

https://dspace.org/

Modelling of the propulsion mechanism for a miniaturized corona ionization thruster

Krommenhoek, Marinus Frans

2015-10-30
http://hdl.handle.net/10539/20450

Downloaded from a DSpace repository. https://dspace.org/

Modelling of the Propulsion Mechanism for a Miniaturized Corona Ionization Thruster

By: Marinus Frans Krommenhoek

A dissertation submitted to the Faculty of Science, University of Witwatersrand, Johannesburg, in fulfilment of the requirements for the degree of Master of Science



School of Physics
South Africa
Supervisor: Dr. Phil Ferrer
Johannesburg, March 2015

Declaration

I declare that this dissertation is my own, unaided work. It is being submitted for the Degree of Master of Science at the University of the Witwatersrand, Johannesburg. It has not been submitted before for any degree or examination at any other University.

_____

(Signature of candidate)

_____day of_____20_____in_____

Abstract

In this dissertation a recipe has been outlined on how thrust can be calculated using the conservation of momentum in continuum form. With the aim of modelling a CORION (corona ionization) like thruster in mind it was then argued using a much simpler system and stochastic calculus why a statistical description of the system is necessary. From this the one-particle distribution emerged as a natural tool for the description of a system sufficient for the determination of the system's thrust.This was followed by a short investigation into the background of non-equilibrium statistical mechanics, both classical and quantum, necessary to understand how one-particle distributions could be derived formally and in a physically consistent way. Mass flow and current-voltage experiments of the CORION like thrust system, necessary for characterization of part of the system, were conducted. This led to a proposal for a modelling strategy, consisting of merging different modelling approaches and descriptions considered throughout the dissertation.

Dedication

This dissertation is dedicated to my family and in memory of my father. I am infinitely grateful for the support, and confidence placed in me by my mother and two younger brothers.

Thanks Renette (mom), Reg and Dirk

Acknowledgements

I would like to thank Dr. Ferrer (my supervisor) for his insights and support, while also thanking my youngest brother Dirk for his assistance with 3D modelling of some of the figures used in this dissertation.

Contents

Declaration iii

Abstract v

Dedication vii

Acknowledgements ix

List of Figures xv

List of Tables xix

Physical Constants and Values Used xxi

1 Introduction 1
- 1.1 CORION Thruster Background . . . 1
- 1.2 Justification for Study and Content of Dissertation . . . 3
- 1.3 A similar system . . . 5
- 1.4 Existing Modelling Approaches . . . 5
- 1.5 Dissertation Outline . . . 5

2 A Generic Thrust Principle 9
- 2.1 The Set-up Under Consideration . . . 10
- 2.2 The Method . . . 11
  - 2.2.1 Continuous Case . . . 11
  - 2.2.2 Discontinuous Case . . . 15
  - 2.2.3 Examples . . . 16
- 2.3 Constructing the control volume's surface ∂V_c and its velocity $\vec{w}$ 18
  - 2.3.1 Constructing the control volume's surface ∂V_c . . . 19
  - 2.3.2 Constructing the velocity field $\vec{w}$ . . . 25
- 2.4 Application of Ideas to Hypothetical Experiment . . . 26

3 Justification for a Statistical Approach to Modelling 29
- 3.1 The Setup under Consideration . . . 29
- 3.2 Applying Stochastic Calculus . . . 30

3.3 Demonstrating Importance of the Neutrals . . . 33
3.4 Deriving an Equation for the Distribution of the Ion System and its Momentum Conservation . . . 36

4 Classical Non-Equilibrium Statistical Mechanics 43
4.1 The Liouville Equation . . . 43
4.2 Reduced Distributions and BBGKY Hierarchy . . . 45
4.2.1 Reduced Distributions . . . 45
4.2.2 The BBGKY Hierarchy . . . 46
4.3 Derivation of Conservation Equations . . . 47

5 Quantum Non-Equilibrium Statistical Mechanics 51
5.1 Von Neumann Density Operator . . . 52
5.2 Wigner Transform and $\star$ - product . . . 53
5.2.1 Un-symmetrized Wigner Transform . . . 54
5.2.2 $\star$ - star operator for un-symmetrized spaces . . . 54
5.2.3 Symmetrized Wigner Transform . . . 55
5.2.4 Extending the star product to symmetrized Wigner Functions . . . 55
5.3 Wigner Distribution Function of the Von Neumann Density . . . 57
5.3.1 Properties and use of The Wigner Distribution . . . 57
5.3.2 Reduced Distributions . . . 58
5.4 Equation of Motion . . . 58
5.5 The Quantum BBGKY Hierarchy . . . 59
5.6 Conservation Equations from the One Particle Distribution . . . 60
5.7 Relevant Distributions and Time Irreversibility . . . 62

6 Mass-flow measurement and calibration 63
6.1 Aim . . . 63
6.2 Background . . . 64
6.2.1 Orifice-plate and Venturi Tube Fundamentals . . . 64
6.3 Mass-flow Estimation Technique and Model . . . 67
6.4 Apparatus . . . 70
6.5 Procedure . . . 74
6.6 Results . . . 75
6.7 Analysis and Discussion . . . 78
6.8 Conclusion . . . 79

7 Thruster Voltage-Current Measurements 81
7.1 Aim . . . 81
7.2 Background - DC Discharges . . . 81
7.2.1 General DC discharge characteristics . . . 82
7.2.2 DC glow discharges . . . 88
7.3 Apparatus . . . 91
7.4 Procedure . . . 96
7.5 Results . . . 97

7.6 Discussion and Conclusion 102

8 Estimates and System Classification 107
8.1 Exit Number Density 108
8.1.1 Estimating Exit Number Density 108
8.2 Flow Classification and micro-tube flow affecting factors 109
8.3 Quantum or Classical 111
8.3.1 Generating a relation for Landau length 111
8.4 Expected Relative Speeds of Interaction 113
8.5 Electron-Ion Interaction 114
8.6 Electron-electron Interaction 115
8.7 Ion-Atom Interaction 115
8.8 Atom-atom Interaction 116
8.9 Electron- Atom Interaction 117
8.10 Non-ideal or Ideal Characterization, Coupling strength Characterization 117
8.10.1 Electron-electron Interaction 119
8.10.2 Electron-ion Interaction 119
8.10.3 Ion-ion Interaction 119
8.10.4 Ion-atom Interaction 120
8.10.5 Atom-atom Interaction 120
8.10.6 Electron-atom Interaction 120
8.11 Degeneracy of electrons 121
8.12 Quantum coupling for electrons 121
8.13 Plasma Parameters 122
8.13.1 Collision Frequency and mean free path length 122

9 Modelling Approach and Difficulties 127
9.1 Note on CTIT models and Boundary Jump Conditions 129
9.2 Modelling Approach 133
9.3 Influence of system characterization on Discharge and Gas flow Modelling 137
9.3.1 Electrons and other plasma constituents outside the thruster system 137
9.3.2 Atoms and other plasma constituents outside the thruster system 138
9.3.3 Ions and other plasma constituents outside the thruster system 139
9.4 Discussion of Boundary Conditions 139

10 Conclusion 141

Appendices 143

A Derivation of conservation equations from One-particle distribution equations 145

B Basic Stochastic Calculus **149**

C Mass Flow Data Results and Analysis **161**
C.1 Error Analysis 166
C.2 Model Justification 167

References **171**

List of Figures

1.1 Oppositely charged needles create a flow of charged particles and neutrals through corona ionization. A plasma bridge ensures continuing operation. 2

1.2 The upper electron plume and lower ion plume are visible. 2

1.3 Diagram illustrating the basic construction of the CORION like system under investigation. 4

1.4 A diagram showing the single needle CORION system (as set up in the laboratory). 7

2.1 A diagram showing how a space craft is first observed with its interaction with the external environment (left) and then how the Space-craft-body V_{scb} and its surface ∂V_{scb} (right) is defined by the modeller. Notice how the nozzles are closed in the picture for V_{scb} to help distinguish internal shuttle contents from external. Modified from [1]. 11

2.2 A diagram illustrating the concept of how to identify the space-craft's-body in order to calculate its thrust. 17

2.3 A diagram illustrating the concept of how to identify the space-craft's-body in order to calculate its thrust. 18

2.4 A conical nozzle of some thruster used to show how Σ_{exit} could be defined. 21

2.5 A: A Cube satellite is used to demonstrate V_M. B: Here ∂V_M is displayed. C: Shows how the exit surface Σ_{exit} is joined on ∂V_M. D: Shows the final surface ∂V_c. 24

2.6 A diagram illustrating the concept of transporting the velocity $\vec{u}$ on ∂V_M^- or Σ_{exit} at some point along the normal $\hat{n}$ to a corresponding point on ∂V_c with normal, say $\hat{n}_c$ to get the velocity there as $\vec{w} = \vec{u}$ for a Euclidean space at least. 26

2.7 Proposed experimental set-up. 27

4.1 Snap shot of an Ensemble of a N particle system in a representation of Γ_N space for a two dimensional system [2, p. 20] 44

6.1 Orifice-plate set-up D is the diameter of the pipe through which gas flows and d is the diameter of the orifice through which gas will be forced [3]. 64
6.2 Nozzle set-up D is the diameter of the pipe through which gas flows and d is the minimum diameter of the nozzle through which gas will be forced [3]. 66
6.3 Nozzle set-up D is the diameter of the pipe through which gas flows and d is the minimum diameter of the nozzle through which gas will be forced [3]. 67
6.4 A diagram showing idea used to establish the mass flow estimate at some time τ and then an instant later. 68
6.5 Extech Differential Pressure Manometer HD750. 71
6.6 Orifice plate box. 71
6.7 Cross-sectional view of the orifice plate box. 72
6.8 A diagram showing the set-up of the experiment from the outside of the vacuum chamber. From left to right: Differential Pressure manometer, Orifice plate, Fine control valve and the two shut-off valves. 72
6.9 A diagram showing the set-up of the experiment from the outside of the vacuum chamber. 73
6.10 Calibration curve of Pressure Difference vs Mass Flow (error set to $\pm\ 2.9 \times 10^{-8}\ kg/s$). 78

7.1 Current voltage characteristic behaviour of DC discharges over a wide current range of gas pressure and electrode geometries. A-B is a region of non-self-sustaining discharge. B-C represents a Townsend dark discharge region. D-E normal glow discharge region. E-F abnormal glow discharge. F-G transition to arcing. G-H arc. The dotted line shows how an increase in applied voltage in a highly inhomogeneous field geometry leads to a corona discharge instead of a normal glow discharge [4, 5]. 82
7.2 A point-to-plane corona geometry, shown here with a positive point. The surface $\alpha^{'} = 0$ marks the outer limit of ionization region, where the production of electrons by ionization just balances the loss by attachment [6]. 86
7.3 General characteristics of DC glow discharges [7, 8]. 89
7.4 Axial potential for high current arc [8]. 91
7.5 The experimental system to be investigated. 92
7.6 hivolt.de T1EP 100 60d p High Voltage Power Supply. 92
7.7 The vacuum chamber used. 93
7.8 The electric stand and gas inlet base used to feed power and gas to the needle. Electric connection inside the chamber to the external power source is shown on the left. 93
7.9 Orthographic views of the experiments set-up: the left hand diagram corresponds to a front view while the right hand diagram corresponds to a side view. 94

7.10 A diagram showing cross-sectional views of the needle and discharge base as used in the experiment. 95
7.11 Results for needle A1 using Argon for a mass flow of 175 $\pm 27 \mu g/s$. Where possible break down voltages with uncertainty $\pm 0.1 kV$ for different trials are included. 97
7.12 Results for needle A3 using Argon for a mass flow of 176 $\pm 28 \mu g/s$. Where possible break down voltages with uncertainty $\pm 0.1 kV$ for different trials are included. 98
7.13 Results for needle A4 using Argon for a mass flow of 159 $\pm 25 \mu g/s$. Where possible break down voltages with uncertainty $\pm 0.1 kV$ for different trials are included. 99
7.14 Results for needle A5 using Argon for a mass flow of 179 $\pm 28 \mu g/s$. Where possible break down voltages with uncertainty $\pm 0.1 kV$ for different trials are included. 100
7.15 Results for needle A6 using air for a mass flow of 117 $\pm 18 \mu g/s$. Where possible break down voltages with uncertainty $\pm 0.1 kV$ for different trials are included. 101
7.16 Needle A4 before the experiment on left, with after the two pictures on the right and bottom. 102
7.17 Typical residue that would be left on the plate in the absence of aluminium foil after firing. The regions A to D have been analysed under a scanning electron microscope (see Figure 7.18). The diameter of the ring is approximately 8mm. [9] 103
7.18 EDS spectra of the regions A to D in Figure 7.17 indicate an increased presence of carbon (peak labeled "C") when compared to aluminium outside the discharge region (far right spectrum).[9] 104

9.1 A diagram showing how the system could be modelled using different modelling techniques in different regions of space where they are most applicable. 128
9.2 A diagram illustrating how the macroscopic view could contain microscopic information about the interface. 132
9.3 A diagram illustrating different non-equilibrium modelling approaches at varying physical scales, modified from [10, p. 5]. . . 134

C.1 A diagram illustrating the set-up for the argument for hydrostatic pressure argument 169

List of Tables

6.1 Table of time taken to evacuate 47 ± $4cm^3$ of Argon and change of pressure across the orifice plate, conducted at a temperature of 294.15 K and with the vacuum chamber stable at 8×10^{-2} $mbar$. 75
6.2 Table of time taken to evacuate 47 ± $4cm^3$ of Argon and change of pressure across the orifice plate, conducted at a temperature of 294.15 K and with the vacuum chamber stable at 9×10^{-2} $mbar$. 76
6.3 Table of time taken to evacuate 47 ± $4cm^3$ of Argon and change of pressure across the orifice plate, conducted at a temperature of 294.15 K and with the vacuum chamber stable at 9×10^{-2} $mbar$. 76
6.4 Table of time taken to evacuate 27 ± $4cm^3$ of Argon and change of pressure across the orifice plate, conducted at a temperature of 294.15 K and with the vacuum chamber stable at $< 10^{-4}$ $Torr$. 77

7.1 Table of discharge types and characteristics [4]. 83

8.1 Summary of system cross-sections, collision frequencies and mean-free path lengths. 124

C.1 Table of time-average volume and mass flow rates for table 6.1 (not taking significant figures into account). 161
C.2 Table of time-average volume and mass flow rates with error estimate for table 6.1. 162
C.3 Table of time-average volume and mass flow rates for table 6.2(not taking significant figures into account). 163
C.4 Table of time-average volume and mass flow rates with error estimate for table 6.2. 163
C.5 Table of time-average volume and mass flow rates for table 6.3 (not taking significant figures into account). 164
C.6 Table of time-average volume and mass flow rates with error estimate for table 6.3. 164
C.7 Table of time-average volume and mass flow rates for table 6.4 (not taking significant figures into account). 165
C.8 Table of time-average volume and mass flow rates with error estimate for table 6.4. 165

Physical Constants and Values Used

Description	Symbol	Values Used
Boltzmann's Constant	k_B	8.6173324×10^{-5} eV/K [11] and 1.3806488×10^{-2} J/K [12]
Relative Atomic Mass of Argon	m_{Argon}	$39.948(1)$ au [13]
Electron Mass (eV)	m_e	$0.510998928(11)$ MeV used 0.510998910 MeV [14]
Electron Mass (kg)	m_e	$9.10938291(40) \times 10^{-31}$ kg used $9.10938215 \times 10^{-31}$ kg [15]
Electric Constant	ϵ	$8.854187817... \times 10^{-12}$ F/m [16] used for Coulomb constant $k_e = 1/(4\pi\epsilon)$
Elementary Charge	e	$1.602176565(35) \times 10^{-19}$ C rounded up to $1.60217657 \times 10^{-19}$ C [17]
Planck's Constant	$\hbar$	$1.054571726(47) \times 10^{-34}$ $J \cdot s$ [18] and $6.58211928(15) \times 10^{-16}$ $eV \cdot s$ [19]

Chapter 1

Introduction

In recent years, research on thruster miniaturisation has been gaining in importance. Miniaturization of general spacecraft components reduces costs associated with payloads and manufacture, while potentially increasing the versatility of space vehicles. Consequently downsizing of propulsion systems for use on smaller spacecraft (with low power availability) has drawn considerable interest, see the review [20]. In miniaturising electric propulsion systems, one aims to retain the high efficiency, exhaust velocity, long lifetime and accuracy of larger systems. While some progress with Hall thrusters has been made [21], despite erosion problems, size reduction of traditional systems is often problematic; for instance gridded electrostatic ion engines lose efficiency on reduction of the discharge chamber [22].

The number of alternative miniaturized electric propulsion systems (total mass < 1kg, operating power < 10 W) has multiplied over the past decade, , see [20]. Work is pursued on thrusters relying on the ejection of charged particles, such as pulsed plasma thrusters [23], the FEEP [24], colloid thrusters [25], Helicon thrusters [26], vacuum arc thrusters [27], micro-particle thrusters [28], hollow cathode thrusters [29] and variations of these. Other alternatives investigate thrust production by various heating mechanisms, such as laser ablation thrusters [30], arc-jet thrusters [31] or relies on interaction with external fields, like the electro-dynamic tethers [32]. Many of these systems have unique strengths and weaknesses, making them candidates for specific mission requirements. The present work can be of benefit in the first category. In this dissertation, we aim to describe elements necessary for the modelling of a corona ionization thruster (like the CORION) and prediction of its thrust.

1.1 CORION Thruster Background

The CORION thruster consists of two hollow stainless steel needles (diameter $O(10^{-1})$ mm) with a potential difference (~1000V) between them, and embed-

ded in an insulator Figure 1.1. A propellant is fed through the needles and escapes into vacuum. The propellant gas leaving through the needle tips experiences a strong electric field and corona ionization is expected to take place. Electrons and negative ions are produced at the negative needle tip, positive ions at the positive needle tip. The charged particles are mainly repelled from their respective needles, but a fraction is attracted by the opposite needle and completes a plasma bridge, which ensures continuing operation. Only about one percent of gas molecules ionize in this fashion, hence the ions repelled from their needle move through a neutral gas background. A photo of the thruster in operation is given in Figure 1.2.

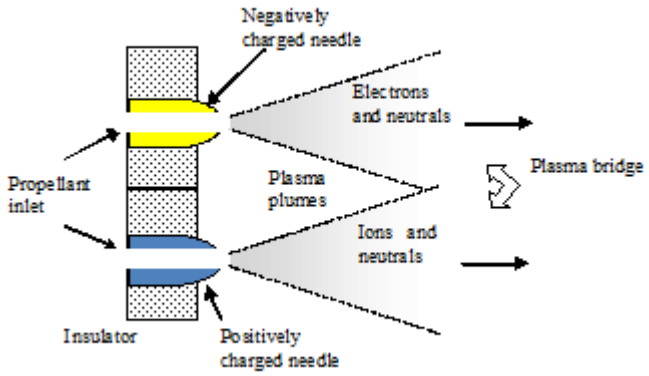


Figure 1.1: Oppositely charged needles create a flow of charged particles and neutrals through corona ionization. A plasma bridge ensures continuing operation.



Figure 1.2: The upper electron plume and lower ion plume are visible.

An analytic model for the radial electric field inside the positive plume was suggested in [33] with the following assumptions:

1. A point charge like electric field produced by the needle tip.

2. The number of neutral particles >> ions.

3. An exhaust plume with a constant spread angle.

4. The current i is the ion current. It is related to the measured current via $i = i_{measured} - i_{sec}$. The i_{sec} is the electron current arising from electrons produced by such secondary effects as photoelectric emission from the plate, positive ion impact, thermionic and field emission. It was not measured and is a free parameter in the theory.

5. Neutralization occurs at the neutralization plane.

6. A uniform neutral gas density decreasing as $1/r^2$.

7. A negligibly small plasma region (the plume is dominated by ions).

Some assumptions were found to be unrealistic [9]. Specifically, electrons cannot be neglected, and the plasma region extends throughout the plume beyond the needle tip. Equally serious was the abnormally high secondary electron emission coefficient of 0.67 (usually < 0.1) and the plume half angle $\theta = 45°$ (it was estimated to be less than 6 degrees, see the aluminium foil in chapter 7). In addition, the onset voltage had to be derived from the data. In this dissertation however, we will not directly discuss the two needle (needle-needle) system above, but rather investigate an assumed simpler configuration involving a positively charged needle and a grounded plate. Some of the shortcomings of previous work is addressed in this dissertation especially inclusion of electrons.

1.2 Justification for Study and Content of Dissertation

The reason for performing the studies and compiling this dissertation is of an entirely practical nature. The CORION thrust system having already displayed thrust potential in previous work [34] is a very small and "simple" thrust system (only several centimetres in dimension) in comparison to hall thrusters (even some miniature versions) [35] and other thrust systems currently employed in satellite orbit control [36]. Having a smaller and lighter thrust system would allow greater propellant (or fuel) accommodation and additional instrumentation on satellites for a given payload cost to be inserted in space. Such an economical advantage would allow for smaller conventional satellite manufacture and deep space probes, thus obviously advancing space science and studies. The problem however is that there is no satisfactory model of the CORION's physical operation making assessment of its practicality and range of functionality in these scenarios impossible without potentially great cost. Consequently, a study on modelling such a system is of great importance to avoid potential uneconomical financing of such a project's development.

Originally this dissertation was to primarily be about the analytic or numerical

modelling of a CORION like thrust system's thrust mechanisms, see [34]. The scenario considered was that of a positively biased needle through which a gas (Argon) is passed and then ionized (presumably just outside the needle) by an incoming stream of electrons 1.3.

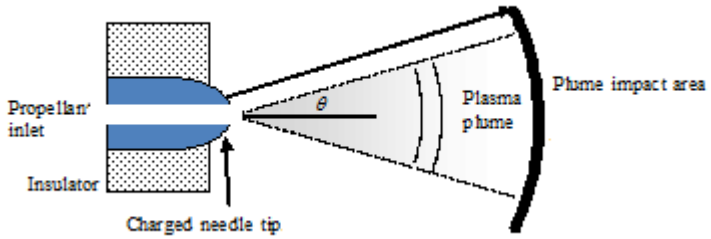


Figure 1.3: Diagram illustrating the basic construction of the CORION like system under investigation.

In the lab the electron stream was supplied by secondary electrons ejected by a plate several hundreds of needle radii from the needle exit, see Figure 1.4. However as investigation and research proceeded the ambitious scope of the initial goal was revealed and had to be abandoned until a later time.

Additional objectives of the dissertation included:

- The description of a formalism, based on continuum mechanics, that can be used to compute thrust and identify thrust mechanisms, but not the methods by which they are generated, for an arbitrary thruster.

- Experiments on electrical behaviour and feasibility of a new construction/set-up for the CORION like system.

- The development of a mass flow measurement technique suitable to low mass flows (~mg/s mass flows).

- A classification of the system's characteristics to assist a reader in developing a model.

These objectives were satisfied. In addition a thorough discussion on a proposed modelling strategy is included which justifies the need for more research in areas such as surface science and computer simulations of strongly coupled classical systems.

1.3 A similar system

A system which appears similar to the Needle to Plate system is the atmospheric-pressure plasma jet [37]. It consists of two concentric electrodes through which a mixture of helium, oxygen and other gases flow into the atmosphere. The gas discharge is ignited by applying a $100-250\ V$ $13.56\ MHz$ RF signal to the inner electrode. Ionized gas exits through the nozzle via the plasma jet with a velocity of $12\ m/s$ and effluent temperature near $150^{\circ}\ C$, under typical operating conditions. Measurements have revealed that the plasma jet posses properties typical of low pressure corona with numerical computation providing additional support for the statement [38]. The atmospheric-pressure plasma jet is different to the system under consideration due to the potential lack of interaction of plasma with shocks formed from the expansion of gas into a vacuum. The systems also have very different boundary conditions for the expected surrounding pressure making comparison difficult. The atmospheric-pressure plasma jet system also has the advantage of not being a multi-scale flow type problem where the system changes from one where fluid descriptions are more appropriate in certain regions of space to kinetic descriptions in other regions of space.

1.4 Existing Modelling Approaches

1.5 Dissertation Outline

The dissertation outline is as follows:

Chapter 2 introduces a generic thrust principle based on manipulation of conservation equations for momentum in a system. Mechanical and aeronautical engineers would recognize this as control volume analysis and application. The derived results show how in general for a non-relativistic system thrust could be derived, as well as how one could go about calculating thrust using the principles introduced. The problem however is that one must often estimate certain physical phenomena (constitutive relations) in order to calculate the thrust within the transport formalism. A formalism that can be used to estimate the unknowns and constitutive equations' forms is introduced in chapters 4, 5 and a section in chapter 9.

Chapter 3 uses Brownian motion based stochastic calculus, for a much simpler hypothetical physical system, to show why it would be necessary to have a statistical method of generating an all inclusive model from which conservation equations for momentum and hence thrust expressions can be derived.

Chapter 4 will introduce Classical Non-equilibrium Statistical Mechanics based on the Liouville equation. From the "moments" and "reduced distributions" of this equation the reader will see how conservation equations can

be derived from the most useful (for the goal of the dissertation) equation to be derived, the equation of motion for the one-particle distribution.

Chapter 5 will be the quantum equivalent to chapter 4, in it the reader will receive a very short introduction to the Wigner-Weyl-Moyal-Groenewold representation of quantum mechanics. This chapter will parallel chapter 4 closely and also show the reader how conservation equations can be derived from a corresponding one-particle Wigner distribution's equation of motion.

Chapter 6 and 7 contain experimental results and analysis for a mass flow measuring technique developed, and electrical results for the CORION like system using a new more stable vacuum chamber as opposed to the chamber used in [34].

Chapter 8 uses information from chapter 6 and previous work on the CORION system for a classification and characterization of its properties pertinent to developing a model for it. It is in this chapter that it becomes evident that, apart from a lack of knowledge about physical boundary conditions and behaviour requiring research in the area of "Surface Science", the system has both quantum and classical behaviour and has components which are strongly coupled (defined and made clear in this chapter). Thereby making it extremely difficult to produce uniformly applicable modelling equations for the system.

Chapter 9 contains ideas to a modelling strategy that could be employed and researched further in order to try and come up with a way to simulate the CORION like system and estimate the thrust. It also serves as a metaphorical "red thread" by connecting what may appear as disconnected and independent chapters together. Thereby validating the use of non-equilibrium statistical mechanics as a modelling tool and the need for additional research.

The dissertation ends with the conclusion.

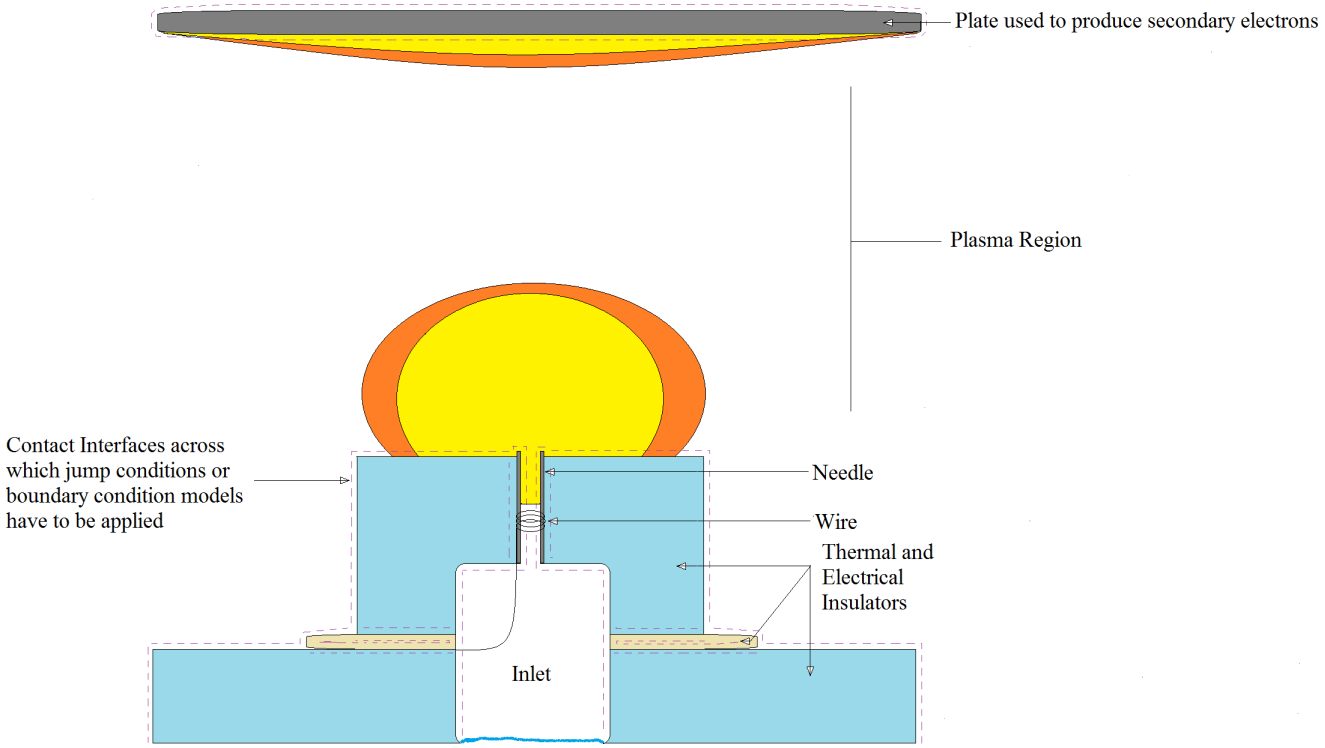


Figure 1.4: A diagram showing the single needle CORION system (as set up in the laboratory).

Chapter 2

A Generic Thrust Principle

In this chapter a basic thrust principle will be developed using ideas from continuum mechanics. The result will naturally be suited to an intuitive definition of thrust for arbitrarily shaped bodies to be "boosted" or "thrusted". It will be applicable to systems using transport equations and conservation equations. This definition will also be applicable to situations where a body and interaction on its surface with external matter for which thrust is required cannot be ignored. In addition this approach will also be useful for situations where a continuum description is not possible, for reasons that will become clear later on when non-equilibrium classical and quantum statistical mechanics is introduced and the "moment equations" (conservation equations) derived.

This formalism or principle is introduced as the author was unable to find any work in the literature which accomplished the goal of having a generic means of defining thrust for an arbitrary body in a convenient way. An exception being perhaps for control volume analysis used in engineering, however there the goals are somewhat different. The advantage of the introduced formalism is that it can be used in many non-relativistic situations and allow one to quickly identify the sources of thrust for a given system.

The chapter is composed of three primary sections. The first introduces the physical situation and setting in which the principle will be introduced. The second section introduces the method used to generate the thrust expression from the situation sketched in the first section and includes examples illustrating the principle. The final section is a logical frame work introduced which can be used to apply the principle in a consistent way to most conceivable physical scenarios of interest.

2.1 The Set-up Under Consideration

Before proceeding, the physical situation to which the method will be applied should be sketched. Of interest will be the situation where the space-craft (and its "internal" propellant as a 3-manifold) V_{sp} is (embedded) in some background (3-manifold) V where V_{ext} the complement (as a set $V_{ext} = V - V_{sp}$) of V_{sp} is the surrounding external environment. Due to stresses and forces acting on the space-craft and its propellant, as well as potential mixing and interaction of the space craft and its propellant with the external environment during the course of its operation there will be deformation of its manifold V_{sp}. The shape of the space-craft and its propellant will change and move through space, a very crude example would be a multi-stage rocket where parts of the original rocket will detach during operation.

In-order to define the thrust of the "space-craft's-body" in an unambiguous way it will become necessary to determine what is meant by the "space-craft's-body" and the external environment. To accomplish this we note that when given the situation of a space craft moving through space we can artificially at each instant in time distinguish "ejected" or "external" propellant from "internal" propellant of a space craft. We can do this by constructing connected surfaces over the nozzle exits (i.e. place where propellant can escape) with their boundaries on the nozzles somewhere (for example on the internal edge of a conical nozzle). We would then consider internal propellant to be that propellant which has not yet passed through the exit surfaces. More generally we would pick the surfaces to have boundary on the space craft with unit normals pointing in the direction along which propellant would escape so as to become part of the external environment, which would then separate the propellant into ejected and internal respectively.

We then extend and connect these surfaces along the physical interfaces between the space-craft (and internal propellant) and the external environment. The closed surface formed in this manner can be used to define the space-craft's-body's boundary denoted ∂V_{scb} while all points internal to it will be called the space-craft's-body and denoted V_{scb}. All points external i.e. $V - (\partial V_{scb} \bigcup V_{scb})$ will then be considered as the external environment still denoted by V_{ext} (note that part of its boundary shares the space-craft's-body's "boundary"). See Figure

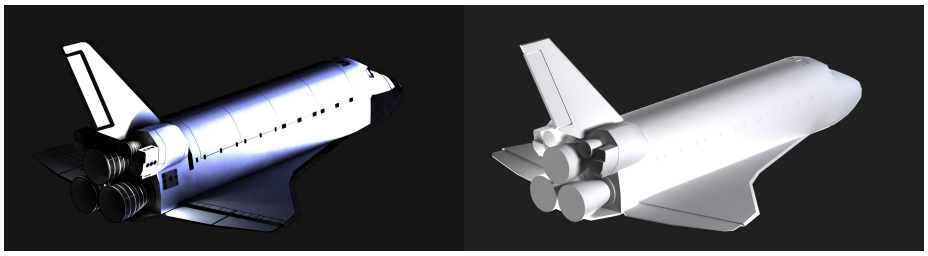


Figure 2.1: A diagram showing how a space craft is first observed with its interaction with the external environment (left) and then how the Space-craft-body V_{scb} and its surface ∂V_{scb} (right) is defined by the modeller. Notice how the nozzles are closed in the picture for V_{scb} to help distinguish internal shuttle contents from external. Modified from [1].

Now with this view in mind we can consider the whole manifold V as a piece of material (or continuum) to which conservation equations can be applied, with an inertial frame of reference used for V's description. And the boundary ∂V_{scb} as a possible moving surface across which discontinuities may occur. By discontinuities it is meant that continuum properties like mass density or temperature may vary rapidly or discontinuously across the surface ∂V_{scb}. This separates the space-craft-body V_{scb} from the external environment as a time varying domain.

2.2 The Method

In this section the method for defining thrust is implemented. A somewhat generic equation of conservation of momentum in "continuum" form will be applied to a space containing a "rocket". The conservation of momentum equation will then be manipulated and used to generate an expression for thrust of the "rocket". Two cases will be considered, a continuous case and discontinuous case. These two cases cover every situation imagined by the author. The continuous case will first be introduced with the notation introduced in it carrying over into the discontinuous case.

2.2.1 Continuous Case

Consider V as the whole space manifold, in which a rocket is embedded, to which conservation equations will be applied, with an inertial frame of reference used for V's description. The only conservation equation of interest here will be the momentum conservation equation, and since we will be considering a non-relativistic system we can consider V as an open subset of E^3 (Euclidean 3-space to exploit its metric and inner product). The conservation equation will then be defined on an open subset of $E \times E^3$ (the additional E is for time). Consequently, for a system with mass density $\rho(\vec{x}, t)$, (t is the time and $\vec{x}$ the position in space of interest) the momentum conservation equation can usually,

be written in the form [39, 40, 41, 42, 43, 44]:

$$\frac{\partial}{\partial t}(\rho\vec{v}) + \nabla\cdot(\rho\overline{\overline{\mathbf{vv}}}) = \nabla\cdot\overline{\overline{\sigma}} + \vec{b} \tag{2.1}$$

Where, the bold letters and $=$ accented letters are tensors. The $\rightarrow$ accented letters are vectors. The un-accented and normal font letters are scalars. $\vec{v}$ is the barycentric velocity of the continuum (i.e. the component density weighted average of the component velocities and the velocity with which V and its boundary ∂V move). $\overline{\overline{\mathbf{vv}}}$ is the dyadic of $\vec{v}$ (basically the tensor product $\vec{v}\otimes\vec{v}$). $\overline{\overline{\sigma}}$ is the stress tensor and $\vec{b}$ a body force density or vector momentum density source. And $\nabla\cdot$ represent divergence operators.

Defining Net Rate of Change of Momentum of a Volume

Now of initial interest to us for the purpose of ultimately deriving an expression for the " thrust vector" of a volume (to be defined later) will be the net rate of change of momentum in the manifold (or volume) V. We begin by integrating the conservation equation 2.1 over the manifold V, i.e.

$$\iiint_V \left[\frac{\partial}{\partial t}(\rho\vec{v}) + \nabla\cdot(\rho\overline{\overline{\mathbf{vv}}})\right]dV = \iiint_V \left[\nabla\cdot\overline{\overline{\sigma}} + \vec{b}\right]dV \tag{2.2}$$

where dV indicates the volume measure on E^3 and the integral is a vector integral (not exactly integration on a manifold, we would need the appropriate "forms" for that). Fortunately from Reynold's Transport Theorem [45] and the use of the Divergence Theorem for tensors [46] we then have that we can identify the **net rate of change of momentum of** V by

$$\frac{d}{dt}(\textit{net momentum of } V) = \frac{d}{dt}\iiint_V \rho\vec{v}dV \tag{2.3}$$

$$\text{By Reynold's Transport Theorem [45]} = \iiint_V \frac{\partial}{\partial t}(\rho\vec{v})dV + \iint_{\partial V}(\rho\vec{v})(\vec{v}\cdot\hat{n})dA \tag{2.4}$$

$$= \iiint_V \frac{\partial}{\partial t}(\rho\vec{v})dV + \iint_{\partial V}\rho\overline{\overline{\mathbf{vv}}}\cdot\hat{n}dA \tag{2.5}$$

$$\text{By Divergence Theorem [46]} = \iiint_V \left[\frac{\partial}{\partial t}(\rho\vec{v}) + \nabla\cdot(\rho\overline{\overline{\mathbf{vv}}})\right]dV\ , \tag{2.6}$$

where dA denotes an area measure and $\hat{n}$ is the unit normal of the surface, chosen to point out of the set V.

Determining the Thrust Vector of a Control Volume

Suppose now that one wants to consider the integral of the conservation equation when restricted to a control volume (denoted V_c again), which will eventually become our space-craft-body V_{scb} contained in V (that is formally as a subset

$V_c \subset V$). For the control volume V_c's boundary ∂V_c (with unit normal $\hat{n}$ pointing out of V_c) we choose a velocity field $\vec{w}$ on it which is not the same as the velocity $\vec{v}$ of the continuum's material on that boundary. We do this to accommodate the case where we would want to superimpose the volume V_c on a rigid rocket such that it moves with the same velocity as the hull of the rocket. And would therefore require that at the nozzles of the rocket the velocity of V_c not be the same as the exit velocity of the propellant. In this case we perform a separation on the above integral 2.2 as follows;

$$\begin{aligned}\iiint_V \left[\frac{\partial}{\partial t}(\rho\vec{v}) + \nabla\cdot(\rho\overline{\overline{\mathbf{vv}}})\right]dV &= \iiint_{V_c\cup(V-V_c)} \left[\frac{\partial}{\partial t}(\rho\vec{v}) + \nabla\cdot(\rho\overline{\overline{\mathbf{vv}}})\right]dV \\ = \iiint_{V_c} \left[\frac{\partial}{\partial t}(\rho\vec{v}) + \nabla\cdot(\rho\overline{\overline{\mathbf{vv}}})\right]dV &+ \iiint_{(V-V_c)} \left[\frac{\partial}{\partial t}(\rho\vec{v}) + \nabla\cdot(\rho\overline{\overline{\mathbf{vv}}})\right]dV \quad (2.7)\end{aligned}$$

where we now note that the velocity of the boundaries of V_c and $V - V_c$, with respect to an arbitrary inertial frame of reference, are $\vec{w}$ and $-\vec{w}$ respectively. We can consider the net rate of change of momentum in V_c and $V - V_c$ respectively using the Reynold's Transport Theorem on equation 2.7. To be specific we would have on application of it to the second last term of equation 2.7

$$\begin{aligned}&\frac{d}{dt}(\textit{net momentum of } V_c) = \frac{d}{dt}\iiint_{V_c}\rho\vec{v}dV \\ &\text{By Reynolds Transport Thm [45]} = \iiint_{V_c}\frac{\partial}{\partial t}(\rho\vec{v})dV + \iint_{\partial V_c}(\rho\vec{v})(\vec{w}\cdot\hat{n})dA\ ,\end{aligned} \quad (2.8)$$

while application to the last term of equation 2.7 yields

$$\begin{aligned}&\frac{d}{dt}(\textit{net momentum of } V - V_c) = \frac{d}{dt}\iiint_{V-V_c}\rho\vec{v}dV \\ &\text{By Reynolds Transport Thm [45]} = \iiint_{V-V_c}\frac{\partial}{\partial t}(\rho\vec{v})dV + \iint_{\partial(V-V_c)}(\rho\vec{v})(-\vec{w}\cdot\hat{n})dA\ ,\end{aligned} \quad (2.9)$$

where $\hat{n}$ here is the unit normal of the boundary $V - V_c$ not V_c. Consequently by adding and subtracting $\oiint_{V_c}\rho\vec{v}\,(\vec{v}\cdot\hat{n})\,dA$ and $\oiint_{V-V_c}\rho\vec{v}\,(\vec{v}\cdot\hat{n})\,dA$ to the above equations we would get for the volume V_c

$$\begin{aligned}&\frac{d}{dt}(\textit{net } \rho\vec{v} \text{ in } V_c) + \oiint_{\partial V_c}\rho\vec{v}\,([\vec{v}-\vec{w}]\cdot\hat{n})\,dA \\ &\qquad = \iiint_{V_c}\left[\frac{\partial}{\partial t}(\rho\vec{v}) + \nabla\cdot(\rho\overline{\overline{vv}})\right]dV\ ,\end{aligned} \quad (2.10)$$

while for $V - V_c$ we get

$$\begin{aligned}\frac{d}{dt}(net\ \rho\vec{v}\ \text{in}\ V - V_c) + \oiint_{\partial(V-V_c)} \rho\vec{v}\,([\vec{v}+\vec{w}]\cdot\hat{n})\,dA \\ = \iiint_{V-V_c}\left[\frac{\partial}{\partial t}(\rho\vec{v}) + \nabla\cdot(\rho\overline{\overline{\mathbf{vv}}})\right]dV\ ,\end{aligned} \tag{2.11}$$

where care must be taken with the interpretation of $\hat{n}$. Additionally, if we perform the same separation of the right hand side for the integrated conservation equation 2.2 we would get

$$\iiint_V \left[\nabla\cdot\sigma + \vec{b}\right]dV = \iiint_{V_c}\left[\nabla\cdot\sigma+\vec{b}\right]dV + \iiint_{V-V_c}\left[\nabla\cdot\sigma+\vec{b}\right]dV\ . \tag{2.12}$$

So that we would get

$$\begin{aligned}\iiint_{V_c}\left\{\left[\frac{\partial}{\partial t}(\rho\vec{v}) + \nabla\cdot(\rho\overline{\overline{\mathbf{vv}}})\right] - \left[\nabla\cdot\sigma+\vec{b}\right]\right\}dV = \\ -\iiint_{V-V_c}\left\{\left[\frac{\partial}{\partial t}(\rho\vec{v}) + \nabla\cdot(\rho\overline{\overline{\mathbf{vv}}})\right] - \left[\nabla\cdot\sigma+\vec{b}\right]\right\}dV\ .\end{aligned} \tag{2.13}$$

Now if the conservation equation remained valid when restricted to the subset V_c we would have that each side equal zero above. Since, by equation 2.1 it holds locally throughout V we conclude

$$\iiint_{V_c}\left\{\left[\frac{\partial}{\partial t}(\rho\vec{v}) + \nabla\cdot(\rho\overline{\overline{\mathbf{vv}}})\right] - \left[\nabla\cdot\sigma+\vec{b}\right]\right\}dV = 0\ , \tag{2.14}$$

and hence that:

$$\frac{d}{dt}(net\ \rho\vec{v}\ \text{in}\ V_c) = \iiint_{V_c}\left[\nabla\cdot\sigma+\vec{b}\right]dV + \oiint_{\partial V_c}\rho\vec{v}\,([\vec{w}-\vec{v}]\cdot\hat{n})\,dA\ , \tag{2.15}$$

with a similar result for the volume $V - V_c$. This then motivates the idea to define the "Thrust Vector of V_c" $\vec{T}_c$ as

$$\vec{T}_c \coloneqq \frac{d}{dt}(net\ \rho\vec{v}\ \text{in}\ V_c)\ , \tag{2.16}$$

that is:

$$\vec{T}_c = \iiint_{V_c}\left[\nabla\cdot\sigma+\vec{b}\right]dV + \oiint_{\partial V_c}\rho\vec{v}\,([\vec{w}-\vec{v}]\cdot\hat{n})\,dA\ . \tag{2.17}$$

On applying the Divergence Theorem [46] we would get:

$$\vec{T}_c = \iiint_{V_c}\vec{b}dV + \oiint_{\partial V_c}\rho\vec{v}\,([\vec{w}-\vec{v}]\cdot\hat{n})\,dA + \oiint_{\partial V_c}\overline{\overline{\sigma}}\cdot\hat{n}dA\ , \tag{2.18}$$

from which it is clear that there are three sources of thrust in the system:

1. Thrust from body forces or momentum sources in the volume V_c, namely $\vec{b}$ (see end of next chapter for an example).

2. Thrust from applied stresses over the boundary of V_c, ∂V_c, namely $\overline{\overline{\sigma}}$ (see the second example of the 2.2.3 subsection).

3. Thrust from momentum flux across the boundary ∂V_c relative to the velocity $\vec{w}$ at which the boundary moves, namely $\rho\vec{v}\left([\vec{w}-\vec{v}]\cdot\hat{n}\right)$ (see the first and second example of the 2.2.3 subsection).

2.2.2 Discontinuous Case

Consider the case where across the boundary ∂V_c discontinuities may be displayed in all quantities used in the conservation equation 2.1. In this case the conservation equations on V are not defined on all of V but are defined on $V-\partial V_c$ and supplemented with "jump conditions" across ∂V_c in-order to ensure physical consistency [39]. Within V_c and $V-(V_c\bigcup\partial V_c)$ we will have that both conservation equations of the form:

$$\frac{\partial}{\partial t}(\rho\vec{v})+\nabla\cdot(\rho\overline{\overline{vv}})=\nabla\cdot\overline{\overline{\sigma}}+\vec{b} \tag{2.19}$$

will hold. On ∂V_c the values of $\rho\vec{v}$ and $\overline{\overline{\sigma}}$ may be different when ∂V_c is considered from the different domains V_c and $V-(V_c\bigcup\partial V_c)$ across the boundary ∂V_c, with the additional possibility that there may be jumps (discontinuous behaviour) across the boundary ∂V_c in $\vec{b}$ (body forces or momentum sources). As an example, momentum associated with ions may be altered by the creation of ions on one side of an interface while being zero on the other side where there is no such ion creation.

With that said we would again have for V_c using the previous definitions for net rate of change of momentum in a volume that;

$$\vec{T}_c=\iiint_{V_c}\vec{b}dV+\oiint_{\partial V_c}\rho\vec{v}\left([\vec{w}-\vec{v}]\cdot\hat{n}\right)dA+\oiint_{\partial V_c}\overline{\overline{\sigma}}\cdot\hat{n}dA\ , \tag{2.20}$$

since within V_c it is defined by its own conservation equation. However, here the values of $\rho\vec{v}$ and $\overline{\overline{\sigma}}$ on the boundary do not have to agree across the boundary with respect to the domain $V-(V_c\bigcup\partial V_c)$ because of the jump conditions. In addition the integral over $\vec{b}$ may be subject to its own jump conditions as well. As a note observe that thrust can also be defined as

$$\vec{T}_c=\oiint_{\partial V_c}\rho\vec{v}\left([\vec{w}-\vec{v}]\cdot\hat{n}\right)dA+\iiint_{V_c}\left[\frac{\partial}{\partial t}(\rho\vec{v})+\nabla\cdot(\rho\overline{\overline{vv}})\right]dV\ , \tag{2.21}$$

which could be extremely useful in systems with "kinetic theory" based descriptions. Kinetic theory based descriptions are covered in the chapters on Non-equilibrium Classical or Quantum Mechanical Statistical Mechanics and indicate how the quantities listed in the above definition can be calculated (or

estimated) (see chapters 4 and 5).

Before continuing with how one could define ∂V_c in systems to associate it with ∂V_{scb} and how one would then go about defining the velocity $\vec{w}$ on ∂V_c, some examples of how the formalism introduced up to now could be used to interpret real thrust, will be given.

2.2.3 Examples

1. Consider a simple thrust system where a box in space moving with velocity $\vec{w}$ simply emits a stream of particles with uniform density ρ and at a velocity $\vec{v}$ from a hole of area A but experiences no stresses or forces. Looking at the Figure 2.2 in order to see how one identifies the space-craft's-body as a simple box we can apply the formula for the thrust vector to get

$$\vec{T}_c = \oiint_{\partial V_c} \rho\vec{v}\left(\left[\vec{w}-\vec{v}\right]\cdot\hat{n}\right)dA = \rho\vec{v}\left[\left(\vec{w}-\vec{v}\right)\cdot\hat{n}\right]A\ , \tag{2.22}$$

   where $\hat{n}$ is the unit normal of the exit. Once we consider the value of the thrust along the unit normal of the exit and identify $\vec{w}-\vec{v}$ as the exit velocity of the stream of particles relative to the space-craft $\vec{v}_{exit}$ and let $\rho\vec{v}\cdot\hat{n}A$ denote the mass-flow rate in the normal direction $\dot{m}_{exit}$ we have the result:

$$\vec{T}_c\cdot\left(-\hat{n}\right) = \dot{m}_{exit}\vec{v}_{exit}\cdot\left(-\hat{n}\right)\ . \tag{2.23}$$

   Thereby giving us the thrust conventionally expected for such a simple system, an example would be the simplified and idealized explanation of a hall thruster's source of thrust [47, p. 21].

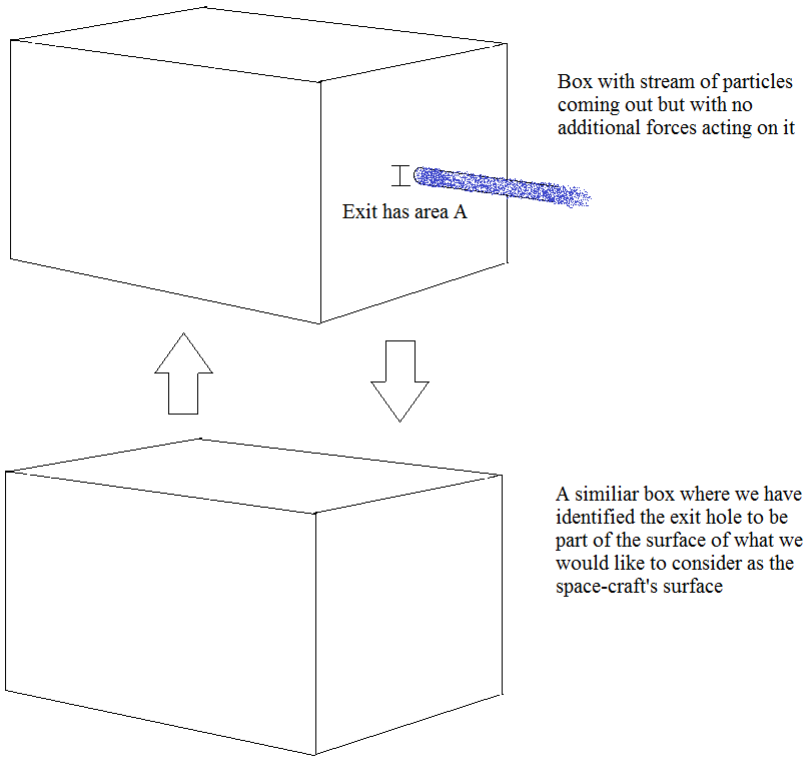


Figure 2.2: A diagram illustrating the concept of how to identify the space-craft's-body in order to calculate its thrust.

2. Consider a simple thrust system where a box in space moving with velocity $\vec{w}$ simply emits a stream of particles with uniform density ρ and at a velocity $\vec{v}$ from a hole of area A and experiences stresses around its surface. To be exact it experiences a pressure P everywhere around it except at the exit where it experiences a pressure P_{exit} due to the stream of particles. Looking at the Figure 2.3 in order to see how one identifies the space-craft's-body as a simple box we can apply the formula for the thrust vector to get

$$\begin{aligned}\vec{T}_c &= \oiint_{\partial V_c} \rho\vec{v}\left([\vec{w}-\vec{v}]\cdot\hat{n}\right)dA + \oiint_{\partial V_c} \overline{\overline{\sigma}}\cdot\hat{n}dA \\ &= \rho\vec{v}\left[(\vec{w}-\vec{v})\cdot\hat{n}_{prop}\right]A + (P-P_{exit})A\hat{n}_{prop}\ , \quad (2.24)\end{aligned}$$

since the pressures P and P_{exit} are equivalent to stresses $-PI$ and $-P_{exit}I$ (see [40]) where I is the identity tensor. Note we have picked the direction

in which the gas particles flow $\hat{n}_{prop}$ as "positive" thus explaining our minus signs. As before if we make the same identifications we get that the thrust would be given by:

$$\vec{T}_c \cdot (-\hat{n}_{prop}) = \dot{m}_{exit}\vec{v}_{exit} \cdot (-\hat{n}_{prop}) + (P_{exit} - P)A \tag{2.25}$$

which can be derived alternatively using thermodynamic arguments as in [48] but with more work.

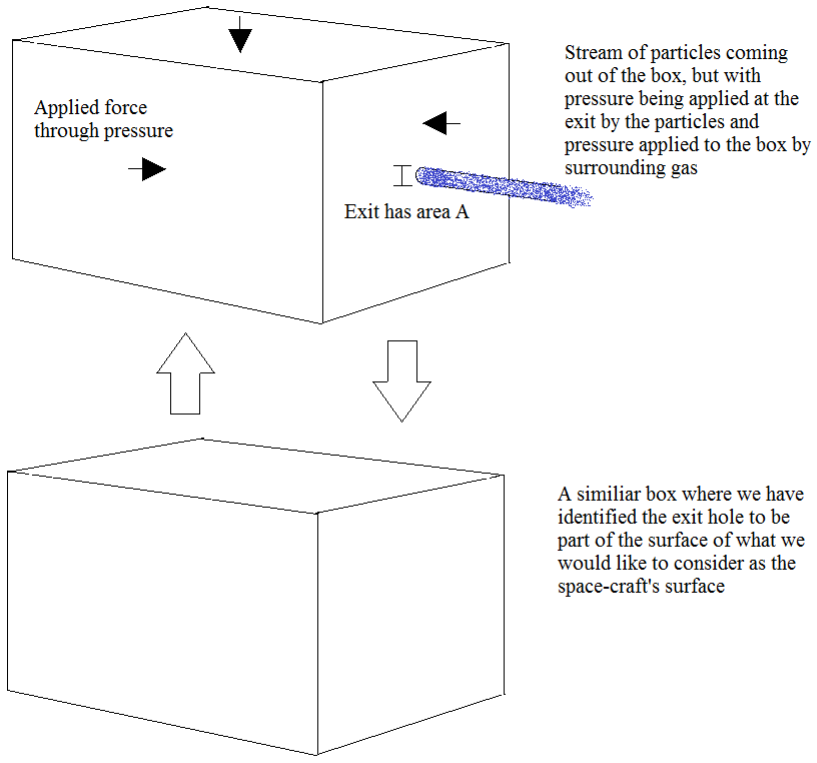


Figure 2.3: A diagram illustrating the concept of how to identify the space-craft's-body in order to calculate its thrust.

2.3 Constructing the control volume's surface ∂V_c and its velocity $\vec{w}$

In this section the method proposed by the author to construct ∂V_c and $\vec{w}$ is described. The control surface ∂V_c will be used to represent and define ∂V_{scb}

(space-craft-body's surface) in applications. While $\vec{w}$, the velocity field defined on ∂V_c, will be constructed such that it would allow application (as outlined by the examples) of the thrust vector's derivation.

How to construct the control volume's surface ∂V_c will first be covered and justified. Then the method to assign a velocity field $\vec{w}$ to ∂V_c appropriate for describing the thrust system will be given.

It should be noted that the construction of an appropriate ∂V_c and its velocity $\vec{w}$ are not unique and different constructions would result in different thrust estimates.

2.3.1 Constructing the control volume's surface ∂V_c

In this section the control volume's surface ∂V_c (and what will be used to represent ∂V_{scb}) along with the control volume will be constructed. However to accomplish this a setting must be introduced to which the definitions and ideas can be applied.

Thus, consider the scenario where one is given a thruster or satellite to run a performance test inside some kind of "testing chamber" (e.g. a vacuum chamber). The thruster once connected to its fuel and energy lines will form say, a "thrust testing unit" inside the "testing chamber".

With the aim of modelling the system in the "testing chamber" mathematically one could then non-uniquely identify an open set (in the Euclidean metric topology) V_M with topological boundary ∂V_M which would "just contain" the "thrust testing unit" and its material boundary whether or not it is in operation. Thereby separating the space in the "testing chamber" in which the "thrust testing unit" is embedded into $V_M \bigcup \partial V_M$ and an external environment.

The problem that emerges is that the notion of "just contains" is not well defined as it is sometimes difficult to reconcile the mathematical description or choice of the open set V_M and its boundary ∂V_M with the "thrust testing unit's" physical occupation of space and its material boundary. As for example, it can become difficult to discern where the macroscopic boundary or interface between different material phases in contact microscopically should be when modelling the system.

However this problem is not a physically inherent problem, but is one generated from a modeller's subjective interpretation of the system. And as a consequence results in non-uniqueness of definitions that could be used by a modeller to identify the material boundary or interface mathematically. Consequently to proceed we will simply assume that the interface or boundary of the "thrust testing unit" is determined by some mathematical means which will be consistent with intuition. To be specific the material boundary or interface will

be defined by a very thin layer of space around the "thrust testing unit" where the "thrust testing unit" and the external environment interact at a microscopic level, but will reduce to a surface at the macroscopic level. Such a definition would be permissible in many cases see for example [49, 50, 51, 52].

Having now decided on how to represent the spatial extent of the "thrust testing unit", that is V_M and its boundary (or interface) ∂V_M we proceed to introduce the notion of "Exit surface" and "Exit surfaces". These surfaces will be used to decide what propellant should be considered inside the thruster when it is operating, and will be denoted Σ_{exit}. We will attach (glue on in a mathematical sense) them to the "thrust testing unit's" surface ∂V_M so that we can ultimately define in a formal way a control volume V_c and its boundary ∂V_c which would allow us to achieve the following goals:

1. It is desirable to include ∂V_M in V_c as the interface can from a physical point of view contain a considerable amount of information. For example consider a satellite in operation in space. As its surface charges the excess surface charge will essentially become part of the interface between the satellite and space and ignoring it will result in neglecting important behaviour such as the migration of the charge over the satellite's body.

2. The exit surface Σ_{exit} will be defined in a way given so that it would conform with what seems to be convention. That is if we had a cylindrical outlet the exit surface would be the defined by the intersection of a plane and the edge of the outlet, see Figure 2.4.

3. With the given definition the operating thruster would be defined to contain the "thrust testing unit" or thruster and all contents (e.g. flowing propellant) up until the exit surface.

4. The definition would also allow us to use the external stresses applied to the contact interface to determine the net stress applied on the thruster instead of having to use jump condition corrected internal stresses at the contact interface, as in the case when we use ∂V_M instead.

We propose to define ∂V_c, in the context of this dissertation, in three stages. First given our thrust testing unit (or spacecraft), and the fact that we have definitions available for V_M and ∂V_M, we will describe the "Exit surface" denoted say by Σ_{exit}. The exit surface/s will be used by the modeller to represent the surfaces through which propellant escapes and can then be considered to be **outside the space craft**:

Proposal 1 *An exit surface Σ_{exit} is a subjectively chosen connected surface with boundary and of minimum area chosen, such that:*

1. *its boundary intersects with the space-craft (or thruster) boundary ∂V_M*

2. *defines a surface through which propellant escapes and can then be considered to be outside the space craft and part of the external environment*

3. *has a consistent orientation (a normal vector) always pointing into the external environment in the general direction of the ejected propellant's direction of movement and mathematically defined by local orthogonal co-ordinates at points lying on the surface (i.e. as the induced orientation of the surface using the orientation on E^3 in which it is immersed)*

The importance of the "exit surfaces" is that they allow us to re-specify the inside of the space-craft or thrust testing unit and what should be considered the external environment. An example of this would be when using a conical nozzle the disk that intersect the inner edge of the nozzle see Figure 2.4.

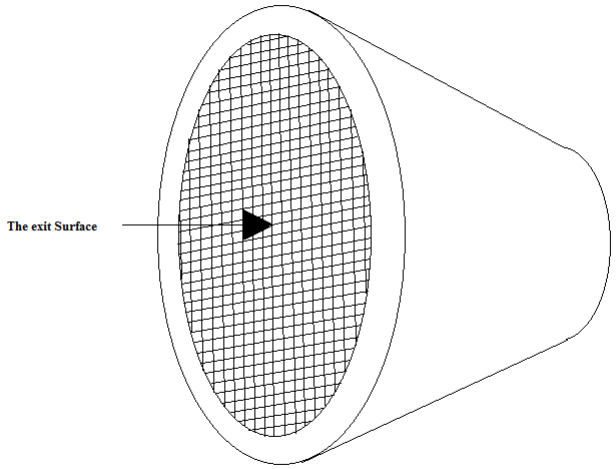


Figure 2.4: A conical nozzle of some thruster used to show how Σ_{exit} could be defined.

With the exit surfaces defined we proceed to describe a temporary surface $\partial V_c'$ which we will call the "outline" used to separate the system into external environment and the space-craft or thrust testing unit's contents. This "outline" $\partial V_c'$ will then be used to define the Space-craft-body V_{scb}'s (or control volume V_c's) surface or boundary ∂V_{scb} (or ∂V_c) and hence define them. We can think of the "outline" as being the three dimensional equivalent of a trace around the "outside" of a two dimensional drawing (see Figure 2.5 C).

Proposal 2 *The " outline" $\partial V_c'$ is the oriented surface given by collecting (into a set) together all points of the space-craft or thrust testing unit's material surface ∂V_M and the exit surfaces Σ_{exit} such that:*

1. *the normal vectors (orientation) of ∂V_M and Σ_{exit} point into the external*

environment, and do not point to either points of V_M or propellant that has not passed through the exit surfaces

2. *the surface $\partial V'$ is then given the same normal vectors at points corresponding to ∂V_M or Σ_{exit} as the normal vectors on those surfaces*

In addition if we denote $Int(\partial V_c')$ to be the interior of the closed surface $\partial V_c'$ we can see that it will contain V_M (i.e. the contents of the space-craft) and all propellant that has not passed through the exit surfaces. With $\partial V_c'$ defined we must next try to define our thruster volume or space-craft-body V_{scb} (or the control volume V_c) and its boundary ∂V_{scb} (or ∂V_c). We do this by introducing the "ϵ-Envelopes of $\partial V_c'$" ∂V_ϵ, which will be used to surround the "outline" $\partial V_c'$ and used to describe ∂V_c or ∂V_{scb} by choosing ϵ to be as small as possible (or useful for the purposes of the modeller). In this way one will be able to choose a surface, ∂V_c or ∂V_{scb}, to "wrap" as tightly as possible (for the purpose of this dissertation) around the outline $\partial V_c'$ and therefore contain the outline and its contents.

Proposal 3 *A "ϵ-Envelopes of $\partial V_c'$" ∂V_ϵ for real $\epsilon > 0$ is a closed smooth surface of minimum surface area such that:*

1. *∂V_ϵ has outward pointing normal vectors (orientation)*
2. *$Int(\partial V_c') \bigcup \partial V_c' \subset Int(\partial V_\epsilon)$, i.e. the contents of ∂V_ϵ must contain V_c' and $\partial V_c'$.*
3. *if $\hat{n}(p)$ is a normal vector on $\partial V_c'$ at a point p and $x_{\hat{n}(p)}$ is the point on ∂V_ϵ to which p is mapped **by the geodesic** with initial tangent vector $\hat{n}(p)$ onto ∂V_ϵ, then we would require that the length L along this curve from p to $x_{\hat{n}(p)}$ satisfy $\epsilon \geq L > 0$ (i.e. we would like the distance of separation to at most be ϵ and as small as possible)*

Note that the "ϵ-Envelopes of $\partial V_c'$" will form a family of surfaces (i.e. as sets), denoted say by $\partial \mathcal{V}$, indexed by the permitted values of $\epsilon > 0$ which we could denote $\Lambda = \{\epsilon > 0 : \partial V_\epsilon \text{ are defined}\}$. It should be obvious that since each member of Λ is bounded from below that Λ will have an infimum (i.e. greatest lower bound) denoted $inf(\Lambda)$. We will now use $inf(\Lambda)$ to pick our control surface ∂V_c or the space-craft-body's surface ∂V_{scb} from the family of sets $\partial \mathcal{V}$, thereby defining them and then use that to define the control volume V_c and space-craft-body V_{scb}.

Proposal 4 *∂V_c the thruster body or ∂V_{scb} space-craft-body's boundary will be considered to be either:*

1. *when $inf(\Lambda) \in \Lambda$, to be the "ϵ-Envelope of $\partial V_c'$" ∂V_δ where $\delta = inf(\Lambda)$*
2. *when $inf(\Lambda) \notin \Lambda$ (i.e. $inf(\Lambda) = 0$), to be the "ϵ-Envelope of $\partial V_c'$" ∂V_δ where $\delta \in \Lambda$ (maximum distance of separation) is chosen by the modeller based on previously defined criteria and modelling parameters, ideally it should be picked so that near surface phenomena can be taken into account to an acceptable level of accuracy for the required application*

Finally the control volume V_c and space-craft-body V_M are then given as the interior of the "ϵ-Envelope of $\partial V_c'$" ∂V_δ (i.e. $Int(\partial V_\delta)$)

See Figure 2.5 which illustrates to some degree the ideas introduced.

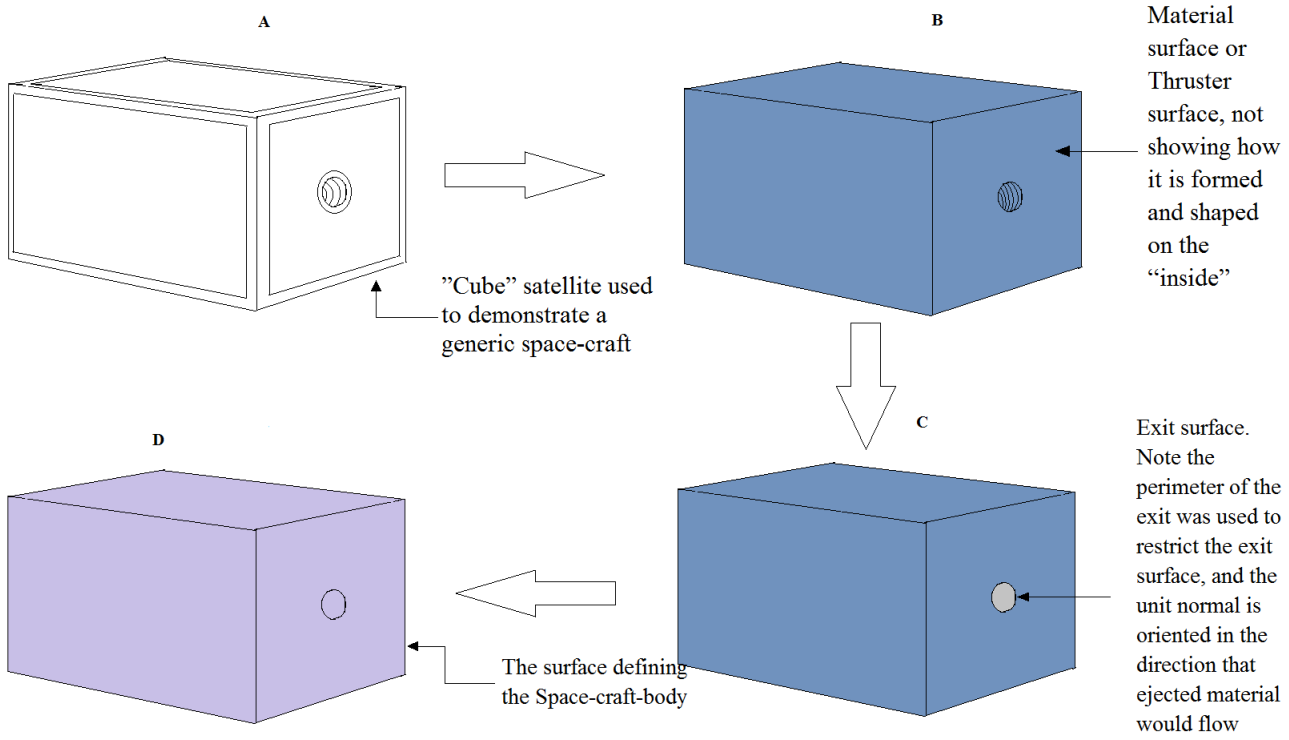


Figure 2.5: A: A Cube satellite is used to demonstrate V_M. B: Here ∂V_M is displayed. C: Shows how the exit surface Σ_{exit} is joined on ∂V_M. D: Shows the final surface ∂V_c.

2.3.2 Constructing the velocity field $\vec{w}$

In-order to apply the derivation of thrust vector as in the examples it would be necessary to describe how the velocity $\vec{w}$ can be described. We propose to define the velocity on ∂V_c, with respect to the context of the dissertation, by using the boundary condition velocities $\vec{u}$ defined on ∂V_M and the yet to be defined velocity $\vec{u}$ on the exit surfaces. Note that due to the orientation that ∂V_M possesses it is possible to identify different sides of it. For instance the side of the surface adjacent to the space into which the normal vector of ∂V_M points can be referred to as ∂V_M^+, while the opposite side can be referred to as ∂V_M^-. In addition ∂V_M has jump conditions associated with the values of the boundary velocities defined about it on the different sides of the surface ∂V_M. That implies that potentially different boundary velocities are defined on the different sides of the surface. The boundary values of ∂V_M that will be used will be the values defined on ∂V_M^-, i.e. the values associated with the space-craft material and not the external environment.

Before proceeding however we will have to specify how one can define a velocity field $\vec{u}$ on the exit surfaces Σ_{exit} that can be used to define the velocity $\vec{w}$ on the control surface ∂V_c.

Proposal 5 (Exit surface velocity field) *Over the exit surfaces Σ_{exit}, the velocity $\vec{u}$ is defined as a velocity field such that:*

1. *the values of $\vec{u}$ on the perimeter of the exit surface Σ_{exit} (points where it intersects with ∂V_M) are provided by the boundary values on ∂V_M^- at those points*

2. *at the point of average distance $x \in \Sigma_{exit}$, from the perimeter of Σ_{exit}, on the exit surface the value of $\vec{u}(x) \equiv \vec{w}_{ave}$ is the average value of $\vec{u}$ on the perimeter of the exit surface (points where it intersects with ∂V_M)*

3. *the vector field $\vec{u}$ is such that the variation of this field (with respect to the value $\vec{w}_{ave}$) over the exit surface (with perimeter values given) is a minimum and satisfies*

$$\min_{\vec{u} \text{ on } \Sigma_{exit}} \delta[\vec{u}] \text{ where } \delta[\vec{u}] = \frac{1}{Area(\Sigma_{exit})} \iint_{\Sigma_{exit}} \|\vec{w}_{ave} - \vec{u}(\vec{x})\|^2 dA \quad (2.26)$$

   where dA is an area measure. This is done in an attempt to stay close to the value $\vec{w}_{ave}$.

Next we construct/choose the velocity field of the space-craft-body's surface ∂V_{scb} $\vec{w}$ as follows:

Proposal 6 (Velocity field $\vec{w}$) *The velocity field on ∂V_c $\vec{w}$ is chosen to be a vector field such that:*

1. *$\vec{w}(x_{\hat{n}(p)}) = \vec{u}(p)$ where $x_{\hat{n}(p)} \in \partial V_c$ are points on the geodesic curve with initial tangent vector $\hat{n}(p)$ (i.e. the normal on $\partial V_c'$ at p) starting at point*

$p \in \partial V_c'$ *and* $\vec{u}(p)$ *is the boundary value velocity field assigned to* ∂V_M^- *or the velocity field assigned to the exit surfaces* Σ_{exit} *depending on* p

2. *if possible* $\vec{w}$ *to be at least smooth (continuous) on* ∂V_c *and only have discontinuous behaviour at points* $x_{\hat{n}(p)} \in \partial V_c$ *which are points on the geodesic curve with initial tangent vector* $\hat{n}(p)$ *(i.e. the normal on* ∂V_M *at* p*) at points* p *on* ∂V_M^- *or* Σ_{exit} *for which* $\vec{u}$ *has discontinuous behaviour*

see Figure 2.6.

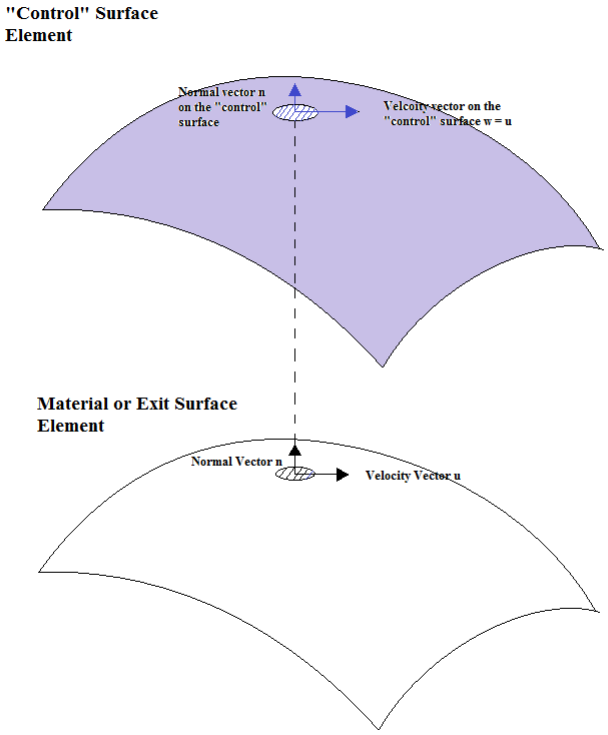


Figure 2.6: A diagram illustrating the concept of transporting the velocity $\vec{u}$ on ∂V_M^- or Σ_{exit} at some point along the normal $\hat{n}$ to a corresponding point on ∂V_c with normal, say $\hat{n}_c$ to get the velocity there as $\vec{w} = \vec{u}$ for a Euclidean space at least.

2.4 Application of Ideas to Hypothetical Experiment

Consider a hypothetical experimental set-up illustrated by Figure 2.7.

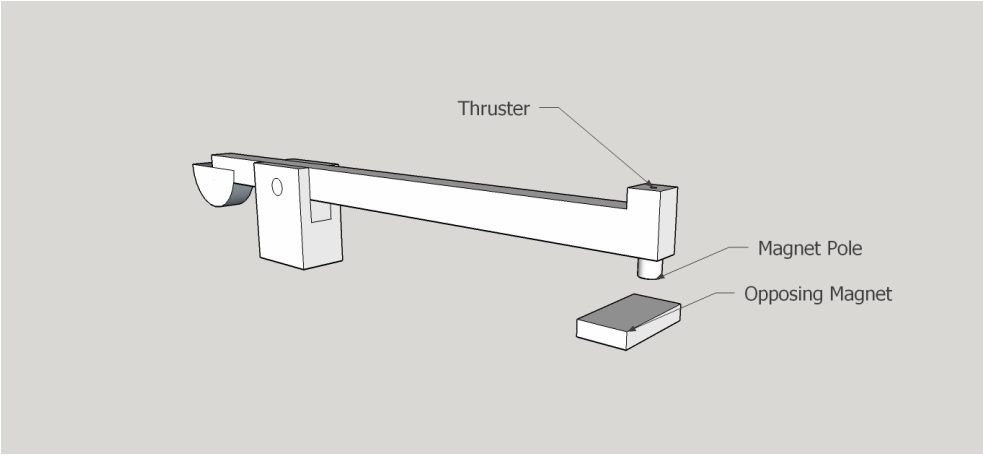


Figure 2.7: Proposed experimental set-up.

In-order to determine the thrust generated by the thruster we consider a frame of reference situated at the thruster with one of its axis parallel to the lever arm and the other perpendicular to the lever and parallel to the direction in which gas is released. As a result once stationary operation has been achieved for a continuously firing thruster the thrust vector will be given by the equation

$$\vec{T}_c = \iiint_{V_c} \vec{b}(\vec{x}) + \vec{g}(\vec{x}) dV - \oiint_{\partial V_c} \rho \vec{v} \left(\vec{v} \cdot \hat{n}\right) dA + \oiint_{\partial V_c} \left(\overline{\overline{\sigma}}_m + \overline{\overline{\sigma}}_p + \overline{\overline{\sigma}}\right) \cdot \hat{n} dA \ , \quad (2.27)$$

where V_c is the thruster and its contents and ∂V_c the boundary around the thruster and its contents. $\vec{b}(\vec{x})$ is the body force density applied to the thruster by the magnet and $\vec{g}$ the gravitational force density. $\overline{\overline{\sigma}}_m$ and $\overline{\overline{\sigma}}_p$ are the electromagnetic and mechanical stress applied by the magnet and plasma on the thruster boundary while $\overline{\overline{\sigma}}$ is a mechanical stress applied on the boundary of the thruster by other sources. At the steady state of operation there will be no change in the net momentum in the volume, as a result if we consider the component of the thrust vector parallel to the direction in which gas leaves the thruster we will have:

$$0 = B + G_{\parallel} - \dot{m} v_{exit} + \hat{n}_{exit} \cdot \oiint_{\partial V_c} \left(\overline{\overline{\sigma}}_m + \overline{\overline{\sigma}}_p + \overline{\overline{\sigma}}\right) \cdot \hat{n} dA \ . \quad (2.28)$$

Since we ultimately use the magnetic force to measure the thrust we would then have that

$$\text{Measured Force} = -B = G_{\parallel} - \dot{m} v_{exit} + \hat{n}_{exit} \cdot \oiint_{\partial V_c} \left(\overline{\overline{\sigma}}_m + \overline{\overline{\sigma}}_p + \overline{\overline{\sigma}}\right) \cdot \hat{n} dA \ . \quad (2.29)$$

If we assume that net contribution of $\overline{\overline{\sigma}}$ over the whole surface of the thruster is zero and that the applied magnetic force is applied by a stationary magnetic field we would then have that the measured force is be given by

$$\text{Measured Force} = G_{\parallel} - \dot{m} v_{exit} + \hat{n}_{exit} \cdot \oiint_{\partial V_c} \left(\overline{\overline{\sigma}}_p\right) \cdot \hat{n} dA \ , \quad (2.30)$$

where we can notice that the right hand side of equation 2.30 is the thrust of the thruster in the absence of the applied magnetic force. It is clear from the equation that the sources of thrust will be from the net flux of momentum out of the thruster and the stress applied by the plasma on the thruster. Unfortunately the form of the stress applied by the plasma is not known, however models for it may be deduced using statistical techniques which will be introduced later in the dissertation.

Chapter 3

Justification for a Statistical Approach to Modelling

In this chapter arguments are made as to why a formulation of the problem of modelling plasma flow of the CORION thruster (or related systems) in-terms of non-equilibrium statistical mechanics is advantageous. More specifically, it will be argued for a hypothetical plasma system consisting of ions, electrons and neutrals, using slightly modified Langevin Equations (Newtonian equations of motion with "random" force terms) for ion motion. These will be used to point out why having idea of how the neutrals behave and interact with the ions is important to the understanding of the plasma system. In addition the equations of motion for the ions will be used to generate an equation of motion for their collective distribution. Then from the equation for the distribution a continuum like momentum conservation equation for the ions will be derived thereby tying this chapter in with chapter 2. These results should then be sufficient for showing why approaching the modelling problem using non-equilibrium statistical mechanics will be advantageous.

3.1 The Setup under Consideration

We consider the hypothetical plasma consisting of ions of one type (positive), neutrals and electrons contained in some volume (specifics about the boundary conditions will be addressed during the course of the derivations) in which a uniform electric field is applied and no chemical reactions occur. Ion-ion and ion-electron interactions will be considered negligible. The only interaction of interest is between ions and a uniform flow of neutrals and ions with an applied electric field. From a physical standpoint the assumption is that the nearby applied electric field is the dominant source of electrically transferred momentum and energy and that interaction between charged species are negligible. With this assumption we note that we can consider the ions to behave independently of one another, but where their motions will be determined by interactions (i.e.

random collisions) with the uniform flow of neutral gas and a uniform applied electric field $\vec{E}$. Thus the classical equations of motion (in 3d-space) of an ion are hypothesized to be of Langevin type:

$$\frac{d}{dt}\vec{v}(t) = \frac{q}{m}\vec{E} - \frac{\gamma}{m}\left[\vec{v}(t) - \vec{u}\right] + \frac{1}{m}\vec{\epsilon}(t) \tag{3.1}$$

$$\frac{d}{dt}\vec{x}(t) = \vec{v}(t)\ , \tag{3.2}$$

where $\vec{v}(t)$ is the velocity of the ion (with initial velocity $\vec{v}(0)$). m is its mass and q is its electric charge. $\vec{E}$ is the applied electric field intensity. $\vec{u}$ is the average velocity of the neutral gas flow. γ is a friction co-efficient simulating "drag like" effects or a gross drift inducing effect, depending on the term in brackets' signs, so a to simulate the net effect of the uniform gas motion on the ions. $\vec{\epsilon}(t)$ is a random force giving the effect of background random collisions with the neutrals and chosen to have the properties of "White-Noise". Namely, the expectation of it at any time is zero ($\langle\vec{\epsilon}(t)\rangle_{\epsilon} = 0$) and its correlation function given by $\langle\epsilon_i(t_1)\epsilon_j(t_2)\rangle_{\epsilon} = g\delta_{ij}\delta(t_1 - t_2)$ (i and j are the vector components and g the strength of the correlation) to validate the white-noise requirement.

The reason for considering such a model is that it will give us an idea as to the dependence of the ion's average kinetic energy on the surrounding neutrals and electric field, as well as how much energy on average is transferred to the ion by the electric field. The difference being the average amount of energy lost via collisions to the neutral gas. It is acknowledged that this model may not have genuine physical significance by using an unrealistic white-noise process, since the noise term may in a real system have finite non-zero correlation time associated with more gradual momentum exchange during collisions (where as the "white noise" has delta function or instantaneous correlations) [53]. But it is used here simply to demonstrate how important knowledge regarding the actual interaction with the neutrals is, and thus why a more formal approach should be used to model the system.

3.2 Applying Stochastic Calculus

Before starting with the calculations the above Langevin equation will be put into a more mathematically acceptable form. This will be done so that Ito-calculus (Brownian motion stochastic calculus see appendix A) can be applied to the solution of the problem. We do this since although we can use the equations 3.1 as above the problem that emerges is that we must apply the theory surrounding "Generalized Stochastic Processes" [54]. Such an approach would detract from the essential simplicity of the model, if everything has to be perfectly justified within this mathematical framework, while we have that Ito-calculus is well developed to handle this problem when recast (see appendix B). Now to introduce the necessary mathematical setting notice that the above equations 3.1 may not have a clear interpretation in the usual sense of a set

of normal differential equations. To be specific the random force may not be continuous at all points in time. In an effort to remove this problem we proceed by performing a normal integration (with respect to time) of the equations to see if the resulting equivalent integral equations would be more accessible to a standard interpretation. Doing this we get:

$$\vec{v}(t) - \vec{v}(0) = \int_0^t \left(\frac{q}{m}\vec{E} - \frac{\gamma}{m}(\vec{v}(\tau) - \vec{u}) \right) d\tau + \int_0^t \frac{1}{m}\vec{\epsilon}(\tau) d\tau \tag{3.3}$$

$$\vec{x}(t) - \vec{x}(0) = \int_0^t \vec{v}(\tau) d\tau \ , \tag{3.4}$$

where for the i'th spatial component $\int \epsilon_i d\tau$ term we could formally associate $\epsilon_i d\tau$ with an infinitesimal change in a stochastic process $U_i(t)$ such that $dU_i(\tau) = \epsilon_i d\tau$ is a stationary Markovian process (see [55]). The process would represent an infinitesimal random change in a momentum component such that the correlation of such a change at any given time between different components satisfy

$$\langle dU_i(\tau) dU_j(\tau) \rangle = \langle \epsilon_i(\tau)\epsilon_j(\tau) \rangle \, d\tau d\tau = g\delta_{ij} d\tau \ , \tag{3.5}$$

where g could represent the strength of the degree of correlation and is by assumption not a function of $\vec{U}$. δ_{ij} is the Kronecker-Delta function used to show that we do not want to have momentum changes in different directions to be correlated with one another. Doing this we could instead of considering integrating with respect to $\epsilon_i d\tau$ consider integrating with respect to $dU_i(t)$. Our problem then would be on how to define such integration. Fortunately on comparison with a multidimensional Wiener Process (multidimensional simple Brownian motion), in this case a 3-dimensional one, denoted $\vec{W}(\tau)$ we could consider $d\vec{U}(\tau) = \sqrt{g} d\vec{W}(\tau)$ in either the Ito-calculus or Stratonovich-calculus sense since g is not a function of $\vec{U}$ by assumption (see appendix B). We could then use the appropriate Stochastic Calculus to define the integration. However one must note that on associating $d\vec{U}(\tau)$ with $\vec{\epsilon}(\tau)d\tau$ in the integral the interpretation of the integral is then in the Stratonovich-calculus sense as required by the Wong-Zakai theorem [56, 57], which regulates which form of Stochastic Calculus is more applicable to physical problems. As a consequence we have:

$$\vec{v}(t) - \vec{v}(0) = \int_0^t \left(\frac{q}{m}\vec{E} - \frac{\gamma}{m}(\vec{v}(\tau) - \vec{u}) \right) d\tau + \int_0^t \frac{\sqrt{g}}{m} \circ d\vec{W}(\tau) \tag{3.6}$$

$$\vec{x}(t) - \vec{x}(0) = \int_0^t \vec{v}(\tau) d\tau \ , \tag{3.7}$$

where for our purposes the Stratonovich style integrals have been bundled together under the $\int \circ d\vec{W}(\tau)$ notation (see appendix B). In addition we will assume that g is a function of time only and will hence have an obvious effect on the integrals which will not be difficult to spot (it will also introduce no effect when we change from Stratonovich formalism to Ito formalism for the differentials). From this it follows that the corresponding Stratonovich style Stochastic Differential Equations (SDE) for the integral equation can be written as

$$d\vec{v}(t) = \left(\frac{q}{m}\vec{E} - \frac{\gamma}{m}(\vec{v} - \vec{u}) \right) dt + \frac{1}{m}\sqrt{g} \circ d\vec{W}(t) \ . \tag{3.8}$$

The novelty (at least at this level of treatment) of the Stratonovich formalism is that we can apply standard calculus change of variable formula (and hence the chain rule for differentials) to the SDE's differentials [58] to obtain

$$d\left(e^{\frac{\gamma}{m}t}(\vec{v}-\vec{u})\right) = \left(\frac{q}{m}e^{\frac{\gamma}{m}t}\vec{E}\right)dt + \frac{1}{m}e^{\frac{\gamma}{m}t}\sqrt{g}\circ d\vec{W}(t)\ . \tag{3.9}$$

In this form we can transform equation 3.9 into the appropriate equivalent Ito-SDE, to exploit the formalism's state of mathematical development and avoid having to do doubly many computations. Fortunately due to the simplicity of the Stratonovich-SDE's form here the Ito-SDE follows as (see appendix B)

$$d\left(e^{\frac{\gamma}{m}t}(\vec{v}-\vec{u})\right) = \left(\frac{q}{m}e^{\frac{\gamma}{m}t}\vec{E}\right)dt + \frac{1}{m}e^{\frac{\gamma}{m}\tau}\sqrt{g}d\vec{W}(t)\ , \tag{3.10}$$

where integration would be performed in the Ito sense [1]. This linear equation can be solved by direct integration, to yield

$$e^{\frac{\gamma}{m}t}\left(\vec{v}(t)-\vec{u}\right) - \left(\vec{v}(0)-\vec{u}\right) = \frac{q}{\gamma}\vec{E}\left(e^{\frac{\gamma}{m}t}-1\right) + \frac{1}{m}\int_0^t e^{\frac{\gamma}{m}\tau}\sqrt{g}d\vec{W}(\tau)\ , \tag{3.11}$$

where the Ito integration is used. From this follows that the momentum of an ion at any time t (within this context) is given by:

$$m\vec{v}(t) = m\vec{v}(0)e^{-\frac{\gamma}{m}t} + \left(m\vec{u} + \left(\frac{m}{\gamma}\right)q\vec{E}\right)\left(1-e^{-\frac{\gamma}{m}t}\right) + \int_0^t e^{-\frac{\gamma}{m}(t-\tau)}\sqrt{g}d\vec{W}(\tau)\ . \tag{3.12}$$

[1] No $\circ$ to indicate Ito formalism

3.3 Demonstrating Importance of the Neutrals

Of paramount interest to us will be the work done on the ion. To calculate this we use the definition of infinitesimal work $d\mathcal{W}$ done:

$$\begin{aligned} d\mathcal{W}(t) &= \vec{F}(t)\cdot d\vec{x}(t) \\ &= \vec{F}(t)\cdot\vec{v}(t)dt \\ &= \left(\vec{F}(t)dt\right)\cdot\vec{v}(t) \\ &= \left(md\vec{v}(t)\right)\cdot\vec{v}(t) \\ &= md\vec{v}(t)\cdot\vec{v}(t) \\ &= m\sum_{i=1}^{3} v_i(t)dv_i(t) \text{ sum is over the spatial components} \\ &= m\sum_{i=1}^{3}\frac{1}{2}dv_i^2(t) \\ &= \frac{1}{2}mdv^2(t) \\ &= d\left(\frac{1}{2}mv^2\right)(t)\ . \end{aligned}$$

Which in-order for all the steps to follow would require a Stratonovich sense of integration (due to the Wong-Zakai theorem [56, 57]) resulting in the following simple result (see appendix B)

$$\Delta\mathcal{W}(t) = \int_0^t \circ d\left(\frac{1}{2}mv^2\right)(\tau) = \frac{1}{2}mv^2(t) - \frac{1}{2}mv^2(0)\ , \tag{3.13}$$

while the infinitesimal electrical work done $d\mathcal{W}_E(t)$ on the ion will be given by

$$d\mathcal{W}_E(t) = q\vec{E}\cdot d\vec{x}(t) = q\vec{E}\cdot\vec{v}(t)dt\ , \tag{3.14}$$

so that $\Delta\mathcal{W}_E(t) = \int_0^t q\vec{E}\cdot\vec{v}(\tau)d\tau$ (interpreted as a Riemann integral). Hence the work done on the "ion by the neutrals" will be given by

$$-\left(\Delta\mathcal{W}(t) - \Delta\mathcal{W}_E(t)\right)\ , \tag{3.15}$$

where the minus is used as a convention to indicate reversed direction. Of primary interest will be the average work done by the " ion on the neutrals" for small times to get an idea of how effective the ion could be at transferring energy to the neutrals. Starting with the shorter case we have from equation

3.12 that

$$\Delta\mathcal{W}_E(t) = \int_0^t q\vec{E}\cdot\vec{v}(\tau)d\tau = \sum_{i=1}^{3} qE_i \int_0^t v_i(\tau)d\tau$$
$$= \sum_{i=1}^{3} qE_i\left(\frac{m}{\gamma}\right)v_i(0)\left[1-e^{-\frac{\gamma}{m}t}\right] + qE_i\left(u_i+\left(\frac{1}{\gamma}\right)qE_i\right)\left[t+\left(\frac{m}{\gamma}\right)e^{-\frac{\gamma}{m}t}-\left(\frac{m}{\gamma}\right)\right]$$
$$+ qE_i\frac{1}{m}\int_0^t\int_0^\tau e^{-\frac{\gamma}{m}(\tau-s)}\sqrt{g}dW_i(s)d\tau \ , \tag{3.16}$$

where the last term simplifies as follows; by change of order of integration we get for any component i:

$$qE_i\frac{1}{m}\int_0^t\int_0^\tau e^{-\frac{\gamma}{m}(\tau-s)}\sqrt{g}(s)dW_i(s)d\tau = \frac{q}{m}E_i\int_0^t -\frac{m}{\gamma}\left[e^{-\frac{\gamma}{m}(t-s)}-1\right]\sqrt{g}(s)dW_i(s)$$
$$= \frac{q}{\gamma}\int_0^t\left[1-e^{-\frac{\gamma}{m}(t-s)}\right]\sqrt{g}(s)dW_i(s) \ .$$

Now to calculate $v^2(t)$ for $\frac{1}{2}mv^2(t)$ we square 3.12 and have after simple but tedious algebra, as well as change of order of integration (and hiding $\sqrt{g}$ which should be in-front of each dW_i for all $i = 1,2,3$ since it is not really involved any where and can be put back at the end):

$$v^2(t) = \sum_{i=1}^{3} v_i^2(0)e^{-2\frac{\gamma}{m}t} + u_i^2\left(1-e^{-\frac{\gamma}{m}t}\right)^2 + \left(\frac{q}{\gamma}E_i\right)^2\left(1-e^{-\frac{\gamma}{m}t}\right)^2$$
$$+ \frac{1}{m^2}\int_0^t e^{-\frac{\gamma}{m}(t-\tau)}dW_i(\tau)\int_0^t e^{-\frac{\gamma}{m}(t-s)}dW_i(s)$$
$$+ 2v_i(0)u_i\left(e^{-\frac{\gamma}{m}t}-e^{-2\frac{\gamma}{m}t}\right) + 2v_i(0)\frac{q}{\gamma}E_i\left(e^{-\frac{\gamma}{m}t}-e^{-2\frac{\gamma}{m}t}\right)$$
$$+ 2v_i(0)\frac{1}{m}\int_0^t e^{-\frac{\gamma}{m}(2t-\tau)}dW_i(\tau) + 2u_i\frac{q}{\gamma}E_i\left(1-e^{-\frac{\gamma}{m}t}\right)^2$$
$$+ 2u_i\frac{1}{m}\int_0^t\left(e^{-\frac{\gamma}{m}(t-\tau)}-e^{-\frac{\gamma}{m}(2t-\tau)}\right)dW_i(\tau)$$
$$+ 2\frac{q}{\gamma}E_i\frac{1}{m}\int_0^t\left(e^{-\frac{\gamma}{m}(t-\tau)}-e^{-\frac{\gamma}{m}(2t-\tau)}\right)dW_i(\tau) \ .$$

To calculate the expectations we can use the following [59, 60], [61, p. 99] :

1. $\langle\int_0^t f(\tau,W)dW(\tau)\rangle = 0$ for a non-anticipating function [2] $f(\tau,W)$ (or an adapted process) (see appendix B)
2. $\langle\int_0^t f(\tau,W)dW(\tau)\int_0^t h(s,W)dW(s)\rangle = \int_0^t\langle f(\tau,W)h(\tau,W)\rangle d\tau$ for non - anticipating functions $f(\tau,W)$ and $h(\tau,W)$ (or adapted processes) (see appendix B)

[2] Note non-anticipating essentially means the function has no functional or otherwise dependence on future values of the Wiener process.

Thus the expected value of $\Delta\mathcal{W}_E(t)$ is

$$\begin{aligned}\langle\Delta\mathcal{W}_E(t)\rangle = &\sum_{i=1}^{3} qE_i\left(\frac{m}{\gamma}\right)v_i(0)\left[1-e^{-\frac{\gamma}{m}t}\right]\\ &+qE_i\left(u_i+\left(\frac{1}{\gamma}\right)qE_i\right)\left[t+\left(\frac{m}{\gamma}\right)e^{-\frac{\gamma}{m}t}-\left(\frac{m}{\gamma}\right)\right]\ ,\end{aligned} \tag{3.17}$$

which to first order in small time t will give

$$\langle\Delta\mathcal{W}_E(t)\rangle = \sum_i qE_iv_i(0)t \text{ where } t \text{ is small}\ , \tag{3.18}$$

while the expectation of $\Delta\mathcal{W}(t)$ follows from 3.17 and the results on the previous page as (when we reintroduce g)

$$\begin{aligned}\langle\Delta\mathcal{W}(t)\rangle = &\sum_i \frac{1}{2}mv_i^2(0)\left(e^{-2\frac{\gamma}{m}t}-1\right)+\frac{1}{2}m\left(u_i^2+\left(\frac{q}{\gamma}E_i\right)^2\right)\left(1-e^{-\frac{\gamma}{m}t}\right)^2\\ &+mu_i\frac{q}{\gamma}E_i\left(1-e^{-\frac{\gamma}{m}t}\right)^2+mv_i(0)\left(u_i+\frac{q}{\gamma}E_i\right)\left(e^{-\frac{\gamma}{m}t}-e^{-2\frac{\gamma}{m}t}\right)\\ &+\frac{1}{2m}\int_0^t e^{-2\frac{\gamma}{m}(t-\tau)}g(\tau)d\tau\ ,\end{aligned} \tag{3.19}$$

which to first order in small t gives

$$\langle\Delta\mathcal{W}(t)\rangle = \sum_{i=1}^{3}\left[v_i(0)\left(\left(u_i-v_i(0)\right)\gamma+qE_i\right)-\frac{g(0)}{2m}\right]t\ , \tag{3.20}$$

where the potential importance of the neutrals is apparent by the presence of the correlation strength $g(0)$ containing term and friction factor γ containing term. In fact we have that:

$$\langle\Delta\mathcal{W}(t)-\Delta\mathcal{W}_E(t)\rangle = \langle\Delta\mathcal{W}(t)\rangle-\langle\Delta\mathcal{W}_E(t)\rangle = \sum_i\left[\gamma v_i(0)\left(u_i-v_i(0)\right)-\frac{g(0)}{2m}\right]t \tag{3.21}$$

If we now treat the initial velocity of the ion $\vec{v}(0)$ as a random variable with expected velocity $\langle\vec{v}(0)\rangle = \vec{u}+\delta\vec{v}$ with $\delta\vec{v}$ being very small when measured in-terms of units of $\vec{u}$ (and with $\vec{u} > \delta\vec{v}$ component-wise). And assuming the ion is initially in thermal equilibrium with the neutrals (i.e. $\langle v_i^2(0)\rangle = (k_BT)/m$ by the equipartition theorem) we have for these small times essentially that

$$\langle\langle\Delta\mathcal{W}(t)-\Delta\mathcal{W}_E(t)\rangle\rangle \approx \sum_i\left[\gamma u_i\left(u_i+\delta v_i\right)-\left(\gamma\frac{k_BT}{m}+\frac{g(0)}{2m}\right)\right]t\ . \tag{3.22}$$

So that even for ions that may start of with a slightly different initial velocity on average from that of the neutrals the friction and binary collision effects cannot

be considered negligible. In fact if we are interested in getting a sense for the potential physical scale associated with the effects of the correlation strength and friction factor we can follow the assumption in Yu.Li.Klimontovich book "Statistical theory of open systems" and use an Einstein fluctuation dissipation relation $g(0) = 2\gamma\left(k_B T\right)/m$, as well as follow Frank. H. Shu's book's "The physics of Astrophysics: Gas Dynamics " reasoning and set $\gamma = \nu\mu$ where ν is the collision frequency between the ion and neutrals and μ the effective mass in an ion-neutral collision. We would then get that

$$\langle\langle \Delta\mathcal{W}(t) - \Delta\mathcal{W}_E(t)\rangle\rangle \approx \sum_{i=1}^{3} \nu\mu\left[u_i\left(u_i + \delta v_i\right) - 2\frac{k_B T}{m}\right]t \ , \tag{3.23}$$

which clearly shows the importance of knowing how neutrals interact with the ions (or at least how frequently in this case) and the relevance of that information.

3.4 Deriving an Equation for the Distribution of the Ion System and its Momentum Conservation

We can in-fact derive more information from the simple stochastic differential equation 3.8 , by using it to generate the equation of motion for a one particle probability distribution $p(\vec{x},\vec{v},t)$ for a collection of ions with their dynamics specified by the very same stochastic differential equation. This probability distribution would give the probability of finding an ion with position and velocity located in the region $(\vec{x},\vec{x}+d\vec{x})$ with velocity in the range $(\vec{v},\vec{v}+d\vec{v})$ by

$$p(\vec{x},\vec{v},t)d^3x d^3v \ . \tag{3.24}$$

In addition we can use this to derive a distribution and an equation for its evolution, for the collection of ions by multiplying it with the number of ions in the system. We could then use that to determine the conservation of momentum equation for the ions, which can be used to determine the origin of thrust for system with respect to the influence of the ions. To begin with the stochastic differential equations that will be of importance are:

$$d\vec{v}(t) = \left(\frac{q}{m}\vec{E} - \frac{\gamma}{m}(\vec{v}-\vec{u})\right)dt + \frac{1}{m}\sqrt{g}d\vec{W}(t) \tag{3.25}$$

$$d\vec{x} = \vec{v}dt \tag{3.26}$$

which are of Ito form (due to the simple form of 3.8 the conversion is simple, see appendix B).

Determining the transition probability

In order to determine one particle probability distribution we must determine a transition probability (to be defined) which would then allow us to find the

one particle probability distribution. Hence following [62], consider an arbitrary function (at least twice differentiable) of $\vec{x}$ and $\vec{v}$ denoted $f(\vec{x},\vec{v})$. In order to eventually relate it to the probability density function we will be interested in its expected rate of change $\langle \frac{df}{dt} \rangle$ at any instant in time for which we can conclude that [62]

$$\frac{\langle df \rangle}{dt} = \langle \frac{df}{dt} \rangle = \frac{d}{dt}\langle f \rangle \ , \tag{3.27}$$

where the expectation is with respect to the position and velocity random variables at an instant in time (an arbitrary time). For the right hand side of equation 3.27 we may assume that $(\vec{x},\vec{v})$ has a conditional probability distribution $p'(\vec{x},\vec{v},t|\vec{x}_0,\vec{v}_0,t_0)$, with initial time t_0 and possible starting values $(\vec{x}_0,\vec{v}_0)$, such that the following holds [62]

$$\frac{d}{dt}\langle f \rangle = \iiint \iiint d^3x d^3v f(\vec{x},\vec{v}) \frac{\partial}{\partial t} p'(\vec{x},\vec{v},t|\vec{x}_0,\vec{v}_0,t_0) \ , \tag{3.28}$$

where integration is over the velocity and position variables. $p'(\vec{x},\vec{v},t|\vec{x}_0,\vec{v}_0,t_0)$ may be interpreted as a transition probability distribution between the states when a particle start of at time t_0 with initial values $(\vec{x}_0,\vec{v}_0)$ but ends up at $(\vec{x},\vec{v})$ at time t.

For the left hand side of equation 3.27 we get using Ito's change of variable formula, the stochastic differential equations 3.26 and the multiplicative and expectation properties for the differentials of the Wiener process that (see appendix B)

$$df = \left\{ (\nabla_{\vec{x}} f)\cdot\vec{v} + (\nabla_{\vec{v}} f)\cdot\left[\frac{q}{m}\vec{E} - \frac{\gamma}{m}(\vec{v}-\vec{u})\right] + \frac{1}{2m^2} g\left(\nabla^2_{\vec{v}} f\right)\right\} dt + (\nabla_{\vec{v}} f)\cdot\frac{1}{m}\sqrt{g}\, d\vec{W}(t) \ . \tag{3.29}$$

So that the expectation of this differential is then given by

$$\langle df \rangle = \langle (\nabla_{\vec{x}} f)\cdot\vec{v} + (\nabla_{\vec{v}} f)\cdot\left[\frac{q}{m}\vec{E} - \frac{\gamma}{m}(\vec{v}-\vec{u})\right] + \frac{1}{2m^2} g\left(\nabla^2_{\vec{v}} f\right)\rangle dt \ , \tag{3.30}$$

where $d\vec{W}(t)$ has expectation equal to 0 (and $\nabla_{\vec{v}} f$ is measurable w.r.t. to the filtration of the Wiener process $\vec{W}(t)$). Consequently we then have that:

$$\frac{\langle df \rangle}{dt} = \iiint \iiint d^3x d^3v \left\{ (\nabla_{\vec{x}} f)\cdot\vec{v} + (\nabla_{\vec{v}} f)\cdot\left[\frac{q}{m}\vec{E} - \frac{\gamma}{m}(\vec{v}-\vec{u})\right] + \frac{1}{2m^2} g\left(\nabla^2_{\vec{v}} f\right)\rangle\right\} p'(\vec{x},\vec{v},t|\vec{x}_0,\vec{v}_0,t_0) \ . \tag{3.31}$$

Using the following integration by parts formulas (see for instance [63]) and Fubini's integration theorem (i.e. change of order of integration), to put the equation in more interpretable form:

1.

$$\iiint_V d^3x\,(\nabla_{\vec{x}} f)\cdot\vec{v}p' = \iint_{\partial V} f\,(\vec{v}p'\cdot\hat{n}_x)\,dA_x - \iiint_V f\nabla_{\vec{x}}\cdot(\vec{v}p')\,d^3x \quad (3.32)$$

where $\hat{n}_x$ is the unit normal of the boundary ∂V of the integration domain V, and the area measure on the boundary is denoted dA_x.

2.

$$\iiint_\Omega d^3v\,(\nabla_{\vec{v}} f)\cdot\left(\vec{F}(\vec{v})p'\right) = \iint_{\partial\Omega} f\left(\vec{F}(\vec{v})p'\cdot\hat{n}_v\right)dA_v - \iiint_\Omega f\nabla_{\vec{v}}\cdot\left(\vec{F}(\vec{v})p'\right)d^3v \quad (3.33)$$

where $\hat{n}_v$ is the unit normal of the boundary $\partial\Omega$ of the integration domain Ω, and the area measure on the boundary is denoted dA_v while $\vec{F}(\vec{v})$ is a vector field dependent on the vector field $\vec{v}$.

3.

$$\iiint_\Omega d^3v hp'\left(\nabla^2_{\vec{v}} f\right) = \iint_{\partial\Omega} hp'\left([\nabla_{\vec{v}} f]\cdot\hat{n}_v\right)dA_v - \iiint_\Omega\left[\nabla_{\vec{v}}\left(hp'\right)\right]\cdot\left[\nabla_{\vec{v}} f\right]d^3v \quad (3.34)$$

where h is an arbitrary scalar function not dependent on $\vec{v}$. However, if we note that

$$\iiint_\Omega d^3v f\nabla^2_{\vec{v}}\left(hp'\right) = \iint_{\partial\Omega} f\left(\left[\nabla_{\vec{v}}\left(hp'\right)\right]\cdot\hat{n}_v\right)dA_v - \iiint_\Omega\left[\nabla_{\vec{v}}\left(hp'\right)\right]\cdot\left[\nabla_{\vec{v}} f\right]d^3v \quad (3.35)$$

it will follow on combining these two expressions to eliminate the common term that:

$$\iiint_\Omega d^3v hp'\left(\nabla^2_{\vec{v}} f\right) = \iint_{\partial\Omega} hp'\left([\nabla_{\vec{v}} f]\cdot\hat{n}_v\right)dA_v + \iiint_\Omega d^3v f\nabla^2_{\vec{v}}\left(hp'\right) - \iint_{\partial\Omega} f\left(\left[\nabla_{\vec{v}}\left(hp'\right)\right]\cdot\hat{n}_v\right)dA_v \quad (3.36)$$

where $\nabla^2_{\vec{v}} \equiv \nabla_{\vec{v}}\cdot\nabla_{\vec{v}}$.

If we now attach the following boundary conditions:

1. $\vec{v}\cdot\hat{n}_x = 0$ on some parts of ∂V while $p' = 0$ on ∂V where $\vec{v}\cdot\hat{n}_x \neq 0$. As in the case when ions stick to a surface or are never allowed to be near an electrode of the same polarity.

2. $p' = 0$ on $\partial\Omega$ with $\nabla_{\vec{v}} p' = 0$ on $\partial\Omega$. Where for clarity we pick Ω to be all possible velocities.

all the boundary terms get set to zero and then the left hand side of expression 3.27 reduces to

$$\frac{\langle df \rangle}{dt} = -\iiint \iiint d^3x d^3v \left\{ (\nabla_{\vec{x}} p') \cdot \vec{v} + (\nabla_{\vec{v}} p') \cdot \left[\frac{q}{m} \vec{E} - \frac{\gamma}{m} (\vec{v} - \vec{u}) \right] - \frac{1}{2m^2} g \left(\nabla_{\vec{v}}^2 p' \right) - 3 \frac{\gamma}{m} p' \right\} f(\vec{x}, \vec{v}, t) \ . \quad (3.37)$$

Thus we have the Fokker-Planck like equation, since $f(\vec{x}, \vec{v}, t)$ was chosen to be arbitrary:

$$\frac{\partial}{\partial t} p' + \vec{v} \cdot \nabla_{\vec{x}} p' = -\left[\frac{q}{m} \vec{E} - \frac{\gamma}{m} (\vec{v} - \vec{u}) \right] \cdot \nabla_{\vec{v}} p' + \frac{1}{2m^2} g \left(\nabla_{\vec{v}}^2 p' \right) + 3 \frac{\gamma}{m} p' \ . \quad (3.38)$$

Deriving the one particle probability distribution

Recall that p' is a conditional probability distribution dependent on the possible initial starting location and velocities $(\vec{x}_0, \vec{v}_0)$. Consequently if the probability distribution for the initial starting location and velocities is given by say

$$p_0(\vec{x}_0, \vec{v}_0) \text{ at time } t_0 \quad (3.39)$$

and assuming it is compatible with the boundary conditions. It would follow that the one particle probability distribution $p(\vec{x}, \vec{v}, t)$ (see equation 3.24) is given by

$$p(\vec{x}, \vec{v}, t) = p'(\vec{x}, \vec{v}, t | \vec{x}_0, \vec{v}_0, t_0) p_0(\vec{x}_0, \vec{v}_0) \quad (3.40)$$

and as a consequence it follows that the equation of motion for it can be derived by multiplying both sides of equation 3.38 by p_0. And as a result we are left with

$$\frac{\partial}{\partial t} p + \vec{v} \cdot \nabla_{\vec{x}} p = -\left[\frac{q}{m} \vec{E} - \frac{\gamma}{m} (\vec{v} - \vec{u}) \right] \cdot \nabla_{\vec{v}} p + \frac{1}{2m^2} g \left(\nabla_{\vec{v}}^2 p \right) + 3 \frac{\gamma}{m} p \ . \quad (3.41)$$

Deriving the ion system's one particle distribution

Now assuming the particle number N of ions in the hypothetical system to be conserved (for simplicity) we could define the distribution by (see chapters 4 and 5)

$$F(\vec{x}, \vec{v}, t) = N p(\vec{x}, \vec{v}, t) \ . \quad (3.42)$$

And as a result its equation of motion would follow as

$$\frac{\partial}{\partial t} F + \vec{v} \cdot \nabla_{\vec{x}} F = -\left[\frac{q}{m} \vec{E} - \frac{\gamma}{m} (\vec{v} - \vec{u}) \right] \cdot \nabla_{\vec{v}} F + \frac{1}{2m^2} g \left(\nabla_{\vec{v}}^2 F \right) + 3 \frac{\gamma}{m} F \ . \quad (3.43)$$

One could then follow the steps outlined in appendix A to generate the conservation of momentum equation for the ions.

Conservation of momentum equation

In order to derive the conservation of momentum equation for the ions we multiply both sides of the equation 3.43 by $m\vec{v}$, integrate over velocity and use the definitions and identifications in appendix A to have the left hand side give

$$\frac{\partial}{\partial t}\left(\rho(\vec{x},t)\vec{v}_{ave}(\vec{x},t)\right) + \nabla\cdot\left(\overline{\overline{P}}(\vec{x},t)\right) \ . \tag{3.44}$$

Where $\overline{\overline{P}}$ is a "pressure tensor" [64, p. 158] defined by

$$\overline{\overline{P}}(\vec{x},t) = \iiint_{\Omega} d^3v m\overline{\overline{vv}}F = \rho\langle\overline{\overline{vv}}\rangle_{\vec{v}} \ . \tag{3.45}$$

While for the right hand side using the integration by parts formulas, see [63]:

1.

$$\begin{aligned} -\iiint_{\Omega} d^3v m v_i\left[\frac{q}{m}\vec{E} - \frac{\gamma}{m}\left(\vec{v}-\vec{u}\right)\right]\cdot\nabla_{\vec{v}}F = \\ \iiint_{\Omega}\nabla_{\vec{v}}\cdot\left\{m v_i\left[\frac{q}{m}\vec{E} - \frac{\gamma}{m}\left(\vec{v}-\vec{u}\right)\right]\right\}F \\ -\iint_{\partial\Omega} dA_v\left\{m v_i\left[\frac{q}{m}\vec{E} - \frac{\gamma}{m}\left(\vec{v}-\vec{u}\right)\right]\cdot\hat{n}_v\right\}F \end{aligned} \tag{3.46}$$

where v_i is the i'th component of $\vec{v}$ and Ω is the integration domain with boundary $\partial\Omega$. And for which we have

$$\begin{aligned} \nabla_{\vec{v}}\cdot\left\{m v_i\left[\frac{q}{m}\vec{E} - \frac{\gamma}{m}\left(\vec{v}-\vec{u}\right)\right]\right\} = m\left[\frac{q}{m}E_i - \frac{\gamma}{m}\left(v_i-u_i\right)\right] \\ - m v_i 3\frac{\gamma}{m} \end{aligned} \tag{3.47}$$

2.

$$\begin{aligned} \iiint_{\Omega} d^3v m v_i\frac{1}{2m^2}g\left(\nabla^2_{\vec{v}}F\right) = -\iiint_{\Omega} d^3v\nabla_{\vec{v}} m v_i\frac{1}{2m^2}g\cdot\nabla_{\vec{v}}F \\ +\iint_{\partial\Omega} dA_v m v_i\frac{1}{2m^2}g\nabla_{\vec{v}}F\cdot\hat{n}_v \end{aligned} \tag{3.48}$$

However since,

$$\begin{aligned} \iiint_{\Omega} d^3v F\nabla^2_{\vec{v}}\left(m v_i\frac{1}{2m^2}g\right) = -\iiint_{\Omega} d^3v\nabla_{\vec{v}} m v_i\frac{1}{2m^2}g\cdot\nabla_{\vec{v}}F \\ +\iint_{\partial\Omega} dA_v F\nabla_{\vec{v}}\left(m v_i\frac{1}{2m^2}g\right)\cdot\hat{n}_v \end{aligned} \tag{3.49}$$

we have on eliminating the common term that

$$\begin{aligned} \iiint_{\Omega} d^3v m v_i\frac{1}{2m^2}g\left(\nabla^2_{\vec{v}}F\right) = \iint_{\partial\Omega} dA_v m v_i\frac{1}{2m^2}g\nabla_{\vec{v}}F\cdot\hat{n}_v \\ +\iiint_{\Omega} d^3v F\nabla^2_{\vec{v}}\left(m v_i\frac{1}{2m^2}g\right) - \iint_{\partial\Omega} dA_v F\nabla_{\vec{v}}\left(m v_i\frac{1}{2m^2}g\right)\cdot\hat{n}_v \end{aligned} \tag{3.50}$$

note that:

$$\nabla_{\vec{v}}^2 \left(m v_i \frac{1}{2m^2} g \right) = 0 \tag{3.51}$$

3.

$$\iiint_\Omega d^3 v m \vec{v} 3 \frac{\gamma}{m} F = 3 \frac{\gamma}{m} \rho \vec{v}_{ave} \tag{3.52}$$

and then impose the boundary conditions on F that follow from those on p we would then get

$$\left[\frac{q}{m} \vec{E} - \frac{\gamma}{m} \left(\vec{v}_{ave} - \vec{u} \right) \right] \rho \tag{3.53}$$

since $F = 0$ and $\nabla_{\vec{v}} F = \vec{0}$ on $\partial\Omega$. So that the conservation of momentum equation for the ions then becomes

$$\frac{\partial}{\partial t} \left(\rho \vec{v}_{ave} \right) + \nabla \cdot \overline{\overline{P}} = \left[\frac{q}{m} \vec{E} - \frac{\gamma}{m} \left(\vec{v}_{ave} - \vec{u} \right) \right] \rho \ , \tag{3.54}$$

where it shouldn't be too difficult to see that its boundary conditions would follow from those imposed on F. However, if we follow appendix A and note that for the random velocity $\vec{v}$ we can decompose it as

$$\vec{v} = \vec{c} + \vec{v}_{ave} \ , \tag{3.55}$$

where $\vec{c}$ is a "new" random variable. The distribution will change as

$$F(\vec{x}, \vec{v}, t) \longrightarrow F(\vec{x}, \vec{c} + \vec{v}_{ave}, t) \equiv F'(\vec{x}, \vec{c}, t) \ , \tag{3.56}$$

since the Jacobian is unity and we would have

$$\vec{0} = \iiint d^3 c \vec{c} F' \ . \tag{3.57}$$

Consequently we can re-write the pressure tensor term $\overline{\overline{P}}$ by defining the relative quantity $\overline{\overline{p}}$

$$\overline{\overline{p}} = \iiint_\Omega d^3 c F' m \overline{\overline{cc}} = \rho \langle \overline{\overline{cc}} \rangle_{\vec{c}} \ . \tag{3.58}$$

Hence we would have

$$\overline{\overline{P}} = \iiint_\Omega d^3 v m \overline{\overline{vv}} F = \iiint_\Omega d^3 c F' m \overline{\overline{(c + v_{ave})(c + v_{ave})}} = \overline{\overline{p}} + \rho \overline{\overline{v_{ave} v_{ave}}} \ , \tag{3.59}$$

and thus the conservation equation would follow as

$$\frac{\partial}{\partial t} \left(\rho \vec{v}_{ave} \right) + \nabla \cdot \left(\rho \overline{\overline{v_{ave} v_{ave}}} \right) = -\nabla \cdot \overline{\overline{p}} + \left[\frac{q}{m} \vec{E} - \frac{\gamma}{m} \left(\vec{v}_{ave} - \vec{u} \right) \right] \rho \ . \tag{3.60}$$

From which one can then identify $-\overline{\overline{p}}$ as a stress term and $\left[\frac{q}{m} \vec{E} - \frac{\gamma}{m} \left(\vec{v}_{ave} - \vec{u} \right) \right] \rho$ as a momentum source. In this way we see how we can go from single particle dynamics to the equation of motion of a distribution of particles to the conservation of momentum for those particles and consequently use that to calculate the component of thrust delivered by these particles. Thereby tying this chapter in with chapter 2 and motivating the use of a statistical description for a many "particle" system.

Chapter 4

Classical Non-Equilibrium Statistical Mechanics

In this section the Liouville equation describing the evolution of a system's phase-space density of states distribution will be introduced and how one can eventually generate conservation equations from this fundamental equation using the one-particle distribution derived from it. We begin with the classical case as the quantum approach also introduced in this thesis has many results and techniques similar to the classical case and hence will allow one to appreciate the quantum approach with less effort.

4.1 The Liouville Equation

In this subsection the Liouville equation will be introduced. The Louville equation is of fundamental importance to classical non-equilibrium statistical mechanics. The Louville equation describes the evolution of the density of phase space states of a system of "particles" and contains all information necessary for the derivation of conservation equations and predictions of expected behaviour for the system.

Consider a system of N particles (with no internal degrees of freedom) whose behaviour and interactions can be described using classical Hamiltonian mechanics. Due to the fact that the particles obey classical mechanics we know that the system can be modelled by trajectories in $6N$ - dimensional phase space (often denoted by Γ_N) where the trajectories are determined by Hamilton's equations and the co-ordinate, position and conjugate momenta, of each of the particles represent the (microscopic) state of the system at the time of evolution. See Figure 4.1

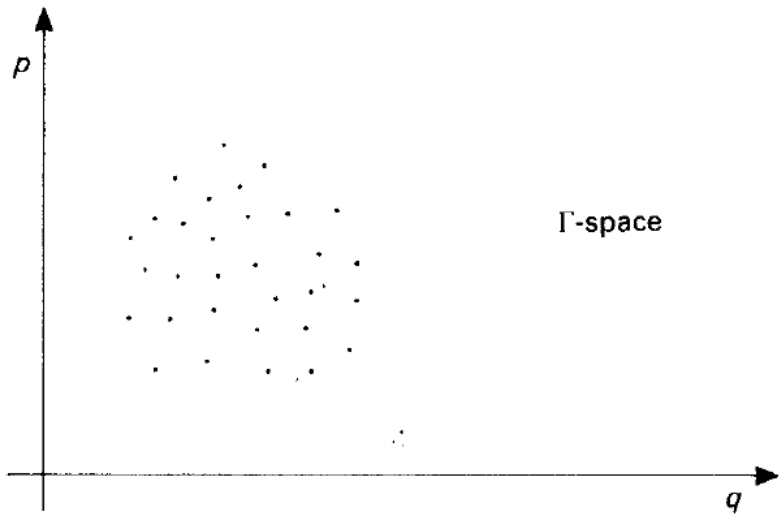


Figure 4.1: Snap shot of an Ensemble of a N particle system in a representation of Γ_N space for a two dimensional system [2, p. 20]

However, even though all the unique trajectories are calculable in theory for a finite number of particles with initial conditions given [2, p. 20] the actual computer aided computation would be expected to be extremely infeasible due to the large computation resources required. In addition, even when a physical system is closed as above (no change in particle number) two problems are almost always present:

1. The initial conditions are often not known with certainty due to external interference (and noise) i.e. the external environment will interact with the system and may introduce randomness.

2. There is always inherent initial conditions measurement uncertainty (even when external environment interference on the measurements can be compensated for).

The best one can potentially do with regards to the description of the initial information is to determine a phase-space density of states distribution of the initial states, or equivalently its total particle normalized counterpart a phase-space probability distribution of the possible initial states.

Consequently, if one was able to generate an equation of motion for the phase-space density of states distribution, one could retrieve an acceptable amount of information for description of expected behaviour of the system and those similar to it, based on what was initially possible.

As it turns out such an equation exists and can be derived using a number of approaches (for a closed system) [2, 65] . In particular if we denote the N - particle phase-space density distribution of states at time t by $F_N(\vec{z}_1, ..., \vec{z}_N; t)$ where $\vec{z} = (\vec{q}, \vec{p})$ (the position and conjugate momentum pair of a particle) for a system of identical particles [1]. Let $\{f, g\}_{sys}$ denote the Poisson bracket for the system i.e.

$$\{f, g\}_{sys} := \sum_{i=1}^{3N} \left(\frac{\partial f}{\partial q_i} \frac{\partial g}{\partial p_i} - \frac{\partial g}{\partial q_i} \frac{\partial f}{\partial p_i} \right) \tag{4.1}$$

where i runs over all the canonical co-ordinates. And let $\mathcal{H}$ denote the Hamiltonian of the system, it then follows that the required equation is given by:

$$\frac{\partial}{\partial t} F_N + \{F_N, \mathcal{H}\}_{sys} = 0 \ , \tag{4.2}$$

which is a partial differential equation for which the initial conditions are determined from the initial distribution $F_N(\vec{z}_1, ..., \vec{z}_N; 0)$. Additional boundary conditions could be imposed to help select a particular solution. In-terms of the interpretation of the distribution one can for a system with constant number of particles divide the distribution by the number of particles to generate a probability distribution from which one can calculate expectations in a normal probabilistic manner.

4.2 Reduced Distributions and BBGKY Hierarchy

In this section reduced distributions of the N-particle distribution and the hierarchy of equations coupling them together the BBGKY hierarchy will be introduced. BBGKY is named after N.N. Bogoliubov, M. Born, H.S. Green and G. Kirkwood and J. Yvon [64].

4.2.1 Reduced Distributions

It has probably become obvious to the reader that solving the Liouville equation could also be impractical and difficult due to the number of variables involved for a large system. In addition although the Liouville equation's solution would be, practically speaking, more flexible and useful it would still contain a tremendous amount of information unnecessary for an acceptable understanding of the system's momentum and energy conservation.

In particular, a one-particle phase-space probability distribution for each particle species of a system consisting of many would posses a sufficient amount of information about the system to determine expected number density and expected energy density [64, p. 158],[66, 67] . For example if the number of

[1] In order to keep notation clean and not unnecessarily introduce complication with interpretation

particles is given by N we could determine the expected number density $n(\vec{q};t)$ by [64, p. 158]

$$n(\vec{q};t) = N \int d^3p f_1(\vec{q},\vec{p};t) \ , \tag{4.3}$$

where $f_1(\vec{q},\vec{p};t)$ is the one-particle phase-space probability distribution.

The one-particle distribution f_1 is in fact a "reduced distribution" of the N - particle distribution $\frac{1}{N}F_N$ and can be derived from it. Any reduced s - particle distribution f_s $(s = 1, ..., N)$ can be derived from the N - particle system using the definition for reduced s - particle distributions [64, p. 37],[68, p. 192] and [69]:

$$f_s = \frac{N!}{(N-s)!} \int dx_{s+1}...dx_N F_N(x_1, ..., x_s, x_{s+1}, ..., x_N) \tag{4.4}$$

where dx_i is short for $d^3q_i d^3p_i$ and $x_i \equiv (\vec{q}_i, \vec{p}_i)$. Due to the particle exchange symmetry (among particles of the same species if it were generalized to system with different types of particles) of the N -particle distribution this definition is equivalent to any other definition where other phase-variables may have been integrated over, see for instance [68, p. 192], [70, 69].

4.2.2 The BBGKY Hierarchy

Having the definition of the reduced distributions the next consideration is the question of whether equations for these are derivable from the N - particle distribution. Fortunately, equations are derivable for each of the reduced distributions by successively integrating the Liouville equation over more and more phase-variable pairs, $(\vec{q},\vec{p})$, and using the definition of the reduced distributions to create a system of equations. However, every equation for a particular s - particle distribution is coupled (dependent) on a $s+1$ - particle distribution (or distributions for many particle species type systems) [68, p. 192],[70, 69]. The system of these N equations is referred to as the BBGKY Hierarchy and it couples the one-particle distribution through its equation to the two-particle distribution. Successive s-particle distributions are intern coupled to other $s+1$ distributions until the $N-1$-particle distribution is finally coupled to the N-particle distribution. In particular for a Hamiltonian $\mathcal{H}$ of the form:

$$\mathcal{H} = \sum_{i=1}^{N} \frac{p_i^2}{2m} + \frac{1}{2}\sum_{i=1}^{N}\sum_{j\neq i}^{N} \Phi_{ij} \tag{4.5}$$

where the potential $\Phi_{ij} = \Phi(|\vec{q}_i - \vec{q}_j|)$, the BBGKY Hierarchy can be written down as [64, p. 82] :

$$\left(\frac{\partial}{\partial t} - \hat{L}_s\right) f_s + (N-s)\sum_{i=1}^{i=s} \frac{\partial}{\partial \vec{p}_i} \cdot \int d\vec{q}_{s+1} d\vec{p}_{s+1} \left[-\frac{\partial}{\partial \vec{q}_i}\Phi_{is+1}\right] f_{s+1} = 0 \tag{4.6}$$

where [64, p. 80]

$$\hat{L}_s = \sum_{j=1}^{s} \frac{\vec{p}_j}{m} \cdot \frac{\partial}{\partial \vec{q}_j} + \sum_{\substack{i=1 \\ i<j}}^{s} \sum_{j=1}^{s} \frac{\partial}{\partial \vec{q}_i} \phi_{ij} \cdot \left\{ \frac{\partial}{\partial \vec{p}_i} - \frac{\partial}{\partial \vec{p}_j} \right\} . \tag{4.7}$$

The BBGKY Hierarchy's usefulness, apart from producing equations for the reduced distributions, lies in the observation that often the higher order distributions are to very good approximation functionally dependent on lower order distributions, thereby closing the system of equations by using the lower order distributions. This would allow for consistent derivation of results associated with the lower order distributions and description of the system with only lower order distributions. Such as in the case of the Boltzmann Equation [71] which is a functional equation only dependent on the one-particle distributions of the system, and naturally derived for short range potentials in the regime of "weak coupling" (which will be defined in chapter 8) [72, 68].

Another functionality of members of the Hierarchy is that although in this case they were argued to be derived for a closed conserved system one can in practice often augment them to account for openness or reactions [73, 74, 75, 76, 77, 78]. As for example when the Boltzmann Equation has ionization or reaction terms included [76, 79] , resulting from the intuitive interpretation of these equations and the need to introduce openness or reactions.

Finally, the one-particle reduced distribution's equation can be used to produce conservation equations, which are of primary interest to this dissertation aim of setting up a strategy to model thrust.

4.3 Derivation of Conservation Equations

In this section the reader will be introduced to the connection between the equation for the one-particle distribution generated from the Liouville equation or through some other means and the conservation equations which can be derived from them. The conservation equations are of fundamental importance to this dissertation as they would be used to model and predict the thrust of the system as well as model transport phenomena necessary for determination of efficiency.

Fortunately, all the necessary conservation equations can be derived from the one-particle distribution's equation. In fact when we consider a some-what generic one-particle distribution equation given by: (for a particular species i of a system of different species collectively denoted by $\mathcal{S}$)

$$\frac{\partial}{\partial t} F_1^i(\vec{q}, \vec{p}, t) + \frac{\vec{p}}{m} \cdot \frac{\partial}{\partial \vec{q}} F_1^i(\vec{q}, \vec{p}, t) + \vec{F} \cdot \frac{\partial}{\partial \vec{p}} F_1^i(\vec{q}, \vec{p}, t) = \left(\frac{\partial F_1^i}{\partial t} \right)_{coll} [\mathcal{S}] \tag{4.8}$$

where in-terms of reduced distributions $F_1^i = Nf_1^i$. When using $\vec{p} = m\vec{v}$ it can also be given by

$$\frac{\partial}{\partial t}F_1^i(\vec{q},\vec{v},t) + \vec{v}\cdot\frac{\partial}{\partial \vec{q}}F_1^i(\vec{q},\vec{v},t) + \frac{\vec{F}}{m}\cdot\frac{\partial}{\partial \vec{v}}F_1^i(\vec{q},\vec{v},t) = \left(\frac{\partial F_1^i}{\partial t}\right)_{coll}[\mathcal{S}] \tag{4.9}$$

where $\vec{F}$ is an externally applied force and the collision term:

$$\left(\frac{\partial F_1^i}{\partial t}\right)_{coll}[\mathcal{S}]\ , \tag{4.10}$$

will represent a model for the change in the distribution not associated with the effects of externally applied forces but due to the mutual interactions between particles. The collision term plays a central role in determining how momentum, energy and particle conservation can be accommodated in a system composed of many particles and species of particles. The collision term can be some approximation of what would be derived in manufacturing the BBGKY hierarchy, thereby taking into account classical coupling between the different species, but can also be of modified form to include re-actions or ionization [73, 74, 75, 76, 77, 78, 79]. Ultimately the collision term is responsible for predicting the form of the stress tensor, heat flux and particle sources for a system and is therefore fundamental to a model describing a thruster's sources of thrust. The one particle distribution also has the advantage of being able to describe turbulence and shock wave phenomena which must be introduced in an effective and discontinuous way , respectively, for conservation equations [80, 81, 82, 83, 84]. Consequently, although macroscopic conservation equations are used to model and explain the sources of thrust for a thruster the use of the one particle distribution is fundamental to the production of an accurate model.

We can begin to derive the conservation equations by first associating some of the moments of the one-particle distribution with the appropriate transport quantities namely [64, p. 158],[66, 67]:

1. particle number density for species i:

$$n^i(\vec{q},t) = \int d^3v F_1^i(\vec{q},\vec{v},t) \tag{4.11}$$

2. momentum density for species i:

$$m^i n^i(\vec{q},t)\vec{u}^i(\vec{q},t) = \int d^3v \vec{v} F_1^i(\vec{q},\vec{v},t) \tag{4.12}$$

3. kinetic energy density for species i:

$$\epsilon_K^i(\vec{q},t) = \int d^3v \left(\frac{1}{2}m^i v^2\right) F_1^i(\vec{q},\vec{v},t) = n^i(\vec{q},t)\langle\frac{1}{2}m^i v^2\rangle \tag{4.13}$$

where with the fluid velocity (average velocity):

$$\vec{u}^i(\vec{q},t) = \frac{\int d^3v \vec{v} F_1^i(\vec{q},\vec{v},t)}{\int d^3v F_1^i(\vec{q},\vec{v},t)} = \langle \vec{v}^i \rangle \tag{4.14}$$

we can define the specular velocity $\vec{c}$ with $\vec{v} = \vec{u} + \vec{c}$ allowing us to define the "Kinetic Temperature" T^i relative to $\vec{u}$ by:

$$\frac{3k_B T^i}{m^i} = \langle (\vec{v} - \langle \vec{v} \rangle)^2 \rangle \tag{4.15}$$

which when a system consists of particles (no internal degrees of freedom) can agree with the thermodynamic temperature (see [64, p. 161]), for which a conservation equation can be derived as well with a simple change of variables. With these definitions in place it is possible to derive conservation equations. The actual derivation of conservation equations from the one particle distribution are outlined in the appendix A, however conservation equations are presented here in generic form for a species $i \in \mathcal{S}$:

Particle Number density Conservation Equation

$$\frac{\partial}{\partial t} n^i + \frac{\partial}{\partial \vec{q}} \cdot \left(n^i \vec{u}^i \right) = \mathcal{J}_n^i[\mathcal{S}] \tag{4.16}$$

where $\mathcal{J}_n^i[\mathcal{S}]$ is some source term. These equations would be important for estimating net current flows while the source terms would give information on the constitutive equations/sources of the current flows, for example temperature gradients leading to current drifts.

Momentum density Conservation Equation

$$\frac{\partial}{\partial t} \left(\rho^i \vec{u}^i \right) + \frac{\partial}{\partial \vec{q}} \cdot \left(\rho^i \overline{\overline{u^i u^i}} \right) = \vec{\mathcal{J}}_{n\vec{u}}^i[\mathcal{S}] \text{ where } \rho^i(\vec{q},t) = m^i n^i(\vec{q},t) \tag{4.17}$$

where $\vec{\mathcal{J}}_{n\vec{u}}^i[\mathcal{S}]$ is some source term. This particular equation would be essential for deriving the thrust expressions from chapter two. The form of a collision term model and its dependence on the different distributions describing the system would ultimately determine the form of the stress applied by a plasma on the thruster in chapter two, thereby allowing one to estimate the thrust.

Energy density Conservation Equation

$$\frac{\partial}{\partial t} E_K^i + \frac{\partial}{\partial \vec{q}} \cdot \left(\vec{u}^i E_K^i \right) = \mathcal{J}_{E_K}[\mathcal{S}] \tag{4.18}$$

where $\mathcal{J}_{E_K}[\mathcal{S}]$ is some source term. These equations would be important for determining energy efficiency or energy consumption by the system while the source term would give constitutive equations/sources of energy flows.

One can also produce conservation equations for the entropy of the system however it was not included in the current study. It should be noted that many more conservation equations can be derived for other transport/conserved quantities or moments of the one-particle distribution other than those listed here, see for instance [85].

Boundary conditions for the conservation equations can be derived from the boundary conditions on the one-particle distribution [86, 85], but details surrounding this is outside the scope of this dissertation. However the reader is referred to [87] for details surrounding the construction of some what generic boundary models and equations.

Chapter 5

Quantum Non-Equilibrium Statistical Mechanics

In this chapter the Wigner-Weyl (or "phase-space") form of quantum mechanics will be introduced with its implementation in Non-equilibrium Statistical Mechanics outlined.

Introducing this representation of quantum mechanics may seem odd, but due to the content of the chapter 8 it transpired that there is a possible non-negligible quantum coupling in the CORION system near the needle exit which would require the introduction of quantum mechanics. The Wigner-Weyl (or "phase-space") form of quantum mechanics is particularly useful as it allows methods from the previous chapters to be employed while ensuring a physically correct method of description. In fact the reason for introducing the reader to this representation of quantum mechanics lies in its similarity to the classical non-equilibrium statistical mechanics of the previous chapter. The similarity allows for the generation of conservation equations in a way similar to that of the classical technique, thus allowing for consistent interpretation of the thrust modelling process from both a quantum and classical level.

This form of quantum mechanics is also particularly well suited to the study of the classical limit and de-coherence according to the reference [88].

The structure of this chapter is as follows. Firstly, the Von Neumann's density operator will be introduced and its equation of motion given which will be the quantum equivalent to the Liouville equation .

Secondly, we will introduce a transform, termed the "Wigner Transform" in this dissertation, of an operator and the use of the Groenewold's $\star$ - star product to help express the Wigner function of a product of operators.

Thirdly, we will introduce the Wigner distribution function for the Wigner Transform of the Von Neumann's density matrix. And then present some of this real function's properties and how it is used as a quasi-probability distribution function to calculate system expectations and properties. The reduced Wigner distributions will also be introduced.

Fourthly, the equation of motion for the Wigner distribution will be given from which the Liouville equation may be retrieved in the classical limit $\hbar \to 0$.

Finally, the BBGKY hierarchy like system of equations will be put forward and how conservation equations could be derived from these.

One reference was found to be extremely practical as it side stepped the second quantization approach normally adopted to describe exchange effects (effects of boson or fermion system symmetry requirements) and should be considered by the interested reader, namely "*Wigner Method in Quantum Statistical Mechanics*" see [89].

5.1 Von Neumann Density Operator

In this section the Von Neumann density operator (also called the density operator) will be defined and its equation of motion given. The Von-Neumann density operator and its equation of motion is fundamental to quantum non-equilibrium statistical mechanics and essential to the derivation of the Wigner distribution.

Consider an arbitrary quantum mechanical system with Hamiltonian $\mathcal{H}(t)$. Although the pure state [1] , in Dirac notation, $|\phi_i(t)\rangle$ (i an index for pure state) of the system corresponding to the particular Hamiltonian $\mathcal{H}(t)$ and its evolution can in principle be found from Schrödinger's equation, it is in practice not always possible to assert in what pure state (namely one of the possible $|\phi(t)_i\rangle$) a real system may be due to a lack of knowledge or experimental uncertainty. Instead what is usually known are the possible pure states $|\phi_i(t)\rangle$ (where i indexes the possible states) and the probability ω_i of their occurrence within the physical set-up.

Consequently, in-order to calculate the expectation value of any of the system's operators A we would have to take double expectation namely [90],[68, p. 27] :

$$\langle A\rangle = \sum_i \omega_i \langle\phi_i|A|\phi_i\rangle \ , \tag{5.1}$$

[1] A pure state is any member of the Hilbert space for the system described by the Hamiltonian $\mathcal{H}(t)$ and therefore includes eigenstates and their superposition. In other words a system is in a pure state if we know exactly what state it is in.

which with respect to an orthonormal basis $\{|u_n\rangle\}$ on which all the pure states are defined have

$$\begin{aligned}\langle A\rangle &= \sum_i \sum_n \sum_m \omega_i \langle \phi_i|u_n\rangle\langle u_n|A|u_m\rangle\langle u_m|\phi_i\rangle \\ &= \sum_i \sum_n \sum_m \langle u_m|\phi_i\rangle\omega_i\langle\phi_i|u_n\rangle A_{nm} \\ &= \sum_n \sum_m \langle u_m|\left[\sum_i |\phi_i\rangle\omega_i\langle\phi_i|\right]|u_n\rangle A_{nm} \\ &\equiv \sum_n \sum_m \rho_{mn}A_{nm} = Tr\left(\hat{\rho}A\right)\end{aligned} \tag{5.2}$$

where $\hat{\rho} \equiv \sum_i |\phi_i\rangle\omega_i\langle\phi_i|$ is the Von Neumann density operator and Tr stand for trace relative to an arbitrary orthonormal basis. With this it becomes apparent that if we know the density operator at any time we can calculate the expectation of any operator A using:

$$\langle A\rangle = Tr\left(\hat{\rho}A\right) \tag{5.3}$$

The problem is that we need to know $\hat{\rho}$ at each time while in practice all that may be available are the initial conditions $\omega_i(0)$ and $|\phi_i(0)\rangle$ due to external conditions and experimental uncertainty. Fortunately an equation for the Von Neumann density operator $\hat{\rho}$ exists regardless of whether the Hamiltonian $\mathcal{H}$ of the system is time-dependent given by application of the Heisenberg equation of motion for operators [72, p. 49],[68, p. 40] :

$$i\hbar\frac{\partial}{\partial t}\hat{\rho} = [\mathcal{H}, \hat{\rho}] \tag{5.4}$$

where $[\mathcal{H}, \hat{\rho}] = \mathcal{H}\hat{\rho} - \hat{\rho}\mathcal{H}$ is the commutator, thus allowing the density operator to be specified at all instants in time using the initial conditions. As can be seen, knowing the Von Neumann density operator and its equation of motion will allow calculation of any expected quantity pertinent to the understanding of the system.

5.2 Wigner Transform and $\star$ - product

In this section, the Wigner transform and $\star$-product will be introduced. Both are essential to the definition of the Wigner distribution function and derivation of its equation of motion. Two versions of the transform will be introduced, the unsymmetrized and symmetrized version necessary for describing spin-less systems (to which Boltzmann statistics may be applied) as well as systems with spin, without having to employ second quantization approaches. Ultimately the Wigner transform will be used to change representation of the equation of motion of the Von Neumann density from operator space to a function space to look and be interpreted like the Liouville equation where we will be able to use it as in the previous chapter.

5.2.1 Un-symmetrized Wigner Transform

The un-symmetrized Wigner Transform or Wigner Equivalent (as in [89]), of a quantum mechanical operator $A(R,P)$ as a function of position R and momentum P operators in a one-dimensional system with phase-space quantization and without additional degrees of freedom for the particles in the system (like spin for example) is denoted by $A_w(r,p)$ and given by [89] :

$$A_w(r,p) \coloneqq \int dz e^{(ipz)/\hbar} \langle r - \frac{z}{2} | A(R,P) | r + \frac{z}{2} \rangle \tag{5.5}$$

where $\{|z\rangle\}$ is the un-symmetrized position (or configuration space) basis for the system and $A_w(r,p)$ represents the Wigner function/equivalent of the operator $A(R,P)$, where R and P as operators have been replaced with their c-number equivalents r and p. If the system is 6n-dimensional in phase space and the particles are still without additional internal degrees of freedom and only phase space quantization is required, the operator A will have indexed arguments like $A(R_i,P_j)$ for example to indicate on what particles it operates and thus the generalization follows as [64, p. 352],[89] :

$$A_w(r_i,p_i) \coloneqq \int dz_1 ... dz_n exp\left((i \sum_{j=1}^{n} p_j z_j)/\hbar \right) \times \\ \langle r_1 - \frac{z_1}{2}, ..., r_n - \frac{z_n}{2} | A(R_i,P_i) | r_1 + \frac{z_1}{2}, ..., r_n + \frac{z_n}{2} \rangle \tag{5.6}$$

where $\{|z_1, ..., z_n\rangle\}$ is the un-symmetrized position basis for the system and each z_i, r_i and p_i is a three vector position and momentum with R_i and P_j being the equivalent operators to the vectors r_i and p_i.

5.2.2 $\star$ - star operator for un-symmetrized spaces

Often, one is interested in the Wigner equivalent of a product of operators AB where A and B are composed of momentum and position operators. Groenewold discovered an operator termed the $\star$ - star operator [91] that would allow one to combine the Wigner equivalents of A and B in a convenient way (for quantized phase space) and take into account the possible non-commutativity of the operators A and B. To summarize, we would have for an n-particle system that the Wigner equivalent of the product AB is given by [89, 92]

$$(AB)_w = A_w \star B_w \ , \tag{5.7}$$

where

$$\star \coloneqq exp\left(\hbar \Lambda / (2i)\right) \ , \tag{5.8}$$

is an operator acting on the respective Wigner functions on its series expansion and by using

$$\Lambda \equiv \sum_{j=1}^{n} \frac{\overleftarrow{\partial}}{\partial p_j} \frac{\overrightarrow{\partial}}{\partial r_j} - \frac{\overleftarrow{\partial}}{\partial r_j} \frac{\overrightarrow{\partial}}{\partial p_j} \tag{5.9}$$

where the arrows indicate on which function, either A_w or B_w, the partial differential operator should act.

5.2.3 Symmetrized Wigner Transform

Although the Wigner equivalent so far has been defined using un-symmetrized basis, when dealing with physical systems consisting of fermions and bosons the bases must posses the appropriate particle exchange symmetry to reflect the physical symmetry of the system [89]. This must be the case even when there is no spin coupling i.e. explicit introduction of this degree of freedom and its quantization.

Consequently one is lead to the notion of a symmetric (or symmetrized) Wigner equivalent of an operator, in this case when only phase-space is quantized [89, 93]. To demonstrate this consider a system of n fermions or bosons i.e. $6n$ dimensional in phase space when ignoring spin [2]. A position basis for such a system could generically be written as [89]

$$|\vec{r}\rangle^{\theta} := |\vec{r}_1, ..., \vec{r}_n\rangle^{\theta} := (N!)^{\frac{1}{2}} \sum_{P} \theta^{|P|} |\vec{r}_{P(1)}, ..., \vec{r}_{P(n)}\rangle \ , \tag{5.10}$$

where $N! \equiv n!$ and where the summation is over the different permutations P of $\vec{r}_1, ..., \vec{r}_n$, $|P|$ is the parity of P, and θ is 1 for bosons and -1 for fermions.

As a result the symmetrical Wigner equivalent of an operator A of the system would be given by [89]

$$A_w^{\theta} := \int d\vec{z} \left(e^{i\vec{p}\cdot\vec{z}/\hbar}\right)^{\theta} \langle \vec{r} - \frac{\vec{z}}{2} | A | \vec{r} + \frac{\vec{z}}{2} \rangle^{\theta} / N! \ , \tag{5.11}$$

where concise notation has been used namely; $d\vec{z} = d\vec{z}_1 ... d\vec{z}_n = d^3 z_1 ... d^3 z_n$ and $\vec{p} \cdot \vec{z} = \sum_{i=1}^{n} \vec{p}_i \cdot \vec{z}_i$, the $\cdot$ between $\vec{p}_i$ and $\vec{z}_i$ being the usual Euclidean inner (dot) product between the two vectors.

5.2.4 Extending the star product to symmetrized Wigner Functions

The $\star$ - product can again be applied to symmetrized Wigner Functions provided that:

1. When applying the $\star$ - product it is necessary to ensure that the operators which are to be individually transformed and correspond to observable quantities first be written down according to the Weyl-ordering (also called completely symmetric ordering) [94]. This ensures that the Weyl-Correspondence [88, p. 6],[72, p. 16] for Hermitian operators holds (for $6n$ dimensional phase-space)

$$\hat{A} = \left(\frac{1}{2\pi\hbar}\right)^{6n} \int d\vec{q} d\vec{p} d\vec{\varepsilon} d\vec{\eta} \exp\left(i\vec{\varepsilon} \cdot (\hat{q} - \vec{q}) + i\vec{\eta}\,(\hat{p} - \vec{p})\right) A(\vec{\varepsilon}, \vec{\eta}) \ , \tag{5.12}$$

[2] Not mixed as this generalization could be built from appropriate basis for such a mixture but would make notation messy and detract from the overall idea.

where A is the phase-space equivalent of the operator $\hat{A}$, $\hat{q}$ and $\hat{p}$ are the operator equivalents of the vectors $\vec{q}$ and $\vec{p}$ and concise notation (section 5.2.3) has once again been used. According to this convention it would then follow that the Wigner-Map [88, p. 22],[92, 89]

$$A(\vec{r},\vec{p}) = \int d\vec{z} \exp\left(i\vec{p}\cdot\vec{z}/\hbar\right) \langle \vec{r} - \frac{\vec{z}}{2}|\hat{A}|\vec{r} + \frac{\vec{z}}{2}\rangle \ , \tag{5.13}$$

holds (the argument could also be reversed as in [89])

2. The form of the $\star$ - product and choice of ordering convention are intimately connected with one another. This connection is as a result of the practice of mapping the quantum operator algebra (with its ordering convention imposed) for its quantum Hilbert space to some corresponding phase-space function space (referred to as Deformation Quantization [88, p. 6],[95, 96]), in a way so that when this mapping is inverted (call this inverted map $\mathcal{W}$ here) the commutator brackets (and or anti-commutator brackets) of the operators are preserved with respect to the product. That is, we would want

$$\frac{1}{i\hbar}\left[\mathcal{W}(f),\mathcal{W}(g)\right] = \mathcal{W}\left(\left[\!\left[f,g\right]\!\right]\right) \ , \tag{5.14}$$

where $\left[\!\left[f,g\right]\!\right] = \frac{1}{i\hbar}\left(f\star g - g\star f\right)$ is the Moyal-Bracket [88, p. 26] for the commutator and $\mathcal{W}(f)$ and $\mathcal{W}(g)$ are the quantum operator versions of the functions f and g. As one can see the goal is to ensure that the algebraic structure be preserved by the transformation through the specifics of the $\star$ - product.

As a result of these two statements, we see that when we impose the symmetry requirement for the basis it actually serves as an additional requirement on the Hilbert space of states, but does not have anything to do with the algebra on the space or the algebra's ordering convention for Hermitian operators. Consequently the $\star$ - product would not be affected directly in the same way that it would not affect the operator algebra directly. In conclusion then, we have for the product of two ordered operators A and B with A at least an observable (or "symmetrical" according to [89]) that [using [89]]

$$(AB)^{\theta}_{w} = A^{\theta}_{w} \star B^{\theta}_{w} \ , \tag{5.15}$$

where A must be "symmetric" otherwise the expression does not easily have this particular form and we would have to digress and cover a substantial section of [89].

Note that if spin were to actually be included as an actual degree of freedom then the $\star$-product would have to be altered.

5.3 Wigner Distribution Function of the Von Neumann Density

Now the Wigner Distribution f_w for a system of N particles with Von Neumann density $\hat{\rho}$ is simply $(2\pi\hbar)^{-3N}$ times the Wigner Equivalent of the Von-Neumann density operator. That is,

$$f_w(\vec{r},\vec{p}) = \left(\frac{1}{2\pi\hbar}\right)^{3N} \int d\vec{z} \exp\left(i\vec{p}\cdot\vec{z}/\hbar\right) \langle \vec{r} - \frac{\vec{z}}{2}|\hat{\rho}|\vec{r} + \frac{\vec{z}}{2}\rangle \ , \tag{5.16}$$

where it should be noted that the symmetrized Wigner distribution (denoted f_w^θ) would follow in the same way, but as a symmetrized Wigner equivalent instead. Note that when the system is known to be characterized by occupation of different "quantum mechanical levels" and transition among them is expected, use of second-quantization is advisable and sometimes more convenient for these systems [97, 98]. This is due to its ability to more naturally accommodate these many particle (or level) phenomena.

5.3.1 Properties and use of The Wigner Distribution

In this section two properties of the Wigner distribution function f_w necessary for justification of its use as a quasi-probability distribution are introduced and then the means by which one would use the Wigner distribution will be presented.

To use the Wigner Distribution function as a quasi-probability distribution it is necessary to note that it has the following two properties [88, p. 3] :

1. It is real
2. It is bounded (and may be negative in parts of phase space that undermine the uncertainty principle)

The first property transforms the problem of considering quantum mechanics in an operator space to considering it in more conventional functional space, while the second property will force us not to interpret the Wigner distribution as a true probability distribution. Of practical importance is to know how to use the Distribution to calculate expectations of an operator A. When not considering symmetrized basis, it follows directly from the Weyl-Correspondence as:

$$\langle A\rangle = Tr\left(\hat{\rho}A\right) = \int d\vec{r}d\vec{p}A_w(\vec{r},\vec{p})f_w(\vec{r},\vec{p}) \tag{5.17}$$

however when using symmetrized basis it was shown in [89] that the expectation of an operator A is conveniently given by:

$$\langle A\rangle = \int d\vec{r}d\vec{p}A_w(\vec{r},\vec{p})f_w^\theta(\vec{r},\vec{p}) \tag{5.18}$$

or (due to the symmetry under permutations of density operator) also:

$$\langle A\rangle = \int d\vec{r}d\vec{p}A_w^\theta(\vec{r},\vec{p})f_w(\vec{r},\vec{p}) \tag{5.19}$$

where it should be recalled that the superscript $^{\theta}$ refers to the symmetrized Wigner equivalent.

5.3.2 Reduced Distributions

The reduced distributions are introduced in the same way as the classical counterpart and posses the same normalization [72, p. 92],[89]. They follow from the (symmetrized) Wigner Distribution as (with $i \equiv (\vec{r}_i, \vec{p}_i)$):

$$f_s^{\theta}(1, ..., s; t) = \frac{N!}{(N-s)!} \int d\vec{r}_{s+1} ... d\vec{r}_n d\vec{p}_{s+1} ... d\vec{p}_n f_w^{\theta} \tag{5.20}$$

where we essentially integrate over all the phase variables except for the first s that we choose to keep, and have used a "generic normalization" [72, p. 92],[89].

The reduced distributions can be used to calculate expectations of operators or observables, in the same way as for the Wigner Distribution, that do not depend on more "phase-variables" than those labelled in the reduced distribution and as a consequence are used for the same reasons as the reduced distributions from the previous chapter. In fact as will be shown later in Appendix A that the one-particle distribution f_1 can be used to estimate the particle number density, momentum density and energy density as well as other "moments" not listed.

5.4 Equation of Motion

In this section the equation of motion for the Wigner distribution function corresponding to the Wigner transform of the Von Neumann density of states will be presented, which will be of fundamental importance as it will be used and interpreted as the quantum version of the Liouville equation. In addition it can be used to generate a quantum version of the BBGKY hierarchy which could then as in the classical case be used to manufacture an equation for a one particle distribution used to derive conservation equations similar to the classical case covered in the previous chapter.

Consider a Hamiltonian $\mathcal{H}$ for a system where spin is not important (i.e. where Boltzmann statistics apply). For such a system we do not need to consider symmetry effects and particle exchange and will, on applying the unsymmetrized Wigner transform and multiplying by $(2\pi\hbar)^{-3N}$ on both sides of the equation of motion for the Von-Neumann density operator equation 5.4 and using the $\star$ - product, that:

$$i\hbar \frac{\partial}{\partial t} f_w = \mathcal{H}_w \star f_w - f_w \star \mathcal{H}_w \ . \tag{5.21}$$

For which expanding the $\star$ - product in the limit $\hbar \to 0$ the Liouville equation is retrieved [99] .

The case when the system posses symmetry under particle exchange or permutations as for Bosonic or Fermionic systems is not much different. One can easily show from the tools developed in [89] and the discussion on the $\star$ - product previously, that for the Hamiltonian and density of states as symmetric operators, on taking the Symmetrized Wigner Transform on both sides of the equation of motion for the Von-Neumann density operator equation 5.4 and multiplying with $(2\pi\hbar)^{-3N}$ throughout that:

$$i\hbar\frac{\partial}{\partial t}f_w^\theta = \mathcal{H}_w^\theta \star f_w^\theta - f_w^\theta \star \mathcal{H}_w^\theta \ , \tag{5.22}$$

where the appropriate symmetrized Wigner Distribution is used as well as the Symmetrized Wigner equivalent of the Hamiltonian. These two equations act as the quantum versions of the Liouville equation, with f_w^θ and f_w acting as quantum versions for the N-particle distribution f_N from the previous chapter. Additionally they can be manipulated and used in essentially the same way as in the previous chapter. Note that depending on the Hamiltonian form, equation 5.22 may reduce to something simpler, specifically when it is "symmetric" as defined in [89] we have:

$$i\hbar\frac{\partial}{\partial t}f_w^\theta = \mathcal{H}_w \star f_w^\theta - f_w^\theta \star \mathcal{H}_w \tag{5.23}$$

where we may then interpret f_w^θ as the appropriate "symmetric" solution to the equation. Alternatively one may keep the (spin-less) un-symmetrized Wigner distribution and instead symmetrize the Hamiltonian as in [93, 100].

5.5 The Quantum BBGKY Hierarchy

The Quantum BBGKY Hierarchy within the Wigner Distribution framework is developed in much the same way as that of the classical case (see previous chapter). That is, by successively integrating the equation of motion of the Wigner distribution (either equation 5.22 or 5.21) over more and more pairs of phase variables , (q, p), until one pair is left while using the symmetry of the Wigner distribution and definition of the reduced distributions to generate the corresponding results. For a general discussion of the Wigner distribution formalism refer to the books [64, 101]. Here, however the BBGKY equations for a N-particle spin-less system (for simplicity) to which Boltzmann statistics may be applied with a specific Hamiltonian $\mathcal{H}$ will simply be given. The Hamiltonian $\mathcal{H}$ is given by

$$\mathcal{H} = \sum_{i=1}^{n}\frac{1}{2}\frac{\hat{p}_i^2}{m} + \hat{V}(\hat{q}_1, ..., \hat{q}_i, ..., \hat{q}_n) \ , \tag{5.24}$$

where each momentum or position operator in equation 5.24 refers to a three-position or three-momentum operator. $\hat{V}(\hat{q}_i)$ is a real interaction potential and could be given by something like

$$\hat{V}(\hat{q}_i) = \sum_{i=1}^{n}\sum_{j>i}^{n}\Phi_{i,j}(||\hat{q}_i - \hat{q}_j||) + \sum_{i}^{n}\Phi_{ext}(\hat{q}_i) \ , \tag{5.25}$$

where $\Phi_{i,j}(\|\hat{q}_i - \hat{q}_j\|)$ only depends on the "distance" between $\hat{q}_i$ and $\hat{q}_j$, while $\Phi_{ext}(\hat{q}_i)$ is some kind of externally applied potential acting on particle i at "position" $\hat{q}_i$. In position basis equation 5.24 reads as

$$\mathcal{H} = -\frac{\hbar^2}{2m}\sum_{i=1}^{n}\frac{\partial^2}{\partial\vec{q}_i^2} + V(\vec{q}_1, ..., \vec{q}_i, ..., \vec{q}_n) \ , \tag{5.26}$$

so that the Quantum BBGKY can be given by [102] as

$$\frac{\partial}{\partial t}f_s + \sum_{i=1}^{s}\frac{\vec{p}_i}{m}\cdot\frac{\partial}{\partial\vec{q}_i}f_s - \sum_{i=1}^{s}\sum_{j>i}^{s}\frac{2}{\hbar}\left\{\sin\left[\frac{\hbar}{2}\left(\frac{\partial}{\partial\vec{p}_i}\cdot\frac{\partial}{\partial\vec{q}_i} + \frac{\partial}{\partial\vec{p}_j}\cdot\frac{\partial}{\partial\vec{q}_j}\right)\right]V\right\}f_s = \sum_{i=1}^{s}(N-s)\int d\vec{q}_{s+1}d\vec{p}_{s+1}\frac{2}{\hbar}\left\{\sin\left[\frac{\hbar}{2}\left(\frac{\partial}{\partial\vec{p}_i}\cdot\frac{\partial}{\partial\vec{q}_i} + \frac{\partial}{\partial\vec{p}_{s+1}}\cdot\frac{\partial}{\partial\vec{q}_{s+1}}\right)\right]V\right\}f_{s+1} \ , \tag{5.27}$$

where s runs from one to N and the $\frac{\partial}{\partial\vec{q}_i}$, $\frac{\partial}{\partial\vec{q}_j}$, $\frac{\partial}{\partial\vec{q}_{s+1}}$, $\frac{\partial}{\partial\vec{p}_i}$, $\frac{\partial}{\partial\vec{p}_j}$ and $\frac{\partial}{\partial\vec{p}_{s+1}}$ operators in the square brackets operate only on the function V. In addition note that sin function is used as short hand notation for its corresponding series expansion with respect to its argument, which in this case happens to be the operators in the square bracket. Note that the boundary conditions used to determine this equation force the distributions to vanish at infinity and the surface terms i.e. gradients as well [102]. For other boundary conditions, different forms of this equation would be derived.

5.6 Conservation Equations from the One Particle Distribution

In this final section we simply indicate the relationship between the one particle distribution and its use to generate conservation equations of quantities of interest to thrust models, and understanding of the overall behaviour.

Just as in the classical case, the novelty of the one-particle distribution's equation lies in its openness to augmentation and alteration to suite a physical situation's requirements, see for instance [103]. Consequently it is, as in the classical case convenient to consider a generic equation, for a system of N identical (spin-less) particles with mass m given by

$$\frac{\partial}{\partial t}f_1 + \frac{\vec{p}}{m}\cdot\frac{\partial}{\partial\vec{q}}f_1 - \frac{2}{\hbar}\left\{\sin\left[\frac{\hbar}{2}\left(\frac{\partial}{\partial\vec{p}}\cdot\frac{\partial}{\partial\vec{q}}\right)\right]V\right\}f_1 = \left(\frac{\partial f_1}{\partial t}\right)_{col} \ , \tag{5.28}$$

where the term in the square brackets acts on the V (as given by equation 5.26) and where $\left(\frac{\partial f_1}{\partial t}\right)_{col}$ represents the effects of collisions and other inter-particle interactions. From such an equation one continues by first introducing the definitions of the transported quantities [104]:

1. Particle number density $n(\vec{q}, t) \coloneqq N\int d^3p f_1$ since f_1 is normalized (see section on reduced distributions).

2. Momentum density $m \times n(\vec{q},t)\vec{u}(\vec{q},t) \coloneqq N \int d^3p\vec{p}f_1$ where $\vec{u}$ is defined as in the appendix A.

3. Once we define the centred distribution by $f_1'(\vec{q},\vec{p},t) \coloneqq f_1(\vec{q},\vec{p}+m\vec{u},t)$ the "Random Kinetic Energy Density" (which is twice the usual definition) follows as $E_k(\vec{q},t) \coloneqq N/m \int d^3p^2 f_1'$

where the energy density could again lead to the "kinetic temperature" [104] but this will not be argued for here.

To develop the conservation equations we proceed exactly as in the classical case for which calculations are in appendix A. The results are Conservation equations of the form:

1. Particle number density conservation:

$$\frac{\partial}{\partial t}n + \frac{\partial}{\partial \vec{q}} \cdot (n\vec{u}) = \mathcal{J}_n \tag{5.29}$$

   where $\mathcal{J}_n$ is a source term including the source. These equations would be important for estimating net current flows while the source terms would give information on the constitutive equations/sources of the current flows, for example temperature gradients and magnetic field gradients leading to specific current drifts.

2. momentum density conservation:

$$\frac{\partial}{\partial t}mn\vec{u} + \frac{\partial}{\partial \vec{q}} \cdot \left(mn\overline{\vec{u}\vec{u}}\right) = \mathcal{J}_{mn\vec{u}} \tag{5.30}$$

   where $\mathcal{J}_{mn\vec{u}}$ is a source term. This particular equation would be essential for deriving the thrust expressions from chapter two.

3. energy density conservation:

$$\frac{\partial}{\partial t}\left[E_k + mn|u|^2\right] + \frac{\partial}{\partial \vec{q}} \cdot \left(\left[E_k + mn|u|^2\right]\vec{u}\right) = \mathcal{J}_{K_k} \tag{5.31}$$

   where $\mathcal{J}_{K_k}$ is a source term. These equations would be important for determining energy efficiency or energy consumption by the system while the source term would give constitutive equations/sources of energy flows.

In general boundary conditions would normally be built into and appended to the one particle distribution's equation and then used to derive the boundary conditions for the transport quantities through use of their definitions, but will not be considered here since it would be outside the scope of this dissertation and is more appropriately addressed by the field of surface science.

5.7 Relevant Distributions and Time Irreversibility

This part of the dissertation will come across as anecdotal (and short) but is actually a very important note to the reader, for actual application of the equations of motion for the classical and quantum distributions to observed real systems. Although, it may not be apparent the equations of motion for the Liouville and Wigner distributions posses time reversal symmetry leading to the prediction of reversal in time of natural phenomena [68, 72]. On its own time reversal symmetry is not a problem except that for observed behaviour this symmetry does not often exist. Consequently, a substantial amount of work has been done on finding out what the origin of the broken time symmetry may be using the equations of motion for the distributions themselves. For instance see [105] for an in-depth discussion on how broken time symmetry may manifest itself "naturally" for certain systems.

In regard to the time reversible equations of the N-particle distributions (introduced in this chapter and chapter 4) there is an aim of developing time irreversible equations of motion for alternative distributions (called Relevant Distributions in [68]). These distributions and their equations are derived from the equations for the N-particle distributions for the description of "real" systems. Several schemes (or programmes) have been developed to achieve this goal, for instance in [72] a programme is produced which can be used to manufacture an equation of motion with broken time symmetry for the appropriate classical relevant distribution (the one associated with observed irreversible phenomena). Alternatively, however the technique presented in [106] was by personal opinion found to be potentially very practical as it tried to maximize the use of experimentally observable information in deriving its equation for an appropriate relevant distribution. It in addition outlined Zwanzig's as well as Robertson's projection methods and the method of ergodic conditions which are all approaches to producing irreversible models [68]. Regardless of these two references the reader should consult the literature on the subject of irreversible models, as some of it may be ideally suited to the problem at hand.

Chapter 6

Mass-flow measurement and calibration

In this chapter a technique is adapted to estimate small mass flows of several hundreds of $\mu g/s$ using orifice plate behaviour will be introduced. The technique was developed for estimation of mass flows through the proposed thrust system which were expected to be of order $\sim \mu g/s$. However, the system developed required analysis and testing. Therefore, the chapter begins with an introduction to the basic operational characteristics and behaviour of orifice plate and venturi mass and volume flow rate measuring systems. It then follows with describing the theory and assumptions used for estimation of the mass flows. This is followed by an outline of the apparatus and experimental technique used. The chapter concludes with the presentation of results of the experiment and their analysis with error analysis and a section for justification of the theoretical model in appendix C.

6.1 Aim

The aim of the tests were to investigate the repeatability and behaviour of a novel low mass flow meter (and calibration system) using an orifice plate construction and differential pressure manometer. The advantages of the proposed calibration system are:

1. Very economical.
2. Versatile and merges with existing technologies e.g. combines with orifice plate and venturi mass flow meters.
3. Robust.
4. Simple.

In addition the tests were conducted to provide information required for estimation of system characterizing parameters introduced in chapter 8.

6.2 Background

6.2.1 Orifice-plate and Venturi Tube Fundamentals

This short section will introduce Orifice-plate, nozzle and venturi flow measurement techniques. Neither of these were used to measure the actual mass flow, however their behaviour was used to indirectly help substantiate the assumption (and physical approximation) of steady flow for the experiments and help "label" (or specify) certain mass flows. The following (including diagrams) section relies heavily on "*Introduction to Fluid Mechanics*" by Y. Nakayama and R. F. Boucher and published by Butterworth-Heinemann p. 187 - 189 [3].

Orifice-plate

The orifice plate with both flange and corner tappings (point across which pressure difference are measured) is shown in the Figure 6.1 below.

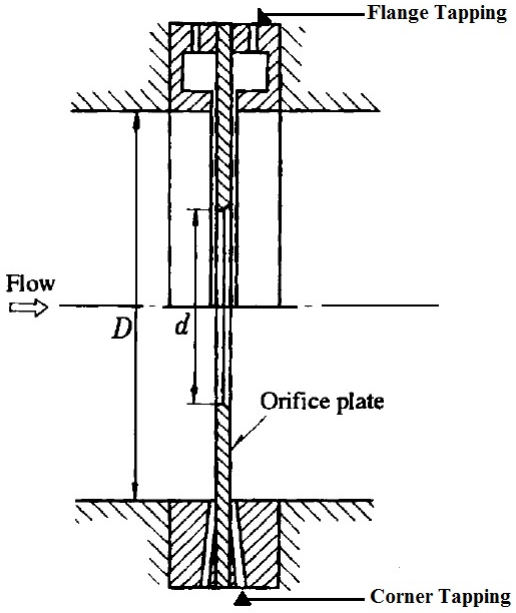


Figure 6.1: Orifice-plate set-up D is the diameter of the pipe through which gas flows and d is the diameter of the orifice through which gas will be forced [3].

The volume flow rate through an orifice plate is given by [3]:

$$Q = \alpha\varepsilon\frac{\pi d^2}{4}\sqrt{\frac{2\Delta p}{\rho_i}} \tag{6.1}$$

whereΔp is the pressure difference across the tappings and ρ_i is the density of the gas on the upstream side of the flow while α and ε are the flow co-efficient

and expansion factor of the gas being used. In addition the mass flow would be given by [3]:

$$\dot{m} = \alpha\varepsilon\frac{\pi d^2}{4}\sqrt{2\rho_i\Delta p} \tag{6.2}$$

which on Taylor expansion for small change in density and pressure difference relative to initial values ρ_i and Δp would yield:

$$\begin{aligned}\delta\dot{m} \approx \alpha\varepsilon\frac{\pi d^2}{4}\frac{1}{\sqrt{2\rho_i\Delta p}}\left[\Delta p(\pm\delta\rho_i) + \rho_i(\pm\delta\Delta p) + (\pm\delta\rho_i)(\pm\delta\Delta p)\right] \\ - \alpha\varepsilon\frac{\pi d^2}{4}\frac{1}{(2\rho_i\Delta p)^{\frac{3}{2}}}\rho_i\Delta p(\pm\delta\rho_i)(\pm\delta\Delta p) \\ = \frac{\dot{m}}{2}\left[\left(\frac{\pm\delta\rho_i}{\rho_i} + \frac{\pm\delta\Delta p}{\Delta p}\right)\right] .\end{aligned} \tag{6.3}$$

From which it can be seen that the mass flow would remain fairly insensitive (and nearly constant) to small changes in the pressure difference Δp and inlet density ρ_i. It could then be argued to within specified acceptable error that the mass flow through the orifice remained constant.

Nozzle

For the sake of completeness we will introduce the nozzle system equivalent of the orifice plate system. The nozzle system depicted below works in essentially the same way as the orifice plate, the only real difference is that the flow loss (loss in stagnation pressure) is less and the flow co-efficient is larger [3].

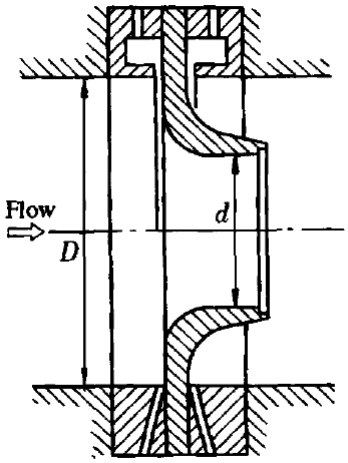


Figure 6.2: Nozzle set-up D is the diameter of the pipe through which gas flows and d is the minimum diameter of the nozzle through which gas will be forced [3].

Venturi

We conclude this section with introduction to the Venturi system which is another alternative to the Orifice Plate system. The Venturi systems depicted below work in essentially the same way as the orifice plate and thus have the same calculations, the only real difference is that the flow loss (loss in stagnation pressure) is less and the flow co-efficient is larger [3] as well.

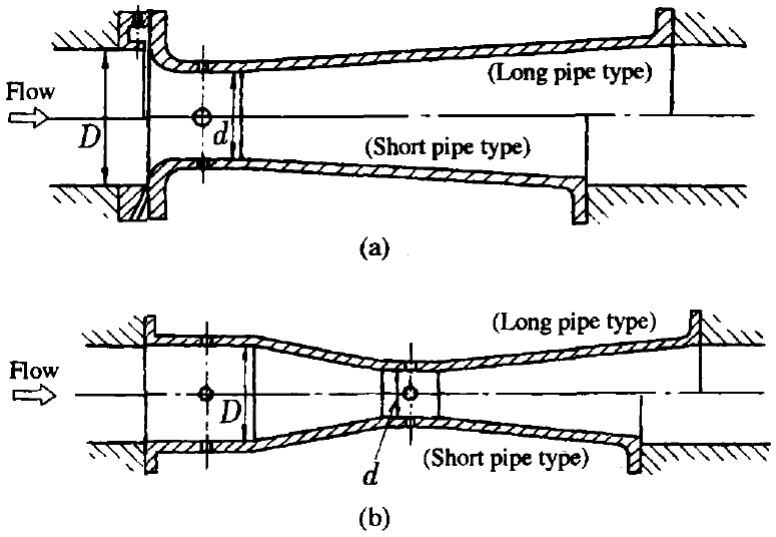


Figure 6.3: Nozzle set-up D is the diameter of the pipe through which gas flows and d is the minimum diameter of the nozzle through which gas will be forced [3].

6.3 Mass-flow Estimation Technique and Model

The technique developed to measure the mass-flow of the system hinges on four aspects and assumptions:

1. The orifice-plate (or venturi tube) behaviour, namely that if the temperature of the gas going into the orifice-plate is known along with its compression characteristic then the volume flow rate is entirely determined by the pressure difference across the orifice-plate [see previous section].

2. The assumption of nearly achievable hydrostatic equilibrium between the inlet chamber gas pressure and water column pressure and gravity effects [see diagram C.1 and section C.2].

3. The verification that the flow in a large fraction of the inlet chamber was iso-thermal.

4. The assumption that gas flow in the inlet chamber was slow enough for a large fraction of the inlet chamber to be near equilibrium and thus well approximated by some equilibrium equation of state.

From the orifice-plate background covered in the previous section we know that volume flow through the orifice is dependent on the pressure difference across the orifice-plate and the temperature of the gas on one side of the plate. Thus

if the temperature at the inlet side of the orifice-plate does not vary greatly, the pressure difference essentially determines the mass-flow through the orifice for slow changing pressure difference and can be used as a label to identify a particular mass-flow, however since there was no way to measure the temperature (to within verifiable accuracy) in the set-up given, the actual mass-flow must be computed alternatively.

This alternative approach's technical details are outlined and justified in appendix C. The basic idea is that we use the rate of change in volume of the inlet and the justified assumption of near hydrostatic equilibrium in the inlet reservoir, as well as essentially constant temperature throughout most of the chamber to estimate the mass-flow out of the inlet chamber. We then combine this with the orifice-plate set-up to label (essentially calibrate) for different pressure differences.

Derivation of Mass Flow Estimate

To make things clear the derivation of the mass flow model will be given. Consider diagram 6.4 defining the inlet chamber at "a point in time τ's state of operation" of the control volume (a non-stationary volume) $V_c(t)$.

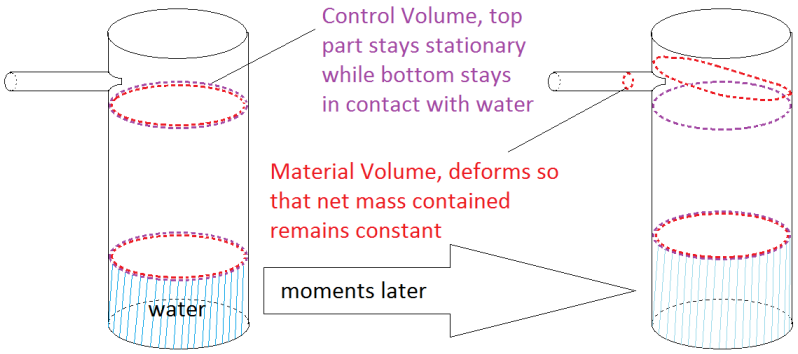


Figure 6.4: A diagram showing idea used to establish the mass flow estimate at some time τ and then an instant later.

From Reynold's transport theorem we have for the net mass in the control volume:

$$\frac{d}{dt}\mathcal{M}(t)|_{t=\tau} = \frac{d}{dt}\int_{V_c}\rho(t)dV = \int_{V_c}\frac{\partial}{\partial t}\rho(t)|_{t=\tau}dV + \int_{\partial V_c}\rho(\tau)\vec{v}_{b(c)}\cdot d\vec{A} \qquad (6.4)$$

where $\vec{v}_{b(c)}$ is the velocity of the control volume's boundary ∂V_c and ρ the density of the gas. However at the same instant in time one can consider a material volume $V_m(t)$ (a volume of gas) that only coincides with the control volume at that instant τ (see diagram 6.4), but for which its evolution in time

for the mass contained in $\mathcal{M}_m(t)$ it is determined by the conservation of mass [107]:

$$0 = \frac{d}{dt}\mathcal{M}_m(t) = \int_{V_m} \frac{\partial}{\partial t}\rho(t)dV + \int_{\partial V_m} \rho(t)\vec{v}_{b(m)} \cdot d\vec{A} \tag{6.5}$$

for all times, where $\vec{v}_{b(m)}$ is the velocity of the material volume's boundary ∂V_m. Since we chose the volumes to coincide at time τ we have that:

$$\frac{d}{dt}\mathcal{M}(t)|_{t=\tau} = \int_{\partial V_c(\tau)} \rho(\tau)\left[\vec{v}_{b(c)} - \vec{v}_{b(m)}\right] \cdot d\vec{A} \tag{6.6}$$

Assuming the density is well approximated by a single value in the two volumes and also the velocity of the gas, the result would reduce to:

$$\frac{d}{dt}\mathcal{M}(t)|_{t=\tau} = -\rho(\tau)v^{+}_{b(m)}(\tau)A := -\dot{m}(\tau) \tag{6.7}$$

where $v^{+}_{b(m)}$ is the velocity through the top of the material volume (other sides are zero either by requirement or by no-slip boundary condition and cancellation) and the mass-flow at time τ is defined by $\dot{m}(\tau) = \rho(\tau)v^{+}_{b(m)}(\tau)A$. Thus to find $\dot{m}$ at any time we must determine $-\mathcal{M}$ ($\mathcal{M}$ is the mass in the control volume) and it first derivative. To do this we have to estimate $\mathcal{M}$. We do this as follows; we assume that the density at time t in the control volume is well approximated by a single value $\rho(t)$ then we have that:

$$\mathcal{M}(t) = \rho(t)V_c(t) \tag{6.8}$$

So that it follows that:

$$\frac{d}{dt}\mathcal{M} = \left(\frac{d}{dt}\rho(t)\right)V_c(t) + \rho(t)\left(\frac{d}{dt}V_c(t)\right) \tag{6.9}$$

for which it then becomes apparent that we need an estimate for the density. This estimate is produced using the ideal gas law (essentially assuming density to be uniform in the control volume and close to equilibrium like behaviour) [108]:

$$\rho(t) = \mathfrak{m}\frac{P(t)}{RT} \tag{6.10}$$

with $\mathfrak{m}$ the molar mass and R the universal gas constant, $P(t)$ and T the pressure and temperature respectively. T was verified to remain constant ($\sim 20 - 21\ C^{\circ}$) through out most of the control volume with a temperature difference occurring only near the water surface for which the consequences were ignored. The system can also be argued to remain near hydrostatic equilibrium (see model justification section) with the pressure $P(t)$ given by:

$$P(t)A' = P_{atm}A' \tag{6.11}$$

where ρ_{water}, V_{water}, g , P_{atm}, A' and A are the water density, water column volume, gravitational acceleration, atmospheric pressure, control volume cross-sectional area and water reservoir cross-sectional area. We therefore have that:

$$\mathcal{M}(t) = \frac{\mathfrak{m}}{RT}\left[P_{atm}\right]V_c(t) \tag{6.12}$$

Thus we have for $\frac{d}{dt}\mathcal{M}$:

$$\frac{d}{dt}\mathcal{M}(t) = -\frac{\mathfrak{m}}{RT}\left[P_{atm}\right]\dot{V}_{water}(t) \tag{6.13}$$

since $V_c = V_{ref} - V_{water}$ and thus we have:

$$\dot{m}(t) = \frac{\mathfrak{m}}{RT}\left[P_{atm}\right]\dot{V}_{water}(t) \tag{6.14}$$

however what will be reported is the averaged time averaged mass-flow rate since the flows took long times (several tens of seconds) to establish small changes in pressure (relative to atmospheric pressure) and fill the inlet chamber's control volume at an approximate constant rate i.e.

$$<< \dot{m}(t) >>=< \frac{1}{\Delta t}\int \dot{m}(t)dt >= Ave\left(\frac{1}{\Delta t}\int \dot{m}(t)dt\right) \tag{6.15}$$

where:

$$\frac{1}{\Delta t}\int \dot{m}(t)dt = \frac{\mathfrak{m}}{RT}\left[P_{atm}\right]\frac{\Delta V_{water}}{\Delta t} \tag{6.16}$$

Note that $V_{ref} \neq V_{water}(0)$ which is not necessarily zero.

6.4 Apparatus

The set-up of the experiment from the outside of the vacuum chamber is given by Figures 6.8 and 6.9. It included the following components:

1. Extech Differential Pressure Manometer HD750 used to measure pressure differences, see Figure 6.5.
2. Orifice plate, see Figures 6.6 and 6.7.
3. Fine control valve and two simple open and shut valves, see Figure 6.8.
4. A measuring cylinder or a transparent container with volume measurement etchings.
5. A vacuum chamber with vacuum pumps.



90

Figure 6.5: Extech Differential Pressure Manometer HD750.

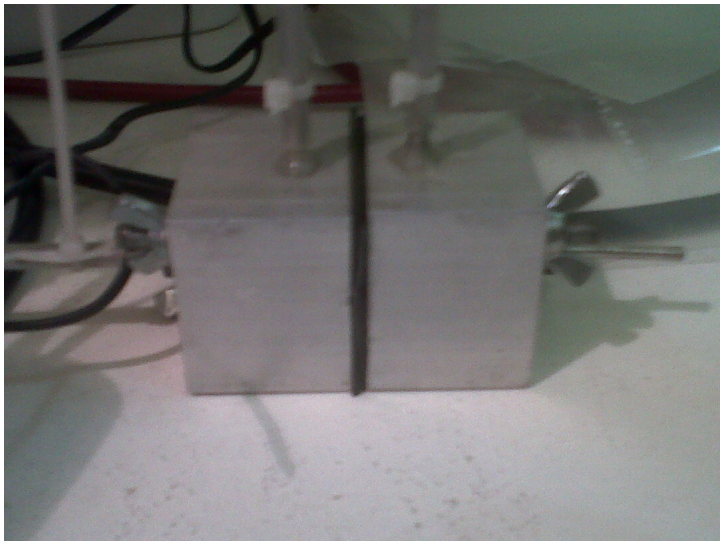


Figure 6.6: Orifice plate box.

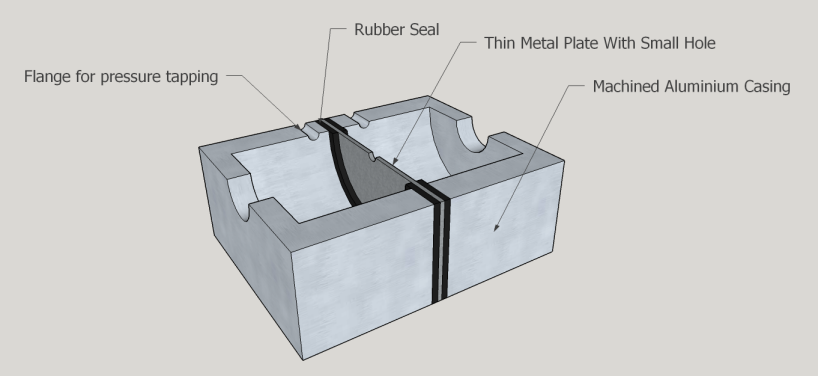


Figure 6.7: Cross-sectional view of the orifice plate box.

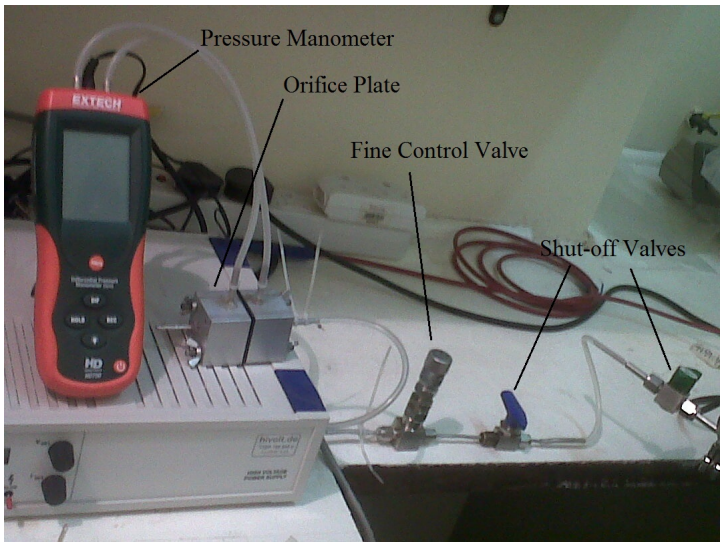


Figure 6.8: A diagram showing the set-up of the experiment from the outside of the vacuum chamber. From left to right: Differential Pressure manometer, Orifice plate, Fine control valve and the two shut-off valves.

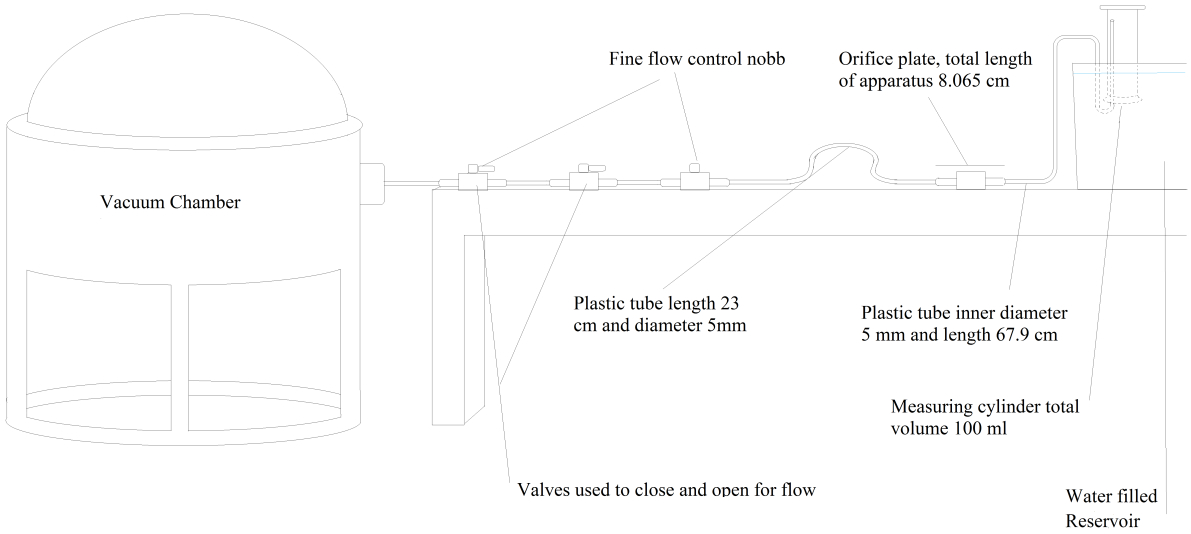


Figure 6.9: A diagram showing the set-up of the experiment from the outside of the vacuum chamber.

6.5 Procedure

With the set-up as shown in the Figure 6.8 and 6.9, the two valves and micrometer screw are all closed and the vacuum chamber evacuated to its maximum level (which for the set-up used was 10^{-8} $Torr$). Once the vacuum chamber is evacuated to the required level, bubble the chosen gas into the inlet chamber until the liquid level in the cylindrical measuring tube is flush with the reservoir liquid level. Then, fully open the valves leading to the chamber, see figure 6.9, and slowly turn to open the micrometer screw until a particular pressure difference [1] (measured using the manometer), for which calibration is to be found, is established across the orifice plate (see Figures 6.8, 6.6 and 6.7). Allow the liquid level to rise until some preferred starting level (point at which start of volume flow rate measurements begin) on the measuring cylinder is achieved. It must be noted that the pressure difference across the orifice-plate (or Venturi tube) should remain as constant as possible with the starting level chosen to ensure that the starting pressure in the inlet is close to the atmospheric pressure, ideally exactly the same.

While adjusting the micrometer screw ensure that the inlet chamber does not evacuate beyond a certain percentage (35% in our case), so that the pressure difference across the orifice would not be allowed to change by more than one unit of error (in our case two millibar). That is try and keep the pressure difference across the orifice plate constant to within an acceptable error margin. If the desired pressure difference is exceeded close the valves but leave the micrometer screw at it set location, then bubble the gas into the inlet chamber to the required initial conditions (correct starting level, pressure and temperature) and begin again by opening the valves [2] while continuing to adjust the micrometer screw until a favourable pressure difference (basically until a desired volume flow rate) is achieved.

Once a desirable pressure difference is achieved close the valves and do not further adjust the micrometer screw, re-set to the required inlet conditions (i.e. liquid at the starting level or near to it, gas at the appropriate pressure and temperature)[3]. Once initial conditions have been met open the valves and once the liquid level in the measuring cylinder reaches the starting level begin to record the time for a percentage of the inlet chamber to be evacuated (here it was either 35% or 20% i.e. 47 cm^3 or 27 cm^3) by using the height of the water column as an indication. Ensure that the evacuated volume is not too large to change the pressure difference across the orifice beyond acceptable error margin. Repeat for many trials leaving the micrometer screw fixed, although sensitive

[1] This must be done carefully as the pressure difference readings were found to be very sensitive to adjustments in the micrometer screw tightness, however the vacuum chamber itself tended to a steady state operation while adjustments were made for the small mass flows considered.

[2] Expect a sudden surge in pressure difference across the orifice plate.

[3] If necessary the outlet conditions as well.

to vibration it may consequently require resetting periodically.

If necessary repeat the last paragraph's instruction, without taking measurements, for several tens of trials (in our case 10 times exactly) to reduce the concentration of air in the chosen gas-air mixture in the inlet chamber.

6.6 Results

Four batches of eight to ten trials each were run all using Argon. The results for time taken to evacuate the required inlet volume and fluctuation of the pressure difference of the orifice plate from the beginning to end for the associated trial are presented. Note that IP and FP stands for Initial and Final Pressure respectively, while Diff and Time stands for change in pressure and time taken.

IP (± 0.2 $mbar$)	FP (± 0.2 $mbar$)	Diff ($mbar$)	Time (± 3 s)
5.5	5.4	-0.1	464
5.4	5.4	0	462
5.6	5.7	0.1	459
5.6	5.5	-0.1	468
5.6	5.6	0	459
5.6	5.5	-0.1	467
5.6	5.5	-0.1	464
5.6	5.5	-0.1	472
5.4	5.5	0.1	462

Table 6.1: Table of time taken to evacuate $47 \pm 4cm^3$ of Argon and change of pressure across the orifice plate, conducted at a temperature of 294.15 K and with the vacuum chamber stable at 8×10^{-2} $mbar$.

IP (± 0.2 $mbar$)	FP (± 0.2 $mbar$)	Diff ($mbar$)	Time (± 3 s)
10.4	10.2	-0.2	329
10.3	10.2	-0.1	326
10.4	10.2	-0.2	328
10.3	10.1	-0.2	328
10.3	10.1	-0.2	333
10.3	10.1	-0.2	324
10.3	10.1	-0.2	330
10.2	10	-0.2	336
10.3	10	-0.3	335
10.1	9.9	-0.2	336

Table 6.2: Table of time taken to evacuate 47 ± $4cm^3$ of Argon and change of pressure across the orifice plate, conducted at a temperature of 294.15 K and with the vacuum chamber stable at 9×10^{-2} $mbar$.

IP (± 0.2 $mbar$)	FP (± 0.2 $mbar$)	Diff ($mbar$)	Time (± 3 s)
15.2	14.8	-0.4	266
15.4	14.8	-0.6	273
15.1	14.7	-0.4	273
15	14.6	-0.4	271
15.5	15.1	-0.4	264
15.3	15.1	-0.2	265
15.2	14.9	-0.3	265
15.3	14.9	-0.4	271
15.2	14.8	-0.4	275
15.1	14.8	-0.3	268

Table 6.3: Table of time taken to evacuate 47 ± $4cm^3$ of Argon and change of pressure across the orifice plate, conducted at a temperature of 294.15 K and with the vacuum chamber stable at 9×10^{-2} $mbar$.

IP (± 0.2 $mbar$)	FP (± 0.2 $mbar$)	Diff ($mbar$)	Time (± 3 s)
4.6	4.45	-0.15	253
4.6	4.3	-0.3	268
4.7	4.5	-0.2	253
4.7	4.6	-0.1	257
4.6	4.4	-0.2	257
4.6	4.5	-0.1	263
4.6	4.5	-0.1	259
4.7	4.6	-0.1	261

Table 6.4: Table of time taken to evacuate 27 ± $4cm^3$ of Argon and change of pressure across the orifice plate, conducted at a temperature of 294.15 K and with the vacuum chamber stable at $< 10^{-4}$ $Torr$.

6.7 Analysis and Discussion

The results for time-average volume and mass flow rates and their analysis are in appendix C, as well as the model justification. However analysis indicated good repeatability and well defined average quantities at a confidence level of 95%. Figure 6.10 shows the calibration curve obtained for the pressure differences used with a maximum mass flow rate error of $\pm\ 2.9\times10^{-8}\ kg/s$ chosen for convenience (as there was some variation).

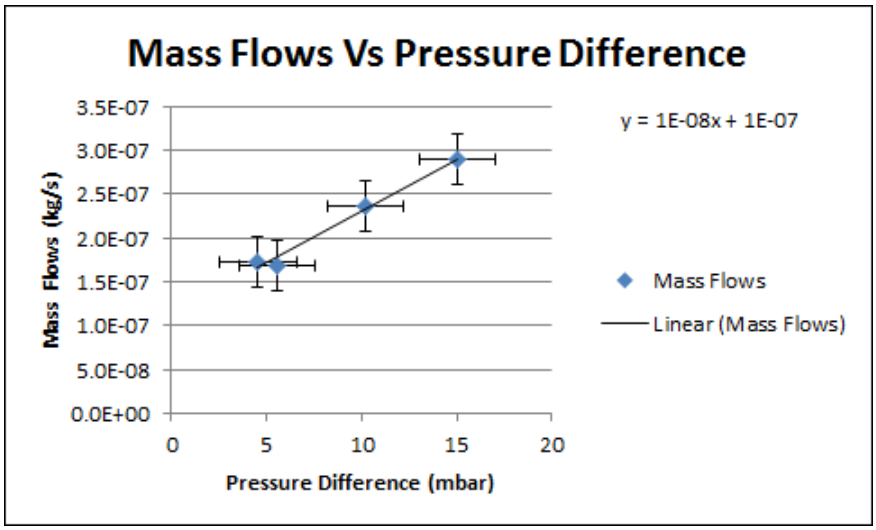


Figure 6.10: Calibration curve of Pressure Difference vs Mass Flow (error set to $\pm\ 2.9\times10^{-8}\ kg/s$).

Statistical tests were performed on the data and their residuals before error estimation against the hypothesis that the data was normally distributed to assert whether the experiments were repeatable. As a consequence two tables for each batch of experiments are included in the appendix: one where significant figures are taken into account and corresponding error estimates are given, while in the other significant figures are not taken into account during algebraic operations so that statistical analysis could be applied. Since no more than eight to ten data points were available for each set of trials recorded, the Anderson-Darling test (with test statistic denoted D) was used. Use of Chi square test would have been to sensitive and subjective to SAS's "binning" of data where as the Anderson-Darling test does not use such an approach and is a non-parametric test suitable to small data sets [109].

The actual analysis was carried out using SAS Enterpriseguide 6.1 distribution test function. Only the results pertinent to establishing conclusions for repeatability of experiments and validation of the statement that statistical error associated with each batch was less than estimated error were presented.

This was accomplished with the following values used for calculations (and the assumption that the gas was dry):

1. $\mathfrak{m} = 39.948(1)\ g/mol$ [13].
2. $R = 8.3144621(75)\ JK^{-1}mol^{-1}$ [110].
3. $T = 294 \pm 1\ K$.
4. $P_{atm} = 101 \pm 5\ kPa$ as pressures tended to fluctuate during the day and between sessions.

6.8 Conclusion

In these tests a technique was developed to measure the mass flow rates for small mass flow rate systems. Data for the experiment indicated a high degree of precise repeatable and time averaged data well within uncertainty, as calculated in the appendix. Mass flows as low as $170 \pm 16\ \mu g/s$ were measured using the technique.

However to improve the validity of the model it would be necessary to increase the volume of the inlet chamber while decreasing the ratio A'/A (see appendix C) so as to improve the conditions necessary for near hydrostatic equilibrium behaviour as outlined in the model justification section. As well as use some kind of liquid thermal insulator (instead of water) to prevent the transfer of heat to and from the inlet chamber to the liquid and thereby ensure more independent and perhaps uniform temperature distribution in the inlet chamber to completely justify ignoring the cooling effects of the water. If possible it would also be desirable to pick the liquid insulator so that it does not evaporate easily into the inlet volume so as to keep the gas in the inlet more pure. In addition to ensure that conditions downstream from the chamber remained sufficiently constant as well, a temperature sensor placed at the entrance to the venturi tube or orifice plate system would be necessary to ensure that the system was monitored to be behaving close to some kind of constant and uniform distribution of temperature.

If possible it would also be desirable to place multiple pressure sensors in the control volume and take readings at different positions in the control volume during the discharge, to ensure that the density would actually be well approximated by the uniform density assumption within the control volume. Since the flow is essentially assumed to be subsonic through the control volume so that it is locally well approximated by equilibrium thermodynamic equations of state verification of uniform pressure distribution would, along with verification of nearly uniform temperature distribution justify the model.

Chapter 7

Thruster Voltage-Current Measurements

In this chapter the current-voltage relationship of a CORION like system will be investigated. To be specific a needle through which gas will be fed will be connected in a circuit to a plate hovering over the needle and high voltage ($O(kV)$) applied across the needle and plate (see Figure 7.5 on p. 92), while exposed to a vacuum environment. For the mass flows considered in the experiment the voltage will be varied until breakdown/discharge occurs. Once the discharge occurs the voltage will continue to be varied to investigate the electrical behaviour of the system. The chapter will commence with an introduction to common DC discharges as well as background in glow and corona discharges. The apparatus, experimental technique used, results and discussion with conclusion will then complete the chapter.

7.1 Aim

The aim of the discharge tests was to investigate the feasibility of a new experimental set-up to study the discharge characteristics of a CORION like system as well as conduct voltage vs current experiments of the CORION like system, see Figure 7.5 on p. 92.

7.2 Background - DC Discharges

In this section discharges across a gap of a container filled with some gas, with the gas at different initial pressures, between two electrodes at opposite ends of the container will be considered. One must note that in the following discharges there is no actual flow of gas (initially) and that the experimental set-up consists

of a power source connected in series with a ballast resistor [1] connected in series with the gap (container).

7.2.1 General DC discharge characteristics

Before breakdown the current through a voltage biased gap will be very low until at least the breakdown voltage [2] is applied across the gap leading to a discharge. Figure 7.1 (taken from [4]) shows a general discharge profile (before and after breakdown), for high and low gas pressure systems, with gap voltage against gap current where as table 7.1 summarizes the different dominant discharge types and regimes identifiable for the systems.

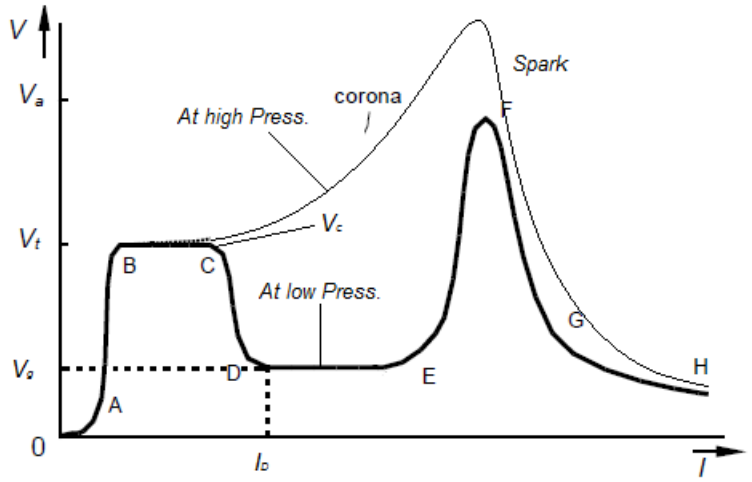


Figure 7.1: Current voltage characteristic behaviour of DC discharges over a wide current range of gas pressure and electrode geometries. A-B is a region of non-self-sustaining discharge. B-C represents a Townsend dark discharge region. D-E normal glow discharge region. E-F abnormal glow discharge. F-G transition to arcing. G-H arc. The dotted line shows how an increase in applied voltage in a highly inhomogeneous field geometry leads to a corona discharge instead of a normal glow discharge [4, 5].

[1] Allows control of current through the gap and voltage drop across the gap once breakdown occurs.

[2] Voltage at which the gas in the gap becomes conductive.

Type of Discharge	**Characteristics**
cosmic rays (not a discharge)	low rate of ionization, important before Townsend as it provides 'seeds' for the other discharge processes
Townsend dark discharge	none or very little light emission with cathode potential drop of 100 volts
Corona discharge	positive and negative corona, may be sporadic, bulk of ionization restricted to region near active electrodes
Glow discharge	may be stable or pulsed, sharply non-uniform distribution of potential across the gap
Low temperature non-thermal plasma	large temperature difference between electrons and ions
Arc discharge	when the current through the gap is at about 1 amp the glow discharge cascades down to an arc, high gap current at low gap voltage with respect to the other glowing discharge types

Table 7.1: Table of discharge types and characteristics [4].

Note that V_a is the gap voltage and V_t is the *transition voltage (ignition voltage)* i.e. "*the voltage at which a self sustained current becomes manifest and leads to an electrode voltage drop for homogeneous fields, and may correspond to the breakdown voltage* "[4]. What follows is brief summary of the different regimes present in Figure 7.1.

Regime O-A The electric fields between the electrodes collect any stray charges created by ionization of the gas molecules by external radiation and any charges emitted from the electrode by the same radiation [8]. The current saturates at a value determined by the external source. This refers to the cosmic rays discharge in table 7.1.

Regime A-B(first Townsend region) The stray electrons as formed in Regime O-A gain enough energy between collisions from acceleration by the field to ionize atoms by collision. The secondary electrons in turn produce others i.e. an avalanche process using only the gas's generated electrons [8]. The current is thus linear in the source current and exponential in the ionization cross-section, neutral density and gap spacing for one dimensional electrode geometries [8].

Regime B-C (second Townsend region) In addition to the process for Regime A-B the ions created from it gain enough energy between collisions from the field to emit electrons from the cathode by bombardment of it by the ions [8]. Internally generated radiation may also contribute to emission of electrons from the cathode by photo-emission [8]. This forms part of the Townsend Dark discharge in table 7.1.

Regime C-D "Beyond the point C, denoted by the *sparking potential* V_c, the ion bombardment of the cathode and/or radiation on the cathode by the discharge gas becomes sufficiently intense that the discharge becomes momentarily unstable and "runs away" to a new lower voltage with the remaining voltage distributing itself across the ballast resistor" [8]. V_c is strongly dependent on all the properties that may affect the discharge gap [8]. Beyond point C the discharge behaviour depends on the voltage source, gas pressure and electrode geometry [8]. If the electrodes are such that they produce inhomogeneous fields and gas pressure is high a corona will form [8]. If they are smooth such that they produce homogeneous fields and the gas pressure is low a normal glow will form, with current determined by the source [8]. (In the case that the source cannot supply the minimum current I_D the gap will spark, return to C, spark again et.) [8].

Regime D-E (normal glow discharge) see subsection 7.2.2 DC glow discharges.

Regime E-F (abnormal glow) Increase of voltage appears primarily across the cathode-fall-region (also called the Cathode Sheath or Crookes dark space see fig 7.3 p. 89) [8], where the ion current density and bombardment energies increase enough to heat the cathode substantially [8].

Regime F-G (glow-arc transition) At point F new emission mechanisms take place at the cathode [8]. The cathode-fall region becomes sufficiently hot so that the cathode can thermionic-ally emit electrons, supported by strong local fields and perhaps photo-emission from the adjacent gas [8]. As the cathode-fall voltage then drops, a high current arc sets in [8].

Regime G-H The arc resistance (resistance of the gap) drops faster than the current can rise and unless protected by a ballast resistor the current will run away to values of 1000 amps vaporizing the electrodes and becoming extremely hot ($> 10^4 K^\circ$) [8]. An arc discharge is recognized by relatively high currents (several amps and higher) at relatively low electrode voltages (less than 100 volts for short arcs) [8].

Townsend Discharge or Regime B-C

The Townsend dark discharge is a self sustained discharge. This discharge is made self sustained by applying the ignition potential across the electrode gap [4]. This potential ensures the constant stationary ejection of electrons from the cathode and their attraction to the anode. Charges are multiplied in avalanches and the entire space charge region is weakly positive in polarity [4]. The current is usually between 10^{-10} and $10^{-5} A$ depending on the circuit and electrode surface [4].

The Townsend discharge is dark because during its regime of existence excitement of atoms by electron impact is negligible (the field is to weak and collisions occur to often for sufficient gain in energy) and ionization events are to few for noticeable production of light [4]. Impact ionization is the dominating ionization mechanism and contributor to the space charge density in this regime [4]. However, it is to be noted that the space charge density and overall number is not great enough to perturb the potential distribution in the gap appreciably [4].

The reason for the length of the horizontal line in the regime B-C is because of the dependence of the current on the emission area i.e. the area where field strength is similar on the electrode surface [4]. It is to be noted that attempted operation at either edge of the second Townsend region leads to unstable current as the state of the electrodes are not constant [4].

Corona Discharge

A corona discharge is a gas discharge (often occurring as a pulse [111]) where the geometry confines the gas ionizing process to high field ionization regions around the active electrodes with the existence of a low field drift region connecting the ionization regions or the low field, passive electrodes (see Figure 7.2)[6].

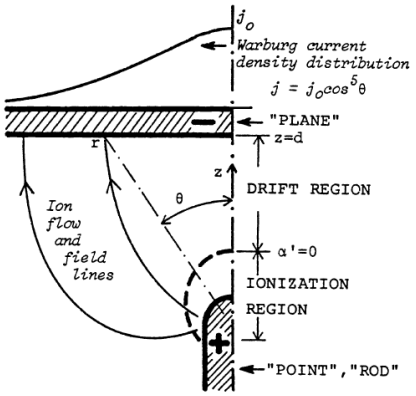


Figure 7.2: A point-to-plane corona geometry, shown here with a positive point. The surface $\alpha' = 0$ marks the outer limit of ionization region, where the production of electrons by ionization just balances the loss by attachment [6].

A corona discharge requires that the potential gradient (field) be intense enough in a region near an electrode to initiate field ionization of the gas there [4]. Electrons and ions are then accelerated to their respective electrodes driving ionization and photo-excitation (glow) [4]. However, for a region of space between the electrodes the field is no longer strong enough to sustain continued break down and glow in the same way (as other mechanisms like streamers exist [4] to allow ionization or charge propagation) in this region [112, 4, 6]. Hence there is a dimming of the glow to nothing as ions and electrons lose energy for visible photo-excitation collisions due to less energetic inelastic collisions [112, 4, 6]. However, if the potential difference is increased an arc will form where it is important to note that for a corona discharge the inter-electrode distance must be much greater than the characteristic size of the electrodes or else a spark will form (transient or short lived arcs)[4].

The corona geometry is named positive, negative, bipolar, AC, or HF, according to the polarity of the active electrodes [6]. While the current conduction in any corona region is called unipolar or bipolar depending on whether positive and or negative charge carrier polarities are of importance. In unipolar conduction coronas, the drifting ions/electrons will always be of the corona polarity (i.e. current in the drift region is due to the charge carriers that leave the ionization region [4]) and their space charge field will be the dominating factor in determining both the corona current/voltage characteristic and the current density distribution in the discharge gap [6]. In most gases essentially two different kinds of DC (or low AC) coronas exist [6]

Unipolar Conduction Coronas Note the following statements are taken from [6]. Also called positive glow coronas, negative Trichel pulse coronas and negative glow coronas, all have ionization regions that stay very concentrated and very close to the active electrode [6]. They either burn or at a constant rate or, more often, in short pulses of such high repetition rate that the ion flow in the drift region is practically continuous, at micro-

Amperes and above [6]. The predominant ions are of the corona polarity, that is, positive ions in positive coronas and negative ions in negative [6]. The part of the drift region current in negative air coronas carried by the corona's electrons is usually small, below $10 - 20\mu A$ of the total current, because of electron attachment [6]. At higher currents, the space charges make the electric field distribution more uniform [6]. This, and the higher applied voltage, sharply increase the drift region field, increasing the electron/negative ion ratio [6]. Note that the rapidly pulsed nature of the ionization region processes is very important for the corrosion of the negative point electrode [6]. This may affect the drift region and plane electrode by sputtering or evaporation of the point metal and the corrosion products [6]. It is advised to think of the drift region as an over grown boundary sheath connecting the ionization region (often a plasma) with the low field electrode [6].

Streamer (bipolar) Conduction Coronas Note the following statements are taken from [6]. These occur at higher point to plane currents, especially at positive point polarity [6]. Under positive polarity of the point electrode, the ionization region produces a conducting plasma faster than the plasma can be absorbed by the point electrode [6]. Consequently a conductive plasma filament of some $30\mu m$ grows out of the point towards the plane, carrying the plasma producing ionization region ahead of it with velocity of $10^6 m/s$ (in atmospheric density air) [6]. When this streamer hits the plane, a cathode spot is produced, the gap field is redistributed along the plasma channel, and this channel either dies out (by electron attachment) or later converts to a thermally ionized spark channel [6]. A positive streamer hitting a plane cathode will subject it to a pulsed glow discharge treatment, bombarding it with positive ions with energies that may exceed $100eV$ [6]. This is in contrast to the mainly thermal energy ion influx (increased pressure) to the plane in unipolar current coronas [6].

Note that both corona forms may coexist [6].

Development of visible corona discharge

The current density at which the field and discharge structure are considerably modified and which manifests the beginning of dark to glow transition of discharge in a inhomogeneous field is given within an order of magnitude by [4]:

$$\frac{j_L}{p^2} \approx \frac{(\mu_+ \cdot p)(E_t/p)^2}{8\pi(pL)} = \frac{(\mu_+ \cdot p)V_t^2}{8\pi(pL)^3} \tag{7.1}$$

j is the current density, μ mobility, p pressure, E_t transition field strength, L characteristic length and V_t transition voltage.

When a positive potential is applied the first corona phenomena observed is the onset of a streamer from the active electrode followed quickly by the formation of a "Hemstein glow" (an apparently continuous glow) [4]. The current is

limited by the space charge in the outer region [6].

The development steps of a positive corona are [4]

1. A high voltage is applied.
2. 'Seed' charges are present.
3. An avalanche builds up and leaves a space charge area behind, however onset streamers precede the formation of glow.
4. Photons from the avalanche create new charge carriers outside the space charge area.
5. New avalanches form closer to the anode.

A negative corona has the same initialization condition as a Townsend discharge whereas in a positive corona the electrons are produced by photo processes [4]. It is to be noted that the ignition of a laboratory corona can also be observed by the jump in current [4]. The mechanism of multiplication of electrons is essentially dependent on the polarity of the electrode surrounded by the corona, but generally manifests itself through an avalanche process [4]. Secondary processes that take place are emission of electrons from the cathode by secondary emission and production of electrons in the outer region by photo-ionization [4].

In contrast to the homogeneous glow about a negative corona, a positive corona displays luminous filaments running away from the electrode [4]. The onset voltage of a positive corona V_{C+} is in general somewhat greater than that of a negative corona V_{C-}, where the difference is gas dependent, and can be estimated using "Peek's law" or an appropriate alternative [4].

7.2.2 DC glow discharges

A DC glow discharge occurs when a potential of several hundred volts is applied across electrodes in a chamber at low pressure (0.1 - 10 torr however they can be observed at atmospheric pressures) [7] and surrounding photons and exotic particles of sufficient energy collide with neutrals causing ionization, followed by an electron avalanche process which starts and causes a multiplication of electrons and ionization events (present in nearly every discharge) throughout the gap. Through out the chamber once the d.c. glow discharge has established itself a glow profile is observed characteristic of glow discharges consisting of light and dark regions indicating different thermodynamic (equilibrium an non-equilibrium) behaviours and potential profiles [7]. Figure 7.3 illustrates the basic characteristics of a glow discharge and profile.

Positive column

The length of the positive column can be adjusted by changing the distance between the electrodes at constant pressure and approximately constant voltage

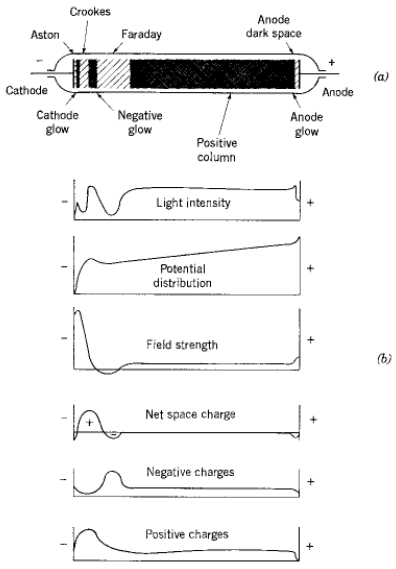


Figure 7.3: General characteristics of DC glow discharges [7, 8].

drop, while the other component lengths and dimensions remain constant [7]. Consequently the positive column can be analysed per unit length where as the other components must be analysed in their entirety [7], basically it is uniform on its cross-section.

As a result we can think of the Positive Column as an axially uniform plasma that is sustained by the input power $J \cdot E$ (E the applied electric field) integrated over the cross-section of the plasma, however this must balance the energy loss per ion-electron pair created under the assumption that the loss is radially uniform [7]. To be specific the power lost per electron-ion pair goes into excitation, ionization, electron-neutral elastic scattering energy losses and the kinetic energy of the electrons and ions striking the walls [7]. As a property, a normal glow discharge tends to have a negative voltage-current relationship (i.e. negative differential resistance dV/dI) which is stabilized by an external resistor [7]. And since the power balance determines the weak E field necessary to sustain the positive column from which the drift velocity of the electrons can be determined, using the d.c. electron mobility, it follows consequently that the current density in the Positive Column can be found [7].

Cathode sheath

This region is also known as the *cathode fall* or *Crooke's dark space*, it is the region over which most of the gap voltage is dropped [7]. Electrons, which carry most of the current in the positive column, are prevented from reaching the cathode by an accumulation of ions there [7]. Additionally the more massive ions, which cannot produce the full current, cause secondary emission

of electrons from the cathode by bombardment of it by the energetic ions [7]. This consequently produces a current that is built up from ionization within the sheath, that is driven by avalanche processes using the secondary emitted electrons accelerated by the strong fields in this region, see Figure 7.3 [7]. The electron density and flux grow exponentially from the cathode and the exponent is known to be the *first Townsend coefficient* [7].

Negative glow and Faraday dark space

The Faraday dark space is a region between the cathode and positive column, of approximately half a mean free path length, in which electrons that have lost nearly all their energy by a complex process are re-accelerated by a weak electric field towards the positive column before entering at its equilibrium conditions [7]. This space is created essentially in order to dissipate the energy of high velocity electrons, by elastic and inelastic collisions, as produced by the secondary emission and avalanche processes in the cathode region, where their density behaves exponentially, and decrease the intense field there to establish the positive column [7].

Anode Fall

The anode fall occurs between the Positive Column and the anode see fig 7.3. Since the drift velocity of electrons in the weak field of the positive column is less than the thermal velocity of the electrons, a retarding field is necessary to prevent the thermal current of the electrons from reaching the anode [7]. Fortunately the anode is positive relative to the positive column to maintain the current thereby forming a *double layer* and establishing the Anode Fall [7]. The anode fall region is much smaller than any of the others but can be analysed by a diffusion-drift approximation (for higher than usually considered pressures of 40 - 80 Torr) [113].

Arcs

The formation of an arc was previously described from the glow to arc transition as a result of the increase of thermionic ionization and photo-ionization processes. For an arc the cathode fall is typically less than 20 V [8], and the cathode surface emits electrons at a tremendous rate (10^3 to 10^7 A/cm^2) through a combination of thermionic, photoelectric and field emission processes [8]. The anode fall and spatial extent is approximately the same as the cathode fall's, and for both regions ionization is driven primarily by field accelerated ions [8]. There is a net negative space charge near the cathode and the opposite at the cathode and both are non-equilibrium regions, where as the positive column (which occupies all remaining space between the electrodes) is approximately a thermal plasma, see Figure 7.4 [8].

It consists of a strongly radiating mixture of electrons, ions and neutrals all

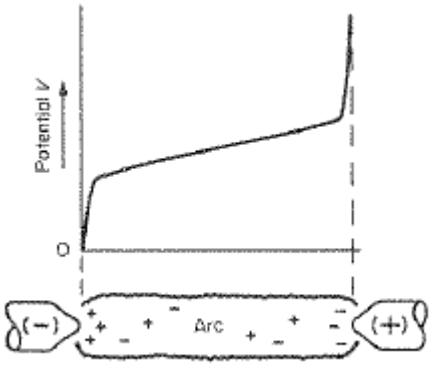


Figure 7.4: Axial potential for high current arc [8].

nearly at the same temperature (500 to $5000K$) with ionization from a few percent to complete or total ionization [8]. The predominant mechanisms of ionization in the positive column are electron collisions and photo-ionization due to the fact that the electrons thermal velocity greatly exceeds their drift velocity in the column (weak electric field region) [8]. Current conduction in the column and anode sheath are determined primarily by diffusion-dominated drift of electrons where as ions contribute greatly to the current in the cathode sheath due to their acceleration there by the cathode fall region [8].

7.3 Apparatus

The experimental set-up when constructed inside the vacuum chamber is represented in Figure 7.5. It consisted of the following components:

1. A hivolt.de T1EP 100 60d p High Voltage Power Supply see Figure 7.6 p. 92 connected in series with the steel plate (through electric stand and gas inlet base see Figure 7.5) and needle.
2. Retort Stand clasping Steel Plate.
3. A vacuum chamber and air pump, see Figure 7.7 p. 93 for vacuum chamber.
4. The electric stand and gas inlet base used to feed power and gas to the needle, see Figure 7.5, 7.9 p. 94, 7.10 p. 95 and 7.8 p. 93.
5. The mass flow set-up from the previous chapter.

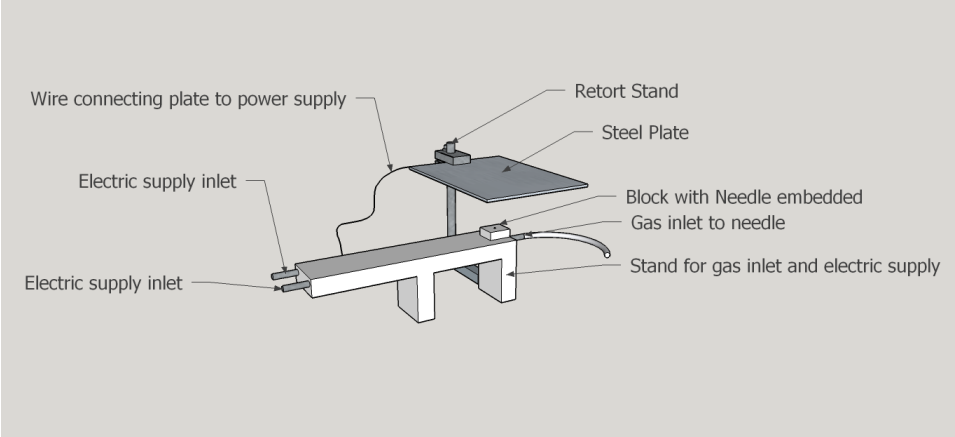


Figure 7.5: The experimental system to be investigated.

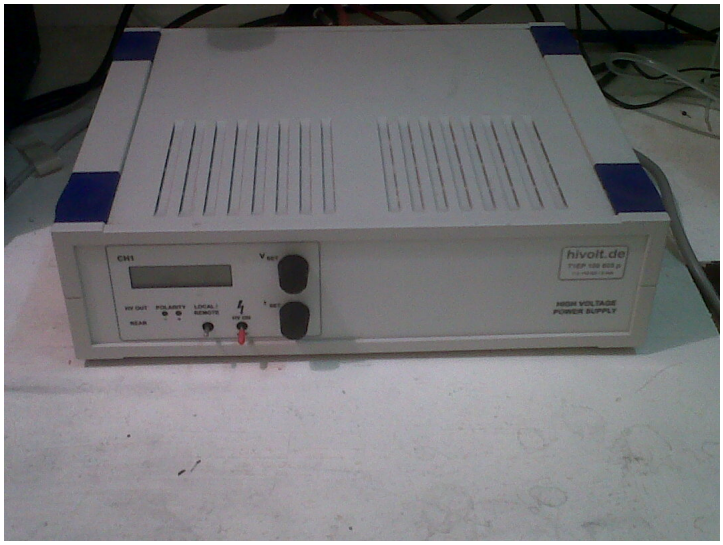


Figure 7.6: hivolt.de T1EP 100 60d p High Voltage Power Supply.



Figure 7.7: The vacuum chamber used.

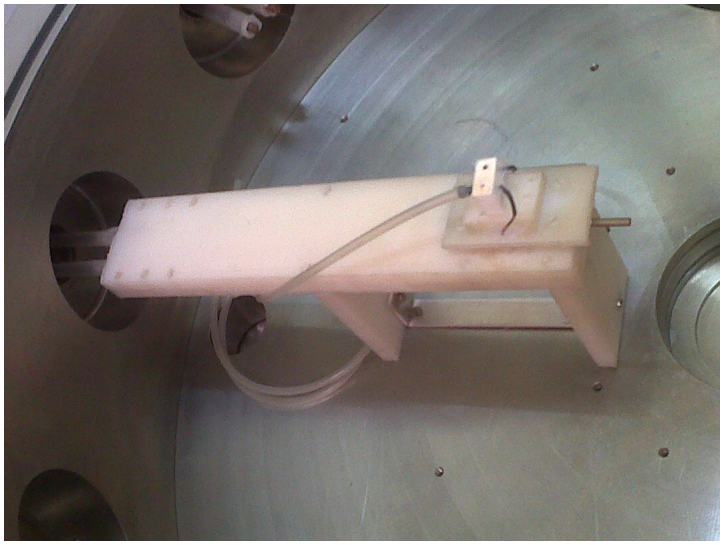


Figure 7.8: The electric stand and gas inlet base used to feed power and gas to the needle. Electric connection inside the chamber to the external power source is shown on the left.

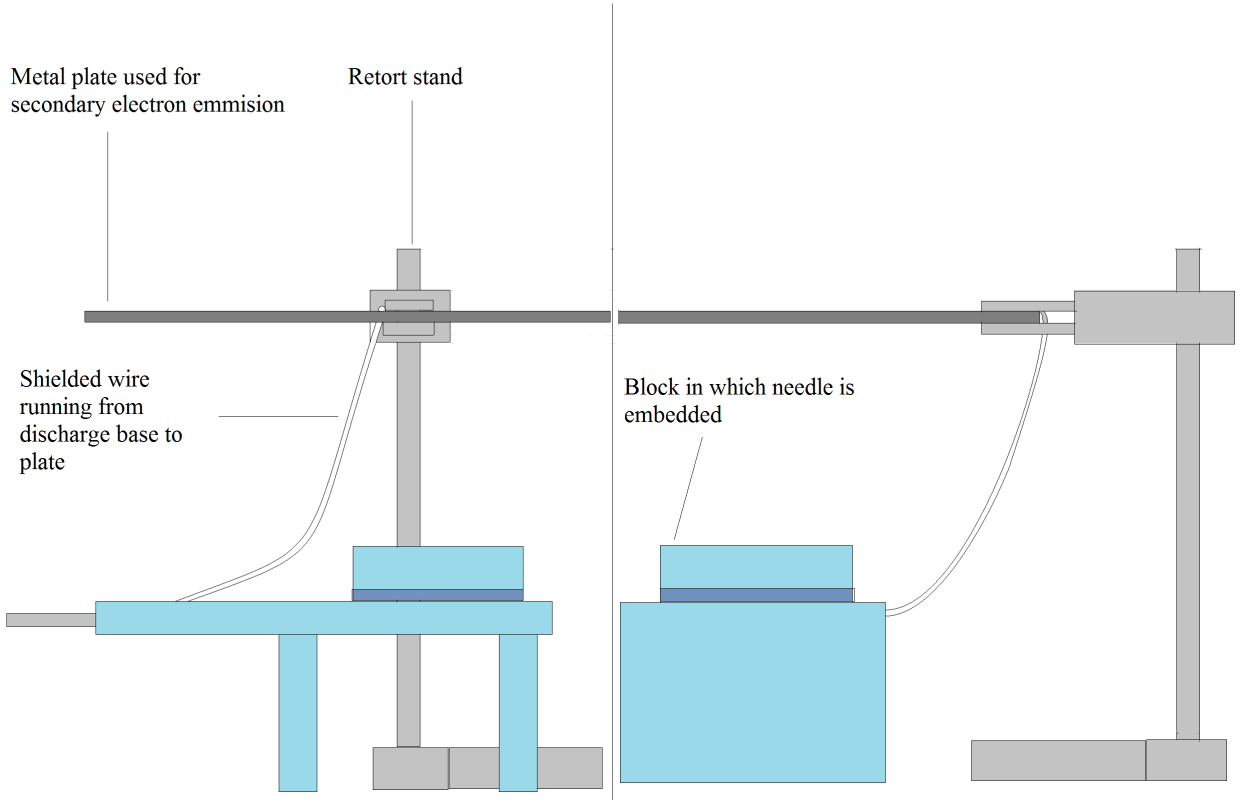


Figure 7.9: Orthographic views of the experiments set-up: the left hand diagram corresponds to a front view while the right hand diagram corresponds to a side view.

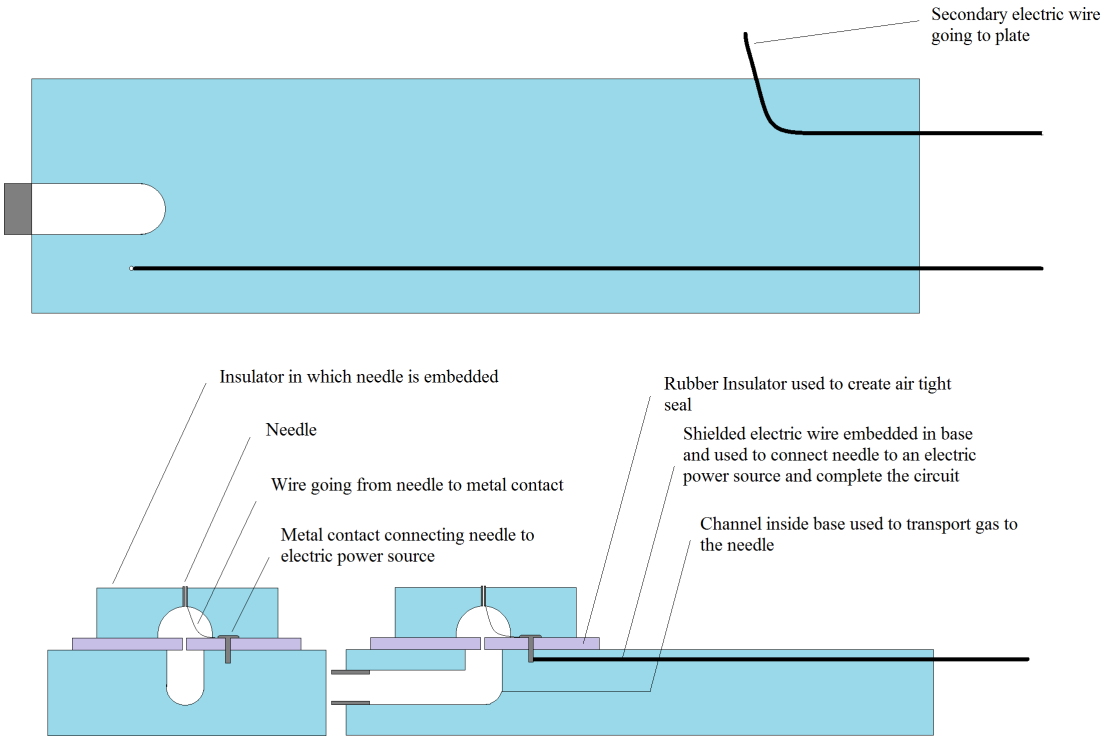


Figure 7.10: A diagram showing cross-sectional views of the needle and discharge base as used in the experiment.

7.4 Procedure

Begin by setting the needle system on the support as in the Figures 7.10 and 7.8. Place the support inside the chamber and connect the gas feed and electrical inputs, Figure 7.8 and 7.10, to the chamber's gas inlet and electrodes respectively. Connect the chamber's gas outlets to the mass flow system (described previously) i.e. gas input system and the power supply to the chamber's electrical outlets. Set the retort stand so that it will hold the steel plate (covered with Aluminium foil) directly over and perpendicular to the needle at a desired height (in our experiments the height was 4 cm). Connect the steel plate to electric stand using an insulated wire at the provided outlet, see Figure 7.10.

Close the chamber and repeat the steps in the mass-flow measurement section (with the chosen inlet gas) for evacuation of the chamber and to establish a particular mass-flow for a particular pressure difference across the orifice plate (or venturi tube). Once the adjustments have been made to achieve the desired mass-flow and the position of the micrometer screw has been found to give this desired flow, as in the mass-flow section make sure the valves are closed and pressurize the inlet chamber to the required pressure, see Figure 6.9. Then, open the valves and allow the gas to leave the inlet chamber, while this happens pump the gas with which testing is being done into the inlet chamber and adjust the rate at which gas enters until a steady state is achieved [3](i.e. the liquid no longer rises or falls in the measuring cylinder [4]) [5].

Once the steady state operation has been achieved switch on the power-supply (it is important that it starts with $0V$ and $0A$) then slowly raise the voltage and current (with needle positively biased relative to the plate) until breakdown occurs (i.e. conduction of non-zero sustained current begins and is detected by the power-supply). Record the breakdown voltage value and current value as accurately as possible using the power supply[6].

Once breakdown occurs, within one minute (to prevent to much damage to the needle), vary voltage first above and then below the breakdown point and record the corresponding current values using the power supply[7]. In this version of the experiment only current values stationary to three significant values were recorded. Record the switch off voltage and current when below breakdown if possible, as the transition can occur rather quickly. Then after this, set the

[3]It was important to try and make sure that the stationary point achieved and indicated by the water level was close to the initial or starting point of the experiment associated with a particular pressure difference across the orifice plate to ensure that the desirable mass-flow rate was sustained.

[4]For the low mass-flow rates used this was possible.

[5]Try to ensure that the pumped gas is close to the same temperature and pressure as the gas was initially when the inlet chamber was pressurized.

[6]Note: a transient current spike may occur as the needle collects surrounding electrons while raising the voltage do not attempt to record this value or interpret it as breakdown.

[7]The current was not allowed to exceed 150 mA to prevent damage to the needle.

power-supply current and voltage to zero and wait for some time (waiting time ranged from 20 seconds to two minutes), and then repeat with the same needle all steps involving the power-supply for a sufficient or physically viable number of trials before replacing the needle[8]. Ensure that the needle remains positively biased with respect to the plate during the experiment.

7.5 Results

Results for four stainless steel gauge 34 needles (7 mm to 10 mm long at 34G with internal diameter of 0.06 mm) three used with Argon and one with air are presented next. For each needle four trials were run and current measurements were taken for currents at least stable to μA. For the mass flow rates the gases were assumed to be dry and the method from the previous chapter used to estimate mass flows. The steel plate was set at a height of 4 cm above the needle.

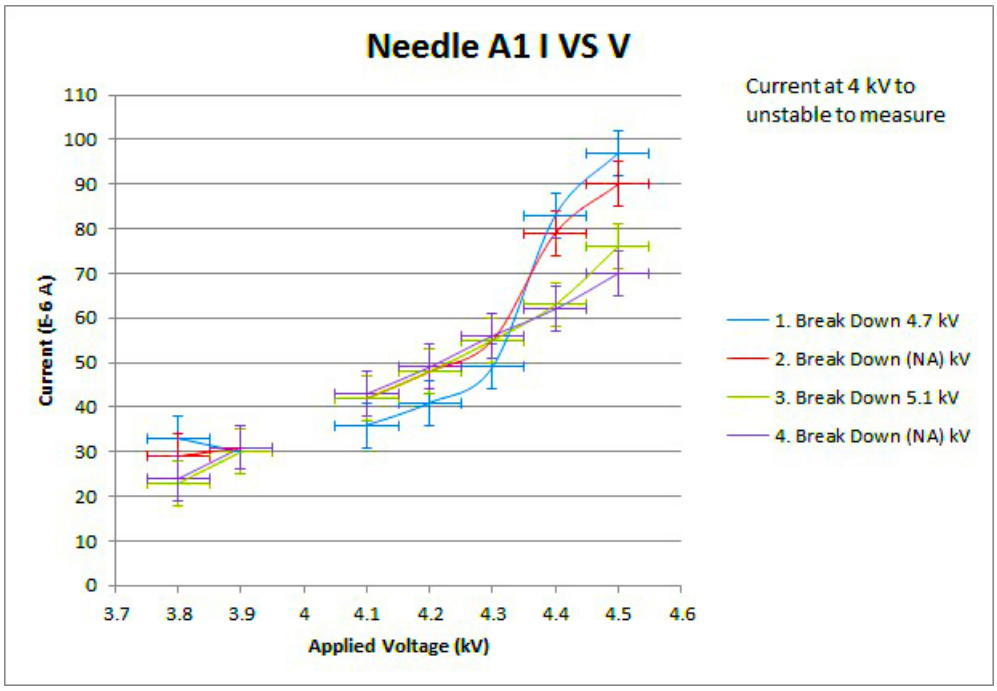


Figure 7.11: Results for needle A1 using Argon for a mass flow of 175 $\pm 27 \mu g/s$. Where possible break down voltages with uncertainty $\pm 0.1 kV$ for different trials are included.

[8]Reproducible results among different needles was found to be difficult.

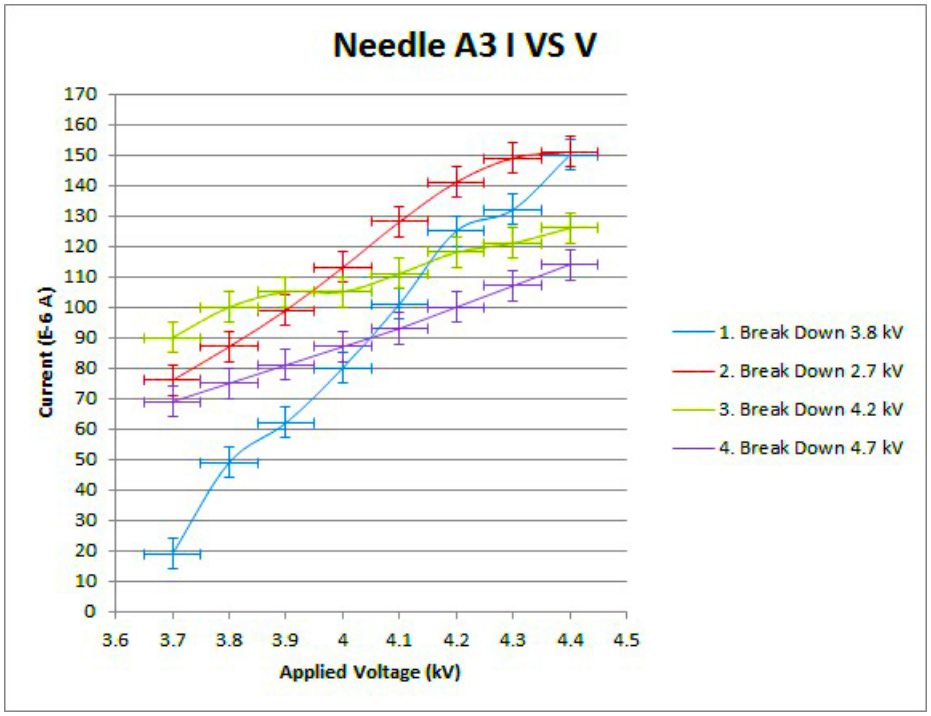


Figure 7.12: Results for needle A3 using Argon for a mass flow of 176 $\pm 28 \mu g/s$. Where possible break down voltages with uncertainty $\pm 0.1 kV$ for different trials are included.

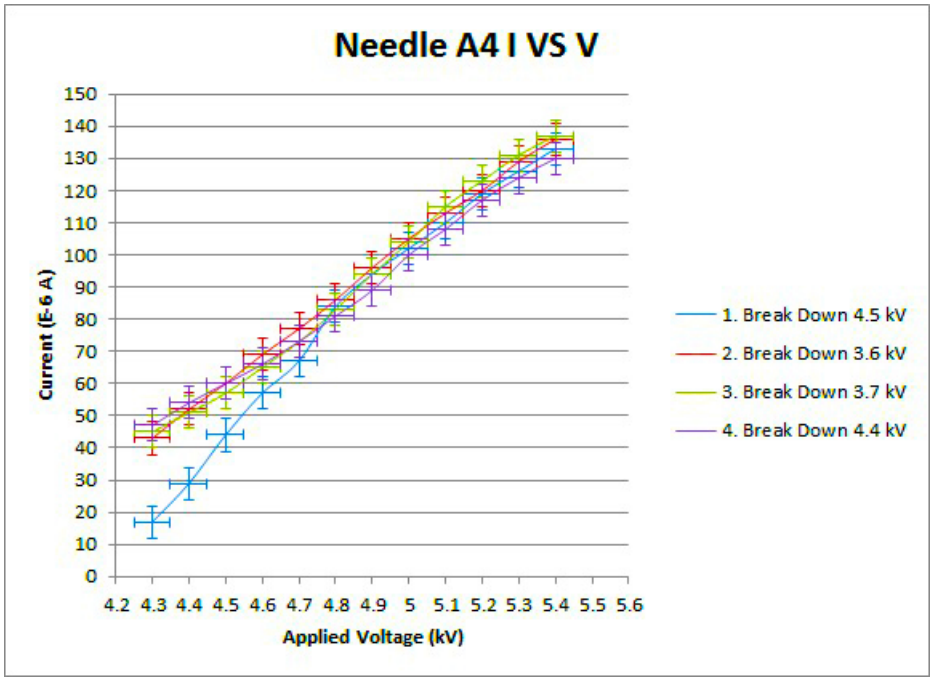


Figure 7.13: Results for needle A4 using Argon for a mass flow of 159 $\pm 25 \mu g/s$. Where possible break down voltages with uncertainty $\pm 0.1 kV$ for different trials are included.

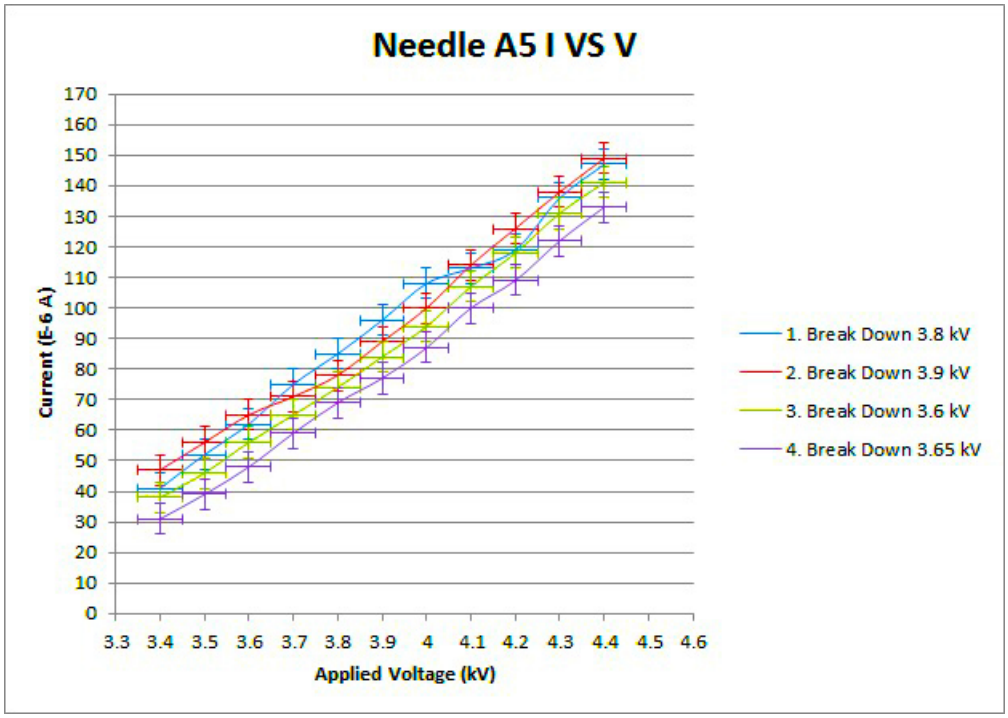


Figure 7.14: Results for needle A5 using Argon for a mass flow of 179 $\pm 28 \mu g/s$. Where possible break down voltages with uncertainty $\pm 0.1 kV$ for different trials are included.

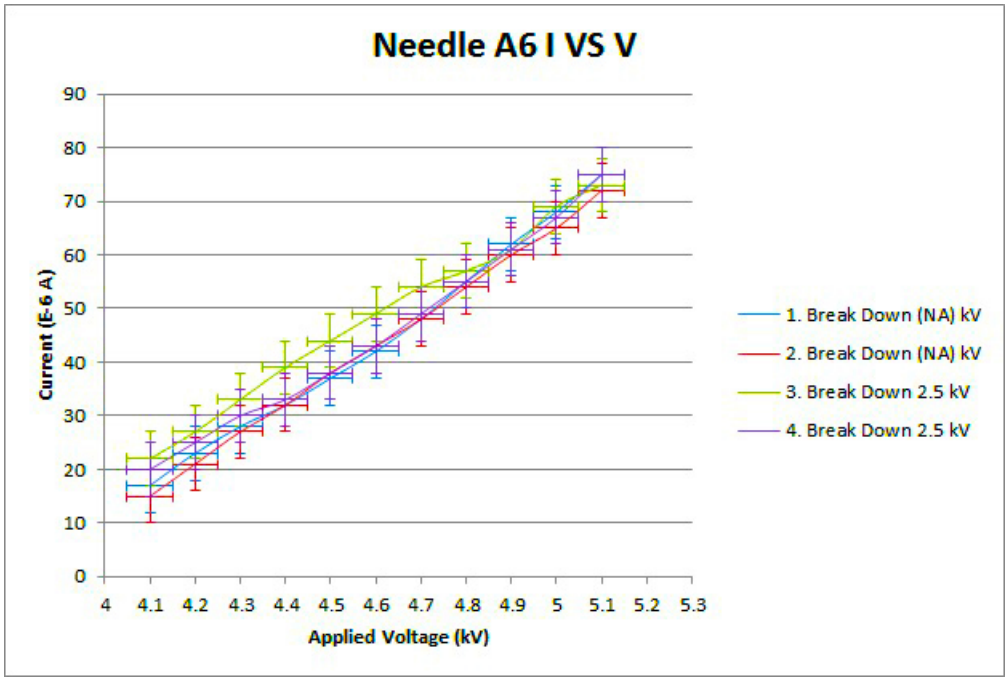


Figure 7.15: Results for needle A6 using air for a mass flow of 117 $\pm 18 \mu g/s$. Where possible break down voltages with uncertainty $\pm 0.1 kV$ for different trials are included.

7.6 Discussion and Conclusion

It should be noted that it was discovered when using needle A1 and A3 that before commencing with the experiment the needle and plate system should be brought to discharge and allowed to run for a few seconds. After doing this there was then greater repeatability in the results and the linear like behaviour as in the other needle experiments became evident. It is hypothesized that this may have had a cleaning or smoothing effect (allowing perhaps for more repeatable discharge environments around the needle tips) on the needle because as needle A3's results show after the first two trials its behaviour seemed to approach the linear behaviour of the other needles, however needle A1's behaviour still remains unclear. That said the other needles were first "cleaned" using a short lived discharge and then the experiments conducted.

From the results one aspect of the discharges observed that was unique, was that it could notably exist below the breakdown voltage. Apart from perhaps being a somewhat unique discharge type a possible reason could be that the polyethylene surrounding the needle may have had "clusters" detach or decomposed into simpler compounds and escape into the gap due to melting (either from contact with the needle's heat or plasma) as the pictures 7.16 would indicate resulting in the discharge of constituents (exited polyethylene "cluster"

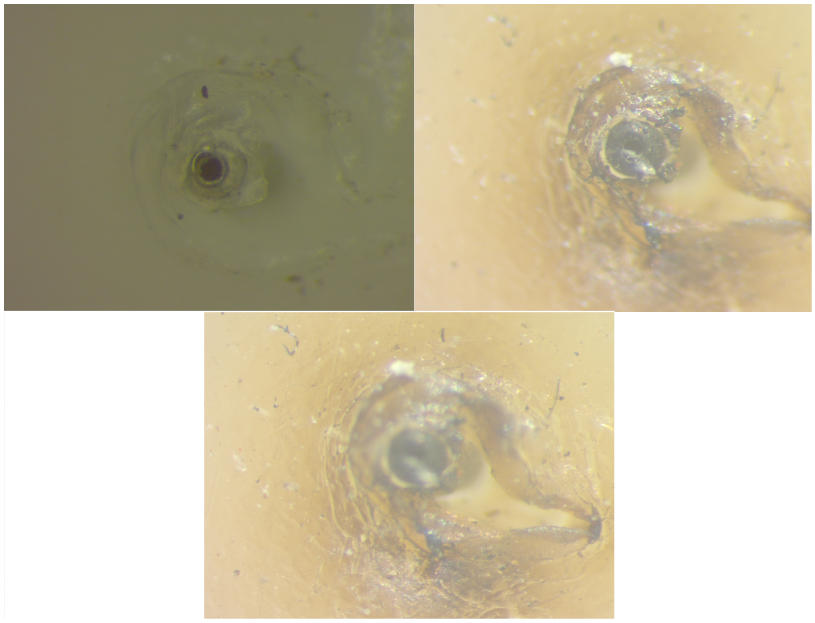


Figure 7.16: Needle A4 before the experiment on left, with after the two pictures on the right and bottom.

perhaps or simpler compounds) into the gap allowing the discharge to be sus-

tained below the breakdown voltage. Further evidence to support this assumption was found from energy dispersive spectroscopic (EDS) analysis of the needle and aluminium foil rapped around the plate which indicated that carbon atoms (probably from the polyethylene) were embedded by the discharge in the foil, see Figures 7.18 and 7.17. Aluminium foil was rapped around the plate, for each trial, in order to protect it from deposits of material generated by the plasma as well as allow study of those deposits. The observation of deposits confirmed contamination of the discharge gap as well as contamination of the steel plate in the absence of the foil. Contamination of the steel plate would have been significant due to its effect on the secondary electron emission coefficient of the plate and would certainly have effected repeatability.

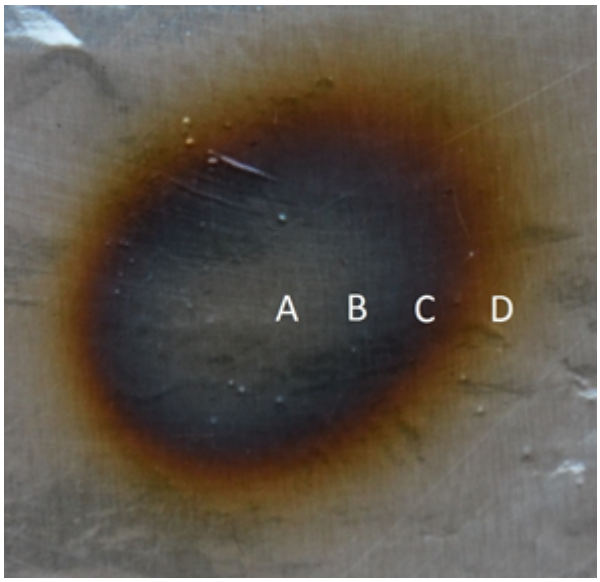


Figure 7.17: Typical residue that would be left on the plate in the absence of aluminium foil after firing. The regions A to D have been analysed under a scanning electron microscope (see Figure 7.18). The diameter of the ring is approximately 8mm. [9]

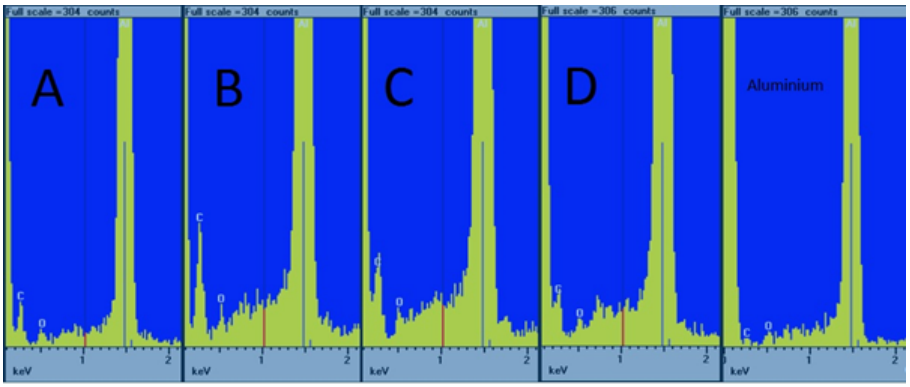


Figure 7.18: EDS spectra of the regions A to D in Figure 7.17 indicate an increased presence of carbon (peak labeled "C") when compared to aluminium outside the discharge region (far right spectrum).[9]

Alternatively it could have been the case that the needle may have been warmed enough by the current to excite large proportions of the ejected gas to lower ionization potentials. Note that the pure air study performed unfortunately did not eliminate questions regarding the effects of impurity in the Argon gas as that particular experiment did not show the same trends. And finally one must note that no ballast resistor was used for the experiment, as a result assuming that the system behaved similar to a glow discharge, it may have been the case that the system on ignition/breakdown jumped to the abnormal glow regime for which we can see, from Figure 7.1, which could allow one to apply voltages below the ignition value and observe currents.

However, the results show that for the recorded values regardless of trial the behaviour was linear (in most cases), but that there are discrepancies among ignition voltages (Break down) among trials as well as changes in the actual currents transferred. Possibly due to needle damage and surface contamination see again the Figure 7.16.

For future experiments it is recommended that the polyethylene be replaced by a medium that would not melt or evaporate during operation. Thereby avoiding contamination of the gap and needle and probably affecting the experiment and breakdown conditions, so as to determine whether the characteristics observed are independent of the polyethylene. It would also be advisable to try and keep the gas as pure as possible so as to try and make exchange reactions of negligible consequence and remove the effects of impurity in the rest gases. If possible it would be desirable to repeat the experiment using a ballast resistor so as to try and eliminate any similarity between this system and conventional DC glow systems.

Additionally it is recommended that the same experiment be repeated several times until complete destruction of the needle is observed as well as run several trials with each needle to measure the durability of the needle (to determine how many start-ups for certain periods of operation can be endured), as neither of these two experiments were performed here. Finally, although expected to be extremely difficult, it would be desirable to generate as many replications of the above study for different needles (with same conditions on the needles and flow rate conditions imposed) as possible to remove uncertainty about the breakdown conditions and shut-off conditions behaviour.

Chapter 8

Estimates and System Classification

The aim of this chapter is to provide information necessary for justifying the use of some modelling equations and strategies applied to the plasma of the CORION thruster system. It is also hoped that this chapter may serve as a future reference. To aid in this it will have to be asserted whether the plasma system can be considered classical or quantum, ideal or non-ideal (and to what degree), collisional or collision-less and if quantum whether the system is degenerate or not.

In what follows for each of the classification concerns listed above, a section on it will be laid out with the pertinent parameters introduced and estimates made for the system, near the needle exit only, with a flow rate of about order 10^{-4} g/s under the assumptions:

1. The discharge is non-neutral with an excess of electrons as based on the previous work [34, 33] assertions.

2. Non-thermal in that the electrons are believed to be at a higher temperature than the ions and neutrals (not in thermal equilibrium) based on the simulation paper's [114, 115] insight and the fact that the system is open so that even when a stationary (steady) state operation is achieved thermal equilibrium is not necessarily established.

3. Partially ionized, based on the previous work [34, 33] roughly 1% of the neutrals are ionized.

In addition to classifying the plasma system, estimates of number density, mean-free path length and Knudsen number at the needle exit will also be made for classification of the neutral gas flow system as rarefied or continuum in-order to assert whether the flow should incorporate the "slip or no-slip" boundary conditions [116, 117].

8.1 Exit Number Density

For many of the estimates an approximate upper-bound estimate for the external-system number density i.e. the needle exit and chamber volume, will be essential. This estimate could perhaps eventually be used to estimate upstream density conditions in the needle using normalized simulation data for a potentially similar system.

In-order to get an estimate of the exit density we will use the estimate for mass-flow (derived previously) rate for the small-volume flow rate experiments considered previously and justified assumptions for the speed of the flow, namely we will use

$$\dot{m}(\tau) = \frac{\mathfrak{m}}{RT} P_{atm} \dot{V}_{water}(\tau) \ , \tag{8.1}$$

where τ is any time. We use the completely tested case where the pressure difference at the device (orifice-plate) was 4.5 $mbar$ at a mass flow of order 10^{-7} kg/s and the steady state chamber pressure was at $< 10^{-4}$ $Torr$.

8.1.1 Estimating Exit Number Density

We can retrieve an estimate for the number density at the needle exit by using

$$\dot{m} = \mathfrak{m} \int_{\Sigma} n\vec{v} \cdot d\vec{A} \ , \tag{8.2}$$

where $\mathfrak{m}$ is the mass of the particle, Σ is the exit surface (a disk with no hole in the center and diameter 0.06 mm), n is the density on Σ while $\vec{v}$ is the velocity of the gas. It would be desirable to have a potential upper-bound on n, however since all details pertaining to the flow through the needle, except for mass-flow rate, are unknown [1] some assumptions will be required. As an assumption we will consider the case where

$$\dot{m} \approx \mathfrak{m} n_{ave} v_{ave} \Sigma \ , \tag{8.3}$$

where n_{ave} is the average exit number density and v_{ave} the average exit speed along the orientation of Σ (along its normal). Additionally we could assume the gas to be ideal. Due to expansion of the gas, of relevance is the case where the gas becomes rarefied (Knudsen number [2] $K_n \geq 1$) and the Mach number (Ma = speed of gas flow/speed of sound in gas) can be above or below the sonic level at the exit [118, 119] (that is subsonic or supersonic) depending on all factors that could affect the gas flow (e.g. heat, friction [120, 121]). The consequences for the number density would then follow from:

$$n_{ave} \approx \left(\frac{\dot{m}}{\mathfrak{m}}\right)\left(\frac{1}{c_{exit}\Sigma}\right)\frac{1}{Ma_{exit}} \approx \left(\frac{\dot{m}}{\mathfrak{m}}\right)\frac{1}{\Sigma\sqrt{\frac{\gamma k_B T}{\mathfrak{m}}}}\frac{1}{Ma_{exit}} \ , \tag{8.4}$$

[1] Near the completion of this thesis cold thrust measurements became available which would have helped in generating estimates however introducing this data would have delayed publication.

[2] This will be introduced at the end of this chapter.

where c_{exit} is the speed of sound of the gas at the exit and by the ideal gas assumption has the estimates $c = \sqrt{\frac{\gamma k_B T}{\mathfrak{m}}}$ [122, p. 88] where γ is the ratio of specific heats and has the approximate value of $\frac{5}{3}$ [64, p. 185] for mono-atomic gas (like Argon, which was used) while M_{exit} is the Mach number at the exit (the ratio of exit speed to speed of sound at the exit), k_B is the Boltzmann constant and T temperature of the gas. Hence from the mass flow rate of order $10^{-7}kg/s$ we would have

$$n_{ave} \approx \left[\dot{m}\left((\mathfrak{m}\gamma k_B)^{\frac{1}{2}}\,\Sigma\right)^{-1}\right]\frac{1}{Ma\sqrt{T}} \sim \frac{1}{Ma\sqrt{T}} \times O(10^{25})\ . \tag{8.5}$$

Depending on the degree of slip (or momentum accommodation) at the boundary the flow could be subsonic or supersonic, for examples view [118, 119, 117]. Based on simulation and numerical results, [118, 119], a choice on bounds for Ma_{exit} is anything of order 10^{-1} to 10^{0}. Since for Knudsen numbers greater than or equal to one (or close to it) the effects of friction and heat transferred could be to induce subsonic flow at the exit, however as long as the gas does not become very viscous the flow might not be strongly subsonic [120, 121]. Alternatively due to heat transfer and friction the exact opposite could be said and based on simulations supersonic flow can be expected at the exit [120, 121]. However no simulations were found which indicated Mach number greater than order 10^{0} in size, for which [118, 119] were used.

Consequently we have that with T of order 10^2K and considering Argon that n_{ave} is between order $10^{25}/m^3$ to $10^{24}/m^3$ number of particle for $Ma_{exit} \sim O(10^{-1})$ and $O(10^{0})$ respectively i.e. $10^{19}/cm^3$ and $10^{18}/cm^3$.

8.2 Flow Classification and micro-tube flow affecting factors

A classification of the flow is essential for proper boundary conditions or implementation of proper boundary models. The most important parameter worth estimating for a micro-thruster in-terms of flow of gas through its "tubes" is the Knudsen number K_n, which gives a system relative estimate of the degree of rarefaction in the system. It will allow one to determine whether "no-slip" $K_n << 1$ or "slip" $0.01 < K_n < 0.1$ (or also referred to as full momentum accommodation and partial accommodation)[3] boundary conditions should be investigated and applied, which will have an affect on all other flow boundary conditions [123, p. 2] . It is also essential to know K_n as it will substantiate the use of a kinetic description $K_n \geq 1$ or fluid description $K_n << 1$ [123, p. 2]. K_n is defined as

[3]No-slip boundary conditions correspond to the physical situation where a boundary layer forms next to a surface over which a gas flows that sticks to that surface (i.e. is stationary relative to the surface). The alternative being Slip conditions where the boundary layer does not stick to the surface.

follows:

$$K_n := \frac{\text{mean free path length}}{\text{characteristic system length scale}} \ , \tag{8.6}$$

where the "characteristic length scale" in the system is going to be determined by a length of the smallest geometry (geometrical shape) through which or "over" which gas flows and represents the physical scale at which the least amount of accuracy would be necessary. For us this would be the diameter or radius of the thruster nozzle (which is cylindrical in our set up and for which the diameter was 0.06 mm). An estimate for the mean-free path [64, p. 179] is given by:

$$l = \frac{1}{\sigma n} \ , \tag{8.7}$$

where σ is the effective cross-section for collision of gas atoms with one-another and where n is the number density of the gas (for which we have order of magnitude estimates). Note we can change σ and n to different values depending on what components of the gas may be colliding with what other components to get upper bounds to the mean-free path lengths. However for the plasma the Coulomb potential is long ranged and an effective cross-section, unless shielding occurs, which won't diverge cannot be given so that we can only really determine the Knudsen number for the K_n Argon atoms. In-order to not formally have to calculate the cross-section (since the next sections will show a whole range of coupling strength and appropriate potentials) we will simply use the "hard shell" approximation of the Argon atoms to calculate values for σ of the Argon atoms only, namely [124] :

$$\sigma = \frac{\pi}{4}\left[D_1 + D_2\right]^2 \ . \tag{8.8}$$

Where D_1 and D_2 are the diameters (something of an effective potential range) of the colliding particles, for Argon we would let D be two times its atomic radius. Consequently we would have:

$$K_n = \frac{1}{\sigma n R} \text{ where } R \text{ is the radius of the tube .} \tag{8.9}$$

Using the Van der Waals radius of Argon as 188 pm [125] i.e. diameter of 376 pm, and the density of Argon as of order of magnitude 10^{24} per cubic meter we have $K_n \sim O(10^{-2})$ to $O(10^{-3})$. As a result we can conclude that the flow is somewhat rarefied and we might not be able to use Navier Stoke's models without modification for Argon-Argon behaviour, we will have to use Burnett equations [126] as a possibility instead since we may be in the slip regime [123, p. 5]. Additionally appropriate slip-boundary conditions will have to be researched.

Additionally we should also address a list of flow affecting factors which would require greater investigation when building models for gas (plasma) flow in micro-tubes. What becomes of greater concern in tubes of this size scale are

axial heat conduction and heat diffusion processes, due to the increase in the ratio of surface area to volume [120]. As well as the earlier than expected onset of turbulent flow in all of these tubes, the effect of enclosure surface roughness, predominate forces at the scale of interest, surface electric charge collection and finally the compressibility effects of the gas must all be considered as well [120]. However, no data was available to address these concerns and therefore digression into these requirements was not made.

8.3 Quantum or Classical

In order for us to be able to consider the system of ions and neutrals and electrons as essentially classical, it is generally accepted that these particles rarely be found within distances of each other comparable to their respective thermal de Broglie wavelengths [76]

$$\lambda_\alpha = \frac{\hbar}{\sqrt{m_\alpha k_B T_\alpha}} \text{ where } \alpha \text{ is the species .} \tag{8.10}$$

Where $\hbar, m_\alpha, T_\alpha, k_B$ are respectively reduced Planck's constant, mass of particle species α, temperature of species α and Boltzmann's constant. Or alternatively, that the same statement holds for the de Broglie wave length $\lambda_{\alpha,\beta}$ of the interacting pair of particles α and β [127]

$$\lambda_{\alpha,\beta} = \frac{h}{\mu g_{\alpha,\beta}} \ , \tag{8.11}$$

where h, μ and $g_{\alpha,\beta}$ are Plank's constant, the effective mass of the interacting pair and the relative speed of interaction. In order to assert whether the system is classical we would then at least require that the classical distances of closest approach, the Landau lengths $(R_L)_{\alpha\beta}$, be much greater than the de Broglie lengths λ_α and $\lambda_{\alpha,\beta}$ for all species α and β [76].

The Landau-length $(R_L)_{\alpha\beta}$ for interaction between an α-species and a β-species particle [4] is defined as the distance at which the interaction energy (basically the potential energy) is the same as the (average) kinetic energy in the center of mass frame of the interacting pair, i.e. distance of closest approach [76]. This definition is general in that the species (types) of interacting particles can be different and that $(R_L)_{\alpha\beta}$ will change as the kinetic energy in the center of mass frame of the interacting pair changes.

8.3.1 Generating a relation for Landau length

In order to generate a relation for the Landau length suppose an α-particle has momentum $\vec{p}_\alpha$ and mass m_α while a β-particle has momentum $\vec{p}_\beta$ and mass m_β. When in the center of mass frame for a "collision" between the two particles they

[4] α and β are used for notation and do not refer to He_4 and e^-.

essentially behave as a single particle in the field of a potential, if the interaction between them is central, particle with reduced mass $\mu := m_\alpha m_\beta/(m_\alpha + m_\beta)$ and effective momentum [128]:

$$\vec{p}_{\alpha\beta} := \frac{m_\alpha \vec{p}_\beta}{m_\alpha + m_\beta} - \frac{m_\beta \vec{p}_\alpha}{m_\alpha + m_\beta} = \mu \vec{g} \ . \tag{8.12}$$

$\vec{g}$'s definition as the relative velocity of the pair is obvious, thus the kinetic energy of the pair in this frame follows as [128]:

$$\frac{1}{2}\mu g^2 = \frac{1}{2\mu}\left[\left(\frac{m_\alpha}{m_\alpha + m_\beta}\right)^2 p_\beta^2 + \left(\frac{m_\beta}{m_\alpha + m_\beta}\right)^2 p_\alpha^2 - \frac{2\mu}{m_\alpha + m_\beta}\vec{p}_\alpha \cdot \vec{p}_\beta\right] \ . \tag{8.13}$$

Assuming particle α's momentum's components are not correlated with particle β's momentum's components over times greater than some characteristic correlation time, we have that for a distribution of the system with a much larger characteristic time-scale of description that the expected kinetic energy then follows as

$$\langle\frac{1}{2}\mu g^2\rangle = \frac{1}{2\mu}\left[\left(\frac{m_\alpha}{m_\alpha + m_\beta}\right)^2 \langle p_\beta^2\rangle + \left(\frac{m_\beta}{m_\alpha + m_\beta}\right)^2 \langle p_\alpha^2\rangle\right] \tag{8.14}$$

$$= \left(\frac{m_\beta}{m_\alpha + m_\beta}\right)\frac{1}{2m_\alpha}\langle p_\alpha^2\rangle + \left(\frac{m_\alpha}{m_\alpha + m_\beta}\right)\frac{1}{2m_\beta}\langle p_\beta^2\rangle \ . \tag{8.15}$$

In addition if we realize that every α and β type particle may have a well defined "centred" velocity $\vec{u}$ we could write $\vec{p}_\alpha = m_\alpha\vec{u} + \vec{k}_\alpha$ and $\vec{p}_\beta = m_\beta\vec{u} + \vec{k}_\beta$ where $\vec{k}_\beta$ and $\vec{k}_\alpha$ are measured in frames of reference moving with velocities $\vec{u}$ respectively. It would then become prudent to consider the contribution to $\langle\frac{1}{2}\mu g^2\rangle$ by these "random momenta" (and requiring $\langle\vec{k}_\alpha\rangle = \langle\vec{k}_\beta\rangle = \vec{0}$), namely the terms:

$$\left(\frac{m_\alpha}{m_\alpha + m_\beta}\right)\frac{1}{2m_\beta}\langle k_\beta^2\rangle + \left(\frac{m_\beta}{m_\alpha + m_\beta}\right)\frac{1}{2m_\alpha}\langle k_\alpha^2\rangle \ , \tag{8.16}$$

and then consider an interaction not only in the center of mass frame but (for a non-relativistic system) first put in a frame moving with velocity $\vec{u}$ so that $\vec{p}'_\alpha = \vec{k}_\alpha$ and $\vec{p}'_\beta = \vec{k}_\beta$ in that frame and then switching to the center of mass frame to get:

$$\langle\frac{1}{2}\mu g^2\rangle = \left(\frac{m_\alpha}{m_\alpha + m_\beta}\right)\frac{1}{2m_\beta}\langle k_\beta^2\rangle + \left(\frac{m_\beta}{m_\alpha + m_\beta}\right)\frac{1}{2m_\alpha}\langle k_\alpha^2\rangle \ . \tag{8.17}$$

With this we would as is convention in "kinetic theory" [64, p. 161] identify

$$3k_B T_\alpha := \frac{1}{m_\alpha}\langle k_\alpha^2\rangle \text{ and } 3k_B T_\beta := \frac{1}{m_\beta}\langle k_\beta^2\rangle \ . \tag{8.18}$$

A central potential like interaction between particles [5] in the center of mass frame, takes place on a plane reducing the number of degrees of freedom from 6 to 4 (for point particles) for the equivalent problem. It will also ensure that the kinetic energy associated with one of the degrees of freedom is entirely conserved [128]. Thus only one degree of freedom will take place or actually be augmented by the interaction and consequently instead of considering the "full kinetic energy in interaction":

$$\langle \frac{1}{2}\mu g^2 \rangle = \frac{3}{2}k_B \left[\left(\frac{m_\alpha}{m_\alpha + m_\beta} \right) T_\beta + \left(\frac{m_\beta}{m_\alpha + m_\beta} \right) T_\alpha \right] := \frac{3}{2}k_B T_{\alpha\beta} \ , \tag{8.19}$$

we restrict interest to the one degree of freedom in which interaction takes place. And therefore define $(R_L)_{\alpha\beta}$ for interaction potential energy $\mathcal{U}(r)$ by the equation

$$|\mathcal{U}\left((R_L)_{\alpha\beta}\right)| = k_B T_{\alpha\beta} \ . \tag{8.20}$$

Here the only problem is a suitable choice of $\mathcal{U}(r)$ as it may have to be something of an approximation for quantum mechanical systems, as for example the interaction of a scattered electron with an atom (the quantum mechanical many particle system).

In order to find a potential candidate for $\mathcal{U}(r)$ one must develop estimates for the relative speeds of the scattering bodies prior to the event as this could have substantial effect on the approximation for $\mathcal{U}(r)$. For instance as in the cases when an atom interacts with a "fast" or "slow" electron. In the first case the atom may not be able to polarize and thus scattering will be different from the case where the atom could become polarized, due to the slowness of the electron [129, p. 60] .

Thus a digression is necessary in which estimates for the relative speed of particles have to be made to justify what approximations for $\mathcal{U}(r)$ to use in this estimate.

8.4 Expected Relative Speeds of Interaction

From the previous section we know that we can estimate the expected relative speed of interaction $g_{\alpha\beta}$ for particles of species α and β from equation 8.17, namely

$$g_{\alpha\beta} = \sqrt{\frac{3k_B T_{\alpha\beta}}{\mu}} \ , \tag{8.21}$$

where

$$T_{\alpha\beta} = \left[\left(\frac{m_\alpha}{m_\alpha + m_\beta} \right) T_\beta + \left(\frac{m_\beta}{m_\alpha + m_\beta} \right) T_\alpha \right] \ , \tag{8.22}$$

[5] An interaction depending solely on the mutual distance of separation and the only interactions to be considered in this chapter.

for which we can make some simplifying observations. For interaction between an electron and Argon ion (or Argon atom) we have that $m_{Argon} >> m_e$ (m_e is mass of electron) for which it then follows that:

$$T_{\alpha\beta} \approx T_e \text{ temperature of the electrons .} \tag{8.23}$$

While for Argon atom-atom, atom-ion and ion-ion interactions we would have that

$$T_{\alpha\beta} \approx \frac{1}{2}\left(T_\alpha + T_\beta\right) \equiv T_{ave} \ , \tag{8.24}$$

since the masses are so comparable. Hence assuming the maximum temperature of the Argon is of physical order $10^2\ K$ and the ion temperature is also of the same order due to the spectroscopic measurements made (as reported in [9]) we would have that $T_{\alpha\beta}$ for ions and neutrals be of $10^2\ K$.

While for the electrons we assume them to be of about $10^5\ K$, which is customary for low pressure processing plasma [129, p. 60] at equilibrium (that is roughly three physical orders of magnitude greater than the ions or neutrals).

From these order of magnitude assumptions we would then have for equation 8.21 that:

1. $g \approx \sqrt{\frac{3k_BT_e}{m_e}} \approx 6.743\times10^3\sqrt{T_e}(m/sK^{\frac{1}{2}}) \sim O(10^6)m/s$ for electron-atom (or ion interaction).
2. $g \approx \sqrt{\frac{3k_BT_{ave}}{m_{ion}/2}} \approx 35\sqrt{T_{ave}}(m/sK^{\frac{1}{2}}) \sim O(10^2)m/s$ for ion-ion or ion-atom interactions.
3. $g \approx \sqrt{\frac{3k_BT_{ave}}{m_{atom}/2}} \sim O(10^2)m/s$ for atom-atom interactions.

We can now shift back to making the required estimates.

8.5 Electron-Ion Interaction

For this kind of interaction it is sufficient to consider $\mathcal{U}(r)$ as the classical Coulomb potential energy for two charges $Z_\alpha e$ and $Z_\beta e$ [129, p. 57] separated by distance R_L with Coulomb constant k_e (ignoring polarization effects of the surrounding plasma), since the expected relative interaction speed estimate is non-relativistic. We have:

$$k_e\frac{|Z_\alpha|e^2}{R_L} = k_BT_e \ , \tag{8.25}$$

so that

$$R_L = |Z_\alpha|e^2\left(\frac{k_e}{k_B}\right)\frac{1}{T_e} \tag{8.26}$$

$$\approx \frac{|Z_\alpha|}{T_e}1.7\times10^{-5}(K\cdot m) \sim 10^{-11} \text{ to } 10^{-10} \ . \tag{8.27}$$

Consequently we can see that since

$$m_e T_e < m_\alpha T_\alpha \text{ for any } \alpha \ , \tag{8.28}$$

we have the de Broglie lengths $\lambda_e > \lambda_\alpha$ and can thus verify:

$$\frac{\lambda_e}{R_L} \approx \left(\frac{\hbar}{k_e |Z_\alpha| e^2} \sqrt{\frac{k_B}{m_e}} \right) \sqrt{T_e} \approx \frac{1}{|Z_\alpha|} 1.8 \times 10^{-3} \sqrt{T_e} (1/K^{\frac{1}{2}}) \tag{8.29}$$

hence

$$\frac{\lambda_e}{R_L} \sim \frac{1}{|Z_\alpha|} O\left(10^{-1}\right) \text{ to } \frac{1}{|Z_\alpha|} O\left(10^{0}\right) \ , \tag{8.30}$$

therefore quantum mechanical interaction is not negligible.

8.6 Electron-electron Interaction

This has essentially also been considered in the above derivation and therefore the same estimate holds, all that changes is $Z_\alpha \to 1$. Consequently, quantum mechanical interaction is not negligible.

8.7 Ion-Atom Interaction

Since the relative interaction speed is obviously far from relativistic and is much less than the characteristic speed of an electron in the atom, which is of order $10^6 \ m/s$ [see [129, p. 60]], the appropriate potential would be the polarization potential [130, p. 61], as the electrons in the atom will have sufficient time to respond to (polarize the atom) the ion's field. Consequently $\mathcal{U}(r)$ is of the form

$$\mathcal{U}(r) = -\frac{1}{2} k_e \left(Z_\alpha e\right)^2 \frac{\gamma}{r^4} \text{ in vacuum} \ , \tag{8.31}$$

where γ is the polarizability of the atom and $Z_\alpha e$ the charge of the ion.

Thus

$$R_L = \left[\frac{\gamma}{2} \frac{\left(Z_\alpha e\right)^2 k_e}{k_B T_{\alpha\beta}} \right]^{\frac{1}{4}} \tag{8.32}$$

$$\approx Z_\alpha^{\frac{1}{2}} \left(T_{\alpha\beta}\right)^{-\frac{1}{4}} 1.9 \times 10^{-9} (m \cdot K^{\frac{1}{4}}) \sim O(10^{-10}) m \tag{8.33}$$

for Argon $\gamma \approx 1.64 \times 10^{-30} m^3$ [130, p. 62]. For Argon atoms and ions their masses are nearly the same and by assumption their temperatures are of the same order of magnitude namely $10^2 \ K$ hence we have

$$\lambda = \frac{\hbar}{\sqrt{m_{Argon} k_B T_{Argon}}} \tag{8.34}$$

$$\approx \frac{1}{\sqrt{T}} 3.5 \times 10^{-12} (m \cdot K^{\frac{1}{2}}) \sim O(10^{-13}) m \ . \tag{8.35}$$

Thus we have $\lambda/R_L < O(10^{-3})$ at the very least and therefore there is negligible quantum mechanical coupling between ions and atoms.

8.8 Atom-atom Interaction

Before moving onto the most challenging case electron-atom interaction we will consider atom-atom interaction. Since the temperature of the gas is assumed to be of order 10^2 K and the relative interaction speed estimated to be of order 10^2 m/s. The interaction energy is estimated to be:

$$\frac{1}{2}\mu g^2 \approx \frac{1}{4} m_{atom} g^2 \sim O(10^{-2}) eV \tag{8.36}$$

where $m_{atom} \approx 39.9 au$ [13], for elastic collisions. Consequently we may consider these to be slow atomic collisions but not to slow for strong quantum mechanical interaction thus the use of an "optical potential" or effective potential is acceptable and thus it is proposed that something like the Lenard-Jones potential be used to simulate elastic collisions for large angle scattering [131] . Hence we let [132, 127]:

$$\mathcal{U}(r) = 4\epsilon \left[\left(\frac{\sigma}{r} \right)^{12} - \left(\frac{\sigma}{r} \right)^{6} \right] \tag{8.37}$$

where for Argon $\epsilon = 0.0104$ eV and $\sigma = 3.40$ $\mathring{A}$ (angstrom) [133]. Hence we have:

$$\begin{aligned} |\mathcal{U}(r)| &= k_B T_{Argon} \\ \Rightarrow |x^2 - x| &= (k_B T)/(4\epsilon) \text{ wher } x = \left(\frac{\sigma}{r} \right)^6 \\ \Rightarrow |x(x-1)| &= (k_B T)/(4\epsilon) \\ \Rightarrow x|x-1| - \mathcal{A} &= 0 \\ \Rightarrow -x(x-1) - \mathcal{A} = 0 \text{ for } x < 1 \text{ and } x(x-1) - \mathcal{A} &= 0 \text{ for } x > 1 \ . \end{aligned} \tag{8.38}$$

For which we have

$$x = \frac{1 \pm \sqrt{1 \pm 4\mathcal{A}}}{2} \ , \tag{8.39}$$

and then picking the smallest positive we would get

$$R_L = \sigma \sqrt[6]{\frac{2}{1 \mp \sqrt{1 \pm 4\mathcal{A}}}} \ , \tag{8.40}$$

since T is of order 10^2 K we have that $\mathcal{A}$ is of order 10^{-1} to 10^0 hence $1 - 4\mathcal{A}$ is not considered, however $1 + 4\mathcal{A}$ will be of order 10^0 hence $\sqrt{1 + 4\mathcal{A}}$ is either 10^0 or 10^{-1}. So that

$$\frac{2}{1 + \sqrt{1 + 4\mathcal{A}}} \ , \tag{8.41}$$

is order 10^0 or 10^{-1} if we picked $1 + \sqrt{1 + 4\mathcal{A}}$ to be of order 10^0. Consequently we consider the effect of sixth root, provided its argument is of order 10^0 its

result will stay 10^0 while if it is 10^{-1} its result will decrease. It seems that it will be order 10^0 since by assumption T is expected to be something like $273K$ to $293K$ (i.e. close to room temperature or a bit colder due to expansion of the gas). Thus we have:

$$R_L \text{ of order } 10^{-10} \text{ to } 10^{-9} \ ,$$

however $\lambda \approx 10^{-13}m$ by the previous work thus we again have $\lambda/R_L < O(10^{-3})$ at the very most and therefore negligible quantum mechanical coupling.

8.9 Electron- Atom Interaction

For this particular the speed of the electrons are estimated to be of the same order of magnitude as the characteristic speed of the orbital electrons [130] . Since the estimate for the speed is of order 10^6 m/s some degree of polarization by the atom is expected. Fortunately the energy of interaction is approximately given by $k_B T_e$ so that we can consider the energy range $k_B 1 \times 10^5$ eV to approximately $k_B 9.9 \times 10^5$ eV, which is the same as 8.6173324 eV to 85.31159076 eV for which a useful phenomenological potential is given by (units in Rydberg i.e. 13.6 eV) [134, 135, 136] :

$$V(r) = -\frac{2}{r} Z\Omega(r) - \frac{\gamma}{\left(r^2 + d^2\right)^2} \ . \tag{8.42}$$

Where Z is the nuclear charge and $\Omega(r) = \left[H(e^{r/D} - 1) + 1\right]^{-1}$ (for which $H = D(Z-1)^{0.4}$ with $D = 0.862$ for Argon), also γ is the electrostatic polarizability of Argon 11.08 a_o^3 (units in Bohr radius cubed) and $d^4 = \left(\frac{1}{2}\gamma\right) Z^{-1/3}$ [134, 135, 136]. This potential is satisfactory for the estimation of the Landau lengths, however since the potential is very non-linear solving

$$|V(R_L)| = k_B T \ , \tag{8.43}$$

for the energy limits had to be done numerically (using wxMaxima 15.08.2 software), the results were approximately 1.1 a_0 for $k_B 9.9 \times 10^5$ eV while for the lower energy limit we have 2.3 a_o for $k_B 1 \times 10^5$ eV so that we could conclude that $R_L \sim O\left(10^{-11}\right)$ to $O\left(10^{-10}\right)$ m. Hence since we have that:

$$\lambda_e = \frac{\hbar}{\sqrt{m_e k_B}} \frac{1}{\sqrt{T_e}} \approx 3 \times 10^{-8} \frac{1}{\sqrt{T_e}} \ m \cdot K^{1/2} \ , \tag{8.44}$$

we can conclude that $\lambda_e / R_L \sim O\left(10^{-1}\right)$ at worst. So that there is non-negligible quantum coupling.

8.10 Non-ideal or Ideal Characterization, Coupling strength Characterization

Although the previous sections showed that there is quantum coupling between some of the components in the system others showed potential for classical

behaviour. Therefore, in an effort to kill two birds with one stone and establish whether the system is ideal and weakly coupled or not in a classical sense we will estimate the classical coupling parameter [64, p. 88] :

$$\Gamma = \frac{E_{inter}}{E_{kin}} \ , \tag{8.45}$$

i.e. the ratio of expected interaction energy too the expected kinetic energy of the interacting pair (which for the classical case was already given a form, see equation 8.17) . If it can be established that $\Gamma << 1$ we may conclude that for the given interacting pair of interest the behaviour is ideal (collision-less) and weakly coupled [64, p. 88], while when $\Gamma \geqq 1$ it would indicate non-ideal behaviour and strong coupling [64, p. 88].

The relevance of this parameter lies in its use to justify the use of kinetic theory [6] as a tool for the modelling of a system as well as motivates the use of certain models within the kinetic theory framework to model a plasma [137] or substantiate the need for computational simulations instead [138, 139]. When the coupling parameter $\Gamma << 1$ we may use a one particle distribution equation like equation 4.8 instead of having to use the whole N-particle distribution Liouville equation 4.2.

Since we have available the interaction potential energies $\mathcal{U}(r)$ from the previous section it is sensible to use $|\mathcal{U}(r_o)|$ for the interacting energy where r_o is the expected inter-particle spacing. We can make an order of magnitude estimate for the inter-particle spacing distance using the Wigner-Seitz cell relation [139, p. 2]

$$\frac{4}{3}\pi n r_o^3 = 1 \ , \tag{8.46}$$

where n is the suitable number density of interest. Since from the mass-flow section we have estimates for the number densities (of applicability here) we can generate estimates for r_o.

In particular, since it is expected from the assumption that only about 1% of the neutrals are ionized we have that a mixture of ions and neutrals or electrons and neutrals with densities of orders of magnitude 10^{25} to 10^{24} particles per cubic meter will produce densities of the ions and electrons of 10^{23} or 10^{22} particles per cubic meter (two orders less since only 1% of neutrals ionized). Consequently estimates for the order of expected inter-particle distances are:

1. neutral-neutral, ion-neutral and electron-neutral:

$$r_o \sim \left(\frac{3}{4\pi n}\right)^{\frac{1}{3}} \sim 0.62 \times O(10^{25})^{-\frac{1}{3}} \text{ to } 0.62 \times O(10^{24})^{-\frac{1}{3}} \tag{8.47}$$

[6] For systems that are weakly coupled the use of one particle distributions (and perturbations of them) introduced in previous chapters for their descriptions is completely valid and Kinetic theory is thus formulated around this criteria.

hence

$$r_o \sim O(10^{-9}) \text{ to } O(10^{-8})m \tag{8.48}$$

2. ion-ion, ion-electron and electron-electron:

$$r_o \sim \left(\frac{3}{4\pi n}\right)^{\frac{1}{3}} \sim 0.62 \times O(10^{23})^{-\frac{1}{3}} \text{ to } 0.62 \times O(10^{22})^{-\frac{1}{3}} \tag{8.49}$$

hence

$$r_o \sim O(10^{-8})m \tag{8.50}$$

8.10.1 Electron-electron Interaction

Here $\mathcal{U}(r)$ is the Coulomb potential interaction and thus (we are ignoring polarization effects by the surrounding plasma i.e. using vacuum value):

$$\Gamma_{ee} = e^2 \left(\frac{k_e}{k_B}\right) \frac{1}{r_o T_e} \tag{8.51}$$

$$\approx 1.671 \times 10^{-5} \frac{1}{r_o T_e} (m \cdot K) \tag{8.52}$$

$$\sim O(10^{-3}) \text{ worst case } O(10^{-2}) \ , \tag{8.53}$$

since $E_{kin} = k_B T_{\alpha\beta}$, hence weakly non-ideal with non-negligible coupling and thus non-ideal behaviour must be taken into account.

8.10.2 Electron-ion Interaction

Here again we use the same potential :

$$\Gamma_{ei} = |Z_\alpha| e^2 \left(\frac{k_e}{k_B}\right) \frac{1}{r_o T_e} \sim O(10^{-3}) \text{ to } O(10^{-2}) \ , \tag{8.54}$$

but with, $T_{\alpha\beta} \approx T_e$ and where z_α is the multiple of charge, thus the same conclusions can be made. (note we are ignoring polarization effects by surrounding plasma)

8.10.3 Ion-ion Interaction

Here $T_{\alpha\beta}$ is the temperature of the ions i.e. $T_{\alpha\beta} \sim O(10^2)K$ but the potential is essentially of the same form hence:

$$\Gamma_{ei} = |Z_\alpha Z_\beta| e^2 \left(\frac{k_e}{k_B}\right) \frac{1}{r_o T_{\alpha\beta}} \sim O(10^{-1}) \text{ to } O(10^1) \ . \tag{8.55}$$

Thus the ions are non-ideal and strongly coupled. It should be noted that if polarization of the surrounding plasma is taken into account it would reduce the value of $k_e = 1/(4\pi\epsilon)$ where ϵ is the permittivity of the medium. It was avoided here since a description at a scale only two orders of magnitude greater than the

inter-particle spacing was required. Additionally it was not known whether at this scale, spatial correlation effects on permittivity would change smoothly so that introducing polarization effects into the estimates could undermine their validity by inappropriately motivating characterization as ideal.

8.10.4 Ion-atom Interaction

As before we use (assuming relative permittivity equal to one i.e. vacuum value):

$$|\mathcal{U}(r)| = \frac{1}{2}k_e|Z_\alpha|^2e^2\frac{\gamma}{r^4} \ , \tag{8.56}$$

hence we have

$$\Gamma_{ia} = \frac{\gamma}{2}\left(\frac{k_e}{k_B}\right)|Z_\alpha|^2e^2\frac{1}{r_o^4T_{\alpha\beta}} \approx |Z_\alpha|^2 1.4\times10^{-35}\frac{1}{r_o^4T_{\alpha\beta}} \sim O(10^{-1}) \ , \tag{8.57}$$

with $T_{\alpha\beta} \sim O(10^2)K$. So that we would then conclude weakly non-ideal with non-negligible coupling, thus further research into modelling approaches is necessary with the possibility of needing a computer simulation of this aspect of the system requiring interest.

8.10.5 Atom-atom Interaction

As before we use (ignoring polarization effects):

$$|\mathcal{U}(r)| = \left|4\epsilon\left[\left(\frac{\sigma}{r}\right)^{12} - \left(\frac{\sigma}{r}\right)^{6}\right]\right| \ , \tag{8.58}$$

$\epsilon = 0.0104\ eV$ [133] and $\sigma = 3.40\ \mathring{A}$ [133] . Hence with $k_B = 8.6173324\times10^{-5}\ eV/K$ [140] :

$$\begin{aligned}\Gamma_{aa} = \left|4\epsilon\left[\frac{\sigma^{12}}{r_o^{12}k_BT} - \frac{\sigma^{6}}{r_o^{6}k_BT}\right]\right| &\approx \left|4.83\times10^2\left[\frac{\sigma^{12}}{r_o^{12}} - \frac{\sigma^{6}}{r_o^{6}}\right]\frac{1}{T}\right| \\ &\sim \left|4.83\times10^2\left[O(10^{-12}) - O(10^{-6})\right]\frac{1}{T}\right| \\ &\sim 4.83\times10^2O(10^{-6})\frac{1}{T} \\ &\sim O(10^{-4})\frac{1}{T} \sim O(10^{-6}) \ .\end{aligned} \tag{8.59}$$

Thus ideal and weakly coupled.

8.10.6 Electron-atom Interaction

We will as before use the potential:

$$V(r) = -\frac{2}{r}Z\Omega(r) - \frac{\gamma}{\left(r^2+d^2\right)^2} \ . \tag{8.60}$$

Due to its form the coupling parameter was calculated for a range of distances and kinetic energy values, fortunately it was inferred from a graph using the graphing function in wxMaxima 15.08.2 that the worst case estimate was atleast $\Gamma_{ea} \sim O\left(10^{-13}\right)$. So that the coupling is very weak and kinetic theory, depending on the time-scales involved, could be implemented if the requirement for classical treatment had been met.

8.11 Degeneracy of electrons

Since it has been established that the electrons have non-negligible quantum mechanical interaction with each other and the other constituents, it is important to assert what statistics should be used. (i.e. include spin effects or not). That is determine whether the system is degenerate or not. To establish whether the system is non-degenerate all that is required is to verify that [139, p. 2] :

$$n_e \lambda_e^3 << 1 \ , \tag{8.61}$$

which clearly holds since λ_e is $O(10^{-10})$ to $O(10^{-11})$ and n_e (electron density) is $O(10^{23})$ to $O(10^{22})$ so that the results easily holds. In addition the degeneration parameter appropriate to application in this scenario [139, p. 2]

$$\xi = \frac{\varepsilon_F}{T} \text{ where } T \text{ is in } eV \ , \tag{8.62}$$

$$\varepsilon_F = \frac{\left(3\pi^2 n_e\right)^{\frac{2}{3}} \hbar^2}{2m_e} \ , \tag{8.63}$$

where ε_F is the Fermi energy of the electrons, is also much less than unity justifying classical Boltzmann statistics.[7]

8.12 Quantum coupling for electrons

This is necessary to establish whether quantum coupling between electrons and essentially ions and neutrals is weak or not i.e. determine whether the system is quantum mechanically ideal and weakly coupled. To do this we compute the quantum version of Γ, Γ^q defined as the ratio of expected interaction energy to the Fermi energy of the electrons in our case [139, p. 3] (but would usually use the quantum equivalent of expected kinetic energy). Note that a general choice for expected quantum kinetic energy exists see [101, p. 16], however it would introduce undue complexity into the estimation of the coupling parameter for our purposes. We expect the electrons to be the main contributors to the kinetic energy due to their small mass. Thus the Fermi energy will be a very good basis for a kinetic energy estimate, since if we have weak coupling for it, we will definitely have weak coupling for greater kinetic energies at higher

[7] The conversion between K Kelvin and eV Electron Volt is given approximately by $1/k_B(eV) \equiv 11604.5(K)$.

temperatures for a given potential energy. Thus we perform estimates for the electron-electron, electron-ion and electron-neutral interactions (the different potentials) as the condition for classical treatment of the electrons was not met. As before $\Gamma^q << 1$ would imply a quantum kinetic description or use of a one particle distribution equation such as equation 5.28 instead of the full equation 5.21 or 5.22.

electron-electron Using the Coulomb potential from the previous sections we would essentially have

$$\Gamma^q_{ee} \approx k_e e^2 n_e^{\frac{1}{3}} / \varepsilon_F = \frac{k_e e^2 \left(3\pi^2\right)^{\frac{2}{3}} \hbar^2}{2m_e} n_e^{-\frac{1}{3}} << 1 \tag{8.64}$$

hence negligible quantum coupling and therefore quantum kinetic theory is applicable.

electron-ion Essentially we have

$$\Gamma^q_{ei} = |Z_\alpha| \Gamma^q_{ee} \tag{8.65}$$

so that the same conclusions could be made.

electron-atom We use the same interaction potential as previously but due to its form the worst case estimate of coupling parameter was calculated using Maxima to be $\Gamma^q_{ea} \sim O\left(10^{-4}\right)$. So that the system is very weakly quantum coupled with the application of quantum kinetic theory being acceptable.

8.13 Plasma Parameters

Although the parameters mentioned in previous sections are essential to characterization of the system, additional parameters such as collision frequency and mean free paths specific to particular collisions provide information about time and length scales in the system. Additional parameters specific to characterization of classical plasma, such as Debye length, will also be introduced and their importance explained.

8.13.1 Collision Frequency and mean free path length

In a system of colliding particles of type a and b the frequency with which a-particles collide with b-particles, by means of a particular collision process i, is estimated by [141]:

$$\nu^i_{ab} = n_b g \sigma^i_{ab}, \tag{8.66}$$

where σ^i_{ab} is the collision cross-section for process i and n_b is the number density of the b-particles. g is the speed of interaction. If Λ denotes the index set of all

collision processes i of a-particles with b-particles the total collision frequency of a-particles with b-particles is given by [141]:

$$\nu_{ab} = n_b g \sum_{i}^{\Lambda} \sigma_{ab}^{i}. \tag{8.67}$$

In addition if there are more than one type/species of b-particles the total collision frequency of a-particles with all b-particles is:

$$\nu_a = \sum_b \nu_{ab}. \tag{8.68}$$

Dependent on the total collision frequency is the mean free path length of a-particles between collisions l_a, defined by [141]:

$$l_a = \frac{g}{\nu_a} = \frac{g}{\sum_b \nu_{ab}} = \frac{g}{\sum_b \sum_i^{\Lambda} \nu_{ab}^{i}} \ , \tag{8.69}$$

that can be approximately decomposed into the mean free path lengths associated with different collision processes i using [141]:

$$l_a^i \approx \left(\frac{\nu_a}{\nu_a^i} \right)^{\frac{1}{2}} l_a \ , \tag{8.70}$$

where i represents a particular collision process. Before estimating the collision frequency and mean free path length of the respective processes and particles in the plasma it is worth noting that non-elastic collisions between heavy particles (Argon atoms and Argon ions) may provisionally be ignored provided that the *"non-adiabatic condition"* is not met [141]. The *"non adiabatic condition"* approximately asserts that cross-sections of non-elastic collisions, between heavy particles, resulting in a change of electronic internal energy $\Delta\epsilon$ become comparable to, the usually larger, elastic cross-sections when [141]:

$$\frac{a\Delta\epsilon}{hg} \lesssim 1 \ , \tag{8.71}$$

holds. a is the range of interaction between the particles, g the relative speed of interaction and h Plank's constant. If we consider Argon atom and ion collisions with an interaction range of order $O(10^{-10})$ m and use an interaction speed of order $O(10^2)$ m/s (from the previous sections) we find that $\Delta\epsilon \lesssim 0.0007$ eV must be satisfied for the *"non adiabatic condition"* to hold. Fortunately the interaction energy of Argon atom and ion collisions is of order $O(10^{-2})$ eV and we may therefore provisionally ignore the non-elastic collisions in the estimation of collision frequency and mean free path length.

Without going into the details, the collisions frequency and mean free paths for certain collision processes is summarized in Table 8.1. From Table 8.1 it is seen that the greatest collision frequency is determined by elastic collisions

Species	$\frac{1}{2}\mu g^2$ (eV)	g (m/s)	Cross-section Type	σ (m^2)	ν (Hz)	l (m)
e vs e	8.617	10^6	Energy average momentum transfer [141]	3.37×10^{-19}	3.37×10^{10}	3.45×10^{-7}
e vs A^+	8.617	10^6	Energy average momentum transfer [141]	3.37×10^{-19}	3.37×10^{10}	3.45×10^{-7}
e vs A	8.617	10^6	Elastic σ [a]	2.48×10^{-17}	2.48×10^{14}	4.02×10^{-9}
e vs A	8.617	10^6	Inelastic σ (upper bound) [142, 143, 144]	$O(10^{-19})$	$O(10^{12})$	$O(10^{-8})$
e vs A	8.617	10^6	Inelastic σ (lower bound) [142, 143, 144]	$O(10^{-21})$	$O(10^{10})$	$O(10^{-7})$
A vs A	0.01	10^2	Rigid sphere collision model	4×10^{-19}	4×10^8	3×10^{-9}
A vs A^+	0.01	10^2	Viscosity σ [141]	1×10^{-14}	1×10^{11}	2×10^{-10}
A vs e	8.617	10^6	Elastic σ	2.48×10^{-17}	2.48×10^{12}	3.91×10^{-11}
A vs e	8.617	10^6	Inelastic σ (upper bound) [142, 143, 144]	$O(10^{-19})$	$O(10^{10})$	$O(10^{-10})$
A vs e	8.617	10^6	Inelastic σ (lower bound) [142, 143, 144]	$O(10^{-21})$	$O(10^8)$	$O(10^{-9})$
A^+ vs A^+	0.01	10^2	Momentum transfer σ [141]	3×10^{-17}	3×10^8	2×10^{-9}
A^+ vs e	8.617	10^6	Energy average momentum transfer [141]	3.37×10^{-19}	3.37×10^{10}	1.45×10^{-10}
A^+ vs A	0.01	10^2	Viscosity σ [141]	1×10^{-14}	1×10^{13}	7×10^{-12}

Table 8.1: Summary of system cross-sections, collision frequencies and mean-free path lengths.

[a] The cross-section was calculated using the potential introduced previously and using the technique outlined in [134].

between electrons and Argon atoms with the viscosity cross-section collision frequency between Argon atoms and ions an order of magnitude less. The smallest mean free path length however is determined by Argon ion and atom collisions with Argon atom and electron collisions being an order of magnitude greater. The large collision frequency between Argon ions and atoms in conjunction with the corresponding mean free path length support the previous estimates establishing that ions and atoms interact strongly. In addition the Debye length of the electrons is estimated to be 7×10^{-8} m [141] thereby asserting that each electron's effective range of interaction is approximately an order of magnitude less than the mean free path between electron collisions. Thus, further justifying the assertions previously that electrons are weakly coupled. The impact parameter of the electron is estimated to be 5.6×10^{-11} m such that the Debye logarithm follows as $7.1 > 1$ which indicates that electrons collectively shield one another [141]. Finally the ratio of electron-electron and electron-Argon collision frequency ν_{ee}/ν_{ea} is of $O(10^{-4})$ and therefore the system is weakly ionized [145].

Chapter 9

Modelling Approach and Difficulties

This chapter essentially serves as a discussion and part of the conclusion of the dissertation. In this chapter a proposed approach and formalism to modelling the CORION like system encountered in chapter 7 will be outlined. Contact is made with the estimates calculated in chapter 8 and the non-equilibrium statistical mechanics introduced in chapters 4 and 5 in order to substantiate the proposed modelling strategy. Difficulties in trying to simulate and model the system, in order to estimate the thrust, will be outlined and discussed as well.

The chapter begins with a short introduction to the Classical Theory of Irreversible Thermodynamics (CTIT). It is presented here as it (or potential generalizations of it) will be proposed to be used as a formalism for modelling the solid components in the system.

Following the introduction to CTIT will be a section on the presentation of a proposed modelling strategy represented in Figure 9.1. In this section the modelling approach will be broken down into component parts and reasons with justification given for the modelling choices. It will however transpire that additional research will be necessary.

The chapter concludes with discussion of boundary conditions and behaviour and the need for more research in the area of surface science. The effects of chapter eight's system classification and parameter estimations on choice of modelling strategy will be discussed and summarized as well.

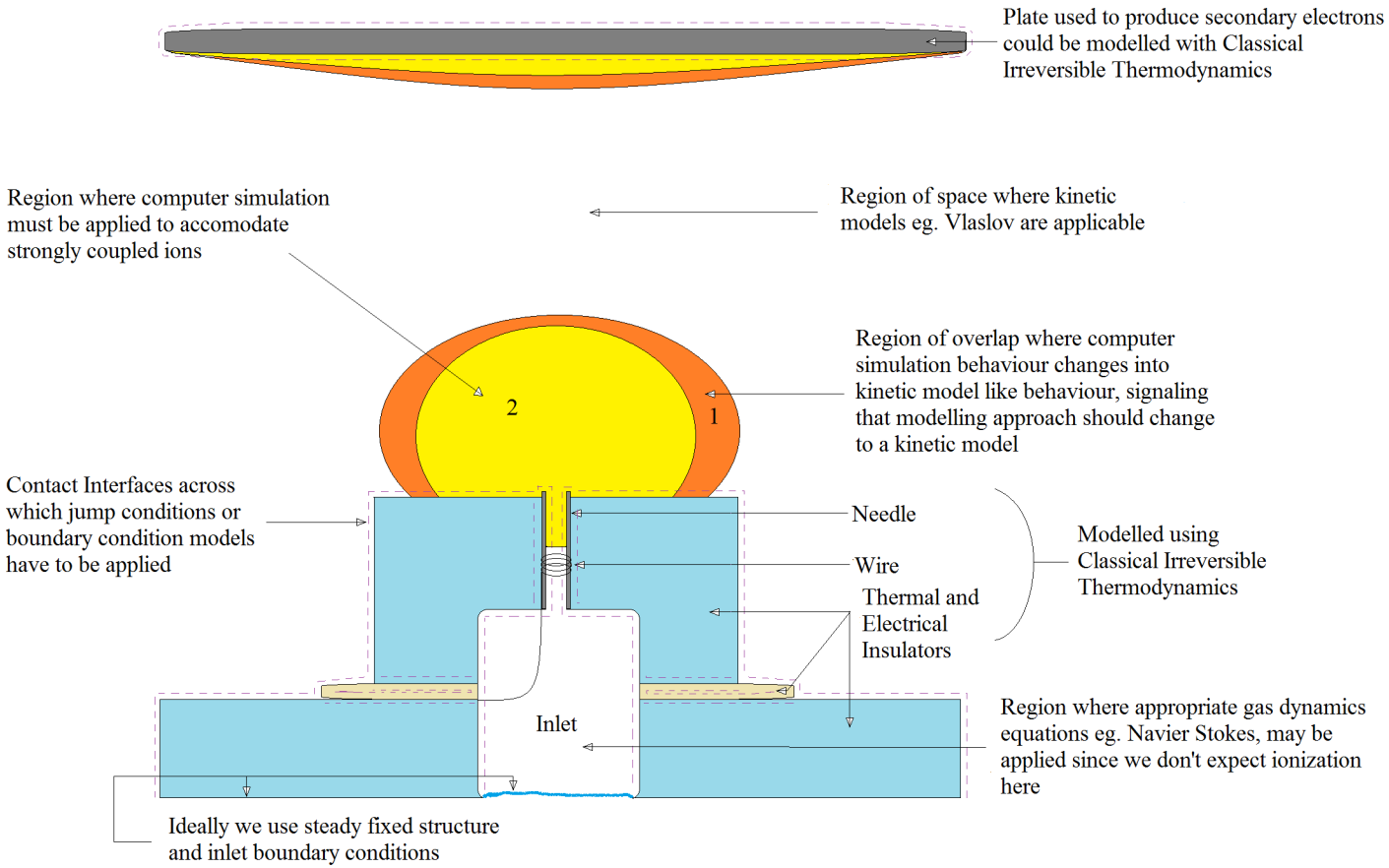


Figure 9.1: A diagram showing how the system could be modelled using different modelling techniques in different regions of space where they are most applicable.

9.1 Note on CTIT models and Boundary Jump Conditions

CTIT (Classical Theory of Irreversible Thermodynamics) essentially constitutes the formalism used to manufacture transport equations (and models) for a system from the primary assumption (since there are a few more) that large systems are in "local thermodynamic equilibrium" or alternatively worded "*the local and instantaneous relations between thermodynamic quantities in a system out of equilibrium are the same as for a uniform system in equilibrium*" [146]. A vast amount of literature surrounds this approach, extensions and generalizations of it [147, 148, 149, 10]. Generic forms for conservation equations are similar to those presented in chapter four on classical non-equilibrium statistical mechanics. Namely, if we have a system consisting of multiple species with index $i \in S$ to indicate a member of the set of species S [150, 151] we will have:

Mass density transport

$$\frac{\partial \rho_i}{\partial t} = -\nabla \cdot (\rho_i \vec{v}_i) + \sum_{j=1}^{S} \nu_{ij} \mathcal{J}_j \tag{9.1}$$

where the terms $\nu_{ij}\mathcal{J}_j$ are production terms for mass of species I generated from potential coupling with the other species (denoted by j).

Momentum density transport When the total density of the system is conserved (and denoted by ρ) and we have defined the barycentric velocity $\vec{v}$ we then have that:

$$\frac{\partial \rho \vec{v}}{\partial t} = -\nabla \cdot \left(\rho \overline{\overline{vv}} + \overline{\overline{\sigma}} \right) + \sum_{j}^{S} \rho_j \vec{F}_j \tag{9.2}$$

where $\overline{\overline{\sigma}}$ is an applied stress and $\rho_j \vec{F}_j$ is an applied force density, while ρ is the whole system's mass density.

Energy density transport The conservation of kinetic energy density $\frac{1}{2}\rho v^2$ and potential ϕ energy density :

$$\frac{\partial}{\partial t}\left(\frac{1}{2}\rho v^2 + \phi\right) = -\nabla \cdot \left(\rho \left(\frac{1}{2} v^2 + \phi \right) \overline{\overline{\sigma}} \cdot \vec{v} + \sum_i \phi_i \vec{J}_i \right) + \overline{\overline{\sigma}} : \nabla \vec{v} - \sum_i \vec{J}_i \cdot \vec{F}_i \tag{9.3}$$

where $\vec{J}_i$ is an applied energy flux and the : means take (appropriate) product and then take the trace (or in other-words a double contraction of the tensor product $\overline{\overline{\sigma}} \otimes \nabla \vec{v}$).

The method used to manufacture these equations is generic and the steps involved can be outlined. What follows here are the steps used to derive conservation equations using the CTIT hypothesis and the thermodynamic laws, note that the following follows from [152].

Step 1 Choose the state variables that will be used to model the systems. According to the local thermodynamic equilibrium hypothesis these variables will be determined by the ensemble of extensive thermodynamic variables appearing in the (local form of) Gibb's equation and the "velocity" at which these variables are transported [152]. These will often be the variables we are interested in measuring i.e. mass density, momentum density and energy density.

Step 2 Assume that the equations determining the evolution of the state variables are determined by balance equations appropriate for their type of variable. In other words if the state variable is a scalar the balance equation will be that for a scalar function while when dealing with a vector or tensor it will be the appropriate equation. See [152] for examples of the equations considered as admissible and the generic conservation equations listed above.

Step 3 Assume that the local source of entropy production σ_s is greater than zero (for irreversible processes) and use the evolution equations from step 2 and the Gibb's equation to determine the form of the source of entropy production. In general one will end up with it consisting of a sum of products of so called thermodynamic fluxes J_i and thermodynamic forces X_i [152]

$$\sigma_s = \sum_i J_i X_i \ . \tag{9.4}$$

The thermodynamic forces are normally associated with gradients of the intensive state variables while the fluxes are associated with fluxes of the extensive ones like fluxes of energy, momentum and mass [152].

Step 4 Assume, based on observation for many systems, that the thermodynamic fluxes are linearly dependent on the thermodynamic forces [152]i.e.

$$J_i = \sum_j L_{ij} X_j \ . \tag{9.5}$$

These flux-force relations are called phenomenological or constitutive equations or relations and express the relation between cause and effect [152].

Step 5 Use material symmetry or Curie's law to reduce the number of thermodynamic forces coupled to the respective thermodynamic fluxes from the previous step [152]. In actuality one is applying representation theorems of isotropic tensors and the main rule here is that depending on what kind of tensor a particular flux is, it can only be manufactured out of similar tensors and it is forbidden to couple fluxes and forces of different tensorial character [152].

Step 6 Impose restrictions on the signs of the constitutive coefficients L_{ij} such that the source of entropy production remains greater than or equal to zero. Consequently from algebraic arguments it follows that the following conditions must be met [152]:

1. $L_{ii} \geq 0$
2. $L_{ii}L_{jj} \geq \frac{1}{4}\left(L_{ij} + L_{ji}\right)^2$

Step 7 Apply the Onsager-Casimir's reciprocal relations appropriate to the setting being considered to establish restrictions on L_{ij} due to time reversal behaviour. See [152] for more on this.

The difficulty with applying CTIT is that in many cases physically different systems will share a "contact interface" through which and along which transport properties will be transferred, like when a gas is in contact with a solid there will have to be some kind of interface forming through which heat could as an example be transferred (see Figure 9.2 p. 132).

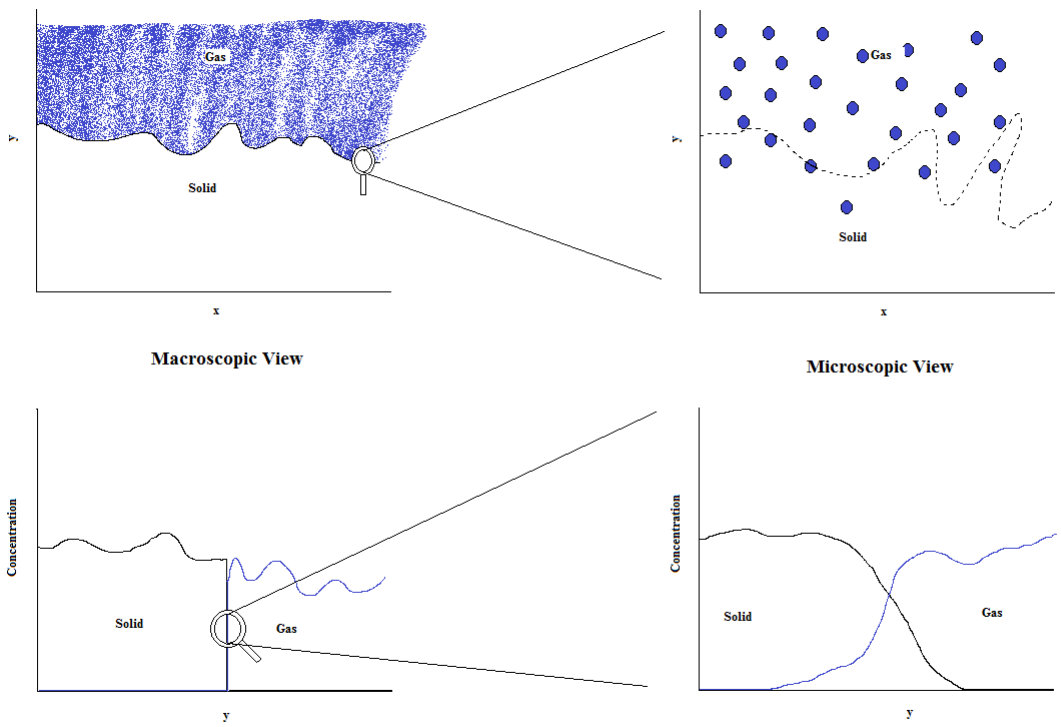


Figure 9.2: A diagram illustrating how the macroscopic view could contain microscopic information about the interface.

In general the contact interface of two physical systems (as in Figure 9.2) or multiple systems in physical contact is defined by the modeller, mathematically [49] , and is therefore not necessarily uniquely defined for a system, but is normally on a microscopic scale a system in itself consisting of constituents from all systems in contact as in Figure 9.2. As a result even when a macroscopic description of the overall system is being made and the thickness of the contact interface at the length scale of the description shrinks to an infinitesimally small quantity (i.e. becomes a surface see Figure 9.2) this should not necessarily be ignored and in practice transport and conservation equations for the interface are also derived (usually using distributions to handle the fact that the quantities of interest are restricted to a surface). The upside to this approach is that the boundaries/contact interfaces have their own transport and conservation equations and thus allows one to consistently model the whole system as well as model the transport phenomena along or through the interface [50] .

The downside is that one must develop transport equations for the interface which can be very challenging depending on how the interface has been defined and how well such a system is actually understood within the CTIT frame work.

Regardless of the difficulties encountered, for systems where such an approach is permissible the value of the information provided usually trumps the practical disadvantages. This is particularly the case in fuel cell research where transport along interfaces can explain electric charge or energy transfer [51, 52] .

The interested reader is strongly advised to consult the given references, since a detailed study is beyond the scope of this dissertation.

9.2 Modelling Approach

In this section an approach or strategy to modelling the entire discharge, gas flow and solid body thrust system for a slightly more ideal system than that considered in chapter 7 will be introduced. The idealization is introduced primarily to get around the fact that it was observed in chapter 7 that the polyethylene melted around the needle of the CORION like system and may have contaminated the gap of the discharge. Thus we instead consider the system to behave as that of Figure 9.1 (p. 128) with the idealization that material surrounding the needle does not melt, evaporate or separate in any way.

In what follows we present further justification for the modelling approach presented in Figure 9.1. Further modelling concerns associated with the characterization estimates generated in chapter 8 and boundary conditions will be addressed with independent sections at the end of this section. It should be understood that Figure 9.1 essentially summarizes the author's opinion on an approach to modelling the system. It is based on the decomposition of modelling non-equilibrium systems outlined in Figure 9.3, for which all previous chapters

have been presented to aid justification.

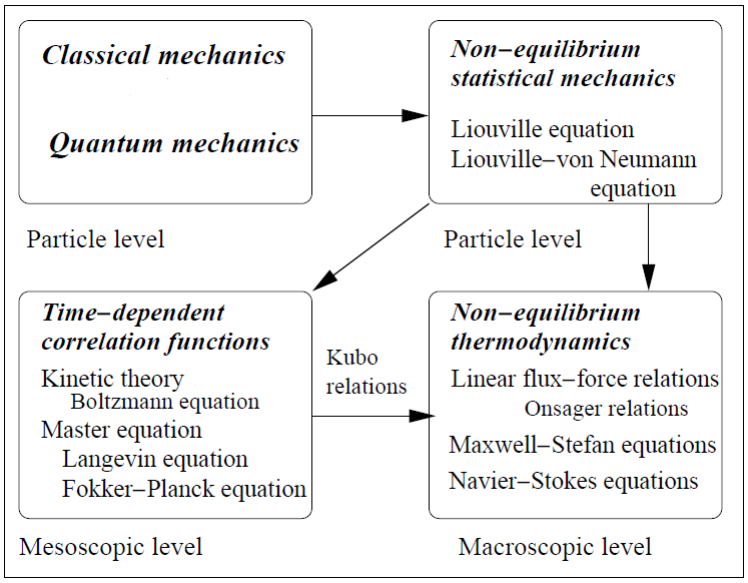


Figure 9.3: A diagram illustrating different non-equilibrium modelling approaches at varying physical scales, modified from [10, p. 5].

Gas Flow Leading into the Needle

For gas flow leading into the needle (see Figure 9.1 p. 128) it is assumed that an appropriate fluid model can be applied to model gas flow there. This assumption is based on the estimate of Knudsen number, from chapter 8, at the needle exit, which indicated gas flow would (ignoring all other components of the discharge and plasma) be effectively modelled by some kind of fluid model with appropriate slip boundary conditions. Since the gas at the needle exit is more rarefied than that of the gas upstream, due to expansion, the resulting estimate of Knudsen number as we move upstream would improve justification for a fluid description. In addition ionization may not extend all the way down the needle and into its inlet chamber thus implementing a fluid description would be further justified.

Gas Flow and Discharge System (orange (1) and yellow (2) areas in Figure 9.1)

The methods to be used for modelling the gas, ions and electrons will primarily be those of non-equilibrium statistical mechanics, both classical and quantum as previously introduced. For the classical formulation use of the Liouville equation 4.2 will be made while for the quantum formulation use of the Phase-Space

quantum mechanical equations 5.21 and 5.22 will be made. In each case the equations will generate phase-space density distribution for the system which could be used to estimate transport momenta like mass, momentum and energy.

In addition based on the characterization of the system performed earlier it will become clear (see later sections) why a formalism based entirely on conservation equations for the system would not be viable and why simulation (since analytic expressions would also be difficult to produce) of at least the one-particle distributions would be critical to accurately estimating the thrust. In particular the yellow areas in Figure 9.1 represent regions where strong coupling is expected to occur and would thus potentially require computer simulation, of equations 4.2 and 5.21 or 5.22, as a one-particle distribution kinetic equation (such as equations 5.28 and 4.8) would not be able to take all necessary correlations characteristic of strongly coupled systems into consideration [68]. From this simulation one would then have to "sample" the appropriate one-particle distributions so that estimation of the thrust would be possible. As a note the area near the plate is assumed to require computer simulation as ions will be accelerated to the plate and collect there as well as generate secondary electrons, thus potentially creating a strongly coupled system but would require more research to assert with certainty.

The orange regions indicate transitional regions where a computer simulation may become impractical and inefficient due to weakening of coupling (decrease in coupling parameter values, see equation 8.45), and as a proposal would have to be "merged" with the use of a kinetic theory (one particle distribution equations such as equations 5.28 and 4.8) based approaches in those same areas which will become more practical. It is hypothesized that such an approach may become necessary as the neutral gas in the plasma would continue to expand into the vacuum, with the ions and electrons behaving in a similar way, resulting in a weakening of coupling thereby justifying the transition to a Kinetic description. It was not known by the author what simulation and kinetic theory approaches would be acceptable for the situation as more research was required. In addition determining how boundary conditions and error propagation would have to be merged and transferred between the different descriptions will require further research.

Plasma Area Between Yellow (2) and Orange (1) Areas in Figure 9.1

The area between the yellow and orange areas will be assumed to be modelled by classical kinetic equations for gas flow and plasma. The proposal is based on the knowledge that the gas will continue to expand into the vacuum and become more rarefied (low density), with the assumption that the ions and electrons would be of low density relative to the neutrals in that area and therefore all constituents of the plasma weakly coupled (as supported by [33]). Literature review indicated many potential candidates for modelling equations (see [**?**] as an example), however a critical variable of the system to know in this area will

be the degree of ionization. It is assumed that the system may be weakly ionized in this region but experimentation will be necessary to confirm.

Rigid and Solid Structures

Although polyethylene structures in the actual thruster melted and evaporated next to the needle (see chapter 7), in order to assert whether this system could produce thrust without the polyethylene it would be necessary to remove this behaviour in a simulation or model. Thus the actual needle and remainder of the thruster system (thrust stand, wires etc...) will be assumed to be modelled by some idealized system where the behaviour of the polyethylene is absent. The chosen mathematical framework for modelling will be conservation equations with appropriate transport equations similar to those in continuum mechanics or CTIT (see Figure 9.1 p. 128 and section 9.1). We justify this by assuming that the currents drawn and temperatures experienced (or assumed to be experienced) would not be to excessive for these idealized systems to be far from behaviour justifying the application of CTIT. Another reason for choosing such a description is that the characteristic length scales (i.e. internal diameter of needle and needle thickness) used for the system's thrust description would be much greater than the characteristic microscopic and atomic length scales of the solid structures, thereby justifying the use of CTIT further [53] (see any of the listed references of section 9.1). A final reason is convenience, the plasma and gas flow system's modelling would generate sufficient complexity to warrant the practical pursuit of simplifying the model and pursuing a macroscopic description where permissible as substantiated by Figure 9.3 p. 134.

Electrodynamics of System

The electrodynamics of the system will be modelled using macroscopic electrodynamics. Even though the needle was the smallest element among the macroscopic elements and set the smallest observable length scale of interest to describing the thrust, its characteristic length scales (primarily its thickness) were much greater than $10^{-8}\ m$. In addition observation times of the system are expected to be much greater than any kind of characteristic times (for instance atomic vibration periods and time between atomic collisions) in the system. Thus allowing the application of macroscopic electrodynamics to consistently model the behaviour of the electromagnetic fields in the system [153].

Electric Behaviour of System

There has to be an electric circuit model (either ideal or realistic) to account for the power-supply's response and behaviour effects to and on the system (for instance fluctuations in the current could be due to the power-supply and not the system itself). This model would have to take into account how the power-source behaves. However, since conductivity or impedance in the system exterior to it can be derived from the transport coefficients of the charge transport

equations and their solutions [52, 10] , deriving a model should be possible but will depend on the evolution of the system thereby introducing a coupling between the two models. It should be noted that due to the Voltage-Current relationship recorded for the thruster system in chapter 7 that the power-supply for the "stable" currents recorded appeared to behave relatively ideally in that the applied voltage was not affected by the breakdown and the current followed the voltage so that the initial use of an ideal voltage power supply could be justified. A sketch of the whole system with the proposed modelling approaches labelled is given, see Figure 9.1 p. 128, to summarize the proposal.

9.3 Influence of system characterization on Discharge and Gas flow Modelling

In this section the effects of the previous chapter's characterization, and system estimates, on choice of modelling strategy for the discharge system will be presented. This section validates the previous chapter as well as provides justification for the need for future research. It will concern itself with the electrons, atoms and ions of the discharge system near the needle exit. Its fundamental aim is to present what in the author's opinion may be acceptable modelling approaches as well as (to restate) indicate why more research is necessary.

9.3.1 Electrons and other plasma constituents outside the thruster system

Since the electrons very close to the needle exit are weakly coupled , both classically and quantum mechanically, to themselves and everything else (see chapter 8 sections 8.10 and 8.12) a kinetic model of some kind would be advised (as weak coupling is one of the major requirements of such an approach [154, 155]), provided characteristic time scales in the system would also accommodate such an approach [156, 157] . Additionally, since the electrons are quantum mechanically coupled to themselves and the other constituents of the plasma outside the needle exit (see chapter 8) a quantum model like those of the one-particle Wigner distribution's equations (see equation 5.28) would be essential for a correct description. Fortunately the system is expected to be non-degenerate, at least outside the needle and throughout most of the discharge due to expansion of the gas, (see chapter 8 section 8.11) so that spin derived symmetry and statistics should not be a major concern and thus Boltzmann statistics like behaviour is expected [158]. Thus one does not necessarily have to consider appropriately symmeterizing the Wigner distributions and since the quantum coupling is weak for the electrons with the other constituents of the plasma one may attempt, initially, a completely classical approach.

Proposed Quantum Mechanical Modelling Strategy

If a quantum mechanical kinetic description is pursued, interaction between ions, neutrals and electrons (excluding ionization and recombination) may be accounted for using "optical" or effective potentials [131, 159]. These are used in scattering models to account for elastic scattering of electrons with the ions and atoms and side step the many-particle nature of those interactions [131, 159]. Ionization and recombination interactions can be handled phenomenologically, see [160] for an example.

One major problem with pursuing a quantum description is that the ions and atoms essentially behave as a classical system, except for the ionization, recombination and probable charge transfer interactions. This would introduce the difficulty of producing an acceptable description for the quantum electrons using classical behaviour of the ions and atoms without to much error being introduced. In other words if one did want to pursue a quantum kinetic description of the electrons, such a description would be functionally dependent on the distributions of the ions and atoms (like in the classical cases). However, since the distributions for the ions and atoms would be well approximated at a particular time and length scale by classical distributions the problem would be to find or justify a quantum kinetic description of the electrons on those length and time scales. Such a description would have to ensure that the quantum nature of the ions and atoms becomes negligible, but that a consistent quantum description of the electrons is still possible. Essentially we have a multi-scale problem which would have to be carefully analysed. However with that said one would still have to postulate or derive a kinetic equation for this system and defend its appropriateness for the problem, but this is beyond the scope of this dissertation.

9.3.2 Atoms and other plasma constituents outside the thruster system

The use of a kinetic description and in particular the use of the Boltzmann equation is perfectly justified. This is due to the small coupling between atoms (see chapter 8 section 8.10) and the estimated time-scale between collisions being much larger than the time-scale associated with collisions themselves [157, 156] i.e.

$$\tau = l/v_T >> \tau_o = r_o/v_T \ , \tag{9.6}$$

where v_T, r_o and l are the thermal velocity, inter-particle average distance of separation and mean free path distance respectively. The problem is that the atoms are quantum mechanically coupled to the electrons , although very weakly (also weakly coupled in a classical sense), and classically to the ions, but more strongly (see the chapter 8 section 8.10) . One could use "optical" or effective potentials for interaction between atoms and electrons and something phenomenological for the ionization and charge exchange interactions. Given the slow speed of

the ions and atoms possibility is to use polarized potentials for their interaction and still argue for a kinetic description. However, the strong interaction with the ions would undermine an all inclusive kinetic modelling approach and require computer simulation of the system [161], which would require further investigation.

9.3.3 Ions and other plasma constituents outside the thruster system

The ions are classically strongly coupled to themselves and the neutrals while very weakly quantum mechanically coupled to the electrons (and also weakly classically coupled). And thus this system suffers from the same modelling difficulty as that of the atoms (neutrals).

9.4 Discussion of Boundary Conditions

In modelling this problem the most useful information are the transport quantities and their gradients so that the thrust of the system can be computed. For the solid structures in the thruster reliance on continuum mechanics like conservation equations would be justified by assumption that they have very small response and characteristic time (and length) scales in comparison to that of the gas and thrust observation time (and length) scales (as argued in section 9.2). However, use of only continuum mechanics like conservation equations for the plasma system would not be advisable due to their inability to describe non-linear behaviour (i.e. turbulence) and resolve shocks, which may occur due to expansion of the gas into vacuum from the needle [126, 162, 53]. It would instead be necessary to know the one-particle distributions and their gradients. As we would then be able to retrieve the transport quantities and their gradients as well as observe and study shocks in the system [162].

The problem which needs to be addresses is to ensure "physically consistent" agreement between the different modelling techniques about the physical interfaces which separate them and where they "merge" (orange areas (1) and boundaries in Figure 9.1 p. 128).

A proposal to handle the situation of consistently merging the different descriptions/models about the contact interfaces between the plasma/gas system and solids is simple. It requires that near interface transport quantities of the plasma (or discharge), derived from the boundary equations for the one-particle distributions, on the interface satisfy the jump conditions imposed by the continuum mechanics description on these quantities about the interface. In-other words what ever the one-particle distribution may estimate near the interface for quantities like density, momentum and energy density etc. we would want the jump conditions used to describe the solids' boundary conditions to agree. In this way we can ignore the probably very complicated physical behaviour of the inter-

faces. And will have to only accommodate the interfaces in a phenomenological way when considering the boundary equations for the one-particle distributions.

As a side note the interface is often considered an independent thermodynamic system with its own transport equations and thermodynamic behaviour when ever possible [50], which may be of use when building the models.

In regions where descriptions "merge" different computational simulations or mathematical equations or both (like the orange (1) areas in Figure 9.1) research would have to be done on how to propagate errors between the descriptions. And on how to supply sufficient information between the descriptions, so that the descriptions leading into the merged areas would remain valid. To be specific each description would have to supply boundary information to the others in a way that reduces error and vice versa, thereby coupling them together.

Chapter 10

Conclusion

In this dissertation a recipe has been outlined on how thrust can be calculated using the conservation of momentum equations derived from continuum mechanics, as a moment of the one-particle distributions or application of CTIT. With the aim of modelling a CORION like thruster in mind it was then argued using a much simpler system and stochastic calculus why a statistical description of the system is necessary. From this the one-particle distribution emerged as a natural tool for the description of a system sufficient for the determination of the system's thrust and other physical quantities, such as energy and particle number.

This was then followed by a short investigation into the background of non-equilibrium statistical mechanics, both classical and quantum, necessary to understand how one-particle distributions could be derived formally and in a physically consistent way. Within this investigation the Wigner-Weyl-Moyal-Groenewold representation of quantum non-equilibrium statistical mechanics was introduced due to its similarity to the classical approach. It however emerged that additional research in the areas of surface science and physical boundary modelling is necessary.

The dissertation then continued with mass flow and current-voltage experiments important to the CORION like thrust system and necessary for characterization of the system. To be specific a novel mass flow and calibration set-up was tested, while a new voltage vs current set-up's feasibility was tested for determination of a CORION like system's electrical behaviour.

A characterization of the system near the needle was then performed in chapter 8 so as to assert what modelling approaches and strategies may be implemented with respect to the non-equilibrium statistical mechanics introduced previously. Within this section of the dissertation it was established what species of the plasma were quantum and classically mechanically coupled, and how strongly. Additionally the degeneracy of the electron system was verified justifying use

of Boltzmann statistics and a classification of the gas flow near the needle performed.

Finally this led to the proposal for a modelling strategy of the CORION like system, consisting of merging different modelling approaches and descriptions considered throughout the dissertation (and alluding to others not considered), by implementing the system characterization. It transpired from a discussion on boundary condition modelling and merging of descriptions/ modelling methods that further research is required. In particular research into how to merge different modelling approaches (equations) and their boundary equations or models effectively and consistently, as well as on how to combine differently physically scaled modelling approaches, is recommended.

Appendices

Appendix A

Derivation of conservation equations from One-particle distribution equations

In this appendix the way to generate the left hand side of the continuum mechanics like conservation equations in the previous chapters is given. The method is the same for both the classical and quantum one-particle distribution equations for particles with mass, say m^α and momentum $\vec{p}^\alpha := m^\alpha \vec{v}^\alpha$ (in the classical case where $\vec{v}^\alpha$ is the velocity of the particle). Consider an equation for the one particle distribution for particles of mass m^α, say α-type particles, $f_1^\alpha(\vec{q},\vec{p},t)$ given by

$$\frac{\partial}{\partial t} f_1^\alpha + \frac{\vec{p}}{m^\alpha} \cdot \frac{\partial}{\partial \vec{q}} f_1^\alpha = \mathcal{J}_{stuff}^\alpha \ , \tag{A.1}$$

where $\mathcal{J}_{stuff}^\alpha$ would contain all the other terms relevant to a particular one particle distribution's equation. We now note that that [163, 104]:

$$F_1^\alpha = N^\alpha f_1^\alpha \tag{A.2}$$

(in both the classical and quantum cases) where N^α are the number of α-type particles in the system and we assume it to be constant for convenience. From this we then introduce the definition of the momentum-expectation of a quantity $\Phi^\alpha(\vec{q},\vec{p},t)$, for α-type particles, which could be scalar, vector or a tensor of some kind, as [85]

$$\langle \Phi^\alpha \rangle_{\vec{p}}(\vec{q},t) := \int \Phi^\alpha(\vec{q},\vec{p},t) F_1^\alpha(\vec{q},\vec{p},t) d^3\vec{p} \ . \tag{A.3}$$

The reason for this is the following, the definition of number density [163, 104] can be written as

$$n^\alpha(\vec{q},t) = \langle 1 \rangle_{\vec{p}}(\vec{q},t) = \int 1 \cdot F_1^\alpha(\vec{q},\vec{p},t) d^3\vec{p} \ , \tag{A.4}$$

additionally we then define the conditional-momentum-expectation of a quantity $\Phi^\alpha(\vec{q},\vec{p},t)$, for α-type particles by

$$\overline{\Phi^\alpha}(\vec{q},t) = \frac{\int \Phi^\alpha(\vec{q},\vec{p},t)F_1^\alpha(\vec{q},\vec{p},t)d^3\vec{p}}{\int F_1^\alpha(\vec{q},\vec{p},t)d^3\vec{p}} \tag{A.5}$$

and from this the definition of fluid velocity of the α-particles (or average velocity density) follows as [163, 104]

$$\vec{u}^\alpha(\vec{q},t) \coloneqq \frac{\int \vec{p}F_1^\alpha(\vec{q},\vec{p},t)d^3\vec{p}}{m^\alpha \int F_1^\alpha(\vec{q},\vec{p},t)d^3\vec{p}} \ . \tag{A.6}$$

Using this we would then define the centred distribution (change of variable for the measure i.e. $F_1^\alpha(\vec{q},\vec{p},t)d^3\vec{p}d^3\vec{q}$) using $\vec{c}+m^\alpha\vec{u}^\alpha=\vec{p}$ as [163, 104]:

$$\mathcal{F}_1^\alpha(\vec{q},\vec{c},t) \coloneqq F_1^\alpha(\vec{q},\vec{c}+m^\alpha\vec{u}^\alpha,t) \tag{A.7}$$

Using the centred distribution we can identify terms like the "thermal" (or random) kinetic energy density [163, 104]:

$$E_K^\alpha(\vec{q},t) \coloneqq \int \frac{1}{2m^\alpha}c^2\mathcal{F}_1^\alpha(\vec{q},\vec{c},t)d^3\vec{c} \tag{A.8}$$

while using the original one-particle distribution we can identify the kinetic energy density [163, 104]

$$\varepsilon_K^\alpha(\vec{q},t) = \int \frac{1}{2m^\alpha}p^2\mathcal{F}_1^\alpha(\vec{q},\vec{p},t)d^3\vec{p} \ , \tag{A.9}$$

the relationship between them being given by [163]

$$\varepsilon_K^\alpha = E_K^\alpha + \frac{m^\alpha n^\alpha \left(u^\alpha\right)^2}{2} \ , \tag{A.10}$$

note that

$$\int \vec{c}\mathcal{F}_1^\alpha(\vec{q},\vec{c},t)d^3\vec{c} = 0 \ , \tag{A.11}$$

hence we consider a change in variables transformation of equation A.1 under $\vec{c}+m^\alpha\vec{u}^\alpha=\vec{p}$ and multiply it by N^α. The change in variables and multiplication would have the following effect on the left hand side of equation A.1:

$$\frac{\partial}{\partial t}F_1^\alpha(\vec{q},\vec{p},t) + \frac{\vec{p}}{m^\alpha}\cdot\frac{\partial}{\partial\vec{q}}F_1^\alpha(\vec{q},\vec{p},t) \longrightarrow \frac{\partial}{\partial t}\mathcal{F}_1^\alpha(\vec{q},\vec{c},t) + \frac{\vec{c}+m^\alpha\vec{u}^\alpha}{m^\alpha}\cdot\frac{\partial}{\partial\vec{q}}\mathcal{F}_1^\alpha(\vec{q},\vec{c},t) \tag{A.12}$$

while the right hand side of equation A.1 will change form appropriately when the change of variables is applied i.e. we would have:

$$\frac{\partial}{\partial t}\mathcal{F}_1^\alpha(\vec{q},\vec{c},t) + \frac{\vec{c}+m^\alpha\vec{u}^\alpha}{m^\alpha}\cdot\frac{\partial}{\partial\vec{q}}\mathcal{F}_1^\alpha(\vec{q},\vec{c},t) = Stuff \tag{A.13}$$

With these two equations then we could derive the transport equations as follows, multiply equation A.13 by the desired quantity $\Phi^\alpha(\vec{q},\vec{c}+m^\alpha\vec{u}^\alpha,t)$ for which momentum expectation is desired (we have already performed the change of variables) [164, 163, 104], note if not obvious the Jacobian of the transformation is 1 i.e.

$$\Phi^\alpha(\vec{q},\vec{c}+m^\alpha\vec{u}^\alpha,t)\left[\frac{\partial}{\partial t}\mathcal{F}_1^\alpha(\vec{q},\vec{c},t)+\frac{\vec{c}+m^\alpha\vec{u}^\alpha}{m^\alpha}\cdot\frac{\partial}{\partial\vec{q}}\mathcal{F}_1^\alpha(\vec{q},\vec{c},t)\right]=\Phi^\alpha(\vec{q},\vec{p},t)Stuff\ . \tag{A.14}$$

$Stuff$ is just the right hand side. Now we integrate both sides over momentum [164, 163, 104] i.e. $\vec{c}$. This results in the right hand side turning into some kind of source term $\mathcal{J}_{\Phi^\alpha}$ while the left hand side yields (using integration by parts):

$$\begin{aligned}&\frac{\partial}{\partial t}\int\Phi^\alpha\mathcal{F}_1^\alpha d^3\vec{c}+\frac{\partial}{\partial\vec{q}}\cdot\int\frac{(\vec{c}+m^\alpha\vec{u}^\alpha)}{m^\alpha}\otimes\Phi^\alpha\mathcal{F}_1^\alpha d^3\vec{c}\\&-\int\left\{\frac{\partial}{\partial t}\Phi^\alpha+\frac{\partial}{\partial\vec{q}}\cdot\left[\frac{(\vec{c}+m^\alpha\vec{u}^\alpha)}{m^\alpha}\otimes\Phi^\alpha\right]\right\}\mathcal{F}_1^\alpha d^3\vec{c}\end{aligned} \tag{A.15}$$

where $\otimes$ implies the correct kind of multiplication since we could be dealing with tensor multiplication, and $\cdot$ should be understood as the correct kind of inner-product or contraction (see [78] but note that in this reference$\cdot$ is replaced with :). Hence we are left with the equation:

$$\frac{\partial}{\partial t}\langle\Phi^\alpha\rangle_{\vec{p}}+\frac{\partial}{\partial\vec{q}}\cdot\langle\frac{(\vec{c}+m^\alpha\vec{u}^\alpha)}{m^\alpha}\otimes\Phi^\alpha\rangle_{\vec{p}}-\langle\left\{\frac{\partial}{\partial t}\Phi^\alpha+\frac{\partial}{\partial\vec{q}}\cdot\left[\frac{(\vec{c}+m^\alpha\vec{u}^\alpha)}{m^\alpha}\otimes\Phi^\alpha\right]\right\}\rangle_{\vec{p}}=\mathcal{J}_{\Phi^\alpha} \tag{A.16}$$

Now when we pick Φ^α to be equal to the following:

1. For $\Phi^\alpha=1$ we get particle number conservation equation [164, 163, 104].
2. For $\Phi^\alpha=\vec{p}=\vec{c}+m^\alpha\vec{u}^\alpha$ we get the momentum conservation equation [164, 163, 104].
3. For $\Phi^\alpha=\frac{1}{2m^\alpha}p^2=\frac{1}{2m^\alpha}(c^2+(m^\alpha)^2(u^\alpha)^2+2\vec{c}\cdot m^\alpha\vec{u}^\alpha)$ we get the "Random" kinetic energy conservation equation [164, 163, 104].

And this completes the appendix section on how conservation equations are derived from the respective one particle distributions. As a final note when the particle number fluctuates in time one will normally only use an equation for F_1^α not f_1^α when deriving the BBGKY-hierarchy or when simply postulating a modelling equation.

Appendix B

Basic Stochastic Calculus

In this appendix basic stochastic calculus (particularly Brownian motion or otherwise also known as Wiener process stochastic calculus) will be introduced, along with the notion of a stochastic differential equation, Ito's change of variable formula and the relationship between Stratonovich and Ito stochastic differential equations.

Definition 1 ***(Stochastic Process)*** *A stochastic process often denoted $X(j)$ or X_j where $j \in Z$ (an index from the index set Z) is actually a family (indexed set) of Random variables $\{X(j), j \in Z\}$ each defined on a common probability space, denoted $(\mathcal{M}, \Omega, \mu)$ [1]. Where $\mathcal{M}$ is the sample space while Ω is the σ-algebra of sets for the probability measure μ and sample space [61, p. 24],[55, p. 10].*

As an example j could be the time , say $j \in [0, 1]$ where the interval is in seconds, at which the "same" kind of experiment's outcome is observed denoted say by $X_\omega(j)$ (where ω characterizes the particular kind of experimental run so that different runs with exactly the same outcomes for all j have the same ω). Hence, every time ordered set of observations $\{X_\omega(j), j \in [0, 1]\}$ (i.e. defining a function $x_\omega(j) = X_\omega(j)$) of different experimental runs over the whole time interval would each be members of the sample space $\mathcal{M}$. Thus one could then think of $(\mathcal{M}, \Omega, \mu)$ as the set of all possible "paths" (functions x_ω) the experiment could produce and then given a probability measure μ on the σ-algebra Ω of this set of paths. The outcome of the experiment at a time $j = t$ is then random and denoted by X_t or $X(t)$ with its probability measure derived from the probability measure μ [165].

With this said it is then often convenient to think of the Stochastic process as a function of two variables (ω, j) where ω would index an element of the sample space $\mathcal{M}$ [55]. One could then interpret $X(\omega, j)$ as a function (in the

[1] And taking values in some algebra or field since things can be generalized to manifolds and vector spaces.

conventional sense) in j when ω is kept constant while when j is kept constant as a random variable on the probability space $(\mathcal{M}, \Omega, \mu)$ for which we have $\omega \in \mathcal{M}$. Next we introduce Brownian motion with respect to time or also known as the Wiener process.

Definition 2 ***(One Dimensional Brownian Motion)*** *denoted conventionally by $B(t)$ or $W(t)$ (when referring to it as a Wiener process) is a stochastic process taking values in R with the following properties [61, p. 56]:*

1. *(Independent Increments) $B(t) - B(s)$ where $t > s$ is independent (uncorrelated with itself) of the past, meaning the increment $B(t) - B(s)$ is independent of $B(u)$ for $0 \leq u \leq s$.*
2. *(Normal/Gaussian Increments) $B(t) - B(s)$, where $t > s$, has a normal distribution with mean zero and standard deviation $t - s$.*
3. *(Continuous paths) The paths for $B(t)$ for $t \geq 0$ are continuous functions of t.*

A multivariate Brownian motion or Wiener process depending on time denoted $\vec{B}(t)$ or $\vec{W}(t)$ can be defined using one-dimensional Brownian motions as a (column or row) vector $[B_1(t), ..., B_n(t)]$ where n would represent the dimension of the Brownian motion and each $B_j(t)$ is a one-dimensional Brownian motion [166].

A motivation for Stochastic calculus will now be introduced as well as used to indirectly define a Stochastic differential equation (more specifically a diffusion type stochastic differential equation). Suppose we have differential equation for some kind of one-dimensional phenomena dependent on time $X(t)$ given by

$$\frac{d}{dt}X(t) = A[X(t), t] \ , \tag{B.1}$$

where A is functionally dependent on $X(t)$ and explicitly dependent on time denoted by $A[X(t), t]$. However suppose it turns out that it is discovered that this kind of phenomena actually has a degree of randomness present during its evolution so that a more correct modelling differential equation would be

$$\frac{d}{dt}X(t) = A[X(t), B(t), t] + C[X(t), B(t), t]\dot{B}(t) \ , \tag{B.2}$$

where A and C are functionally dependent on $X(t)$ and $B(t)$, and explicitly dependent on time t. $B(t)$ could be a one-dimensional Brownian motion as introduced above or some other Stochastic process while $\dot{B}(t)$ would denote its "derivative", we assume (for the time being) that the paths themselves are smooth enough to allow interpretation of a derivative in the conventional sense. It would, still assuming we could interpret the derivative of the stochastic process, then hold that this differential equation would be equivalent to the integral equation (by assuming straight forward integration holds)

$$X(t) = X(0) + \int_{s=0}^{s=t} A[X(s), B(s), s]ds + \int_{s=0}^{s=t} C[X(s), B(s), s]\dot{B}(s)ds \ . \tag{B.3}$$

One immediate problem becomes clear, that is we might not actually have a conventional interpretation of $\dot{B}(s)$, since in the specific case of Brownian motion it is known that the paths are nowhere differentiable [167]. However if we still carry on with our assumptions we could write

$$X(t) = X(0) + \int_{s=0}^{s=t} A[X(s), B(s), s]ds + \int_{s=0}^{s=t} C[X(s), B(s), s]dB(s) \ , \quad \text{(B.4)}$$

where the interpretation of the increment $dB(s)$ may actually be something more conventional and attainable with in the more normal limits of the calculus we are employing. To be specific we want to work with "normal" functions and Stochastic processes, not generalized functions and Stochastic processes and then have to recast the above differential equation into a frame work that would "always" (since it has its limits as well) allow for an interpretation of the derivative of the Stochastic process [54].

The problem however that we then face is that we have no idea as to how to define the integral:

$$\int_{s=0}^{s=t} C[X(s), B(s), s]dB(s). \quad \text{(B.5)}$$

Fortunately Kiyoshi Itô managed to identify the necessary frame work for the "integration" of stochastic processes with respect to Brownian motion [61]. The approach will now be introduced starting with the "integration of non-random simple processes".

Definition 3 ***(Non-random Simple Process)*** *$X(t)$ is a function of t and does not depend on the Brownian motion $B(t)$ such that for an interval $[0,T]$ there exist times $0 = t_0 < t_1 < ... < t_n = T$ and constants c_0, c_1, ..., c_{n-1} so that $X(t)$ has the expansion:*

$$X(t) = c_0 + \sum_{i=0}^{n-1} c_i \chi_{(t_i, t_{i+1}]}(t) \quad \text{(B.6)}$$

where $\chi_{(t_i,t_{i+1}]}(t)$ are characteristic functions on the respective intervals [168].

for which its Ito stochastic integral is defined by

Definition 4 ***(Integration of Non-random Simple Process)*** *of Non-random Simple Process $X(t)$ over the interval $[0,T]$ is defined by [168]:*

$$\int_{s=0}^{s=T} X(s)dB(s) := \sum_{i=0}^{n-1} c_i \left(B(t_{i+1}) - B(t_i)\right). \quad \text{(B.7)}$$

Now to integrate a Stochastic process we would have to allow that the coefficients themselves be "random" [168], denote it hence by say ξ_i. If this becomes the case the coefficients themselves could be functionally dependent on the Brownian motion i.e. $\xi_i[B(s)]$ for the interval $s \in [t_i, t_{i+1}]$. The problem then becomes

how to choose the actual value the variable should take on the interval i.e. what should the value of s be in the interval. Regardless though of how we choose said value, the requirement to be met would be that we want to make sure that each coefficient only depends on the Brownian motion within the time interval, it is broken up into and not future values of the Brownian motion i.e. depend on values outside $[t_i, t_{i+1}]$. To specify such a requirement in a mathematically consistent way before defining the appropriate integral we have to introduce the notion of a σ-algebra generated by a stochastic process, a filtration, a filtration generated by a stochastic process (in our case the Brownian motion) and the notion of an "adapted stochastic process". Thus we begin with:

Definition 5 ***(σ-algebra generated by a Random Variable)*** *Since a Random Variable X is actually a measurable mapping from a probability space, say $(\mathcal{M}, \Omega, \mu)$, into some measure space $(\mathcal{N}, \Lambda, \nu)$:*

$$X : \mathcal{M} \longrightarrow \mathcal{N} \tag{B.8}$$

for example the Real numbers with the Lebesgue integration measure defined on the Borel sets for the Reals, we can use the Random Variable and the co-domain to which the space $\mathcal{M}$ is mapped to select (i.e. generate) a σ-algebra contained in Ω as follows: The σ-algebra generated by Random Variable X denoted $\sigma(X)$ is σ-algebra generated by the family of sets defined by:

$$\sigma(X) \coloneqq \left\{X^{-1}(S) | S \in \Lambda\right\} \tag{B.9}$$

where X^{-1} is the pre-image of X i.e.

$$X^{-1}(S) = \{\omega \in \mathcal{M} | X(\omega) \in S\} \tag{B.10}$$

since X is a measurable mapping we would have $\sigma(X) \subseteq \Omega$ [61, p. 24],[55, p. 8].

Before defining σ-algebra generated by a Stochastic Process a discussion will be entered into since it seems somewhat unnecessary and paradoxical to introduce this concept if we already have that a stochastic process will **by definition** posses its own σ-algebra. Recall that in the definition of a stochastic process it was necessary to use an index set Z for the j in the identification of each X_j in the stochastic process. From a modelling point of perspective one would choose or discover Z to be some kind of set that should encompass all desired behaviour, and then with respect to this set we would label the Random variables that constitute the stochastic process. But what happens if, when we run our experiments or record and track our observations we do not use the entire index set Z's indices , what if in fact we only track phenomena in some subset Z' of Z ($Z' \subset Z$)(for instance instead of observing a phenomena over a time interval $[0, T]$ we observe it over a time interval $[0, \tau]$ with $\tau < T$)? The situation that then occurs is that we must analyse our observations with respect to only this subset and find out what "events" or elements in our sample space $\mathcal{M}$ could explain the phenomena on this subset Z' as using the whole Z (if possible) may include to much information (or require data not available to us

due to our restricted observation). In other words we would need to find out whether a σ-algebra with respect to the restriction of the stochastic process to the index set Z' can be found to encode the "observable events".

As it turns out one can manufacture such a required σ-algebra but will first have to define "cylinder sets" and then construct the "cylinder σ-algebra" before σ-algebra generated by a Stochastic Process can be defined. Recall the identification we made earlier that a stochastic process can be viewed as a mapping in two variables, namely

$$X : Z \times \mathcal{M} \longrightarrow \mathcal{N} \ , \tag{B.11}$$

such that

$$(j, \omega) \in Z \times \Omega \longrightarrow X(j, \omega) \in \mathcal{N} \ . \tag{B.12}$$

In addition to this identification we could also note that this mapping could be considered a mapping from $\mathcal{M}$ into a subset of the space $\mathcal{N}^Z$ (the space of all maps from Z to $\mathcal{N}$) i.e.

$$X : \mathcal{M} \longrightarrow \mathcal{N}^Z \ , \tag{B.13}$$

such that by denoting $X(\cdot, \omega)$ (a function on Z) by $\omega(\cdot)$ we can see that we would have the mapping:

$$\omega \in \mathcal{M} \longrightarrow \omega(\cdot) \in \mathcal{N}^Z \ . \tag{B.14}$$

With respect to this mapping and the fact that (w.r.t to the identification just made)

$$X(\mathcal{M}) \subseteq \mathcal{N}^Z \ , \tag{B.15}$$

we can introduce the notion of a cylinder set, appropriate to application here.

Definition 6 ***(Cylinder Set)*** *$C_{(z_1,...,z_n)}(B) \subset \mathcal{N}^Z$ is a set given by [169, p. 2],[61, p, 47]:*

$$C_{(z_1,...,z_n)}(B) = \left\{ \omega \in \mathcal{N}^Z \middle| \, (\omega(z_1), ..., \omega(z_n)) \in B \right\} \tag{B.16}$$

where $n \geq i \geq 1$, $z_i \in Z$ and $B \in \Lambda^{\otimes n}$. Where $\Lambda^{\otimes n} \equiv \Lambda \otimes ... \otimes \Lambda$ is the n-product σ-algebra of the σ-algebra Λ of $\mathcal{N}$ i.e. the smallest σ-algebra containing all subsets of $\mathcal{N}^n$ ($\mathcal{N} \times ... \times \mathcal{N}$ is the n-times Cartesian product) of the form:

$$(A_1, A_2, ..., A_n) \in \mathcal{N}^n \ \textit{where} \ A_i \in \Lambda \tag{B.17}$$

Definition 7 ***(Cylinder σ-algebra)*** *If we consider the class of all cylinder sets (i.e. collection of all cylinder sets) constructed from $\mathcal{N}^Z$ denoted $\mathcal{C}(\mathcal{N}, Z)$ or simply $\mathcal{C}$ (and is an algebra of sets):*

$$\mathcal{C}(\mathcal{N}, Z) := \bigcup_{n \geq 1}^{\infty} \bigcup_{\substack{z_1,...,z_n \in Z \\ B \in \Lambda^{\otimes n}}} C_{(z_1,...,z_n)}(B) \tag{B.18}$$

we can use it to generate a σ-algebra of sets by considering the Cylinder σ-algebra denoted $\sigma(\mathcal{C})$ (or $\sigma(\mathcal{C}(\mathcal{N}, Z))$to be the smallest σ-algebra to contain the class $\mathcal{C}$ i.e. all its elements namely all the different cylinder sets [169, p. 2].

At this point it probably doesn't come as a surprise (due to the identifications earlier) but we would then consider a Stochastic process X to be the measurable map

$$X : (\mathcal{M}, \Omega) \longrightarrow (\mathcal{N}^Z, \sigma(\mathcal{C}(\mathcal{N}, Z))) \ , \tag{B.19}$$

where the σ-algebra on $\mathcal{M}$ would still be Ω due to the "measurable" requirement while the σ-algebra on $\mathcal{N}^Z$ would be $\sigma(\mathcal{C}(\mathcal{N}, Z))$. However it is possible for an alternative σ-algebra to be induced, by using the map X and the σ-algebra $\sigma(\mathcal{C})$ on $\mathcal{N}^Z$, for the set $\mathcal{M}$ which we would denote $\sigma(X)$ (unfortunately this notation seemed to be convention) [169]. This connection is made formal using the Kolmogrov theorems [61, p. 47]. We already made sure by definition right at the start of this appendix that $X(j)$ is a measurable function between the measure spaces $(\mathcal{M}, \Omega)$ and $(\mathcal{N}, \Lambda)$ for all $j \in Z$ that $\sigma(X) \subseteq \Omega$ or $\Omega \subset \sigma(X)$. Hence we have by the previously mentioned definition that X is measurable with respect to $(\mathcal{N}^Z, \sigma(\mathcal{C}(\mathcal{N}, Z)))$ on $(\mathcal{M}, \Omega)$ and use the definition of σ-algebra induced by a stochastic process to generate the required result. Consequently, everything manufactured may seem redundant except when you want to perhaps check whether it would be possible to construct a stochastic process from some subset of a space of maps of some kind. Of immediate practical value is the scenario where we already have our model stochastic process but only have data for $j \in Z' \subset Z$ such that we would need to restrict our stochastic model to this subset when applying analysis techniques in a way that would keep everything consistent. Thus we are lead to (as a practical requirement)

Definition 8 ***($\sigma_{Z'}$-algebra generated by a Stochastic Process)*** *Assuming that $X : \mathcal{M} \longrightarrow \mathcal{N}^{Z'}$ is a stochastic process for $Z' \subset Z$ i.e. we have $(\mathcal{M}, \Omega, \mu)$ a probability space, $(\mathcal{N}, \Lambda, \nu)$ a measure space with measure ν, $(\mathcal{N}^{Z'}, \sigma(\mathcal{C}(\mathcal{N}, Z')))$ a measure space and finally X measurable function between the two spaces. We can proceed to define the σ-algebra generated by a Stochastic Process X on Z' denoted as $\sigma(X)$ as the σ-algebra [170]:*

$$\sigma(X) \coloneqq \left\{ X^{-1}(B) \subset \mathcal{M} | B \in \sigma(\mathcal{C}(\mathcal{N}, Z')) \right\} \tag{B.20}$$

where the set on the right can be checked to be σ-algebra using $\sigma(\mathcal{C}(\mathcal{N}, Z'))$

Now important to the introduction of filtration generated by a stochastic process we will have to introduce the notion of an augmented σ-algebra with respect to a probability measure μ denoted $\mathcal{F}$.

Definition 9 ***(Augmented σ-algebra)*** *Given a stochastic process:*

$$X : \mathcal{M} \longrightarrow \mathcal{N}^{Z'} \tag{B.21}$$

on the probability space $(\mathcal{M}, \Omega, \mu)$ and the σ-algebra $\sigma(\mathcal{C}(\mathcal{N}, Z'))$ induced on $\mathcal{M}$ by it, the augmented σ-algebra w.r.t the probability measure μ denoted $\mathcal{F}_{Z'}$ is the σ-algebra generated by the family of sets [169, p. 21]:

$$\sigma(\mathcal{C}(\mathcal{N}, Z')) \bigcup \mathfrak{N}_\mu \text{ where } \mathfrak{N}_\mu \coloneqq \{ A \in \mathcal{M} | \mu(A) = 0 \} \tag{B.22}$$

in other words:

$$\mathcal{F}_{Z'} \coloneqq \sigma(\sigma(\mathcal{C}(\mathcal{N}, Z')) \bigcup \mathfrak{N}_\mu) \tag{B.23}$$

This σ-algebra simply makes sure that we always include the zero probability events which the experiments would never be able to display and which the restricted stochastic process may ignore. In this way this σ-algebra contains all events we would possibly associate with the index set Z' and all experimental outcomes observed for it. Now to introduce a filtration appropriate to the application in this appendix and thesis.

Definition 10 ***(Filtration)*** *A filtration F is a family of σ-algebras on the same space, indexed and ordered according to a linear totally ordered (in general it only needs to be totally ordered) index set (denoted here by Γ) such that when $i, j \in \Gamma$ with $i \preceq j$ (i precedes j at most) and $\mathcal{F}_i, \mathcal{F}_j \in F$ then $\mathcal{F}_i \subseteq \mathcal{F}_j$ holds [169, p. 21].*

Definition 11 ***(Filtration Generated by a Stochastic Process)*** *Using a linear totally ordered index set Z for a stochastic process X the filtration generated by the stochastic process X is the family of σ-algebras:*

$$F \coloneqq \{\mathcal{F}_i | i \in Z\} \tag{B.24}$$

where $\mathcal{F}_i$ is the augmented σ-algebra for the restricted stochastic process running up to $i \in Z$ [169, p. 21].

Using the filtration we can upgrade our probability space to a filtered probability space where the filtration could be built from a specific stochastic process, in our case Brownian motion. With the filtration we can now introduce the notion of an adapted process.

Definition 12 ***(Adapted Process)*** *Consider stochastic process $Y(j)$ defined on $(\mathcal{M}, \Omega, \mu)$ with $j \in Z$ where in addition $(\mathcal{M}, \Omega, \mu)$ has a filtration $F = \{\mathcal{F}_i | i \in Z\}$ (where each $\mathcal{F}_i$ $i \in Z$ could have been generated by another stochastic process $X(j)$). $Y(j)$ will be called adapted if for $j = t$ we have $Y(t)$ is $\mathcal{F}_t$ measurable [61, p. 50].*

This would have the consequence that such a process, possibly only ever observed up to $j = t$, would not depend on future behaviour but can be analysed using at least the events and our understanding of them in $\mathcal{F}_t$.

With all this said we can finally move on to define the second last tool for integration of stochastic process with respect to Brownian motion. We introduce the notion of the integral for a simple adapted process, necessary for the construction of any stochastic integral.

Definition 13 ***(Integration of Simple Stochastic Process)*** *Assume we have a filtered probability space $(\mathcal{M}, \Omega, \mu)$ with $F = \{\mathcal{F}_i | i \in Z\}$ being generated by Brownian motion. Then a simple adapted stochastic process $X(j)$ on $Z = [0, T]$*

is such that there exist "times" $0 = t_0 < t_1 < ... < t_n = T$*, a constant* ξ_0 *(not entirely necessary) and* $\mathcal{F}_{t_i}$ *measurable Random Variables* ξ_i *with* $E[\xi_i^2] < \infty$ *for* $i = 0, 1, 2, ..., n$ *so that it can be put in the form:*

$$X(j) = \xi_0 + \sum_{i=0}^{n-1} \xi_i \chi_{(t_i, t_{i+1}]} \tag{B.25}$$

The Ito integral of an adapted simple process follows:

$$\int_0^T X(s)dB(s) := \sum_{i=0}^{n-1} \xi_i \left(B(t_{i+1}) - B(t_i)\right) \tag{B.26}$$

which we can see is a random variable itself [168].

Finally we can conclude this talk of integration with the last definition.

Definition 14 ***(Stochastic integral of a Stochastic Process)*** *Let* $\{X^n(j)\}_{j\geq 1}$ *be a sequence of simple adapted stochastic processes convergent in probability to the stochastic process* $X(j)$ *i.e. If the following limit exists [61, p. 95],[171]*

$$\lim_{n\to\infty} \mu(\{|X^n(j) - X(j)| > \varepsilon\}) = 0 \ \ \forall \varepsilon > 0, \forall j \in Z \tag{B.27}$$

where $|\cdot|$ *indicates the norm in the space to which the stochastic processes are mapped. Then the stochastic integral of the process* $X(j)$ *denoted* $\int_0^T X(s)dB(s)$ *is the limit in probability (when it exists) of the sequence of Random Variables:*

$$J^n := \int_0^T X^n(s)dB(s) \tag{B.28}$$

in other words as a random variable $J = \int_0^T X(s)dB(s)$ *we would require:*

$$\lim_{n\to\infty} \mu(\{|J^n - J| > \varepsilon\}) = 0 \ \ \forall \varepsilon > 0 \tag{B.29}$$

However using the limit in probability isn't the only way to go, but is weak, an alternative is to replace it with the $\mathcal{L}^2(\mu)$ as is usual in Lebesgue integration theory, since convergence in $\mathcal{L}^2(\mu)$ guarantees convergence in the probability sense [171],[167, p. 14].

As a final note, when breaking down a stochastic process $X(j)$ into sequence of simple processes $\{X^n(j)\}_{n>1}$ it will often be the case that we could represent these sequences as

$$X^n(j) = \sum_{i=0}^{n} X(s_n)\chi_{[f_-(i,n), f_+(i,n))} \ , \tag{B.30}$$

where $X(s_n)$ would represent some "appropriate" value of $X(j)$ on the interval $[f_-(i,n), f_+(i,n))$, for which $f_-(i,n), f_+(i,n)$ would be used to determine upper and lower limits on the interval. Now two choices are conventional [171]:

1. Ito's choice $s_n = f_-(i,n)$, using the bottom value guarantees you that you won't be trying to look into the future.

2. Stratanovich's choice $s_n = (f_-(i,n) + f_+(i,n))/2$, considered more useful for work in generalizing to manifolds as change of variable formula look the same as in conventional calculus.

These two choices are related with a small digression at the end of the appendix indicating the relationship. However regardless, two results used in the dissertation are note worthy and will be mentioned namely: Ito's change of variable formula and the relationship between Stratonovich and Ito stochastic differential equations. We start with Ito's change of variable formula suitable to application in the dissertation by introducing the notion of a Ito-process and stochastic differential equation.

Definition 15 ***(Ito-process and Stochastic Differential Equation)*** *An Ito-process on the interval* $[0,T]$ *is a stochastic process* $X(t)$ *which has the form [61, p. 108]:*

$$X(t) = X(0) + \int_{s=0}^{s=t} A[X(s),B(s),s]ds + \int_{s=0}^{s=t} C[X(s),B(s),s]dB(s) \quad \text{(B.31)}$$

where $X(0)$ *is* $\mathcal{F}_0$*-measurable, the processes* $A[X(s),B(s),s] \equiv A(s)$ *and* $C[X(s),B(s),s] \equiv C(s)$ *are* $\mathcal{F}_t$*-adapted such that:*

1. $\int_0^T |A(s)|\,ds < \infty$

2. $\int_0^T C(s)^2 ds < \infty$

hold. When this is the case the process $X(t)$ *is said to have the "stochastic differential" on* $[0,T]$

$$dX(t) = A[X(t),B(t),t]dt + C[X(t),B(t),t]dB(t) \text{ where } 0 \le t \le T \quad \text{(B.32)}$$

however one must interpret it as an alternative notation for the integral form B.31. When the conditions for an Ito process cannot be asserted and one does not know what $X(t)$ *is, then an equation of the form B.32 is referred to as a "Stochastic Differential Equation" driven by Brownian motion [61, p. 126] [note this is the Ito form of a stochastic differential equation since integration is implied in the Ito sense].*

With this at hand we can introduce Ito's change of variable formula for Ito-processes.

Definition 16 ***(Ito's change of variables for functions with multiple variables)*** *Let* $\vec{X}(t) = (X_1(t), X_2(t), ..., X_n(t))$ *be a vector Ito-process and* $f(x_1,...,x_n)$ *be an atleast twice differentiable function i.e. member of the* C^2

set of functions, of n-variables. Then $f(X_1(t),...,X_n(t))$ is an Ito-process and in addition its stochastic differential is given by [61, p. 119]:

$$df(X_1(t),...,X_n(t)) = \sum_{i=1}^{n} \frac{\partial}{\partial x_i} f(X_1(t),...,X_n(t))dX_i(t) + \frac{1}{2}\sum_{i=1}^{n}\sum_{j=1}^{n} \frac{\partial^2}{\partial x_i \partial x_j} f(X_1(t),...,X_n(t))d[X_i,X_j](t) \quad \text{(B.33)}$$

where $d[X_i,X_j](t)$ is the stochastic differential of the quadratic variation [61, p. 103]:

$$[X_i,X_j](t) = \lim \sum_{l=0}^{n-1} \left(X_i(t_{l+1}^n) - X_i(t_l^n)\right)\left(X_j(t_{l+1}^n) - X_j(t_l^n)\right) \quad \text{(B.34)}$$

where for each n the sequence $\{t_l^n\}_{l=0}^n$ is a partition of $[0,t]$, and the limit is taken over all partitions with $\delta_n = max(t_{l+1}^n - t_l^n) \to 0$ as $n \to \infty$ with convergence/limit result determined through convergence in probability.

Fortunately one can compute the stochastic differential of the quadratic variation of Ito-processes $X_i(t)$ and $X_j(t)$ using their stochastic differentials as [61, p. 119]

$$d[X_i,X_j](t) = dX_i(t)dX_j(t)\ . \quad \text{(B.35)}$$

One would then multiply out the product on the right using the stochastic differentials of $X_i(t)$ and $X_j(t)$ which should have forms similar to equation B.32 (since they are Ito-processes) and then use the following "**formal**" results to simplify further [61, p. 110],[172, p. 96]:

1. $dB_i(t)dB_j(t) = \delta_{ij}dt$ since $X_i(t)$ and $X_j(t)$ may depend on multiple Brownian motions
2. $dB_i(t)dt = 0$ for any i
3. $(dt)^2 = 0$

With this complete we can proceed to relate the Stratanovich integral to Ito's and also relate their respective stochastic differential forms (used colloquially), which could then be used to show how Stratanovich stochastic differential equations can be transformed into Ito-stochastic differential equations.

Definition 17 ***(Stratanovich Integral and Stochastic Differential interms of Ito counterparts)*** *Let $X(t)$ and $Y(t)$ be continuous adapted processes such that the Ito-integral $\int_0^t Y(s)dX(s)$ is defined. The Stratanovich integral is then defined by [61, p. 145]:*

$$\int_0^t Y(s) \circ dX(s) = \int_0^t Y(s)dX(s) + \frac{1}{2}[Y,X](t) \quad \text{(B.36)}$$

while the Stratanovich stochastic differential associated with it is given by [61, p. 145]:

$$Y(s) \circ dX(s) = Y(s)dX(s) + \frac{1}{2}d[Y,X](t) \quad \text{(B.37)}$$

Using Ito's change of variable formula and the above definition of Stratanovich stochastic differentials in-terms of Ito's stochastic differentials it is possible to show how Stratanovich stochastic differential equations are related to Ito stochastic differential equations, namely:

Theorem 1 (Conversion of Stratanovich SDE to Ito SDE) *Suppose that a stochastic process $X(t)$ satisfies the following SDE in the Stratanovich sense:*

$$dX(t) = A[X(t),t]dt + B[X(t),t] \circ dB(t) \tag{B.38}$$

with B twice differentiable in X. Then $X(t)$ satisfies the Ito SDE [61, p. 147]:

$$dX(t) = \left[A[X(t),t] + \frac{1}{2}\left(\frac{\partial}{\partial X}B[X(t),t]\right)B[X(t),t]\right]dt + B[X(t),t]dB(t) \tag{B.39}$$

Appendix C

Mass Flow Data Results and Analysis

In this appendix results of the analysis of mass flow is given as well as error analysis and model justification. Note that this section may appear repetitious but the results are for different experiments.

VF (cm^3/s)	MF (kg/s)
0.101293103	1.67644E-07
0.101731602	1.6837E-07
0.102396514	1.6947E-07
0.10042735	1.66211E-07
0.102396514	1.6947E-07
0.100642398	1.66567E-07
0.101293103	1.67644E-07
0.099576271	1.64803E-07
0.101731602	1.6837E-07

Table C.1: Table of time-average volume and mass flow rates for table 6.1 (not taking significant figures into account).

VF (cm^3/s)	Error (cm^3/s)	MF (kg/s)	Error (kg/s)
0.10	± 0.009	1.7E-07	± 1.7E-08
0.10	± 0.009	1.7E-07	± 1.7E-08
0.10	± 0.009	1.7E-07	± 1.7E-08
0.10	± 0.009	1.7E-07	± 1.6E-08
0.10	± 0.009	1.7E-07	± 1.7E-08
0.10	± 0.009	1.7E-07	± 1.6E-08
0.10	± 0.009	1.7E-07	± 1.7E-08
0.10	± 0.008	1.7E-07	± 1.6E-08
0.10	± 0.009	1.7E-07	± 1.7E-08

Table C.2: Table of time-average volume and mass flow rates with error estimate for table 6.1.

For volume flow rate data un-altered by error estimates, Anderson-Darling test under assumption of normal data yielded p-value greater than 0.250 with D = 0.25490432. Mean was μ = 0.10128 with 95% confidence interval $[0.10056, 0.10199]$ while standard deviation σ = 0.0009312 with 95% confidence interval $[0.0006290, 0.00178]$. For volume flow rate data un-altered by error estimates, Anderson-Darling test of volume flow rate residuals under assumption of normal data yielded p-value greater than 0.250 with D = 0.25490432. Mean was μ = 2.2222E-11 with 95% confidence interval $[-0.0007158, 0.0007158]$ while standard deviation σ = 0.0009312 with 95% confidence interval $[0.0006290, 0.00178]$.

For mass flow rate data un-altered by error estimates, Anderson-Darling test under assumption of normal data yielded p-value greater than 0.250 with D = 0.25490909. Mean was μ = 1.67617E-7 with 95% confidence interval $[1.66432E-7, 1.68801E-7]$ while standard deviation σ = 1.54113E-9 with 95% confidence interval $[1.04097E-9, 2.95245E-9]$. For mass flow rate data un-altered by error estimates, Anderson-Darling test for mass flow rate residuals under assumption of normal data yielded p-value greater than 0.250 with D = 0.25490424. Mean was μ = 2.2222E-16 with 95% confidence interval $[-1.1847E-9, 1.1847E-9]$ while standard deviation σ = 1.54123E-9 with 95% confidence interval $[1.04104E-9, 2.95264E-9]$.

VF (cm^3/s)	MF (kg/s)
0.142857143	2.36434E-07
0.144171779	2.3861E-07
0.143292683	2.37155E-07
0.143292683	2.37155E-07
0.141141141	2.33594E-07
0.145061728	2.40083E-07
0.142424242	2.35718E-07
0.139880952	2.31509E-07
0.140298507	2.322E-07
0.139880952	2.31509E-07

Table C.3: Table of time-average volume and mass flow rates for table 6.2(not taking significant figures into account).

VF (cm^3/s)	Error (cm^3/s)	MF (kg/s)	Error (kg/s)
0.14	± 0.01	2.4E-07	± 2.3E-08
0.14	± 0.01	2.4E-07	± 2.4E-08
0.14	± 0.01	2.4E-07	± 2.3E-08
0.14	± 0.01	2.4E-07	± 2.3E-08
0.14	± 0.01	2.3E-07	± 2.3E-08
0.15	± 0.01	2.4E-07	± 2.4E-08
0.14	± 0.01	2.4E-07	± 2.3E-08
0.14	± 0.01	2.3E-07	± 2.3E-08
0.14	± 0.01	2.3E-07	± 2.3E-08
0.14	± 0.01	2.3E-07	± 2.3E-08

Table C.4: Table of time-average volume and mass flow rates with error estimate for table 6.2.

For volume flow rate data un-altered by error estimates, Anderson-Darling test under assumption of normal data yielded p-value greater than 0.250 with D = 0.32590742. Mean was μ = 0.14223 with 95% confidence interval $[0.14091, 0.14355]$ while standard deviation σ = 0.00184 with 95% confidence interval $[0.00126, 0.00336]$. For volume flow rate data un-altered by error estimates, Anderson-Darling test of volume flow rate residuals under assumption of normal data yielded p-value greater than 0.250 with D = 0.32590742. Mean was μ = 0 with 95% confidence interval $[-0.00132, 0.00132]$ while standard deviation σ = 0.00184 with 95% confidence interval $[0.00126, 0.00336]$.

For mass flow rate data un-altered by error estimates, Anderson-Darling test under assumption of normal data yielded p-value greater than 0.250 with D = 0.32590622. Mean was μ = 2.35397E-7 with 95% confidence interval $[2.3322E-7, 2.37574E-7]$ while standard deviation σ = 3.04314E-9 with 95% confidence

interval $[2.09318E-9, 5.55558E-9]$. For mass flow rate data un-altered by error estimates, Anderson-Darling test for mass flow rate residuals under assumption of normal data yielded p-value greater than 0.250 with D = 0.32590778. Mean was μ = -1.1E-15 with 95% confidence interval $[-2.1771E-9, 2.17705E-9]$ while standard deviation σ = 3.04331E-9 with 95% confidence interval $[2.0933E-9, 5.5559E-9]$.

VF (cm^3/s)	MF (kg/s)
0.176691729	2.92432E-07
0.172161172	2.84934E-07
0.172161172	2.84934E-07
0.173431734	2.87037E-07
0.178030303	2.94647E-07
0.177358491	2.93535E-07
0.177358491	2.93535E-07
0.173431734	2.87037E-07
0.170909091	2.82861E-07
0.175373134	2.9025E-07

Table C.5: Table of time-average volume and mass flow rates for table 6.3 (not taking significant figures into account).

VF (cm^3/s)	Error (cm^3/s)	MF (kg/s)	Error (kg/s)
0.18	± 0.015	2.9E-07	± 2.9E-08
0.17	± 0.015	2.9E-07	± 2.8E-08
0.17	± 0.015	2.9E-07	± 2.8E-08
0.17	± 0.015	2.9E-07	± 2.8E-08
0.18	± 0.015	2.9E-07	± 2.9E-08
0.18	± 0.015	2.9E-07	± 2.9E-08
0.18	± 0.015	2.9E-07	± 2.9E-08
0.17	± 0.015	2.9E-07	± 2.8E-08
0.17	± 0.015	2.8E-07	± 2.8E-08
0.18	± 0.015	2.9E-07	± 2.9E-08

Table C.6: Table of time-average volume and mass flow rates with error estimate for table 6.3.

For volume flow rate data un-altered by error estimates, Anderson-Darling test under assumption of normal data yielded p-value greater than 0.250 with D = 0.42067214. Mean was μ = 0.17469 with 95% confidence interval $[0.17284, 0.17654]$ while standard deviation σ = 0.00258 with 95% confidence interval $[0.00178, 0.00472]$. For volume flow rate data un-altered by error estimates, Anderson-Darling test of volume flow rate residuals under assumption of normal data yielded p-value

greater than 0.250 with D = 0.42067209. Mean was μ = -1E-10 with 95% confidence interval $[-0.00185, 0.00185]$ while standard deviation σ = 0.00258 with 95% confidence interval $[0.00178, 0.00472]$.

For mass flow rate data un-altered by error estimates, Anderson-Darling test under assumption of normal data yielded p-value greater than 0.250 with D = 0.42061730. Mean was μ = 2.8912E-7 with 95% confidence interval $[2.8606E-7, 2.9218E-7]$ while standard deviation σ = 4.27754E-9 with 95% confidence interval $[2.94225E-9, 7.80913E-9]$. For mass flow rate data un-altered by error estimates, Anderson-Darling test for mass flow rate residuals under assumption of normal data yielded p-value greater than 0.250 with D = 0.42067238. Mean was μ = -1E-15 with 95% confidence interval $[-3.0601E-9, 3.0601E-9]$ while standard deviation σ = 4.27773E-9 with 95% confidence interval $[2.94237E-9, 7.80947E-9]$.

VF (cm^3/s)	MF (kg/s)
0.106719368	1.76625E-07
0.100746269	1.66739E-07
0.106719368	1.76625E-07
0.105058366	1.73876E-07
0.105058366	1.73876E-07
0.102661597	1.69909E-07
0.104247104	1.72533E-07
0.103448276	1.71211E-07

Table C.7: Table of time-average volume and mass flow rates for table 6.4 (not taking significant figures into account).

VF (cm^3/s)	Error (cm^3/s)	MF (kg/s)	Error (kg/s)
0.11	± 0.02	1.8E-07	± 2.8E-08
0.10	± 0.01	1.7E-07	± 2.6E-08
0.11	± 0.02	1.8E-07	± 2.8E-08
0.11	± 0.02	1.7E-07	± 2.7E-08
0.11	± 0.02	1.7E-07	± 2.7E-08
0.10	± 0.02	1.7E-07	± 2.7E-08
0.10	± 0.02	1.7E-07	± 2.7E-08
0.10	± 0.02	1.7E-07	± 2.7E-08

Table C.8: Table of time-average volume and mass flow rates with error estimate for table 6.4.

For volume flow rate data un-altered by error estimates, Anderson-Darling test under assumption of normal data yielded p-value greater than 0.250 with D = 0.22611837. Mean was μ = 0.104332 with 95% confidence interval $[0.10263, 0.10603]$ while standard deviation σ = 0.00203 with 95% confidence interval $[0.00134, 0.00413]$.

For volume flow rate data un-altered by error estimates, Anderson-Darling test of volume flow rate residuals under assumption of normal data yielded p-value greater than 0.250 with D = 0.22611838. Mean was μ = 2.75E-10 with 95% confidence interval $[-0.00170, 0.00170]$ while standard deviation σ = 0.00203 with 95% confidence interval $[0.00134, 0.00413]$.

For mass flow rate data un-altered by error estimates, Anderson-Darling test under assumption of normal data yielded p-value greater than 0.250 with D = 0.22611118. Mean was μ = 1.72674E-7 with 95% confidence interval $[1.69863E-7, 1.75485E-7]$ while standard deviation σ = 3.3624E-9 with 95% confidence interval $[2.22313E-9, 6.8434E-9]$. For mass flow rate data un-altered by error estimates, Anderson-Darling test for mass flow rate residuals under assumption of normal data yielded p-value greater than 0.250 with D = 0.22611828. Mean was μ = -8.75E-16 with 95% confidence interval $[-2.8109E-9, 2.81094E-9]$ while standard deviation σ = 3.36229E-9 with 95% confidence interval $[2.22306E-9, 6.84316E-9]$.

C.1 Error Analysis

Here $< \dot{m} >$ will denote the time averaged mass flow rate i.e.

$$< \dot{m} >= \frac{\mathfrak{m}}{RT}\left[P_{atm}\right]\frac{\Delta V_{water}}{\Delta t} \tag{C.1}$$

which we can see is a function of eleven quantities: R, T, $\mathfrak{m}$, Δt, V_{ref} and ΔV_{water}. We can estimated the uncertainty $\delta < \dot{m} >$ by using the formula [173]:

$$\delta f(x_1, x_2, ..., x_n) = \sqrt{\sum_{i=1}^{n}\left(\frac{\partial f}{\partial x_i}\delta x_i\right)^2} \tag{C.2}$$

where δf is the uncertainty of the function f of x_1, x_2 etc each with uncertainty δx_1, δx_2 etc. On applying this formula we would get:

$$\frac{\delta < \dot{m} >}{|< \dot{m} >|} = \sqrt{\left(\frac{\delta\mathfrak{m}}{\mathfrak{m}}\right)^2 + \left(\frac{\delta R}{R}\right)^2 + \left(\frac{\delta T}{T}\right)^2 + \left(\frac{\delta P_{atm}}{P_{atm}}\right)^2 + g} \tag{C.3}$$

where

$$g = g(\delta\Delta V_{water}, \Delta V_{water}, \delta\Delta t, \Delta t) = \left(\frac{\delta\Delta V_{water}}{\Delta V_{water}}\right)^2 + \left(\frac{\delta\Delta t}{\Delta t}\right)^2 \tag{C.4}$$

where

$$\delta\Delta V_{water} = \sqrt{2}\delta V \tag{C.5}$$

δV being the uncertainty in the volume measurement, also note that:

$$\delta\Delta t = \sqrt{2}\delta t \tag{C.6}$$

where δt is the uncertainty in time measurements.

C.2 Model Justification

In this section the "near hydrostatic equilibrium" approximation will be justified. Consider the net force acting on the water in the reservoir and tube see Figure C.1. With the following notation:

1. let F_{net} denote the net upward or downward force on the water.
2. let F_n denote the net normal force acting on the water.
3. let P_{atm} denote the atmospheric pressure acting on the exposed reservoir water.
4. let A denote the exposed reservoir water surface area.
5. let A' denote the cross-sectional area of the tube in which water is drawn up.
6. let P_{gas} denote the pressure of the gas at the surface of water in the tube.
7. let w' denote the weight of water in the tube.
8. let W' denote the weight of water in the rest of the reservoir.

consider the balance of vertical forces:

$$F_{net} - F_n = -\left[P_{atm}A + P_{gas}A' + w' + W'\right] \tag{C.7}$$

for which it would follow that:

$$F_{net} - F_n = -\left[P_{atm}A + P_{gas}A' + \left(hA' + H\bar{A}\right)\rho_{water}g\right] \tag{C.8}$$

where H is the height of the water in the reservoir from the bottom of the container to where it is exposed to the atmosphere, and $\bar{A}$ is the cross-sectional area of the reservoir. h is the height of the water column relative to the surface of water in the reservoir exposed to the atmosphere. Note we let $hA'\rho_{water}g << H\bar{A}\rho_{water}g$ (through out operation) and $A' << A < \bar{A}$. Consequently we have that:

$$\frac{d}{dt}\left(\frac{F_{net} - F_n}{P_{atm}A}\right) = -\left[\frac{\dot{P}_{gas}A'}{P_{atm}A} + \left(\dot{h}\frac{A'}{A} + \dot{H}\frac{\bar{A}}{A}\right)\frac{\rho_{water}g}{P_{atm}}\right] \tag{C.9}$$

since $-\dot{h}A' = \dot{H}\bar{A}$ (balance of volume flow rates and treating water as incompressible) we have that

$$\frac{d}{dt}\left(\frac{F_{net} - F_n}{P_{atm}A}\right) = -\frac{\dot{P}_{gas}A'}{P_{atm}A} \tag{C.10}$$

since the flow was slow (long times for small changes in pressure) and only a small percentage of the inlet was ever evacuated (i.e. $P_{gas} \approx P_{atm}$ when flows were stopped) we would have:

$$\left|\frac{\dot{P}_{gas}A'}{P_{atm}A}\right| << 1 \tag{C.11}$$

hence we would have:

$$\frac{d}{dt}\left(\frac{F_{net}-F_n}{P_{atm}A}\right)\approx 0 \tag{C.12}$$

and therefore (starting from mechanical equilibrium):

$$F_{net}(t)=F_n(t)-F_n(0) \tag{C.13}$$

as an approximation and hence we would have:

$$-F_n(0)=-\left[P_{atm}A+P_{gas}(t)A'+\left(h(t)A'+H(t)\bar{A}\right)\rho_{water}g\right] \tag{C.14}$$

fortunately at time $t=0$ F_n is determined by mechanical equilibrium hence we have that:

$$F_n(0)=\left[P_{atm}A+P_{gas}(0)A'+\left(h(0)A'+H(0)\bar{A}\right)\rho_{water}g\right] \tag{C.15}$$

which reduces to:

$$F_n(0)=P_{atm}\bar{A}+H(0)\bar{A}\rho_{water}g \tag{C.16}$$

from which it then follows that:

$$P_{gas}(t)A'=P_{atm}\left(\bar{A}-A\right)+\left(H(0)-H(t)\right)\bar{A}\rho_{water}g-h(t)A'\rho_{water}g \tag{C.17}$$

Fortunately from $-\dot{h}A'=\dot{H}\bar{A}$ and its definition we have that:

$$h(t)A'=\left(H(0)-H(t)\right)\bar{A} \tag{C.18}$$

and therefore we have the simple result that:

$$P_{gas}(t)\approx P_{atm} \tag{C.19}$$

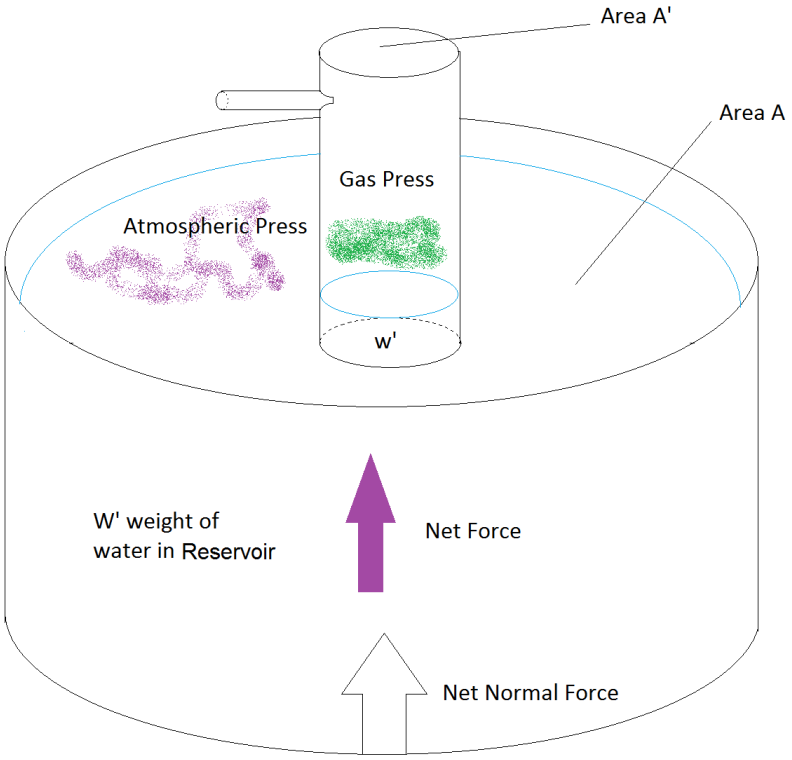


Figure C.1: A diagram illustrating the set-up for the argument for hydrostatic pressure argument

References

[1] Jafit. http://www.blendswap.com/blends/view/61208, 2015. Space Shuttle Orbiter Atlantis Released under Creative Commons Attribution 3.0.

[2] R. L. Liboff, *Kinetic Theory Classical, Quantum, and Relativistic Descriptions*, pp. 1–22. Springer, third ed., 2003.

[3] Y. Nakayama and R. F. Boucher, *Introduction to Fluid Mechanics*, pp. 187 – 189. Butterworth-Heinemann, 1999.

[4] R. G. Longwitz, *Study of gas ionization in a glow discharge and developement of a micro gas ionizer for gas detection and analysis*. Phd, Institut de microélectronique sciences et techniques de L'ingeénieur, École Polytechnique Fédérale de Lausanne, 2004.

[5] A. Descoeudres, *Characterization of Electrical Discharge Machining Plasmas*. Phd, École Polytechnique Fédérale de Lausanne, 2006.

[6] N. Goldman, A. Goldman, and R. Sigmond, "The corona discharge, its properties and specific uses," *Pure and Applied Chemistry*, vol. vol 57, no. no 9, pp. 1353–1362, 1985.

[7] M. A. Lieberman and A. J. Lichtenberg, *Principles of plasma discharges and materials processing*, ch. 14, pp. 450–465. John Wiley and Sons, Inc, 1994.

[8] R. G. Jahn, *Physics of Electric Propulsion*, ch. 6, pp. 110–116. McGraw Hill, 1968.

[9] P. Ferrer and H. Liedberg, "Plume characterization for a miniaturized corona ionization propulsion system," *NA*, 2013. Internal work, publication pending.

[10] S. Kjelstrup and D. Bedeaux, *Non-Equilibrium Thermodynamics of Heterogeneous Systems*, vol. 16 of *Series on Advances in Statistical Mechanics*. World Scientific Publishing Co. Pte. Ltd., 2008.

[11] CODATA Committee on Data for Science and Technology, "The NIST reference on constants, units, and uncertainty." http://physics.nist.gov/cgi-bin/cuu/Value?tkev|search_for=Boltzmann+constant, December 2014. Boltzmann constant (eV/K).

[12] CODATA Committee on Data for Science and Technology, "The NIST reference on constants, units, and uncertainty." http://physics.nist.gov/cgi-bin/cuu/Value?k|search_for=Boltzmann+constant, December 2014. Boltzmann constant (J/K).

[13] M. E. Wieser, "Atomic weights of the elements 2005 (iupac technical report)," *Pure Appl. Chem.*, vol. 78, no. 11, pp. 2051–2066, 2006.

[14] CODATA Committee on Data for Science and Technology, "The NIST reference on constants, units, and uncertainty." http://physics.nist.gov/cgi-bin/cuu/Value?mec2mev|search_for=electron+mass, December 2014. electron mass (MeV).

[15] CODATA Committee on Data for Science and Technology, "The NIST reference on constants, units, and uncertainty." http://physics.nist.gov/cgi-bin/cuu/Value?me|search_for=electron+mass, December 2014. electron mass (kg).

[16] CODATA Committee on Data for Science and Technology, "The NIST reference on constants, units, and uncertainty." http://physics.nist.gov/cgi-bin/cuu/Value?ep0|search_for=electric+constant, December 2014. Electric Constant used for Coulomb constant.

[17] CODATA Committee on Data for Science and Technology, "The NIST reference on constants, units, and uncertainty." http://physics.nist.gov/cgi-bin/cuu/Value?e, December 2014. Elementary charge.

[18] CODATA Committee on Data for Science and Technology, "The NIST reference on constants, units, and uncertainty." http://physics.nist.gov/cgi-bin/cuu/Value?hbar|search_for=universal_in!, December 2014. Planck's Constant Js.

[19] CODATA Committee on Data for Science and Technology, "The NIST reference on constants, units, and uncertainty." http://physics.nist.gov/cgi-bin/cuu/Value?hbarev|search_for=universal_in!, December 2014. Planck's Constant eVs.

[20] W. Wright and P. Ferrer, "Electric micropropulsion systems," *Progress in Aerospace Sciences*, vol. 74, pp. 48–61, April 2015.

[21] E. Ahedo and J. Gallardo, "Scaling down hall thrusters," in *Proc. of the 28th International Electric Propulsion Conference Toulouse, France*, no. 104, 2003.

[22] A. Sengupta, "Magnetic confinement in a ring-cusp ion thruster discharge plasma," *Journal of Applied Physics*, vol. 105, no. 9, p. 093303, 2009.

[23] P. Molina-Cabrera, G. Herdrich, M. Lau, S. Fausolas, T. Schoenherr, and K. Komurasaki, "Pulsed plasma thrusters: a worldwide review and long yearned classification," in *Proc. of the 32nd International Electric Propulsion Conference, Electric Rocket Propulsion Society, Wiesbaden, Germany*, 2011.

[24] M. Tajmar, A. Genovese, and W. Steiger, "Indium field emission electric propulsion microthruster experimental characterization," *Journal of Propulsion and Power*, vol. 20, no. 2, p. 211, 2004.

[25] M. Gamero-Castano and V. Hruby, "Characterization of a colloid thruster performing in the micro-newton thrust range," in *Proc. of the 27th International Electric Propulsion Conference, Electric Rocket Propulsion Society (Pasadena, USA)*, no. 282, 2001.

[26] M. West, C. Charles, and R. Boswell, "Testing a helicon double layer thruster immersed in a space-simulation chamber," *Journal of Propulsion and Power*, vol. 24, p. 134, 2008.

[27] J. Polk, M. Sekerak, J. Ziemer, J. Schein, N. Qi, and A. Anders, "A theoretical analysis of vacuum arc thruster and vacuum arc ion thruster performance," *IEEE Transactions On Plasma Science*, vol. 36, p. 2167, 2008.

[28] K. Avinash and G. Zank, "Micropropulsion in space via dust-plasma thruster," *Physics of Plasmas*, vol. 14, p. 053507, 2007.

[29] A. Grubisic and S. Gabriel, "Understanding hollow cathode thrust production mechanisms," in *Proc. of the 31st International Electric Propulsion Conference, Electric Rocket Propulsion Society (Ann Arbor, USA)*, no. 187, 2009.

[30] C. Phipps, M. Birkan, W. Bohn, H. Eckel, H. Horisawa, T. Lippert, *et al.*, "Review: laser-ablation propulsion," *J. Propul. Power*, vol. 26, no. 4, p. 609, 2010.

[31] B. Wollenhaupt, A. Hammer, G. Herdrich, S. Fasoulas, and H. Roser, "A very low power arcjet (velarc) for small satellite missions," in *Proc. of the 32nd International Electric Propulsion Conference, Electric Rocket Propulsion Society (Wiesbaden, Germany)*, no. 257, 2011.

[32] S. Kawamoto, T. Makida, F. Sasaki, Y. Okawa, and S. Nishida, "Precise numerical simulations of electrodynamic tethers for an active debris removal system," *Acta Astronautica*, vol. 59, p. 139, 2006.

[33] P. Ferrer and M. P. Tchonang, "Miniaturization of electrostatic ion engines by ionization and acceleration coupling," *J. Phys. D. Appl. Phys.*, vol. 44, p. 335204, 2011.

[34] M. T. Pokaha, "Modelling of the corona ionization space propulsion system," Master's thesis, School of Physics, University of Witwatersrand, 2011.

[35] T. Ito, N. Gascon, W. S. Crawford, and M. A. Cappelli, "Further development of a micro hall thruster," in *42nd AIAA/ASME/SAE/ASEE Joint Propulsion Conference & Exhibit*, American Institute of Aeronautics and Astronautics, 2006. Copyright © 2006 Standford University.

[36] R. G. Jahn, *Physics of electric propulsion*. McGraw-Hill Inc, 1968.

[37] A. Schütze, J. Y. Jeong, S. E. Babayan, J. Park, G. S. Selwyn, and R. Hicks, "The atmospheric-pressure plasma jet: A review and comparison to other plasma sources," *IEEE Transactions on Plasma Science*, vol. 26, no. 6, p. 1685, 1998.

[38] Y. Sakiyama and D. B. Graves, "Corona-glow transition in the atmospheric pressure rf-excited plasma needle," *J. Phys. D: Appl. Phys.*, vol. 39, pp. 3644–3652, 2006.

[39] K. Hutter, A. A. F. van de Ven, and A. Ursescu, *Electromagnetic Field Matter Interactions in Thermoelastic Solids and Viscous Fluids*. Springer-Verlag, 2006.

[40] J. H. Spurk and N. Aksel, *Fluid Mechanics*. Springer-Verlag, second ed., 2008.

[41] W. M. Lai, D. Rubin, and E. Krempl, *Introduction to Continuum Mechanics*. Elsevier, fourth ed., 2010.

[42] L. D. Landau and E. M. Lifshitz, *Fluid Mechanics*. PERGAMON PRESS, second ed., 1987.

[43] L. B. FREUND, *Dynamic Fracture Mechanics*. CAMBRIDGE UNIVERSITY PRESS, 1998.

[44] J. P. Freidberg, *Plasma Physics and Fusion Energy*. CAMBRIDGE UNIVERSITY PRESS, 2007.

[45] J. Marsden and A. Tromba, *Vector Calculus*. W. H. Freeman and Company, fifth ed., 2003.

[46] K. F. Riley, M. P. Hobson, and S. J. Bence, *Mathematical Methods for Physics and Engineering*. CAMBRIDGE UNIVERSITY PRESS, third ed., 2006.

[47] D. M. Goebel and I. Katz, *Fundamentals of Electric Propulsion Ion and Hall Thrusters*. John Wiley & Sons, Inc., 2008.

[48] G. P. Sutton and O. Biblarz, *Rocket Propulsion Elements*. John Wiley & Sons, INC., 2001.

[49] S. Kjelstrup and D. Bedeaux, *Non-Equilibrium Thermodynamics of Heterogeneous Systems*, vol. 16 of *Series on Advances in Statistical Mechanics*, pp. 23–29. World Scientific Publishing Co. Pte. Ltd., 2008.

[50] D. Bedeaux, "Nonequilibrium thermodynamics and statistical physics of surfaces," *Advance in Chemical Physics*, vol. LXIV, pp. 105–119, 1986.

[51] D. Bedeaux and A. Albano, "Non-equilibrium electro-thermodynamics of polarizable multicomponent fluids with an interface," *Physica A*, vol. 147, pp. 407–435, 1987.

[52] S. Kjelstrup and D. Bedeaux, *Non-Equilibrium Thermodynamics of Heterogeneous Systems*, vol. 16 of *Series on Advances in Statistical Mechanics*, pp. 127–155. World Scientific Publishing Co. Pte. Ltd., 2008.

[53] Y. L. Klimontovich, *Statistical Theory of Open Systems Volume 1: A Unified Approach to Kinetic Description of Processes in Active Systems*. Fundamental Theories of Physics, SPRINGER-SCIENCE+BUSINESS MEDIA, B.V., 1995.

[54] D. Seleši, *Generalized Stochastic Processes in Infinite Dimensional Spaces with Applications to Singular Stochastic Partial Differential Equations*. PhD thesis, UNIVERSITY OF NOVI SAD FACULTY OF SCIENCE DEPARTMENT OF MATHEMATICS AND INFORMATICS, 2007.

[55] B. Øksendal, *Stochastic Differential Equations An Introduction with Applications*. Springer, sixth ed., 2003.

[56] E. Wong and M. Zakai, "On the relation of ordinary and stochastic differential equations," *Int. J. Engr. Sci.*, vol. 3, pp. 213–219, 1965.

[57] E. Wong and M. Zakai, "On the convergence of ordinary integrals to stochastic integrals," *Ann. Math. Statist.*, vol. 36, pp. 1560–1564, 1965.

[58] C. W. Gardiner, *Handbook of Stochastic Methods for Physics, Chemistry and the Natural Sciences*, pp. 98–101. Springer, second ed., 1985.

[59] C. W. Gardiner, *Handbook of Stochastic Methods for Physics, Chemistry and the Natural Sciences*, pp. 86–87. Springer, second ed., 1985.

[60] F. C. Klebaner, *Introduction to Stochastic Calculus with Applications*, pp. 93–95. Imperial College Press, second ed., 2005.

[61] F. C. Klebaner, *Introduction to Stochastic Calculus with Applications*. Imperial College Press, second ed., 2005.

[62] C. Gardiner, *Handbook of Stochastic Methods for Physics, Chemistry and the Natural Sciences*, pp. 96–98. Springer, second ed., 1994.

[63] T. Arbogast and J. Bona, *Methods of Applied Mathematics*. Department of Mathematics the University of Texas at Austin, 2005.

[64] R. L. Liboff, *Kinetic Theory Classical, Quantum, and Relativistic Descriptions*. Springer, third ed., 2003.

[65] R. Balescu, *Equilibrium and Nonequilibrium and Statistical Mechanics*, pp. 49–53. John Wiley & Sons, 1975.

[66] R. Balescu, *Equilibrium and Nonequilibrium Statistical Mechanics*, pp. 232–239. John Wiley & Sons, 1975.

[67] D. Zubarev, V. Morozov, and G. Ropke, *Statistical Mechanics of Nonequilibrium Processes*, vol. 1, pp. 98–100. Akademie Verlag, 1996.

[68] D. Zubarev, V. Morozov, and G. Ropke, *Statistical Mechanics of Nonequilibrium Processes*, vol. 1. Akademie Verlag, 1996.

[69] R. Balescu, *Equilibrium and Nonequilibrium Statistical Mechanics*, pp. 57–62. John Wiley & Sons, 1975.

[70] R. L. Liboff, *Kinetic Theory Classical, Quantum, and Relativistic Descriptions*, pp. 78–82. Springer, third ed., 2003.

[71] D. Zubarev, V. Morozov, and G. Ropke, *Statistical Mechanics of Nonequilibrium Processes*, vol. 1, pp. 188–248. Akademie Verlag, 1996.

[72] R. Balescu, *Equilirium and Nonequilibrium Statistical Mechanics*. John Wiley & Sons, 1975.

[73] M. Moreau, "Formal study of a chemical reaction by grad expansion of the boltzmann equation. i," *Physica A*, vol. 79, pp. 18–38, 1975.

[74] M. Moreau, "Formal study of a chemical reaction by grad expansion of the boltzmann equation. ii," *Physica A*, vol. 79, pp. 39–51, 1975.

[75] M. Bisi, M. Groppi, and G. Spiga, "Grads distribution functions in the kinetic equations for a chemical reaction," *Continuum Mech. Thermodyn*, vol. 14, pp. 207–222, 2002.

[76] B. V. Alexeev, A. Chikhaoui, J. G. Molans, J. T. Grushin, and L. P. Grushina, "Generalized chapmanenskog method in the kinetic theory of reacting ionized gases," *Phys. Plasmas*, vol. 1, pp. 3199–3210, October 1994.

[77] M. Groppi and G. Spiga, "Kinetic approach to chemical reactions and inelastic transitions in a rarefied gas," *Journal of Mathematical Chemistry*, vol. 26, pp. 197–219, 1999.

[78] B. Alexeev, A. Chikhaoui, and I. T. Grushin, "Application of the generalized chapman-enskog method to the transport-coefficient calculation in a reacting gas mixture," *PHYSICAL REVIEW E*, vol. 49, pp. 2809–2825, April 1994.

[79] G. M. Kremer, *An Introduction to the Boltzmann Equation and Transport Processes in Gases*, pp. 235–297. Springer, 2010.

[80] S. O. Macheret, Y. Z. Ionikh, N. V. Chernysheva, L. M. Azer P. Yalin, and R. B. Miles, "Shock wave propagation and dispersion in glow discharge plasmas," *PHYSICS OF FLUIDS*, vol. 13, no. 9, p. 2693, 2001.

[81] I. V. Adamovich, V. V. Subramaniam, J. W. Rich, and S. O. Macheret, "Phenomenological analysis of shock-wave propagation in weakly ionized plasmas," *AIAAA Journal*, vol. 36, p. 816, May 1998.

[82] S. Ansumalia, I. V. Karlinb, and S. Succid, "Kinetic theory of turbulence modeling: smallness parameter, scaling and microscopic derivation of smagorinsky model," *Physica A: Statistical Mechanics and its Applications*, vol. 338, p. 379394, July 2004.

[83] C. K. Chu, "Kinetictheoretic description of the formation of a shock wave," *Phys. Fluids*, vol. 8, no. 1, p. 12, 1965.

[84] T. I. Gombosi, *Gaskinetic Theory*, vol. 16. Cambridge University Press, 1994.

[85] R. Balescu, *Equilibrium and Nonequilibrium Statistical Mechanics*, pp. 409–413. John Wiley & Sons, 1975.

[86] D. Zubarev, V. Morozov, and G. Ropke, *Statistical Mechanics of Nonequilibrium Processes*, vol. 1, pp. 123–127. Akademie Verlag, 1996.

[87] C. Cercignani, *Mathematical Methods in Kinetic Theory*, pp. 51–55. PLENUM PRESS NEW YORK 1969, 1969.

[88] C. K. Zachos, D. B. Fairlie, and T. L. Curtright, *QUAHTUH MECHANICS IN PHASE SPACE An Overview with Selected Papers*, vol. 34. World Scientific Publishing Co. Pty. Ltd., 2005.

[89] K. Ímre, E. Özizmir, M. Rosenbaum, and P. F. Zweifel, "Wigner method in quantum statistical mechanics," *JOURNAL OF MATHEMATICAL PHYSICS*, vol. 8, pp. 1097–1108, May 1967.

[90] R. Balescu, *Equilibrium and Nonequilibrium Statistical Mechanics*, pp. 44–47. John Wiley & Sons, 1975.

[91] H. J. Groenewold, "Wigner method in quantum statistical mechanics," *Physica*, vol. 12, pp. 405–460, 1946.

[92] B. Lesche, "From classical mechanics to feynman graphs with $\star$ - products," *PHYSICAL REVIEW D*, vol. 29, pp. 2270–2274, May 1984.

[93] V. D. M. Bonitz, *Quantum Kinetic Theory*, pp. 31–85. B. G. Teubner Stuttgart Leipzig, 1998.

[94] C. K. Zachos, D. B. Fairlie, and T. L. Curtright, *QUAHTUH MECHANICS IN PHASE SPACE An Overview with Selected Papers*, vol. 34, pp. 21–24. World Scientific Publishing Co. Pty. Ltd., 2005.

[95] F. Bayen, M. Flato, C. Fronsdal, A. Lichnerowicz, and D. Sternheimer, "Deformation theory and quantization. i. deformations of symplectic structures," *ANNALS OF PHYSICS*, vol. 111, pp. 61–110, 1978.

[96] F. Bayen, M. Flato, C. Fronsdal, A. Lichnerowicz, and D. Sternheimer, "Deformation theory and quantization.ii. physical applications," *ANNALS OF PHYSICS*, vol. 110, pp. 111–151, 1978.

[97] R. Balescu, *Equilibrium and Nonequilibrium Statistical Mechanics*, pp. 89–98. John Wiley & Sons, 1975.

[98] M. Pascoli, P. Bordone, R. Brunetti, and C. Jacoboni, "Wigner paths for electrons interacting with phonons," *PHYSICAL REVIEW B*, vol. 58, pp. 3503–3506, August 1998.

[99] R. L. Liboff, *Kinetic Theory Classical, Quantum, and Relativistic Descriptions*, pp. 356–357. Springer, third ed., 2003.

[100] V. D. M. Bonitz, *Quantum Kinetic Theory*, pp. 323–326. B. G. Teubner Stuttgart Leipzig, 1998.

[101] V. D. M. Bonitz, *Quantum Kinetic Theory.* B. G. Teubner Stuttgart Leipzig 1998, 1998.

[102] R. L. Liboff, *Kinetic Theory Classical, Quantum, and Relativistic Descriptions*, pp. 400–402. Springer, third ed., 2003.

[103] P. A. Markowich, N. J. Mauser, and F. Poupaud, "A wignerfunction approach to (semi)classical limits: Electrons in a periodic potential," *Journal of Mathematical Physics*, vol. 35, p. 1066, 1994.

[104] C. L. Gardner and C. Ringhofer, "The chapman-enskog expansion and the quantum hydrodynamic model for semiconductor devices," *VLSI DESIGN*, vol. 10, no. 4, pp. 415–435, 2000.

[105] R. Balescu, *Equilibrium and Nonequilibrium Statistical Mechanics*, pp. 513–543. John Wiley & Sons, 1975.

[106] D. Zubarev, V. Morozov, and G. Röpke, *Statistical Mechanics of Nonequilibrium Processes*, vol. 1, pp. 96–142. Akademie Verlag, 1996.

[107] J. H. Spurk and N. Aksel, *Fluid Mechanics*, pp. 35–37. Springer, second ed., 2008.

[108] R. D. Zucker and O. Biblarz, *Fundamentals of Gas Dynamics*, p. 6. John Wiley and Sons, Inc., second ed., 2002.

[109] M. Saculinggan and E. A. Balase, "Empirical power comparison of goodness of fit tests for normality in the presence of outliers," *Journal of Physics:ConferenceSeries*, vol. 435, 2013. 2012 iCAST:Contemporary Mathematics, Mathematical Physics and their Applications IOP Publishing.

[110] CODATA Committee on Data for Science and Technology, "The NIST reference on constants, units, and uncertainty." http://physics.nist.gov/cgi-bin/cuu/Value?r|search_for=gas+constant, December 2014. Molar Gas Constant.

[111] A. Bogaerts, E. Neyts, R. Gijbels, and J. van der Mullen, "Gas discharge plasmas and their applications," *Elsivier*, 2001.

[112] Y. P. Raizer, *Gas Discharge Physics*, pp. 324–346. Springer-Verlag, 1991.

[113] R. S. Islamov, "Analytic investigation of the glow discharge of the anode region in elevated pressure electronegative gases," *Journal of Applied Physics*, 1996.

[114] A. Kaminska, B. Lopez, B. Izrar, and M. Dudeck, "Modelling of an argon plasma jet generated by a dc arc," *Plasma Sources Sci. Technol*, vol. 17, 2008.

[115] R. A. Arakoni, J. J. Ewing, and M. J. Kushner, "Microdischarges for use as microthrusters: modelling and scaling," *J. Phys. D: Appl. Phys.*, vol. 41, 2008.

[116] B. V. Alexeev, *Generalized Boltzmann Physical Kinetics*, pp. 124–132. ELSEVIER, 2004.

[117] E. B. Arkilic, M. A. Schmidt, and K. S. Breuer, "Gaseous slip flow in long microchannels," *JOURNAL OF MICROELECTROMECHANICAL SYSTEMS*, vol. 6, pp. 167–178, June 1997.

[118] V. Titarev and E. Shakhov, "Computational study of a rarefied gas flow through a long circular pipe into vacuum," *Vacuum*, vol. 86, pp. 1709–1716, 2012.

[119] V. Titarev, "Rarefied gas flow in a circular pipe of finite length," *Vacuum*, vol. 94, pp. 92–103, 2013.

[120] Z.-Y. Guo and Z.-X. Li, "Size effect on microscale single-phase flow and heat transfer," *International Journal of Heat and Mass Transfer*, vol. 46, pp. 149–159, 2003.

[121] P.-F. Hao, Y.-T. Ding, Z.-H. Yao, F. He, and K.-Q. Zhu, "Size effect on gas flow in micro nozzles," *JOURNAL OF MICROMECHANICS AND MICROENGINEERING*, vol. 15, pp. 2069–2073, 2005.

[122] R. D. Zucker and O. Biblarz, *Fundamentals of Gas Dynamics*. John Wiley & Sons, INC., second ed., 2002.

[123] C. Shen, *Rarefied Gas Dynamics Fundamentals, Simulations and Micro Flows*. Springer, 2005.

[124] R. L. Liboff, *Kinetic Theory Classical, Quantum, and Relativistic Descriptions*, pp. 145–146. Springer, third ed., 2003.

[125] Not Available, "Van der waals radius of the elements." http://periodictable.com/Properties/A/VanDerWaalsRadius.v.html, December 2014. Up to date, curated data provided by Mathematica's ElementData function from Wolfram Research, Inc.

[126] L. Garca-Coln, R. Velasco, and F. Uribe, "Beyond the navierstokes equations: Burnett hydrodynamics," *Physics Reports*, vol. 465, pp. 149–189, 2008.

[127] B. H. Bransden and M. R. C. McDowell, *Charge Exchange and the Theory of Ion-Atom Collisions*, pp. 19–20. Clarendon Press, 1992.

[128] R. L. Liboff, *Kinetic Theory Classical, Quantum, and Relativistic Descriptions*, pp. 138–139. Springer, third ed., 2003.

[129] M. A. Lieberman and A. J. Lichtenberg, *Principles of Plasma Discharges and Materials Processing*. John Wiley & Sons, INC., 1994.

[130] M. A. Lieberman and A. J. Lichtenberg, *Principles of Plasma Discharges and Materials Processing*, pp. 61–66. John Wiley & Sons, INC., 1994.

[131] N. F. Mott and H. S. W. Massey, *The Theory of Atomic Collisions*, pp. 329–331. Oxford University Press, 1965.

[132] R.E.Johnson, *Introduction to Atomic and Molecular Colliisons*, p. 116. Plenum Press, New York, 1982.

[133] A. Rahman, "Correlations in the motion of atoms in liquid argon," *Phys. Rev.*, vol. 136, p. A405, October 1964.

[134] J. E. Purcell, R. A. Berg, and A. E. S. Green, "Potential-scattering model for electons on helium and other atoms," *Physical Review A*, vol. 2, pp. 107–111, July 1970.

[135] J. E. Purcell, R. A. Berg, and A. E. S. Green, "Addendum to: Potential-scattering model for electons on helium and other atoms," *Physical Review A*, vol. 3, pp. 508–510, July 1970.

[136] D. L. Sellin, A. S. Zachor, and A. E. S. Green, "Analytic independent-particle model for atoms," *The Physical Review*, vol. 184, pp. 1–9, August 1969.

[137] D. Zubarev, V. Morozov, and G. Ropke, *Statistical Mechanics of Nonequilibrium Processes*, vol. 1, pp. 209–227. Akademie Verlag, 1996.

[138] S. Jardin, *Computational Methods in Plasma Physics*. Computational Science Series, Chapman & Hall/CRC Press Taylor & Francis Group, 2010.

[139] V. Fortov, I. Iakubov, and A. Khrapak, *Physics of Strongly Coupled Plasma*. CLARENDON PRESS OXFORD, 2006.

[140] A. Beiser, *Concepts of Modern Physics*, p. 0. McGraw-Hill, sixth ed., 2003.

[141] M. Mitchner and C. H. Kruger, *Partially Ionzed Plasma*, vol. 16. John Wiley & Sons Inc., 1992.

[142] Biagi-v7.1 (Magboltz version 7.1), "Cross sections extracted from program magboltz, version 7.1 june 2004." www.lxcat.net, August 2014.

[143] Biagi-v8.9 (Magboltz version 8.9), "Cross sections extracted from program magboltz, version 8.9 march 2010." www.lxcat.net, August 2014.

[144] NGFSRDW database, "A set of excitation cross section to individual fine-structure levels of the noble gases.." www.lxcat.net, August 2014.

[145] F. van Odenhoven, *Kinetic Theory of Transport Processes. In Partially Ionized Gases*. PhD thesis, TECHNISCHE HOGESCHOOL EINDHOVEN, 1983.

[146] G. Lebon, D. Jou, and J. Casas-Vázquez, *Understanding Non-equilibrium Thermodynamics Foundations, Applications, Frontiers*, pp. 39–40. Springer, 2008.

[147] G. Lebon, D. Jou, and J. Casas-Vázquez, *Understanding Non-equilibrium Thermodynamics Foundations, Applications, Frontiers*. Springer, 2008.

[148] H. Kreuzer, *Non-equilibrium Thermodynamics and its Statistical Foundations*. Clarendon Press, 1981.

[149] S. R. D. Groot and E. Mazur, *Non-equilibrium Thermodynamics*. DOVER PUBLICATIONS, INC., NEW YORK.

[150] S. R. D. Groot and E. Mazur, *Non-Equilibrium Thermodynamics*, pp. 11–17. DOVER PUBLICATIONS, INC., NEW YORK.

[151] H. Kreuzer, *Non-equilibrium Thermodynamics and its Statistical Foundations*, pp. 18–25. Clarendon Press, 1981.

[152] G. Lebon, D. Jou, and J. Casas-Vázquez, *Understanding Non-equilibrium Thermodynamics Foundations, Applications, Frontiers*, pp. 45–49. Springer, 2008.

[153] J. D. Jackson, *Classical Electrodynamics*, pp. 248–249. John Wiley & Sons, Inc., third ed., 1999.

[154] D. Zubarev, V. Morozov, and G. Ropke, *Statistical Mechanics of Nonequilibrium Processes*, vol. 1, pp. 209–223. Akademie Verlag, 1996.

[155] R. L. Liboff, *Kinetic Theory Classical, Quantum, and Relativistic Descriptions*, pp. 98–108. Springer, third ed., 2003.

[156] Y. L. Klimontovich, *Statistical Theory of Open Systems: A Unified Approach to Kinetic Description of Processes in Active Systems*, vol. 1, pp. 6–8. SPRINGER-SCIENCE+BUSINESS MEDIA, B.V., 1995.

[157] D. Zubarev, V. Morozov, and G. Ropke, *Statistical Mechanics of Nonequilibrium Processes*, vol. 1, pp. 90–96. Akademie Verlag, 1996.

[158] V. Fortov, I. Iakubov, and A. Khrapak, *Physics of Strongly Coupled Plasma*, p. 2. CLARENDON PRESS OXFORD, 2006.

[159] N. F. Mott and H. S. W. Massey, *The Theory of Atomic Collisions*, pp. 332–334. Oxford University Press, 1965.

[160] V. I. Kolobov, "Advances in electron kinetics and theory of gas discharges," *PHYSICS OF PLASMAS*, vol. 20, p. 101610, 2013.

[161] V. Fortov, I. Iakubov, and A. Khrapak, *Physics of Strongly Coupled Plasma*, pp. 9–10. CLARENDON PRESS OXFORD, 2006.

[162] B. V. Alexeev, *Generalized Boltzmann Physical Kinetics*, pp. 238–240. ELSEVIER, 2004.

[163] R. L. Liboff, *Kinetic Theory Classical, Quantum, and Relativistic Descriptions*, pp. 158–159. Springer, third ed., 2003.

[164] R. Balescu, *Equilibrium and Nonequilibrium Statistical Mechanics*, pp. 423–427. John Wiley & Sons, 1975.

[165] B. Øksendal, *Stochastic Differential Equations An Introduction with Applications*, pp. 10–11. Springer, sixth ed., 2003.

[166] C. Gardiner, *Handbook of Stochastic Methods for Physics, Chemistry and the Natural Sciences*, pp. 67–68. Springer, second ed., 1994.

[167] D. Kannan, *An Introduction to Stochastic Processes*. North Holland, sixth ed., 1979.

[168] F. C. Klebaner, *Introduction to Stochastic Calculus with Applications*, pp. 91–93. Imperial College Press, second ed., 2005.

[169] D. Gusak, A. Kukush, A. Kulik, Y. Mishura, and A. Pilipenko, *Theory of Stochastic Processes With Applications to Financial Mathematics and Risk Theory*. Springer, 2010.

[170] O. Kallenberg, *Foundations of Modern Probability*, pp. 2–6. Springer, second ed., 2002.

[171] B. Øksendal, *Stochastic Differential Equations An Introduction with Applications*, pp. 26–30. Springer, sixth ed., 2003.

[172] C. Gardiner, *Handbook of Stochastic Methods for Physics, Chemistry and the Natural Sciences*. Springer, second ed., 1994.

[173] J. R. Taylor, *An Introduction to Error Analysis The Study of Uncertainties in Physical Measurements*. University Science Books, second ed., 1997.